Synthesis, Photoaffinity Labeling Studies, Biological Evaluation of Photoreactive Probes for HDAC 2 and 8.

BY

ADITYA SUDHEER VAIDYA
B.Tech. Institute of Chemical Technology, Mumbai, 2008

THESIS

Submitted as partial fulfillment of the requirements for the degree of Doctor of Philosophy in Medicinal Chemistry in the Graduate College of the University of Illinois at Chicago, 2013

Chicago, Illinois

Defense Committee:
Pavel A. Petukhov, Chair and Advisor
Gregory R. J. Thatcher
Karol S. Bruzik
Richard B. van Breemen
Jesus Garcia-Martinez (Department of Physiology and Biophysics)

ACKNOWLEDGMENTS

Firstly, I would like to thank my advisor Dr. Pavel A. Petukhov for his unwavering support and guidance during my graduate studies. As a mentor, he has always set the parameters within which my research would be focused, but also has given me immense freedom in trying novel troubleshooting methodologies not only in synthetic chemistry but also in biochemistry for which I had no prior knowledge. This approach has undoubtedly helped me to troubleshoot problems independently. I think the most important contribution he has to my work, are the instructive, inspiring and motivational discussions, that have helped me sail through a number of occasions, when experiments have been inconclusive or have given unexpected results.

Over the past five years, I have received support and encouragement from a number of individuals: Dr. Raghupathi Neelarapu and Dr. Bhargava Karumudi for their continued guidance during the synthesis of the photoreactive probes. Dr. He Bai for guiding me through enzyme kinetics and photoaffinity labeling studies. Emma Mendonca for her efforts in molecular modeling and docking studies. Antonett Madriaga for her efforts in cell-based assays and Hazem Abdelkarim for his efforts in IC_{50} collection for HDAC1 and 3. I would like to thank all the current and past lab members for their constructive critique and lively debates, without which I could not have taken my graduate work to fruition.

I would also like to thank all my teachers/mentors who have taught me during my undergraduate studies at the Institute of Chemical Technology, Mumbai especially, Dr. K. G. Akamanchi, Dr. M.S. Degani for they were the ones, who inspired me to come to pursue higher studies in Medicinal Chemistry.

I also want to thank my fiancée Prajakta, for her unconditional love, support and encouragement at every step during this journey.

ACKNOWLEDGMENTS (CONTINUED)

Finally and most importantly, I would like to thank my parents who have a greater place in my life than my God, without whom I would never have seen this day, or any day for that matter, for their unwavering support and encouragement, for their love and belief in me.

ASV

TABLE OF CONTENTS

CHAPTER 1 BACKGROUND AND INTRODUCTION 1

1.1 Introduction 1

1.2 Histone deacetylases 2

1.2.1 Chromatin, nucleosome and histones 2

1.2.2 Histone deacetylases and transcriptional regulation 3

1.2.3 Classification of histone deacetylases 4

1.2.4 Mechanism of deacetylation mediated by zinc dependent histone deacetylases 5

1.2.5 Inhibitors of histone deacetylases 7

1.3 Research Significance 15

1.3.1 HDAC2 and 8 as potential targets in the multiple therapeutic applications. 15

1.3.2 Therapeutic liabilities of existing HDAC inhibitors present a barrier in their use as therapeutics for long term applications. 18

1.3.3 Exploring secondary binding sites in HDACs for design of ligands lacking a zinc chelating group. 20

1.3.4. Barriers in the pursuit of structure-based drug design of novel HDAC ligands 22

1.4 Affinity-based protein profiling 22

1.4.1 General principles of affinity-based protein profiling 22

1.4.2 Types of photoreactive groups used for photoaffinity labeling. 24

1.4.3. Types of reporter tags used for visualization and purification 30

1.4.4 Types of bioorthogonal reactions used to ligate reporter tags with probe-protein adducts 31

1.4.5 Clickable benzophenone-based probes for profiling HDACs. 34

1.4.6 Diazirine-based probes for profiling HDACs. 35

1.4.7 Binding Ensemble Profiling with photoaffinity labeling (BEProFL) of HDACs with clickable azide-based probes. 36

1.5 Scope of the current study 38

CHAPTER 2: DEVELOPMENT OF AN IN VITRO ASSAY FOR SCREENING LIGANDS FOR HDAC2 40

2.1 Introduction 40

2.2 Types of HDAC activity assays 41

2.3 Radioisotope-labeled functional assays 41

2.4 Non-radioisotope labeled functional assays. 42

2.5 Non-radioisotope labeled binding assays. 49
2.6. Choice of an assay to screen ligands for HDAC2 51
2.7 Materials and Methods. 53
2.7.1 HDAC2 activity assays and enzyme kinetics 53
2.8 Results and Discussion 55
2.8.1 Screening of commercially available HDAC2/substrate pairs. 55
2.8.2 Optimization of amount of HDAC2 used per assay (steady state analysis) 57
2.8.3 Optimization of time of incubation of HDAC2 and substrate. 58
2.8.4 Determination of V_{max} and K_m for the HDAC2 59
2.8.5 Validation of the HDAC2 fluorogenic assay. 60
2.9 Conclusions 62

CHAPTER 3 NOVEL HISTONE DEACTYLASE 8 LIGANDS WITHOUT ZINC CHELATING GROUP: EXPLORING AN UPSIDE DOWN POSE 63

3.1 Introduction 63
3.2 Materials and methods 65
3.2.1 Synthesis 65
3.2.2 HDAC activity assays 65
3.2.3 Photolabeling protocol 66
3.2.4 Molecular modeling studies 67
3.2.5 Cell culture and western blot protocol 68
3.3 Results and Discussion 69
3.3.1 Synthesis 69
3.3.2 Structure-activity trends and docking studies 73
3.3.3 Photoaffinity labeling studies 78
3.3.4 Monitoring H4 and α-tubulin acetylation in SH-SY5Y cells 85
3.4 Conclusions. 86

CHAPTER 4. DESIGN, SYNTHESIS, MODELING, BIOLOGICAL EVALUATION AND PHOTOAFFINITY LABELING STUDIES OF NOVEL SERIES OF PHOTOREACTIVE BENZAMIDE PROBES FOR HISTONE DEACETYLASE 2 88

4.1 Introduction 88
4.2 Materials and methods 90
4.2.1 Synthesis 90

4.2.2 HDAC activity assays 90
4.2.3 Photolabeling protocol 91
4.2.4 Molecular modeling studies 92
4.2.5 Cell culture and western blot protocol 92
4.3 Results and Discussion 93
4.3.1 Synthesis 93
4.3.2 Structure activity trends and docking studies 100
4.3.3 Photolabeling studies 108
4.3.4 Monitoring H4 acetylation in MDA-MB-231 cells. 110
4.4 Conclusions 111

CHAPTER 5. CONCLUSIONS AND FUTURE DIRECTIONS 113

APPENDIX A. SYNTHETIC EXPERIMENTAL PROCEDURES AND COMPOUND CHARACTERIZATION 115

APPENDIX B. COMPOUND CHARACTERIZATION SPECTRA 135

APPENDIX C: COPYRIGHT AGREEMENTS 168

REFERENCES 170

VITA 187

LIST OF TABLES

TABLE I. HDAC8 IC_{50} VALUES FOR COMPOUNDS **52, 52A-H**, **53**, **53A**, AND **54**, **54A**. 75
TABLE II. INHIBITORY PROFILE OF BENZAMIDE PROBES AGAINST CLASS I HDACS. 101
TABLE III. RATIOS OF IC_{50} OF BENZAMIDE PROBES FOR HDAC1, 2 AND 3 WITH RESPECT TO PREINCUBATION TIME AND SELECTIVITY. 102

LIST OF FIGURES

Figure 1. Transcriptional regulation modulated by the acetylation status of histones by histone deacetylases(HDACs) and histone acetyl transferases(HATs) 4
Figure 2. Mechanism of histone deacetylation in zinc dependent histone deacetylases. 6
Figure 3. Structures of Trichostatin A and suberoylanilide hydroxamic acid (SAHA) 7
Figure 4. Numbering of amino acids in cyclic peptide surface binding group. 9
Figure 5. Examples of HDAC inhibitors with cyclic peptides as surface binding group. 10
Figure 6. Examples of benzamide-based HDAC1 and 2 selective inhibitors. 12
Figure 7. Examples of HDAC3 selective inhibitors. 13
Figure 8. Examples of HDAC8 selective inhibitors. 15
Figure 9. General schematic of affinity-based protein profiling using photoreactive ligands. 23
Figure 10. Mechanism of Huisgen (3+2) cycloaddition between terminal alkynes and azides. 32
Figure 11. Mechanism of Staudinger ligation. 33
Figure 12. Clickable benzophenone-based probes for HDACs 35
Figure 13. SAHA capture compound bearing aryl diazirine as a photoreactive group and biotin for visualization and/or enrichment. 36
Figure 14.Schematic of the BEProFL approach. 37
Figure 15. Structures of diazide-based photoreactive probes for HDACs suitable for BEProFL studies. . 38
Figure 16. Generation of thioacetate upon deacetylation by HDAC8 and subsequent reaction with 5,5' – dithiobis(2-nitrobenzoate) to generate 2-nitro-5-thiobenzoate. 43
Figure 17. Deacetylation of Boc-Lys(Ac)-AMC by HDACs 44
Figure 18. Derivatization of deacetylated product via reaction with naphthalene-2,3-dicarbaldehyde. 45
Figure 19. Two step fluorogenic assay using analogs of Boc-Lys(Ac)-AMC. 46
Figure 20. Structure activity studies on analogs of Boc-Lys(Ac)-AMC. 47
Figure 21. Schematic of a three-step bioluminogenic assay. 48
Figure 22. Fluorescently labeled SAHA derivative for fluorescence polarization assay. 50
Figure 23. Structure of furylacryloyl hydroxamic acid (FAHA) 50

LIST OF FIGURES (CONTINUED)

Figure 24. Comparison of fluorescent signal obtained from His-tagged and Flag-tagged HDAC2 with different commercially available substrates. 56
Figure 25. Steady state analysis of His-tagged HDAC2 57
Figure 26. Temporal representation of deacetylation of Boc-Lys(Ac)-AMC by HDAC2. 59
Figure 27. Saturation Kinetics of His-tagged HDAC2 with Boc-Lys(Ac)-AMC. 60
Figure 28. A. Dose response curve for SAHA. B. Z factors obtained in the fluorogenic assay for different preincubation times 61
Figure 29. Therapeutic liabilities of HDAC inhibitors bearing zinc chelating groups. 64
Figure 30. Mechanism of diazotization-azidation using *t*-butyl nitrite/trimethyl silyl azide and sodium nitrite/sodium azide. 71
Figure 31. Structures of ligands/probes tested for HDAC8 inhibition 74
Figure 32. Upside down binding pose proposed for HDAC inhibitors. 76
Figure 33. Proposed binding mode of probes **52**, **52a**, **52g** and **52h** in the HDAC8 binding site. 80
Figure 34. Photoaffinity labeling studies with the upside down probes with HDAC8. 84
Figure 35 Monitoring acetylation status of H4 and alpha tubulin in SH-SY5Y cells upon treatment with probe **52h** and ligand **73** 86
Figure 36. Benzamide inhibitors of HDAC1 and 2 89
Figure 37. Amine and acid precursors used for synthesis of photoreactive probes 94
Figure 38. Probe **75c** docked into the active site of (A) HDAC2, (B) HDAC3, and (C) HDAC8. 104
Figure 39.Overlay of compounds **8b** (green), **8c** (magenta), **8g** (cyan) and **75c** (gold) in the active site of HDAC2. 107
Figure 40. Western blot analysis of probes **52**, **53**, **54**, **8c**, **8d 8e**, **8f**, **75b**, **75c** and **8g** (25 μM) photocrosslinked to HDAC2 (1.25 μM) using streptavidin-HRP and nickel-HRP 109
Figure 41. Western blot analysis of diazide probes **8c**, **8d**, **8e**, **8f**, **75b**, **75c** and **8g** (25 μM) photocrosslinked to HDAC2 (1.25 μM) in the presence or absence of 125 μM of Trichostatin A using streptavidin-HRP and nickel-HRP 110
Figure 42. Western blot detection of acetyl H4 in MDA-MB-231 cell lines following a 24h treatment with various diazide and monoazide-based benzamide probes at 50 μM 111

LIST OF SCHEMES

Scheme 1. Possible routes for conversion of aryl amines into aryl azides..... 25
Scheme 2. Decomposition pathways of azides upon UV irradiation..... 27
Scheme 3. Decomposition pathways of trifluoromethyl diazirines upon UV irradiation..... 28
Scheme 4. Decomposition pathways of benzophenones, upon UV irradiation..... 29
Scheme 5. Synthesis of non ZCG ligands/probes..... 73
Scheme 6. Synthesis of diazide intermediates **77** and **92**..... 95
Scheme 7. Synthesis of mono-Boc protected phenylendiaamines..... 97
Scheme 8. Synthesis of diazide intermediate **78** and monoazide intermediates **84** and **79** 98
Scheme 9. Synthesis of monoazide and diazide-based benzamide probes..... 99

LIST OF ABBREVIATIONS

ABPP	Affinity-based protein profiling
ABPs	Activity-based probes
AMC	Aminomethyl coumarin
Asp	Aspartate
Ala	Alanine
Arg	Arginine
AD	Alzheimer's disease
AChe	Acetylcholinesterase
Aβ	Amyloid beta
BEProFL	Binding ensemble profiling with (f)photoaffinity labeling
BT	Biotin tag
bp	Base pairs
BSA	Bovine serum albumin
CoREST	Co-repressor for element-1-silencing transcription factor
CREB	cAMP response element binding protein
CBP	CREB binding protein
CDI	Carbonyl diimidazole
DNA	Deoxyribonucleic acid
DMSO	Dimethyl sulfoxide
DIPEA	Diisopropylethylamine
DMF	Dimethylformamide
DMAP	N,N-Dimethylaminopyridine
DBU	1,8-Diazabicyclo[5.4.0]undec-7-ene
ECL	Enhanced chemiluminescence

LIST OF ABBREVIATIONS (CONTINUED)

EDCI	1-Ethyl-3-(3-dimethylaminopropyl)carbodiimide
Fluor-de-Lys	Fluorescent deacetylation of lysine
FAHA	Furoylacryoyl hydroxamic acid
FPA	Fluorescence polarization assay
FRET	Fluorescence resonance energy transfer
Gly	Glycine
GAPDH	Glyceraldehyde 3-phosphate dehydrogenase
HATs	Histone acetyltransferases
HDACs	Histone deacetylases
HDLP	Histone deacetylase-like protein
HDAH	Histone interaction domain
His	Histidine
HRP	Horseradish peroxidase
HDLP	HDAC like protein
HOBt	Hydroxybenzotriazole
Leu	Leucine
LAH	Lithium aluminium hydride
LC-MS/MS	Liquid chromatography coupled with tandem mass spectrometry
MALDI	Matrix-assisted laser desorption ionization
MW	Molecular weight
MMP	Matrix metalloprotease
MBD3	Methyl-CpG binding protein
NAD^+	Nicotinamide adenine dinucleotide

LIST OF ABBREVIATIONS (CONTINUED)

NFkB	Nuclear factor kappa-light-chain-enhancer of activated B cells
NDA	Naphthalene 2,3-dicarbaldehyde
NCoR	Nuclear co-repressor
OPD	*o*-Phenylenediamine
PBS-T	Phosphate buffer saline, supplemented with 0.05% Tween-20
PAL	Photoaffinity labeling
PP1	Protein phosphatase 1
Phe	Phenylalanine
RNA	Ribonucleic acid
SAHA	Suberoylanilide hydroxamic acid
SAR	Structure-activity relationship
SBG	Surface binding group
Strep-HRP	Streptavidin-Horseradish Peroxidase
SPA	Scintillation proximity assay
TBTA	Tris((1-benzyl-1H-1,2,3-triazol-4-yl)methyl)amine
TCEP	Tris(2-carboxyethyl)phosphine
TFA	Trifluoroacetic acid
TEA	Triethylamine
TSA	Trichostatin A
THF	Tetrahydrofuran
TsCl	Tosyl chloride
TBST	tris-based saline, supplemented with 0.05% Tween 20
Tyr	Tyrosine

LIST OF ABBREVIATIONS (CONTINUED)

$TMSN_3$	Trimethylsilyl azide
ZCG	Zinc chelating group

SUMMARY

Histone deacetylases (HDACs) are well established epigenetic targets for multiple therapeutic applications. Histone deacetylases 2 (HDAC2) has been shown to be aberrantly recruited and expressed in diseases such as Alzheimer's disease, Duchene muscular dystrophy, consequently HDAC2 is considered as attractive target for these conditions. Recently, the role of histone deacetylase 8 (HDAC8) in cognitive disorders, leukemia and neuroblastoma has been elucidated. Potent and selective inhibitors of HDAC2 and HDAC8 may have therapeutic value not only in neurodegenerative diseases but also malignant conditions such as leukemia and neuroblastoma. Existing HDAC inhibitors typically bear a zinc chelating group (ZCG), as all of them target the substrate binding site/main catalytic site containing Zn^{2+}. The presence of the ZCGs is believed to be associated with a poor metabolic profile and a number of therapeutic liabilities in long term settings. Discovery of HDAC inhibitors lacking a ZCG would be a significant step towards wider application of HDAC inhibitors as small molecule therapeutics.

One of the key challenges impeding the development of HDAC ligands without ZCG is a poor understanding of binding modes of existing ligands in the HDAC binding site and lack of research tools to probe various histone deacetylase complexes in cells. To address this issue, we have established the Binding Ensemble Profiling with (F) photoaffinity labeling (BEProFL) approach, to map experimentally the multiple binding modes of inhibitors of histone deacetylase. This study is focused on the design, synthesis and biological evaluation of novel photoaffinity probes for histone deacetylase 2 and 8 suitable for BEProFL studies in cells.

In Chapter 1, a brief introduction to HDACs, particularly HDACs 2 and 8 and their roles in neurodegenerative conditions, muscular dystrophy is presented. A brief discussion on existing

HDAC inhibitors and the therapeutic liabilities associated with a zinc chelating group are delineated. A comparative discussion on the research strategies and tools required for target identification and mapping of multiple binding modes of ligands in target binding sites with particular emphasis on the BEProFL approach is presented. In this way, the significance, methodology and scope of our study were discussed.

In Chapter 2, a brief discussion on the types of in vitro assays to screen HDAC ligands is presented. The latter part deals with the optimization of fluorogenic assay to assess the potency of photoaffinity probes for HDAC2 is discussed. Particularly optimization of the concentrations of purified recombinant HDAC2, choice and concentrations of substrate Boc-Lys-(AMC) and the time for pre-incubation with potential inhibitors is discussed. Enzyme kinetic studies to determine K_m and V_{max} for the HDAC2 are also presented.

In Chapter 3, the design, synthesis, photoaffinity labeling studies, molecular modeling studies and biological evaluation of a series of HDAC8 inhibitors lacking a zinc chelating group is discussed. Photoaffinity labeling studies and molecular modeling studies indicated that these ligands bind in an “upside-down” fashion to a secondary binding site, proximal to the main catalytic site in HDAC8. The most potent ligand in the series exhibits and IC_{50} of 28 μM for HDAC8 and is found to inhibit the deacetylation of H4 but not α-tubulin in SH-SY5Y cell line.

In Chapter 4, the design, synthesis, molecular modeling studies and biological evaluation of a novel series of photoreactive benzamide probes for HDAC2 is presented. The probes are potent and selective towards HDAC1 and 2 and are efficient in crosslinking to HDAC2 as demonstrated by photoaffinity labeling experiments. The probes exhibit a time dependent inhibition of Class I HDACs and their inhibitory activities are influenced by the positioning of the aryl and alkyl

azido groups necessary for photocrosslinking and attachment of the biotin tag. The probes are shown to inhibit the deacetylation of H4 in MDA-MB-231 breast cancer cell lines indicating they are cell permeable and target nuclear HDACs and suitable for profiling HDAC2 related complexes in cells.

CHAPTER 1 BACKGROUND AND INTRODUCTION

1.1 Introduction

It has been recently discovered that malfunctioning of gene transcription machinery in our cells is linked to several disease conditions. Processes regulating of gene transcription without altering the DNA sequence are collectively termed as "epigenetic" processes. Evolutionary biologists have formed a consensus that environmental factors in the form of chemical stimuli may activate or repress a certain set of genes, that may aid in survival of a species, hence such modifications have been posited as one the crucial factors for the success of a species. [1, 2] Epigenetic modifications have been found to be at the heart of variety of bio chemical processes in humans that regulate cellular development. Deregulation of a variety of homeostatic proteins may be causative for a range of disease conditions such as cancer[3], neurodegenerative conditions.[4] Chemical probes that are capable of delineating the aberrant functioning of epigenetic modifiers may be critical in understanding the pathophysiology of a broad spectrum of diseases.

The purpose of this chapter is to introduce the reader to one such set of epigenetic modifiers, namely histone deacetylases (HDACs), their role in transcriptional regulation and how their inhibition may be used as a potential therapeutic strategy in variety of disease conditions. The latter part of the chapter deals with the therapeutic liabilities of existing HDAC inhibitors and strategies to identify novel targets and binding modes of photoaffinity probes for HDACs. Armed with the knowledge of the spatio-temporal positioning of ligands in the HDAC binding site, a rational drug design strategy can be

pursued to design novel ligands with an improved pharmacodynamic and pharmacokinetic profile.

1.2 Histone deacetylases

1.2.1 Chromatin, nucleosome and histones

Chromatin refers to a set of proteins and deoxyribonucleic acid (DNA) in the eukaryotic nucleus that condenses to form chromosomes.[5] The basic building block of chromatin is referred to as a nucleosome. A nucleosome is composed of a segment of DNA molecule 146 base pair (bp) long wrapped around a highly basic proteins known as histones.[6] The histone proteins form an octamer consisting of two copies of each core histone designated as H2A, H2B, H3 and H4. Linker histones designated as H1 and H5 are positioned near the entry and exit points of the DNA segments. DNA in its condensed formed wrapped around histone proteins (normally referred to as heterochromatin) is inaccessible for proteins that help in gene transcription such as RNA polymerases, transcription factors etc., upon chemical modifications of histones, particularly acetylation, DNA becomes less densely packed around histones(normally referred to as euchromatin) and consequently becomes more accessible to replication machinery.[7, 8] The proteins that mediate histone modifications are termed as "writers", proteins that recognize these modifications are termed as "readers" and proteins that remove such modifications are termed as "erasers".[9] In case of acetylation of histones, histone acetyltransferases[10] are considered as writers as they transfer acetyl groups to certain lysine residues on histones, bromodomains[11] are considered as readers as they recognize and bind to acetylated lysine

motifs and in turn promote recognition of a transcription complex and histone deacetylases[12] are considered as erasers as they remove acetyl groups on certain lysines on histones. A broad consensus has now emerged that understanding the molecular mechanisms by which readers, writers and erasers function may give insights into the biochemical pathways involved in cellular development

1.2.2 Histone deacetylases and transcriptional regulation

Histone deacetylases (HDACs) are a family of hydrolases that catalyze the removal acetyl groups from ε-N-acetyl lysine residues on histones. Besides histones, there are also other intercellular proteins that act as substrates for certain HDAC isoforms. Examples of non-histone substrates for HDACs are hormone receptors such as estrogen receptor alpha,[13] transcription factors such as MyoD,[14] chaperon proteins such as heatshock protein 90[15] and microtubular proteins such as alpha tubulin.[16]

Acetylation status of histones is determined by the dynamic equilibrium between histone acetyl transferases (HATs) and histone deacetylases (HDACs) catalyzed acetylation and deacetylation, respectively. Acetylation status of histones in turn controls magnitude of electrostatic interactions between histones and the negatively charged DNA molecule wrapped around histones.[17] The deacetylation of acetylated lysines in histones, results in augmentation of electrostatic interactions between negatively charged DNA molecule and protonated ε-amino group, in turn condensing the chromatin structure and vice-versa.[18] In general, histone hyperacetylation results in a “relaxed” chromatin structure and better

accessibility for transcription factors, whereas histone deacetylation promotes chromatin condensation and transcriptional repression (Figure 1).

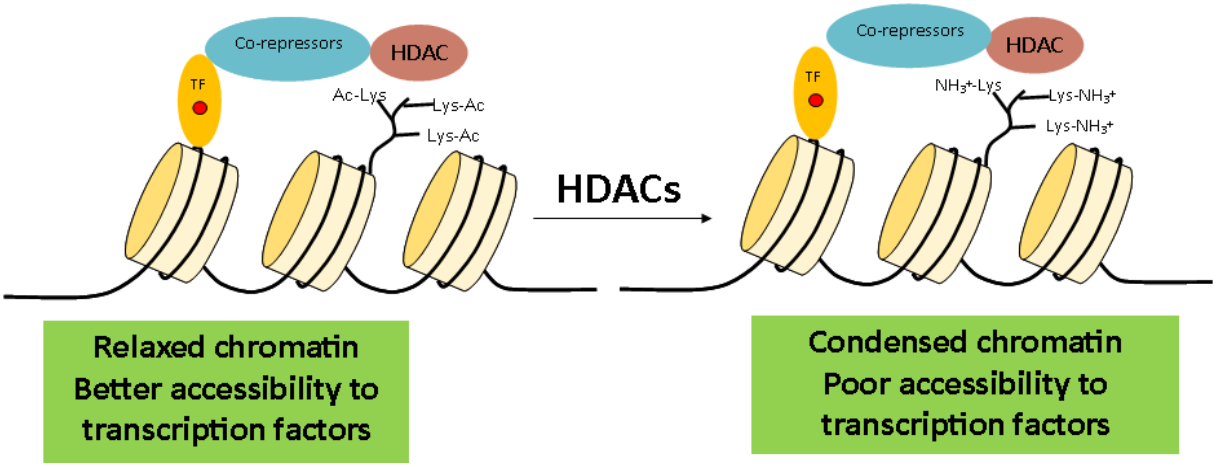

Figure 1. Transcriptional regulation modulated by the acetylation status of histones by histone deacetylases (HDACs) and histone acetyl transferases (HATs)

1.2.3 Classification of histone deacetylases

HDACs are grouped into four classes depending on sequence similarity to yeast homologs and deacetylase domain characterization. Class I HDACs (HDAC1, 2, 3 and 8) are Zn^{+2}- dependent metalloproteases that are localized in the nucleus. Class II HDACs (HDAC4, 5, 7, 9 and 10) are Zn^{+2} dependent metalloproteases that shuttle between the nucleus and the cytoplasm. Class III HDACs (Sirt 1-7) are nicotinamide dinucleotide (NAD^{+}) dependent proteases found in both the nucleus and cytoplasm. Class IV HDAC

(HDAC11) is a zinc dependent metalloprotease that contains conserved residues in the catalytic domain shared by both Class I and Class II HDACs and is mostly localized in the nucleus. Among the 18 known mammalian HDAC isoforms, only Class I HDACs are ubiquitous in all tissues, while distribution of other HDACs is restricted only to certain kinds of tissues. The focus of this dissertation is HDACs 2 and 8.

1.2.4 Mechanism of deacetylation mediated by zinc dependent histone deacetylases

Crystal structures of several zinc dependent histone deacetylases including HDAC1 (PDB: 4BKX[19]), HDAC2(PDB: 4LXZ,[20] 3MAX[21]), HDAC3(PDB: 4A69[22]) and HDAC8(PDB: 2V5W[23] amongst several others)have revealed certain commonalities in the HDAC catalytic site and deacetylase machinery involved. HDACs have catalytic core containing a zinc ion, exhibiting tetrahedral coordination to a of set conserved Asp-Asp-His-water residues/molecules.[24, 25] There are additional Asp/His residues referred to as "charge relay" systems that act as general acid/base catalysts during the catalytic cycle and site directed mutagenesis studies have indicated that at least one of the Asp/His residues in the "charge relay" system and a conserved Tyr residue are essential for catalytic activity.[26]

Figure 2 shows the mechanism of deacetylation mediated by zinc dependent histone deacetylases. The zinc ion in the active site acts as Lewis acid and aids in polarization of the carbonyl oxygen of the amide bond. One of the His residues in the Asp/His "charge relay" system acts as a general base and deprotonates a catalytic water molecule, promoting nucleophilic attack at the carbonyl carbon of the amide bond, leading to the

formation of a tetrahedral oxyanion intermediate. This oxyanion intermediate is stabilized by interactions with zinc ion and a conserved Tyr residue in the active site. A second protonated His residue then acts a general acid, protonating the amine leaving group, leading to the collapse of the tetrahedral intermediate.[27] The acetate ion that gets generated may exit through an "acetate release channel" as seen in case of HDAC8,[28] while the lysine residue which bears the free amine may get displaced by another acetylated lysine residue through a "feed-forward" mechanism as seen in case of deacetylation mediated by HDAC3-NCoR2 complex.[29]

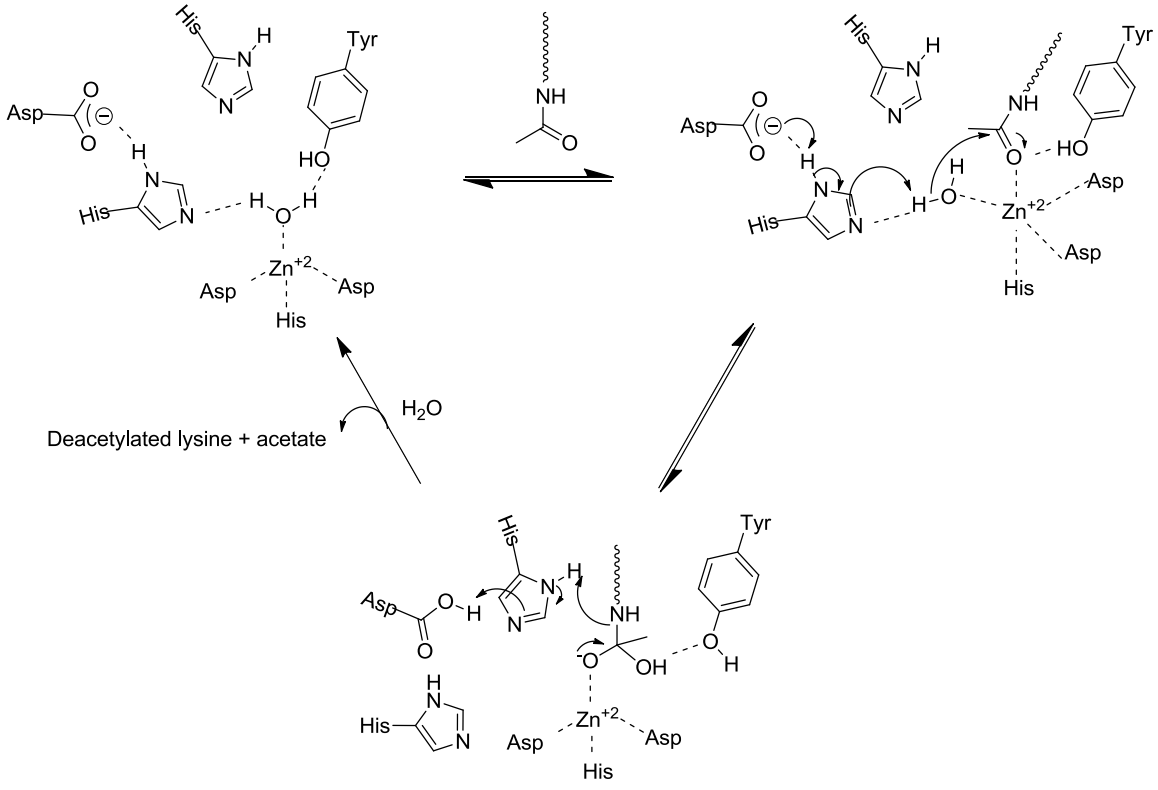

Figure 2. Mechanism of histone deacetylation in zinc dependent histone deacetylases.

1.2.5 Inhibitors of histone deacetylases

The design of existing HDAC inhibitors was inspired from the features of the active site of HDACs, namely a hydrophilic catalytic core containing a zinc ion and a hydrophobic channel connecting the catalytic core to the surface of the protein. Complementary to the above mentioned features, the most popular HDAC pharmacophore reported includes a ***surface binding group or cap group*** (that interacts with residues on the surface of the protein) a ***hydrophobic linker*** (that interacts with hydrophobic residues present between the catalytic core and the surface of protein) and a ***zinc chelating group***. Pan HDAC inhibitors such as Trichostatin A and suberoylanilidehydroxamic acid (SAHA) are typical examples of HDAC inhibitors that follow the above mentioned HDAC pharmacophore. Figure 3 shows the structures of Trichostatin A and SAHA.

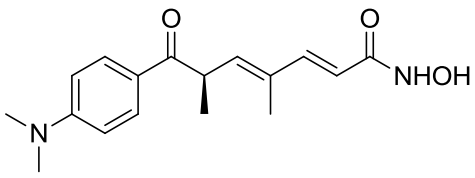

1, Trichostatin A(TSA)
Pan HDAC inhibitor with nM potency

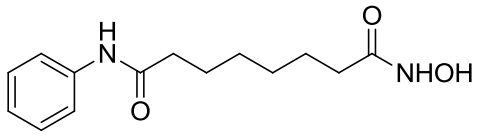

2, Suberoylanilide hydroxamic acid(SAHA)
Vorinostat-FDA approved
Pan HDAC inhibitor with nM potency

Figure 3. Structures of Trichostatin A and Suberoylanilide hydroxamic acid (SAHA)

Until recently, efforts have been mainly focused on the modulation of the HDAC pharmacophore to design isoform selective HDAC inhibitors.[30-32]

It has been reported that a cyclic peptidic moiety as a surface binding group can be used to achieve selectivity towards HDACs 1, 2 and 3 over HDAC6 and 8. Figure 5 shows some HDAC ligands with cyclic peptides as cap groups. A steric argument has been invoked for explaining the observed selectivity patterns of cyclic peptide-based HDAC ligands, comparison of the HDLP (Class I HDAC representative) and FB188 HDAH (a Class II representative) revealed that there are two loops near the entrance of the active site which prevent binding of the bulky peptidic cap groups on the surface of HDAH.[33] Natural products such as trapoxins, chlamydocin, azumamides and a recently FDA approved drug romidepsin[34, 35] and their analogs show nanomolar potency against Class I HDACs and 100-1000-fold selectivity towards HDACs 1, 2 and 3 vs. other HDAC isoforms. The number of amino acids and their stereochemistry in the cyclic peptide has been set as general criteria for classification of cyclic peptide HDAC inhibitors. Ligands such as apicidin have four α-amino acids, hence are grouped under α4 ligands. Azumamides on the other hand have three α-amino acids and one β amino acid and are grouped as α3β ligands. For apicidin, amino acid bearing the spacer or the hydrophobic linker is referred to as aa1. Figure 4 shows the general numbering of amino acids in the cyclic peptide surface binding group.

Extensive SAR studies by Ghadiri et al.[36, 37] using a combinatorial strategy with aa1 bearing an aliphatic linker with six methylene units and a carboxylic acid as a zinc

chelating group with variations at the aa2, aa3 and aa4 revealed the factors which influenced the potency and selectivity of a broad range of cyclic peptide HDAC ligands.

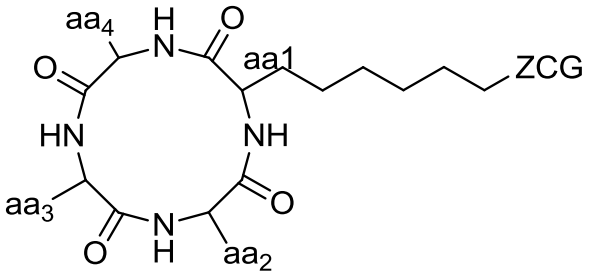

Figure 4. Numbering of amino acids in cyclic peptide surface binding group.

In general, aromatic residues at the aa2 position, amino acids with aliphatic chains at the aa3 position and basic residues such as arginine/lysine at the aa4 position were favored for Class I HDAC inhibition. Stereochemical inversion of amino acids apart from aa3 lead to decrease in activity, in fact the most potent analogs were α4 and α3β analogs with double digit nM activity against recombinant HDAC1, 3. Recently, peptidic ligands similar to apicidin without any linker or a possible zinc chelating group most likely binding at the entrance to the active site exhibit modest potency towards HDACs 1,2 and 3. Docking studies with HDLP[38], revealed that ligands with cyclic peptides from the azumamides series form important hydrophobic interactions and can be accommodated in

pockets delimited by Tyr 91, Tyr 264, Leu 265, Phe 338, Ala 197 residues at the entry of the active site.

Despite the structural diversity of cyclic peptide-based HDAC ligands, only romidepsin, a natural product obtained from bacterium *Chromobacterium violaceum* has been approved for treatment of cutaneous T-cell lymphoma due to their inherent limitations as peptide drugs prone to hydrolysis. Romidepsin, is a prodrug and is stable in the blood, once inside the cells the intramolecular disulphide bridge is reduced by glutathione[39] to generate the active thiol analog which potently inhibits HDACs.[35, 40]

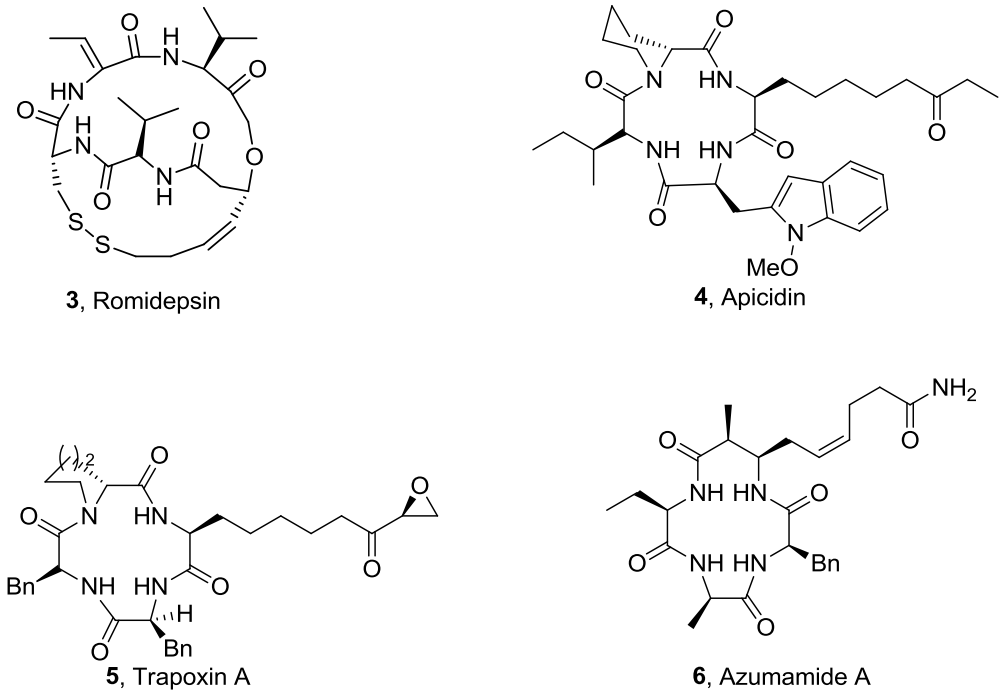

Figure 5. Examples of HDAC inhibitors with cyclic peptides as surface binding group.

Despite the success of the above mentioned cyclic peptide ligands, extensive efforts have been directed over the past few years in modifying the surface binding group by incorporation of small aryl/heteroaryl moieties in conjunction with aromatic linkers, to reduce synthetic efforts and/ or circumvent therapeutic liabilities presented by peptidic drugs.

HDAC ligands with spirocyclic nicotinamides or biaryl moieties in their cap group with an *o*-aminoanilide group as a zinc chelating group have been extensively studied as HDAC1 and 2 selective ligands with nM potency. [21, 41-43]

Figure **6** shows some examples of HDAC1& 2 selective inhibitors. Ligands bearing an *o*-aminoanilide (otherwise known as benzamide HDAC inhibitors) moiety as a zinc chelating group, exhibit time dependent inhibition of Class I HDACs.[21] The slow tight binding kinetics of benzamide ligands has been attributed to the gradual formation of bidentate chelate with the zinc ion and a possible induced fit effect, where a portion of the ligand binds to a secondary binding site. Recently phenylalanine and phenylglycine derivative **10** has been recently identified as potent ligand for HDAC1 with an IC_{50} of 10 nM and approximately 13-5000 selectivity towards HDAC1 vs. other HDAC isoforms.[44]

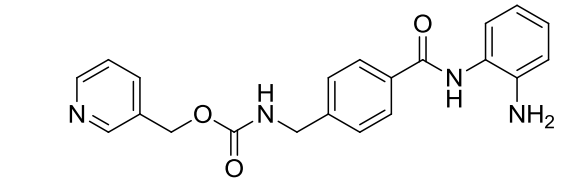

7, MS-275

HDAC1 and 2 selective ligand with nM potency

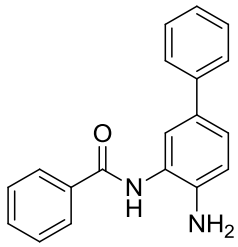

8, LLX

HDAC1 and 2 selective ligand with nM potency

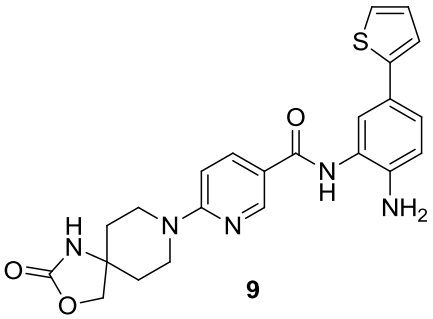

9

Spirocyclic nicontinamide-based HDAC1 and 2 selective ligand

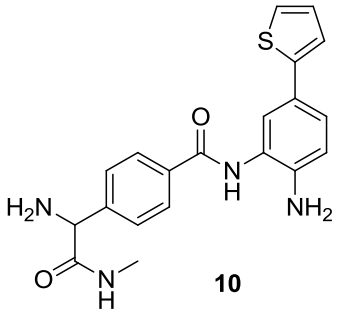

10

Phenylglycine-based selective HDAC1 inhibitor

Figure 6. Examples of benzamide-based HDAC1 and 2 selective inhibitors.

Pimelic diphenlamide ligand **11** is a benzamide-based ligand exhibits a slow tight binding to HDACs 1, 2 and 3 and is potent inhibitor of HDAC3 with K_i value of 14 nM and modest selectivity profile within Class I HDACs. Recently improvements on the pimelic diphenylamide structure using a click chemistry-based combinatorial approach in in the discovery of novel triazolyl-based benzamide ligands potent and selective for HDAC3.[45] Figure 7 shows some examples of HDAC3 selective ligands Benzamide derivatives T247 and T326 have an IC_{50} of 240 nM and 260 nM and are approximately 80 and 384-fold selective towards HDAC3 vs. HDAC1, 8 and HDAC6. Recently ligands with a chiral

heteroaryl containing cap group such as ligand **12** has also been shown to be potent and selective for HDAC3 with an IC_{50} of 12 nM and selectivity of 8-340-fold selectivity within Class I HDACs.[46] Incorporation of an isoxazole moiety in the surface binding group has resulted in success towards design of HDAC3 selective ligands such as **15** with low nM potency and modest selectivity towards HDAC3.[47, 48]

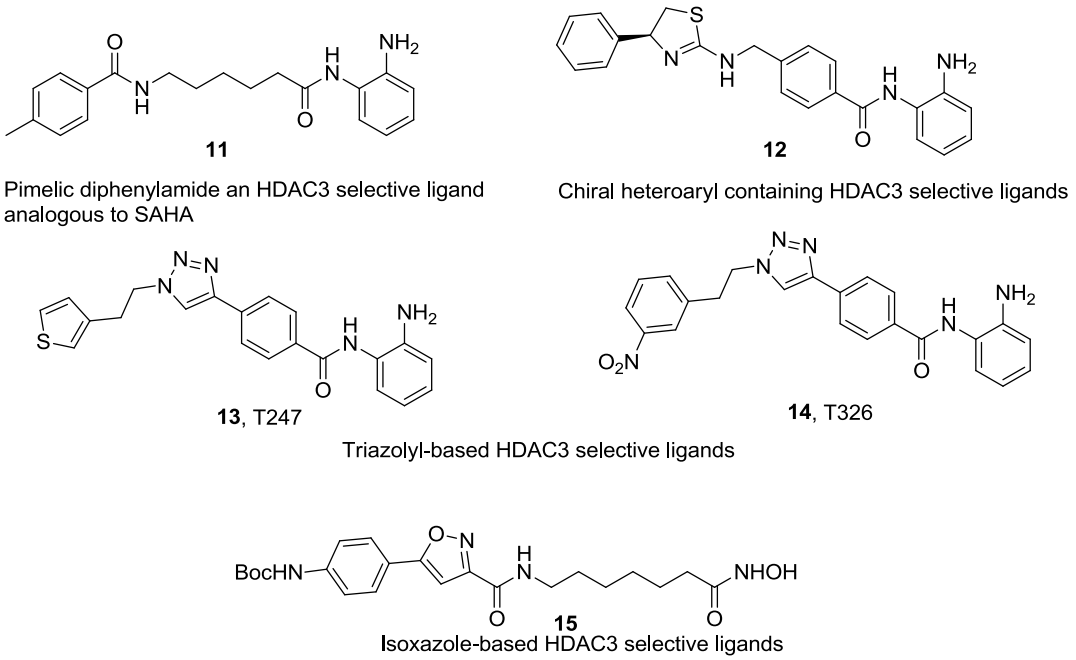

Figure 7. Examples of HDAC3 selective inhibitors

Ample structural data on HDAC8 co-crystallized with a variety of ligands have concluded that modulation of the length and the type of the hydrophobic linker in a ligand can be used to obtain HDAC 8 selectivity, particularly the use of short methylene chain or aryl/heteroaryl moieties in the linker region have been successful, such as in the case of linker-less hydroxamic acid, **17** shown in Figure 8[44, 49]

Another example is ligand **16**, otherwise known as PCI34051, an indole-based ligand with an IC_{50} of 10 nM for HDAC8 and over 100-fold selectivity for HDAC8 vs. other HDAC isoforms.[49] Recently, a combinatorial study using click chemistry has also been successful to discover novel triazole-based HDAC8 selective inhibitors such as **19**[50], shown in Figure 8. Ligand **19** has an IC_{50} of 70 nM for HDAC8 and over 100-fold selectivity for HDAC8 vs. other HDAC isoforms.

A recent high throughput screening campaign led to the discovery of an isoindole-based ligand, **18**[28] with an α-amino ketone motif as a zinc chelating group with an IC_{50} of 90 nM for HDAC8 and over 20-fold selectivity for HDAC8 vs. other HDAC isoforms. X-ray crystallographic studies have identified an internal cavity in HDAC8 where ligand **18** binds. The internal cavity is considered to be the acetate release channel in HDAC8, a tunnel through which an acetate ion is released after the HDAC catalytic cycle. Similar internal cavity has been found in a homologous protein HDLP by X-ray crystallography.

X-ray crystallographic studies have also identified distinct secondary binding sites, proximal to the main catalytic site as seen in the case of trichostatin A where one molecule binds to the primary binding site and another binds to a secondary binding site.[25] The main focus of this thesis is to design ligands that potentially bind to secondary binding sites in HDACs, with improved pharmacodynamic and pharmacokinetic properties.

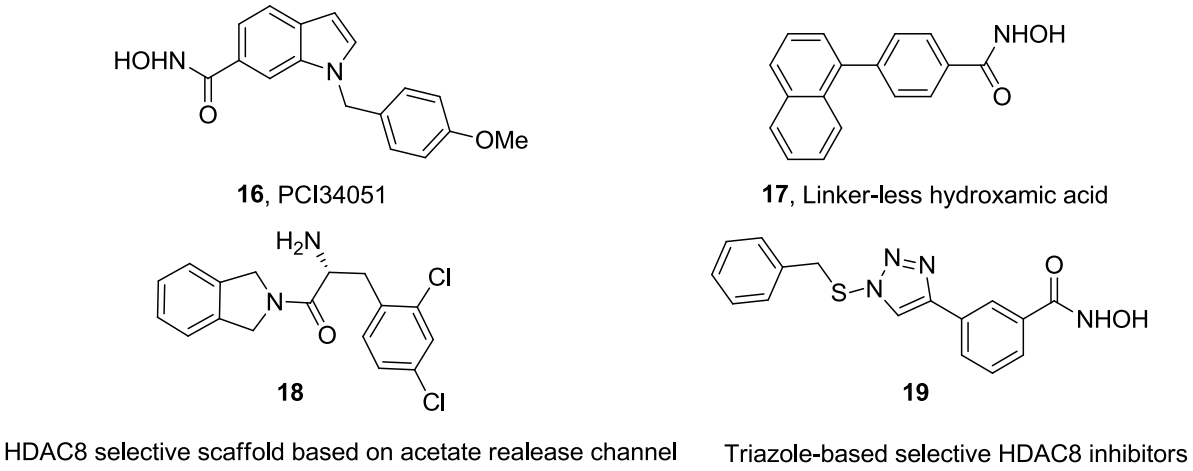

Figure 8. Examples of HDAC8 selective inhibitors.

The most common of the zinc chelating groups in the design of HDAC inhibitors is the hydroxamic acid which forms a bidentate chelate with the catalytic zinc atom, non-hydroxamate zinc chelating groups include carboxylic acids,[51] thiols,[52, 53] mercaptoacetamides, [54] ketones [55-57] etc. Variations of the zinc chelating group, such as azetidinones [58] have shown success in the discovery of HDAC8 selective ligands.

1.3 Research Significance

1.3.1 HDAC2 and 8 as potential targets in the multiple therapeutic applications.

In humans there are 18 histone deacetylase (HDAC) isoforms that are divided into four classes-based on structure, sequence homology, and domain organization.[59] Chemical inhibitors of HDAC have demonstrated promise in treatment of a broad spectrum of neurodegenerative diseases.[60] Neuronal tissues that degenerate in AD patients exhibit

increased oxidative damage, impaired energy metabolism, perturbed calcium homeostasis and show extracellular deposits of amyloid β peptide (Aβ).[61]

Recent reports have demonstrated the efficacy of HDAC inhibitors to reverse contextual memory deficits, modulate long term memory for object recognition and restore cognition in various AD mice models.[62-64] In fact, Tsai et al. have demonstrated that exposure to HDAC inhibitors in transgenic mice models, leads to sprouting of dendrites, increase in number of synapses and reinstatement of learning behavior and access to long term memories. The major role of HDACs is to induce chromatin remodeling and directly influence the transcription of genes. Some of these genes have been found to be associated with modulation of memory and learning behavior.[65] For example, overexpression of HDAC2 in neurons has been implicated in decreasing synaptic plasticity, synaptogenesis and inactivation of the CREB-CBP pathway. [66, 67] Further, co-repressor CoREST may have a key role in repressing neuronal gene expression by recruitment of other proteins to the chromosome interval. It is known that HDAC2 preferentially interacts with CoREST for its functioning; [68, 69] and interactions between HDAC2 and CoREST modulate the expression of neuronal genes. Experimental studies also report that S-nitrosylation of HDAC2 induces chromatin remodeling and activates genes associated with neuronal development particularly the expression of EGR1/c-FOS.[70] Another report suggests that HDAC2 inhibition leads to increased acetylation of RelA (p65) subunit of the transcription factor nuclear actor-kappa B(NF-kB).[71] NF-kB is known to preferentially interact with HDAC2 and negatively regulate gene expression,[72]

thus it has been proposed that enhancement of acetylation of RelA leads to increased NF-kB DNA binding activity which in turn would lead to augmentation in memory.[73]

HDAC2 knockout mice exhibited an increase freezing behavior in context dependent and tone dependent fear conditioning models and had enhanced spatial memory working memory in the T-maze non-matching-to-place task. These experimental data indicate that inhibition of HDAC2 is an attractive therapeutic avenue for neurodegenerative diseases associated with learning and memory impairment, and opens up the possibilities of recovery of long-term memories in patients with dementia.

Recent literature reveals that HDAC8-protein phosphatase1 (PP1) complex can repress CREB mediated transcription of genes important for neuronal survival and development, by dephosphorylating phospho-CREB (pCREB).[74, 75] Thus, one can hypothesize that selective modulators of the HDAC8-PP1 complex can prove to be valuable tools for understanding epigenetic pathways/events besides those mediated by HDAC2 in neuronal development.

Recently, it has also been reported that deletion of HDAC3 in the hippocampus or the hippocampal delivery of a HDAC3 inhibitor RGFP136 [N-(6-(2-amino-4-fluorophenylamino)-6-oxohexyl)-4-methylbenzamide] was shown to increase long term memory formation in mice models.[76] The study does not include a comprehensive HDAC inhibition profile for the ligands in question and only hints at modest selectivity of 3-6-fold for HDAC3 vs. HDAC1 using *in vitro* fluorogenic assays. The inhibition of HDAC2 cannot be ruled out as it is known from previous SAR studies that benzamide-based ligands may exhibit a time dependent inhibition of HDAC2.[21]

Recently, epigenetic modifications by histone deacetylases (HDACs) were suggested to play a role in muscle development.[77] Overexpression of HDAC2 was implicated in loss of fusion and differentiation of satellite cells derived from Mdx mice.[78] Experimental studies using HDAC1 and HDAC2 selective inhibitor MS-275 and HDAC2 siRNA suggest that inactivation of transcriptional factors such as MyoD (which binds to follistatin promoter) by deacetylation of HDAC1 and 2[79] leads to repression of a gene encoding Follistatin, a myostatin antagonist. Follistatin is known to bind to the C-terminal dimer of myostatin preventing myostatin from binding to activin type (II) receptor[80]. The latter inhibits a cascade of biochemical events that control fusion and differentiation of satellite cells to form myotubes.[81-83]

HDAC8 is overexpressed in neuroblastoma cell lines, and its inhibition resulted in decreased cell proliferation, suggesting that targeting HDAC8 should be useful in development of novel small molecules therapeutics against neuroblastoma.[84, 85]

These observations further merit the need to design of novel probes to dissect the interplay of individual HDAC isoforms to gain better insights into the design of novel chemotherapeutics.

1.3.2 Therapeutic liabilities of existing HDAC inhibitors present a barrier in their use as therapeutics for long term applications.

It was observed in Phase I and II studies of current pan HDAC inhibitors that non selective HDAC inhibition leads to numerous side effects such as bone marrow depression, diarrhea, weight loss, taste disturbances, electrolyte changes, disordered

clotting, fatigue and cardiac arrhythmia. These side effects of pan inhibition do not come as a surprise as HDACs are key regulators of chromatin structure and post-translational modifiers of numerous important proteins in cells.[86] The pharmacophoric elements possessed by most of the pan HDAC inhibitors as discussed earlier are surface binding group (SBG), a linker, and a zinc chelating group (ZCG). It has been proposed that a ZCG group is absolutely essential to maintain activity as it chelates to the zinc atom and hampers the fundamental catalytic mechanism of deacetylation.

The most commonly used zinc binding group in design of HDAC inhibitors is the hydroxamate group which shows poor metabolic stability *in vivo* and is rapidly hydrolyzed to carboxylic acid a poor zinc chelating group and hydroxylamine that exhibits mutagenic properties.[87] In addition, hydroxamates are poorly absorbed *in vivo* and show extensive glucuronidation and sulfation.[88, 89] It has also been reported that vorinostat has a half-life of 21-58 min[90] in patients and Trichostatin A (TSA) exhibits no antitumor activity in nude mice bearing xenograft models of human melanoma cells as a consequence of metabolic inactivation.[91] Non-hydroxamate ZCG's include groups such as carboxylic acids (sodium valproate), epoxy ketones(trapoxin), o-amino anilides (MS 275), electrophilic ketones, thiols, N-formyl hydroxylamines, mercaptomides, sulfones and phosphones.[92, 93] Problems associated with these ZCG's are a) carboxylic acids which are less potent than hydroxamic acid derivatives and inhibits HDACs at µM concentration,[94] b) epoxy ketones irreversibly inhibit HDACs and other enzymes by reacting with active site nucleophiles,[92] c) *o*-amino anilides such as MS 275 show modest selectivity towards HDAC but are not as potent as other hydroxamic acids derivatives,

exhibit poor aqueous solubility and short half-lives due to hydrolysis[95] d)trifluoromethyl ketones are rapidly hydrolyzed to inactive alcohols *in vivo* and have poor aqueous solubility,[96] e) thiols mediate redox cycling reactions in cells, leading to generation of free radicals. The very presence of a zinc chelating group is typically associated with inhibition of cellular matrix metalloproteases and generally considered teratogenic.[97] ***Clearly, there is an urgent need to find potent and selective inhibitors of histone deacetylases which do not bear a zinc chelating group.***

1.3.3 Exploring secondary binding sites in HDACs for design of ligands lacking a zinc chelating group.

Targeting secondary binding sites in protein targets has always been an interesting approach to expand the chemical space with an improved pharmacological profile. In fact the very same approach has been used for the design of peptidic inhibitors of matrix metalloproteinases (MMP) MMP2 and MMP9 that do not bear conventional zinc chelating groups.[98] The ligands reported in the study exhibited a modest potency in the μM range and high selectivity (greater than 100-fold for the MMP 2 and 9 over other MMPs) however were unstable *in vivo* due to their peptidic nature.

Recently, we published BEProFL approach that was used to map experimentally the multiple binding poses of the SBGs of HDAC ligands. In this paper we noted that some of the covalent modifications of HDAC8 may correspond to an *upside-down pose* of the probe that would be strikingly similar to that found for one of the two molecules of TSA co-crystallized with HDAC8 (PDB:1T64).[25] Our preliminary molecular modeling studies

revealed that the secondary binding site of HDAC8 has two relatively large sub pockets, providing a room for further modifications of the ligands. Accessibility and the shape of the proximal secondary site appear to be dependent on the scaffold of the HDAC inhibitors. In the X-ray of HDAC8 co-crystallized with one of the linker-less inhibitors (PDB: 1VKG) both sites are almost merged in one large site making the secondary site an excellent candidate for drug discovery efforts. Several molecular dynamics studies,[99, 100] demonstrated that the second binding site can be occupied by the SBG of the HDAC8 ligands.

Based on overall relatively high homology within HDAC isoforms it is quite possible that a similar proximal secondary binding site is available in other class I and II HDAC isoforms. The sequence identity for the area corresponding to the proximal site ranges from 100% for HDAC1 and HDAC2, to 78% between HDAC2 and HDAC3, to 32% between HDAC2 and HDAC8, and 46% between HDAC3 and HDAC8. Despite the homology between the isoforms the expected differences even in the shape of the putative second binding sites of the homology models of HDAC1 and X-ray of HDACs 2, 3 and 8 (class I) are markedly pronounced.[101] A co-crystallization of HDAC2 with N-(2-aminophenyl) benzamide ligand shows that a relatively large cavity proximal to the main catalytic site can accommodate chemical moieties as large as substituted biaryls.[21,102] *These observations merit further efforts to identify ligands that bind to the secondary site of HDAC2 and 8.*

1.3.4. Barriers in the pursuit of structure-based drug design of novel HDAC ligands

Rational drug design in case of histone deacetylases remains a challenge .due to various reasons, the major ones being absence/limited crystal structures of all the isoforms, the malleability of the protein surface leading to uncertainty of the binding poses adopted by the ligands in the solvent exposed binding site[101, 103] and the presence of an additional copy of the HDAC protein in majority of crystal structures. The latter not only shields the bound ligand from the solvent but also directly affects the binding of the ligand. Thus, it is essential that rational design of any isoform selective inhibitors be based on the knowledge of the binding poses adopted by various ligands in the enzyme. Affinity-based protein profiling has emerged as an important technique to not only map the binding sites of the target in question but also to interrogate protein-protein interactions and identify novel targets for ligands of interest.

The following sections extensively dwell on various aspects of affinity-based protein profiling using photoaffinity probes.

1.4 Affinity-based protein profiling

1.4.1 General principles of affinity-based protein profiling

Affinity-based protein profiling as the name suggests is a technique to study protein targets using high affinity probes bearing a reactive group and reporter tag or a ligation handle to attach a reporter tag. The binding of the probe to the target is achieved by using a target recognition fragment- a series of groups/moieties in the ligand, that help form non-covalent interactions with the target, once the probe binds to a given protein target,

the probe-target complex is either irradiated with UV light or the reactive group modifies the protein to form a probe-target adduct. Since, some of the reporter tags hinder the binding of the probe to the target or reduce cell permeability, an alternative two step approach has gained popularity these days, where by the probe-target adduct bears a ligation handle which can be used to attach a reporter tag using a bioorthogonal reaction for further purification and/or visualization in gels. Figure 9 shows a schematic explaining the general principles of two step approach in affinity-based protein profiling using photoreactive groups.

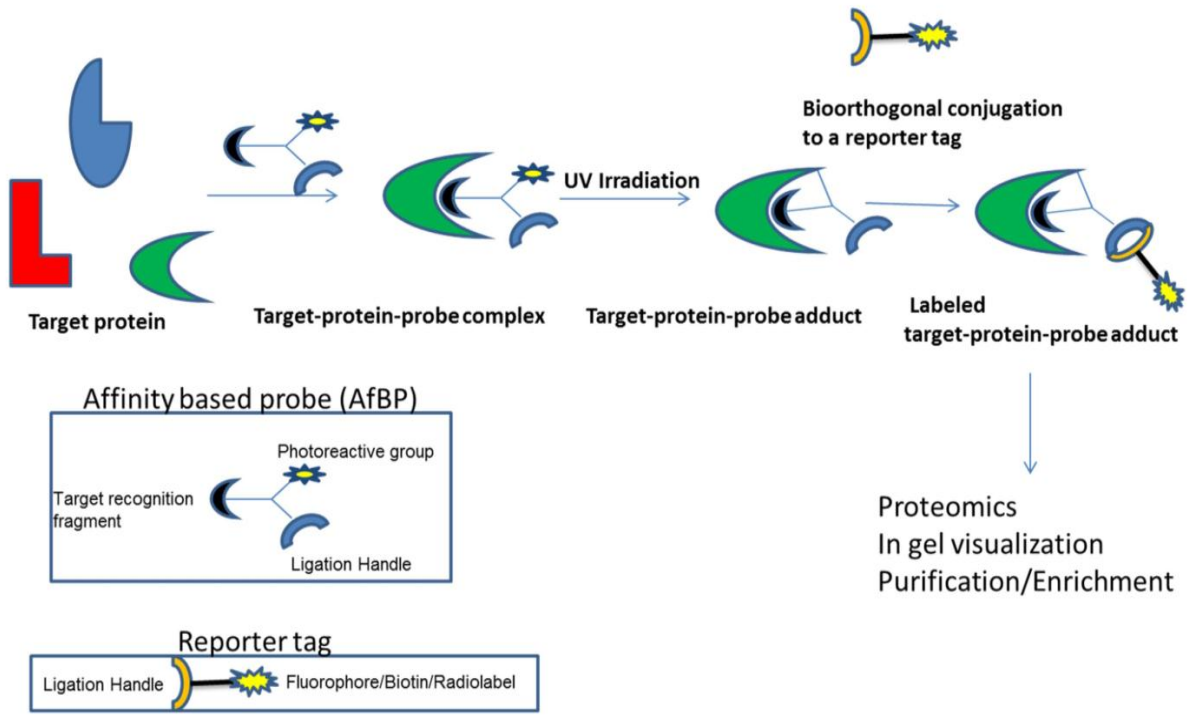

Figure 9. General schematic of affinity-based protein profiling using photoreactive ligands.

1.4.2 Types of photoreactive groups used for photoaffinity labeling.

One of the first photoreactive groups reported for photoaffinity labeling was the diazoacetyl group used to label chymotrypsin by Westheimer et.al[104] in 1962. Since then considerable progress has been made in the area of photoaffinity labeling with the advent of novel photoreactive groups. Aryl azides[105] (first reported in 1969), benzophenones[106] (first reported in 1973) and diazirines[107] (first reported in 1973) are widely used in photoaffinity labeling studies due to the following reasons.

1. Relatively stable to the conditions the biological sample is exposed to especially heat and reducing conditions.
2. Activated by a specific wavelength that does minimal damage to the biological system, else generate reactive species in short irradiation times.
3. Reactive species generated upon UV irradiation have smaller lifetimes, comparable to the lifetime of the probe-target complex, hence ideal for capturing of structural snapshots of ligand binding.
4. Reactive species are able to insert into a variety of chemical bonds, including unreactive ones such as C-H bonds.
5. Relatively small moieties, which do not affect the ligand binding to the target, if the spatial positioning is appropriate.
6. Synthetic accessibility in few steps.

Aryl azides are extensively used as photoreactive group in PAL studies due to the ease of synthesis, easy incorporation into the structure of a ligand without perturbing the overall size of the molecule, short irradiation times, ability to insert into even unactivated

chemical bonds and a short lifespan of the reactive nitrene ($\approx 10^{-4}$s).[108, 109] Several methods are reported to synthesize aryl azides, the most common one being diazotization-azidation of aryl amines with sodium nitrite, mineral acid and sodium azide.[110] Alternatively milder methods which do not employ harsh acidic conditions have also been reported such as diazotization with *t*-butyl nitrite/ amyl nitrite and trimethylsilyl azide[111] or the use of trifyl azide[112] or imidazole-1-sulfonyl azide[113] in presence of a base to form azides in moderate to high yields. Scheme 1 shows some of the routes for synthesis of aryl azides.

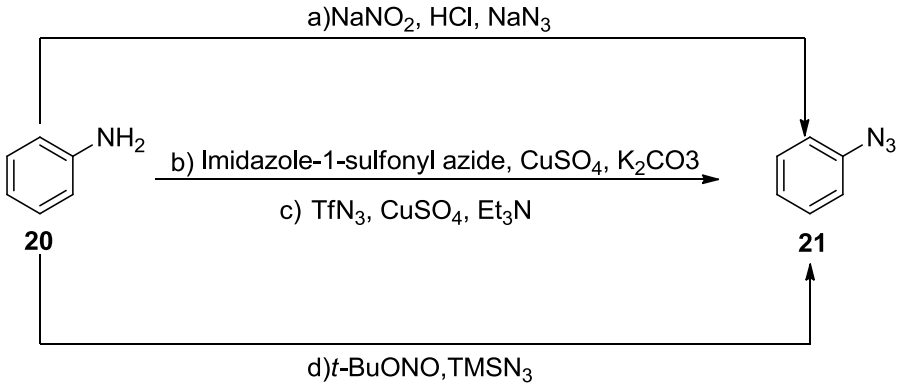

Scheme 1. Possible routes for conversion of aryl amines into aryl azides.
a) diazotization with sodium nitrite, mineral acid and sodium azide, b) with imidazole-1-sulfonylazide, c) with trifyl azide, d) diazotization with *t*-butyl nitrite and trimethylsilylazide.

Upon irradiation by UV light, azides release molecular nitrogen and form highly electrophilic and unstable singlet nitrenes **22** that quickly insert into a chemical bond or alternatively transform into stable triplet nitrenes **23** that exhibit a diradical character. Triplet nitrenes abstract H atoms from C-H bonds to form intermediate **24** which then react with corresponding C- centered radicals to form amines **25**. An alternate pathway of decomposition of singlet nitrenes is the formation of a benzazirine **26** which may react with nucleophilic amino acids in the target to form **27** or rearrange into a dehydroazepine **28** that may also react with nucleophilic amino acids in the target to form **29** It has been reported that perfluorinated azides exhibit a slow conversion to benzazirines/ dehydroazepines.[114]

Despite the above mentioned attractive features, aryl azides do suffer from some drawbacks, irradiation wavelengths are below 300 nm, which may damage biological systems, are susceptible to reduction by thiols,[115] triplet nitrenes susceptible to oxidation to form nitro derivative **30** [116] Scheme 2 shows the possible decomposition pathways of aryl azides upon activation by UV light.

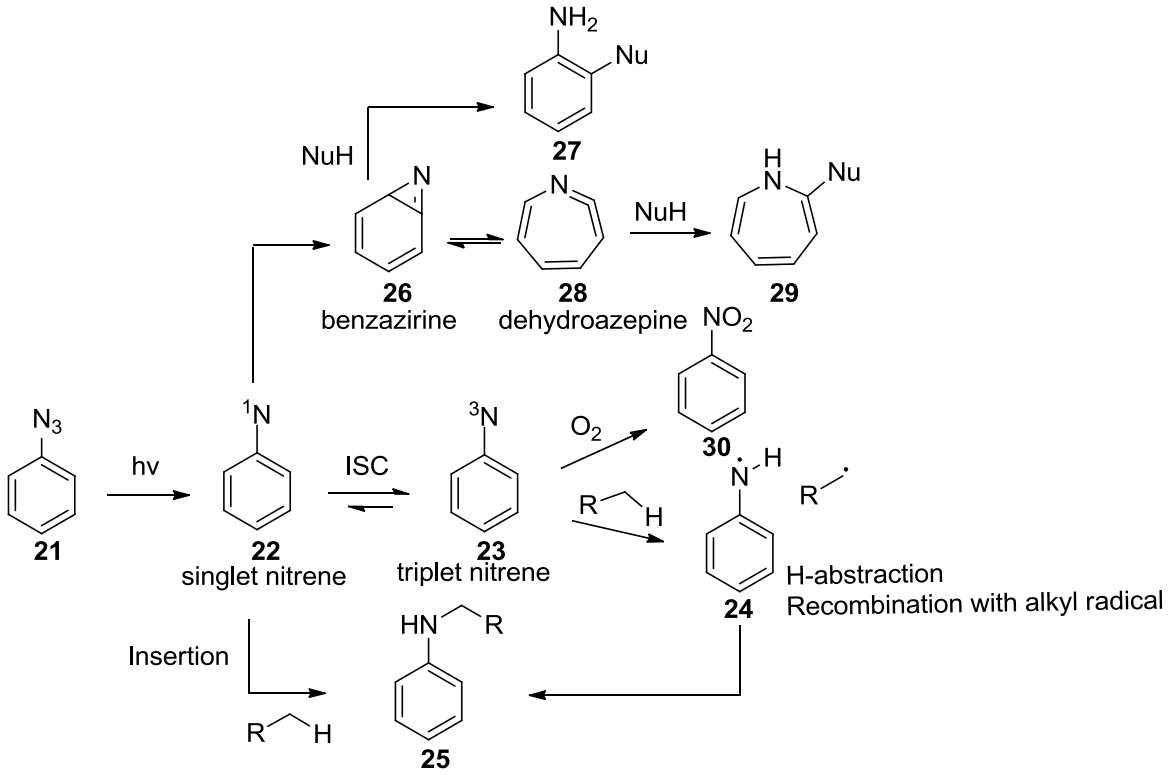

Scheme 2. Decomposition pathways of azides, upon UV irradiation.

Diazirines is another popular group used in PAL studies. Aryl diazirines are activated at 350-380 nm wavelength hence no significant damage to biological systems is observed, however irradiation if often carried out for longer times to get sufficient photocrosslinking. Binding of probes to the targets is often unperturbed due to the small size. Once activated, diazirine **31** forms singlet carbine **33** which gets converted into triplet carbene **34** by intersystem crossing. Singlet and triplet carbenes are similar to singlet and triplet nitrenes in reactivity. A singlet carbene inserts into C-H as well O-H and N-H bonds to form adducts **37**, **38** and **39** respectively, while a triplet carbene abstracts H atom from C-H bonds to form intermediate **36** and later combines with C-

centered radicals to form adduct **37**. Another possible decomposition pathway of diazirines is the formation of a diazo isomer **32** which slowly converts into a singlet carbene, substitution with a trifluoromethyl group, in case of 3-aryl-3-(trifluoromethyl) diazirines is known to retard the isomerization process.[117] Triplet carbene can get oxidized to ketone by molecular oxygen to form trifluormethyl ketone such as **35**.[118] Substituted aryl diazirines are in general more cumbersome to synthesize as compared to aryl azides. Scheme 3 below shows the decomposition pathways of aryl diazirines, upon UV irradiation.

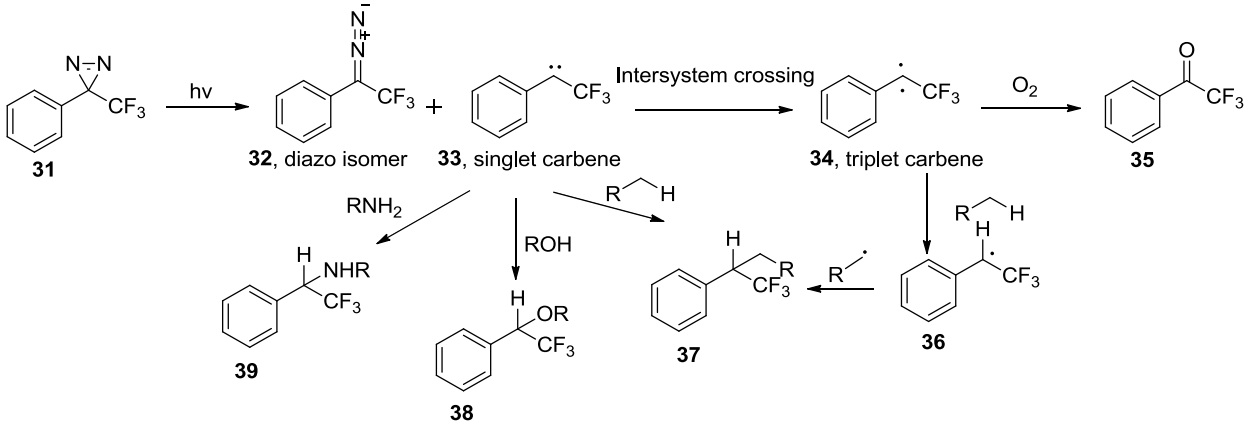

Scheme 3. Decomposition pathways of trifluoromethyl diazirines, upon UV irradiation.

Yet another popular option of photoreactive group are substituted benzophenones which are also activated at wavelengths of 350-380 nm, however require extended period of irradiation at lower temperatures for photocrosslinking to the target. Upon activation of

benzophenone **40**, a triplet benzhydril diradical **41** is formed which abstracts H atom from C-H, N-H or O-H bonds to form a ketyl intermediate **42** which subsequently reacts with the C-centered/ N-centered or O-centered radical to form a benzyhydrol **43**. Alternatively the ketyl intermediate can undergo an intermolecular reaction with another ketyl molecule to form a benzopinacol **44**.[119] Scheme 4 shows the decomposition pathways of benzophenones, upon UV irradiation.

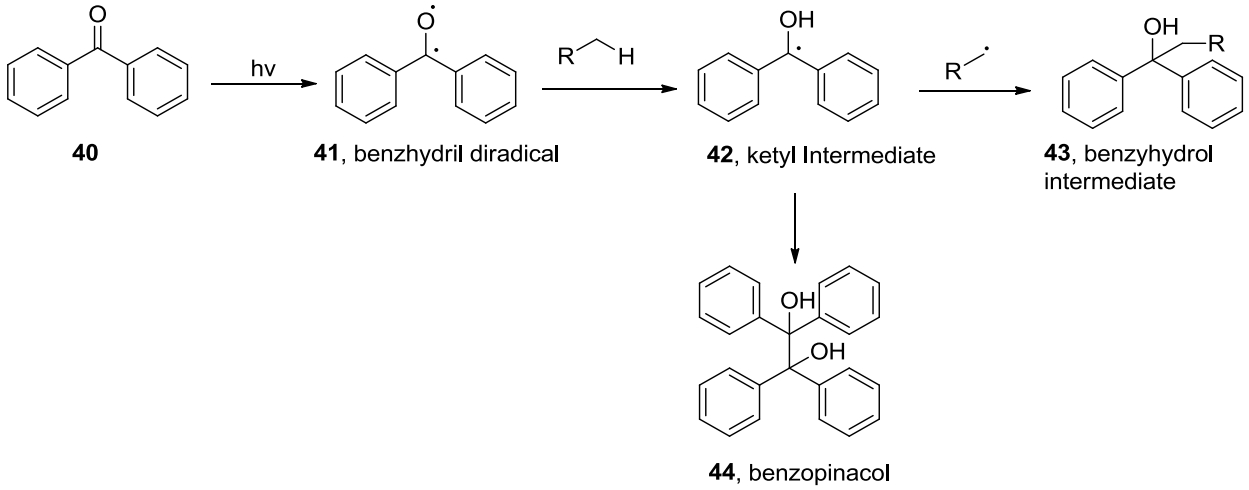

Scheme 4. Decomposition pathways of benzophenones, upon UV irradiation.

One of the major disadvantages of benzophenones is the bulky nature of the group; hence their incorporation into probes leads to a dramatic change in binding affinity of the probe to the target.[120]

1.4.3. Types of reporter tags used for visualization and purification

A reporter tag consists of three essential components, a ligation handle that can be used to react with a probe-protein adduct, a moiety that can help produce a signal proportionate to the number of target molecules tagged and a spacer that separates the ligation handle and the signal producing moiety. Any ligation handle should be small so as to make the reporter tag cell permeable, should be able to react in a bioorthogonal fashion with the probe-target adduct in high yields, in short times.

The most popular ligation handle is an azide or alkyne which can be used to react with an alkyne or azide bearing probe-target adduct using the Huisgen (3+2) cycloaddition reaction or "click chemistry".[121] In general, azides are preferred over alkynes, as alkyne containing tags are known to produce a low non-specific background through reactions with nucleophilic amino acid residues.[122, 123] Azides are also suitable in case one wants to use Staudinger Ligation reaction with activated phosphines.[124] Recently several other ligation handles have been reported including, nitrones,[125] nitrile oxides,[126] alkenes.[127] The chemistry pertaining to the above mentioned handles will not be discussed at length in this thesis; however a brief overview is given in the section of bioorthogonal chemical reactions.

The most commonly used spacers in the design of reporter tags are hydrophilic polyethylene glycol linkers that improve solubility in water and facilitate the bioorthogonal reaction in aqueous biological systems.

There are several moieties that can produce a signal to enable detection of a tagged target molecule. One of the most popular options is the use of a biotin that can be subsequently

recognized by streptavidin/avidin antibodies linked to horse radish peroxidase (HRP) or other fluorophores and sensed by a chemiluminescent or a fluorescence-based detection system respectively. The use of biotin is also advantageous from the point of view of purification/enrichment through commonly used streptavidin/avidin beads which separate biotinylated proteins of interest from other proteins.[128] Alternatively, fluorescent or fluorogenic moieties linked to azides/alkynes are also popular choices for laser confocal microscopy or in-gel fluorescence techniques. Commonly used fluorophores are Alexa dyes[129] which are stable to biological conditions, have high quantum yields and are cell permeable. Other less commonly used moieties include FLAG tag,[130] His tag[131] or HA tag[132] that can be suitable modified to incorporate a ligation handle.

1.4.4 Types of bioorthogonal reactions used to ligate reporter tags with probe-protein adducts.

A bioorthogonal reaction is one that can occur in biological systems without interfering with their function. An ideal bioorthogonal reaction should have the following properties

1. It should be selective only to the ligation handles placed in the reporter tag and the probe-protein adduct.
2. Ligation handles should be chemically inert to intracellular electrophiles and nucleophiles and be should not be metabolized quickly.
3. The reaction should be fast, high yielding and utilize conditions that are non-toxic to cells and the reaction products be stable to biological environment.

Several bioorthogonal reactions have come to forefront in the area of chemical biology but 1,3 dipolar cycloaddition between azides and alkynes, popularly known as “Click Chemistry” has been far the most cited and utilized reaction. First reported by Huisgen more than four decades ago,[133] the reaction required heating to yield regioisomeric triazoles in modest yields. Pioneering efforts by Sharpless, Meldal and co-workers resulted in a Cu (I) catalyzed reaction that yielded the 1,4 regioisomer in high yields.[134, 135]

Figure 10 shows the mechanism of 1,3 dipolar cycloaddition between azides and alkynes in presence of Cu(I) catalyst.

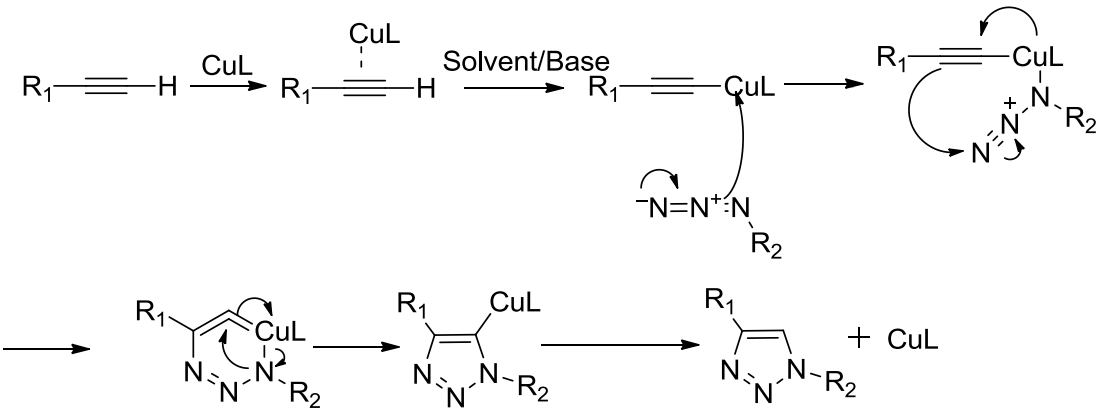

Figure 10. Mechanism of Huisgen (3+2) cycloaddition between terminal alkynes and azides.

Azides and alkynes are not present in biological systems, hence are ideal ligation handles to work with and their synthesis is fairly straightforward. Despite the popularity of the Click chemistry reaction, the use of copper may have cytotoxic effects in cells.[136] To circumvent copper induced cytotoxicity, Bertozzi and coworkers developed strained alkynes[127, 137] that do not require copper catalysis for reaction and react rapidly in aqueous conditions. However, the major hurdle in this approach is the synthetic accessibility of the strained alkynes and possible side reactions with intracellular thiols.[123] Another popular approach used by many researchers is the Staudinger ligation discovered by Bertozzi and co-workers. The reaction employs an azide-phosphine pair, which reacts to form an aza-ylide intermediate which can be subsequently trapped by an electrophilic carbonyl group which upon hydrolysis forms an amide bond.[138] Figure 11 shows the mechanism of Staudinger ligation.

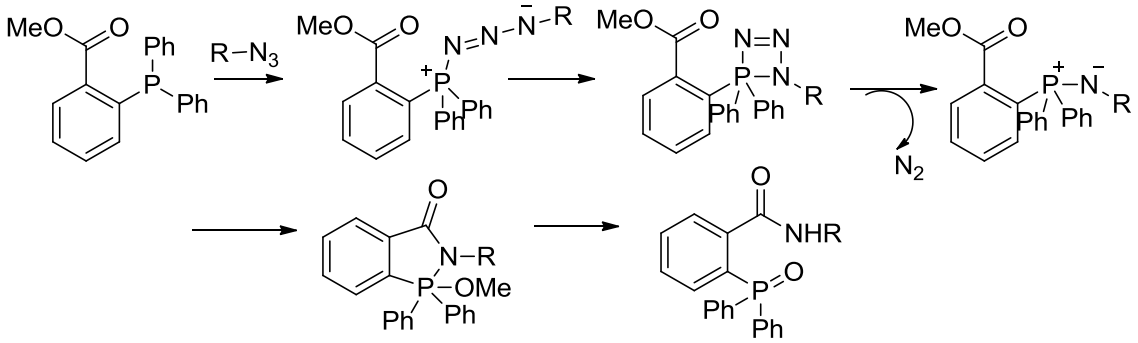

Figure 11. Mechanism of Staudinger ligation.

Though widely used, Staudinger ligation suffers from its own share of drawbacks, including susceptibility of phosphines to oxidation and inferior reaction kinetics as compared to click reactions.[139]

1.4.5 Clickable benzophenone-based probes for profiling HDACs.

Recently Cravatt et.al[140] and Gottesfield et.al[141] have designed benzophenone-based probes for profiling HDACs in proteomes from different cell lines. Probes **45**[120], otherwise known as SAHA-BPyne (Figure 12) is based on the scaffold of a pan HDAC inhibitor SAHA (suberoylanilide hydoxamic acid) and is capable of crosslinking to HDAC1 and 2 in cell lysates from breast cancer and HDAC6 in melanoma cell lines respectively, and was also able to identify potential HDAC binding partners such as CoREST and MBD3. Amongst other benzophenone-based probes shown in Figure 12, SAHA-BPyne was the only probe capable of profiling HDACs in live cells and helped in confirming the lowering of HDAC1 expression levels in cancer cells treated with parthenolide.[140] Despite the success of SAHA-BPyne in photolabeling HDACs, similar attempts to make benzophenone probes based on HDAC1 and 2 selective benzamide scaffolds resulted in probes **49** and **50** with HDAC potency above 180 μM and diminished photocrosslinking ability. The authors attributed this observation to the size and the positioning of the benzophenone group on the probe. Probe **47**[141], slow-tight binding inhibitor of Class I HDACs was able to identify HDAC3 as a unique target in cell lysates from human lymphoblasts and elucidate the role of HDAC3 in Freidrich Ataxia.

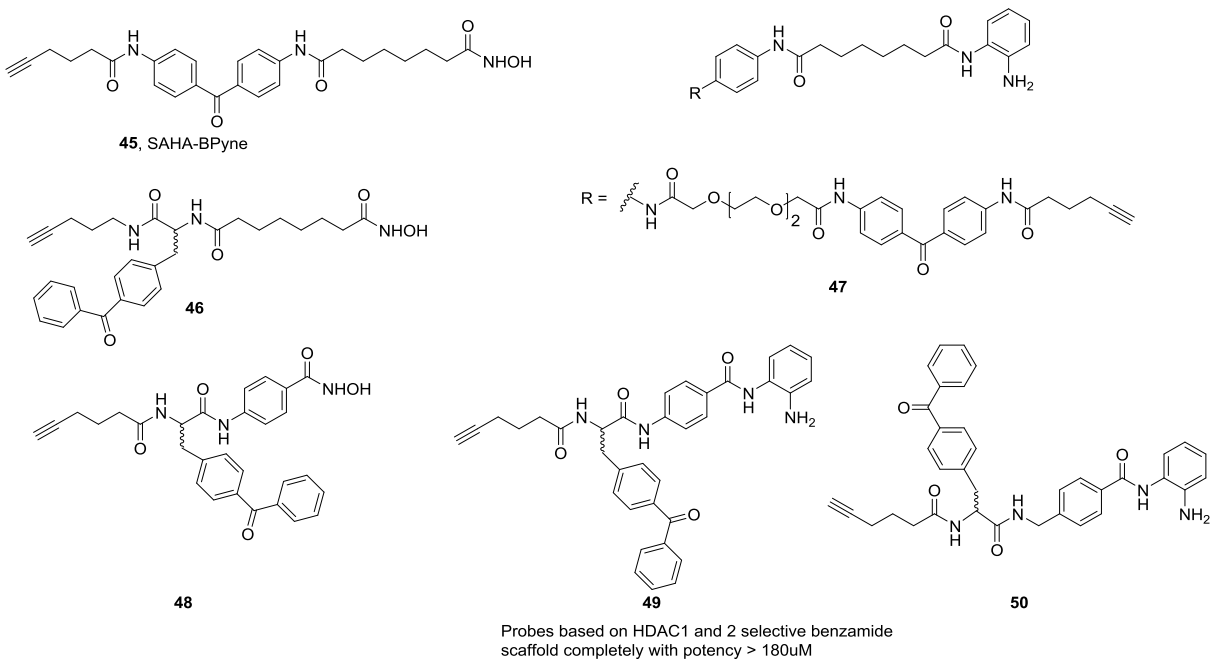

Figure 12. Clickable benzophenone-based probes for HDACs

1.4.6 Diazirine-based probes for profiling HDACs.

Recently, a trifunctional capture compound **51** based on SAHA, otherwise known as SAHA capture compound (SAHA-CC)[142] containing an aryl diazirine as a photoreactive group, biotin as a "sorting functionality" for enrichment and visualization purpose was not only able to identify HDAC3 but also isochorismitase domain containing protein 2 (ISOC2), a putative hydrolase associated with negative regulation of tumor suppressor protein p16 as an additional target for SAHA analogs in HepG2 cell lines. The molecular consequences of binding of SAHA analogs to ISOC2 are still under investigation, and may shed light on possible off-target effects and/or additional mode of action of hydroxamate-based HDAC inhibitors.

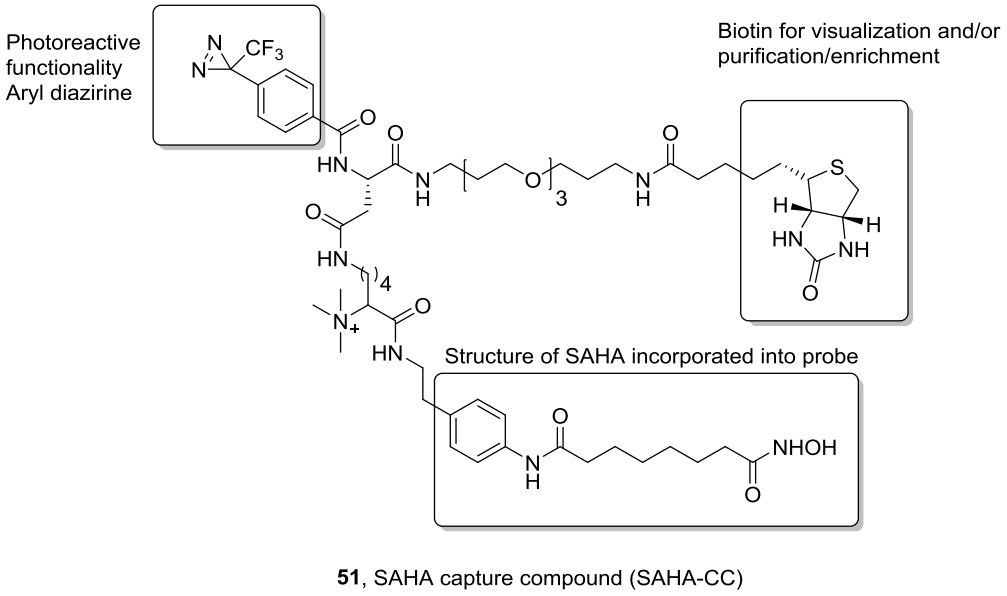

51, SAHA capture compound (SAHA-CC)

Figure 13. SAHA capture compound bearing aryl diazirine as a photoreactive group and biotin for visualization and/or enrichment.

1.4.7 Binding Ensemble Profiling with photoaffinity labeling (BEProFL) of HDACs with clickable azide-based probes.

Our lab has established the Binding Ensemble Profiling with photoaffinity labeling (BEProFL) approach to experimentally map the multiple binding modes of photoreactive HDAC probes. The design of these included the decoration of HDAC ligands with a 3-azido-5-azidomethylene moiety, a photoreactive moiety originally proposed by Suzuki et al. for labeling of catalytic site of HMG-CoA reductase.[143] The aryl azide is used as a photoreactive group and the alkyl azide serves as a ligation handle to attach a fluorescent or biotin tag via click chemistry. The biotinylated HDACs can be subsequently visualized

in gels via chemiluminscent/fluorescent detection systems, else can also be subjected to tryptic digestion and the modified peptides detected by LC-MS/MS. The mass spectrometry data along with molecular modeling techniques such as docking and MD simulations can then help distinguish between multiple binding modes adopted by the probes. Figure 14 shows a schematic explaining the BEProFL approach.

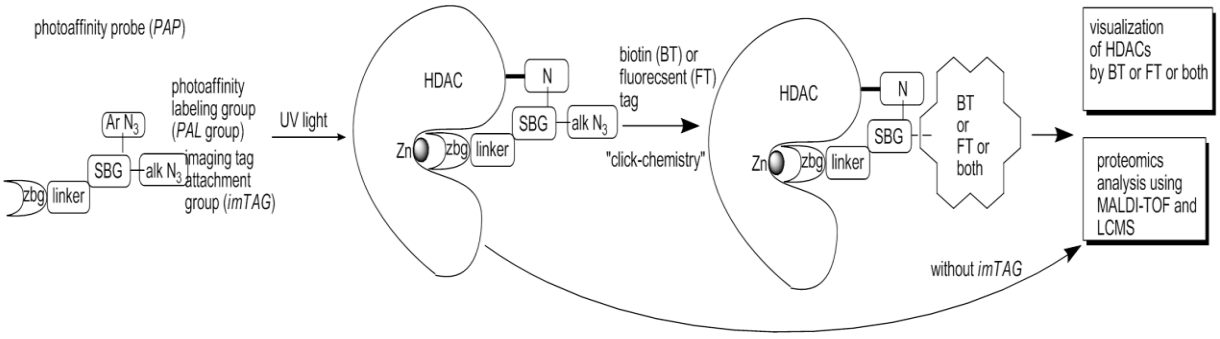

Figure 14.Schematic of the BEProFL approach.

Based on this approach we were successfully able to design and synthesize in few high yielding steps SAHA-like probe **52**, [144] (Figure 15) which enabled us to distinguish between the binding modes of the surface binding group of SAHA analogs on the surface/gorge region of HDAC8 and also discovered a novel “upside down” binding mode in a secondary binding site proximal to the main catalytic site of HDAC8. Recently, we have also reported the design, synthesis and biological evaluation of novel

diazide probes **53** and **54** [48] (Figure 15) potent and selective for HDAC3 and 8 that are cell permeable and exhibit excellent anti-proliferative activities in multiple cancer cell lines.

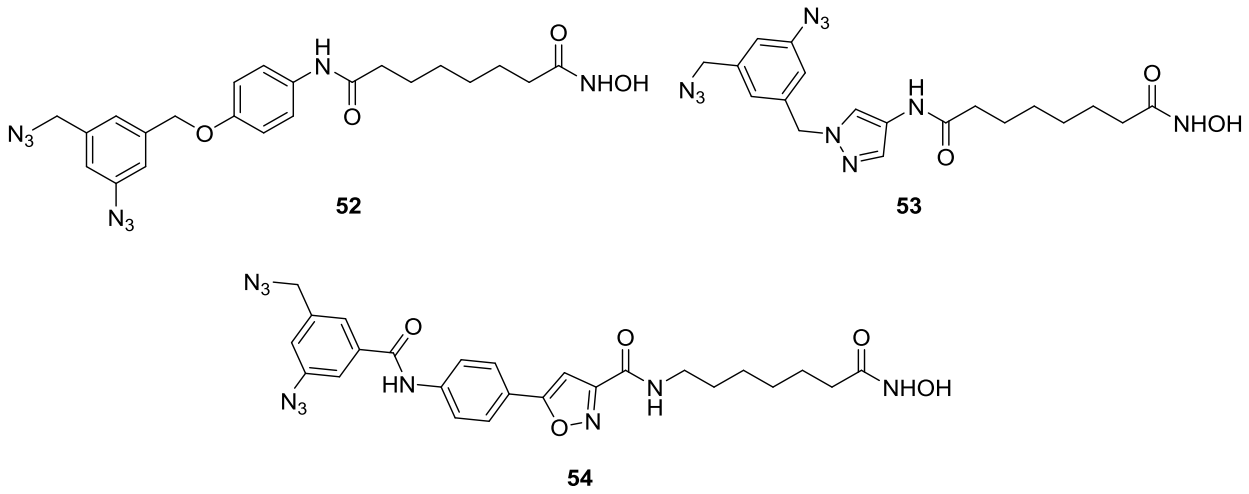

Figure 15. Structures of diazide-based photoreactive probes for HDACs suitable for BEProFL studies.

1.5 Scope of the current study

Histone deacetylases have been identified as promising drug targets for multiple therapeutic applications including cancer, muscular dystrophy and neurodegenerative conditions such as Alzheimer's disease. Existing HDAC inhibitors typically bear a zinc chelating group (ZCG), as all of them target the substrate binding site/main catalytic site containing Zn^{2+} ion. The presence of the ZCGs is believed to be associated with a number of therapeutic liabilities in long-term settings. Discovery of HDAC inhibitors lacking a

ZCG would be a significant step towards wider application of HDAC inhibitors as small molecule therapeutics. One of the strategies to eliminate a ZCG from the HDAC pharmacophore is to explore secondary binding sites in HDACs.

In order to explore secondary binding sites in HDAC 2 and 8, a series of diazide probes were used in Binding Ensemble profiling with Photoaffinity labeling studies for these isoforms with purified recombinant proteins. The design of probes that are potent and selective towards a given HDAC isoform is not trivial; hence the synthesis, structure activity relationships and photoaffinity labeling studies and biological evaluation of the probes will be discussed in detail in the following chapters.

These probes can act as important tools and shall undoubtedly help future investigations in the roles of HDACs 2 and 8 not only in neurodegenerative conditions and cancer but also other diseases.

CHAPTER 2: DEVELOPMENT OF AN IN VITRO ASSAY FOR SCREENING LIGANDS FOR HDAC2

2.1 Introduction

The induction of terminal differentiation in murine erythroleukemia cells by dimethyl sulfoxide, almost 40 years ago by Friend et al.[145] laid the foundations to understanding of the molecular mechanisms of HDAC inhibition as antineoplastic agents. Later, research focused into development of synthetic agents having similar effects to dimethyl sulfoxide lead to the discovery of suberoylanilide hydroxamic acid (SAHA) by Below et al. in 1996.[146] The development of functional and binding assays for screening for histone deacetylases has always been an active area of research since the discovery of SAHA. Despite the important role of HDAC2 in disease conditions such as Alzheimer's disease and Duchene muscular dystrophy, limited efforts have been focused on the development of economical HDAC2 ligand screening strategies. The development of a robust and economical ligand screening protocol is imperative for any drug discovery campaign; hence in this chapter we introduce the reader to existing histone deacetylase inhibition assays and deliberate on their pros and cons. The latter part of the chapter discusses the development, optimization and validation of a fluorogenic HDAC2 inhibition assay using commercially available Boc-Lys(Ac)-AMC substrate and human recombinant purified HDAC2. The assay discussed in this chapter will be used extensively in Chapter 3 and 4 for screening ligands for HDAC2 in a concentration and time dependent fashion.

2.2 Types of HDAC activity assays

In vitro assays for screening HDAC ligands can be divided into (1) radioisotope-labeled and non-radioisotope labeled and (2) binding and functional assays. The following sections dwell on different types of HDAC screening assays with the major emphasis of non-radioisotope labeled functional and binding assays.

2.3 Radioisotope-labeled functional assays.

Radioisotope-labeled assays as the name suggests, employs the use of radioactively labeled substrates/reagents for the design of a ligand screening assay. Radiolabeled histones or radiolabeled oligopeptides based on the N-terminal histone sequence were often used as substrates in isotopic assays. An example of a radiolabeled oligopeptide is as follows

Ac-Gly-Ala-Lys(ε-[^{3}H]Ac)-Arg-His-Arg-Lys(ε-[H^{3}]Ac)-Val-NH_2.[147]

Histones extracted from chicken reticulocytes or calf thymus extracts could be radiolabeled by incubation with ^{14}C-based acetic anhydride or ^{3}H sodium acetate.[148] Radiolabeled histones would then be incubated with an enzyme extract followed by extraction of radiolabeled acetic acid using ethyl acetate and centrifugation. An aliquot from the organic layer is then added to a scintillation cocktail and counted for radioactivity using a scintillation spectrometer. These assays suffered from disadvantages outlined below.

- Production of radiolabeled histones is lengthy and complicated.
- Degree of acetylation of core histones varies from preparation to preparation.

- Requires sacrifice of animals.
- Extraction steps and separation steps limit throughput.
- Exposure of personnel to radioactive materials.
- Disposal of radioactive waste.

To circumvent lengthy and complicated extraction and separation steps and to increase the throughput in screening, a scintillation proximity assay (SPA) was later introduced. In a typical SPA, an oligopeptide histone substrate, radiolabeled with [^{3}H] acetate, containing an N terminal biotin group, gets bound to streptavidin-coated SPA-beads.[149] The binding event leads to proximity of the scintillant containing beads to the radiolabel, resulting in energy transfer and the emission of light. The incubation of the radiolabeled substrate with HDACs releases [^{3}H] acetate, leading to a decrease in light emission. Although the throughput of the SPA was better than the original assay involving quantification of radiolabeled acetic acid, it suffered from similar drawbacks such as exposure of personnel to radioactive material and disposal of radioactive waste.

The limitations of radioisotope-labeled assays prompted the development of non-radioisotope-labeled assays involving techniques such as emission and/or absorption spectroscopy.

2.4 Non-radioisotope labeled functional assays.

One of the first assays to use absorption spectrometry, as a detection technique was designed for screening of ligands for HDAC8. In this assay, thio-acetyl lysine p53 peptide was incubated with HDAC8 to generate thioacetate.[150] Thioacetate is later

derivatized by 5,5'-Dithiobis (2-nitrobenzoate) to form 2-Nitro-5-thiobenzoate which can be monitored at 412 nm. (Figure 16) Although an obvious improvement over radioisotope-labeled techniques, this assay was limited for screening of ligands for HDAC8 as the substrate may not be recognized by other HDAC isoforms and the synthetic accessibility of the peptide presented difficulties.

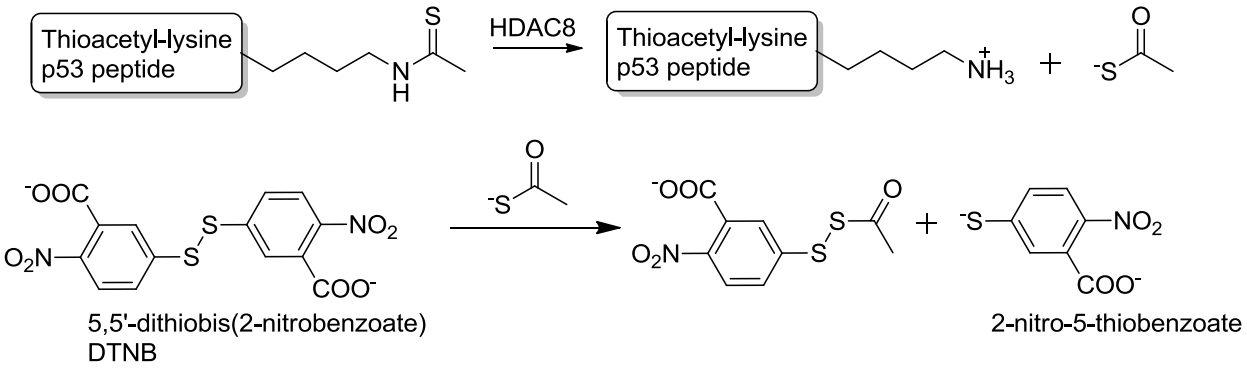

Figure 16. Generation of thioacetate upon deacetylation by HDAC8 and subsequent reaction with 5,5' –dithiobis(2-nitrobenzoate) to generate 2-nitro-5-thiobenzoate.

Fluorogenic peptides-based on the N-terminal histone sequence were first to be screened as substrates for HDACs. The simplest of these peptides was Boc-Lys(Ac)-AMC, **55** shown in Figure 17.[151] The coumarin-based molecule **55** exhibited time dependent conversion into its metabolite **56** when incubated with a preparation showing histone deacetylase activity. The reaction mixture had to be extracted and the product or

remaining substrate, quantified by high performance liquid chromatography (HPLC). Extraction of the product or the unconsumed substrate and quantification via HPLC limited the throughput of the assay. Another limitation of this protocol was inhibitors having overlapping absorption/emission spectra as coumarin may be identified as false negatives.

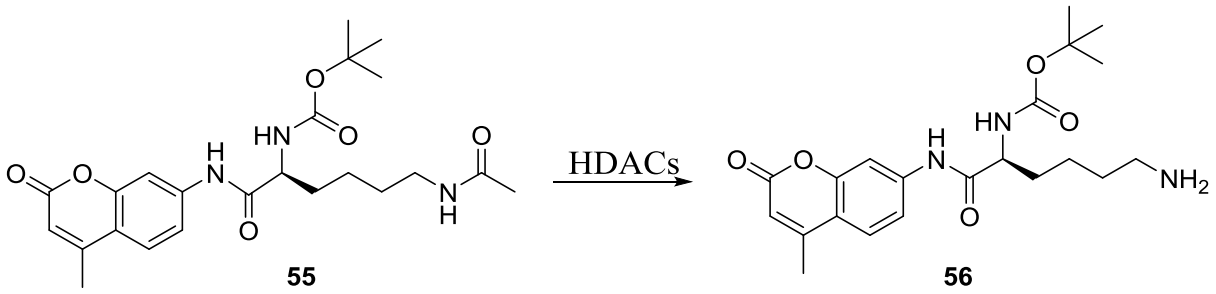

Boc-Lys(Ac)-AMC

AMC- Aminomethyl coumarin

Figure 17. Deacetylation of Boc-Lys(Ac)-AMC by HDACs

The deacetylated product **56** can be converted into an electrophilic imine species via reaction with napthalene-2,3-dicarbaldehyde (NDA). The imine is later trapped with a nucleophile such as 2-ethanethiol to form a fluorescent isoindole derivative **57** (Figure 18) which can be later quantified using fluorescence spectroscopy.

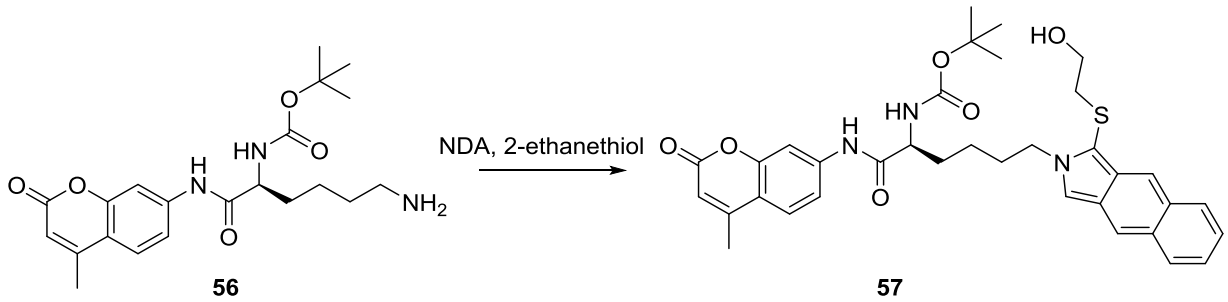

56 57

Figure 18. Derivatization of deacetylated product via reaction with naphthalene-2,3-dicarbaldehyde.

Although the above mentioned modifications to the assay were the first step towards a true homogenous assay, it suffered from the obvious disadvantage of using noxious reagents such as β-mercaptoethanol. Cyanide-based reagents can be used as alternative nucleophiles to β-mercaptoethanol, however they also may be hazardous in the long run. The presence of amine functionalities in the ligand and derivatization of amino/hydroxyl groups on proteins by NDA, may lead to fluorescent adducts which cause non-specific signal and necessitate the use of additional controls in this protocol.

Recently the use of a two-step fluorogenic assay has gained popularity in screening of ligands for HDACs.[152] This assay typically involves the incubation of purified enzyme with coumarin-based peptide in presence or absence of a ligand. Upon deacetylation, the deacetylated substrate is recognized by trypsin to release coumarin and deacetylated lysine derivative. (Figure 19). The free coumarin is detected using a fluorescence spectrophotometer; essentially lower the fluorescence signal detected for a particular concentration of a ligand, the more potent the ligand and lower the IC_{50}

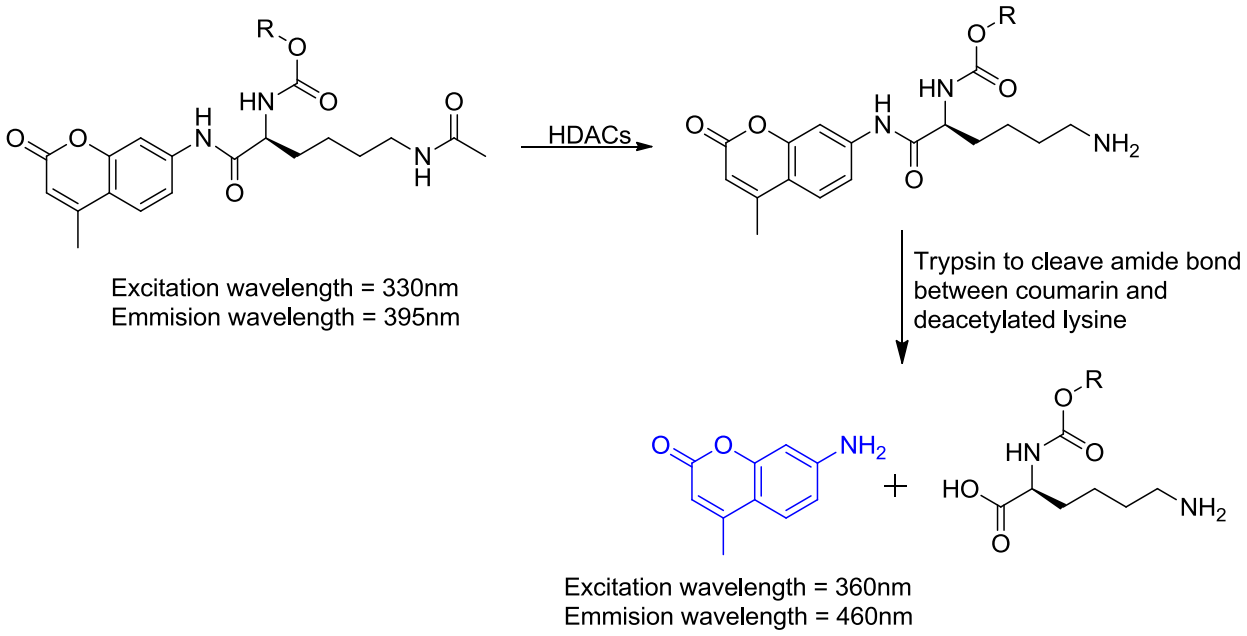

Figure 19. Two step fluorogenic assay using analogs of Boc-Lys(Ac)-AMC.

Extensive structure activity relationship studies have been conducted to design better substrates for HDACs 1, 3, 6 and 8. Essentially the structure of the Boc-Lys(Ac)-AMC was manipulated to yield isoform selective substrates. The use of such isoform selective substrates would be ideal, as the concentration required would be far lower than with a non-selective substrate to yield the same signal/noise ratio in a given amount of time. On the other hand, the synthesis of such substrates might be difficult and/or time consuming, thereby increasing the cost of screening per compound. Another possible limitation of the fluorogenic assays is the excess of trypsin that needs to be added in the second step, to prevent identification of trypsin inhibitors as false positives.

Figure 20 shows the general trends observed during these studies.[153-155]

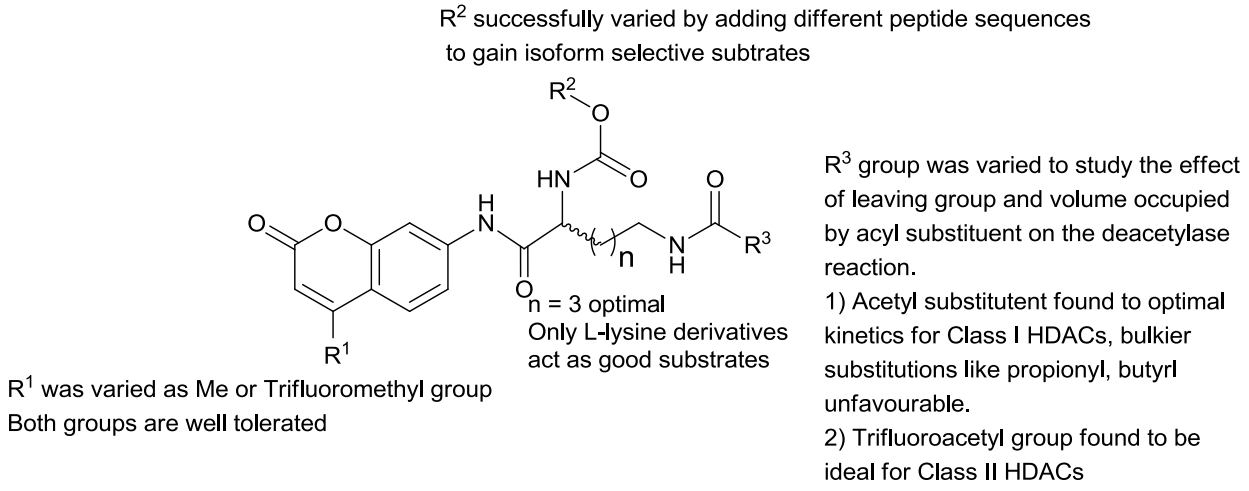

Figure 20. Structure activity studies on analogs of Boc-Lys(Ac)-AMC.

Recently a bioluminogenic activity assay was reported by Halley et al.[156] It is similar to the fluorogenic assays described in the preceding sections. A proluminogenic molecule designed by coupling aminoluciferin to a peptide sequence derived from histone H4 is used a substrate in this assay. HDAC mediated deacetylation of an N-acetylated, aminoluciferin-based substrate results in formation of an intermediate free amine as shown in Figure 21. The free amine generated after deactylation by HDACs is recognized by proteolytic enzymes such as trypsin that cleave the amide bond between aminoluciferin and the rest of the peptide molecule. The aminoluciferin acts as a substrate for luciferase and the amount of light produced in the reaction can be considered as a measure of HDAC activity. Figure 21 shows a schematic for the assay.

An obvious drawback of the biolumnigenic assay is the additional step of adding the luciferase system to generate a luminescent signal from aminoluceferin which ultimately

lowers the throughput of the assay and increases the overall cost of screening per ligand. An additional limitation for this assay is the identification of luciferase inhibitors as false positives

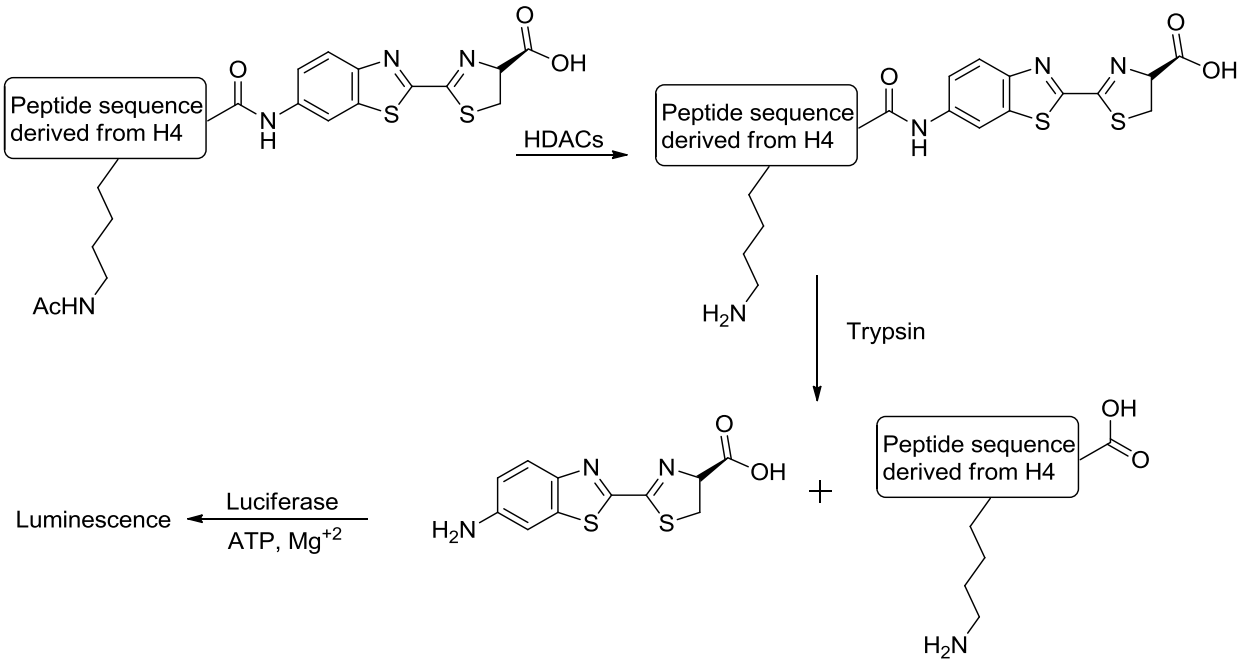

Figure 21. Schematic of a three-step bioluminogenic assay.

Cell-based functional assays are often coupled with above mentioned enzymatic assays to evaluate ligands of interest from the point of cell permeability, metabolism in cellular components.

The most popular assay to assess histone deacetylase activity at the cellular level is an immunoblotting protocol to detect histone hyperacetylation.[157] Alternatively, acetylation levels of non-histone substrates can also be monitored using suitable antibodies to assess selectivity of a ligand at the cellular level, for example HDAC6 selective inhibitors cause an increase in the acetylation levels of α-tubulin[158] (a non-histone substrate for HDAC6) but not histone H3 and H4 in cells.

2.5 Non-radioisotope labeled binding assays.

Recently a fluorescence polarization (FP) assay[159] was developed to overcome limitations of fluorogenic assays discussed in the preceding paragraphs. In a typical FP assay, a fluorescently labeled HDAC inhibitor **58** is incubated with purified enzyme and increasing concentrations of a ligand of interest is added to the HDAC/**58** complex and fluorescence anisotropy is measured at equilibrium. The assay does not allow direct measurement of enzymatic activity; however it correlates well with assays using fluorogenic substrates.

Figure 22 below shows the structure of fluorescently labeled SAHA analog using “click chemistry”

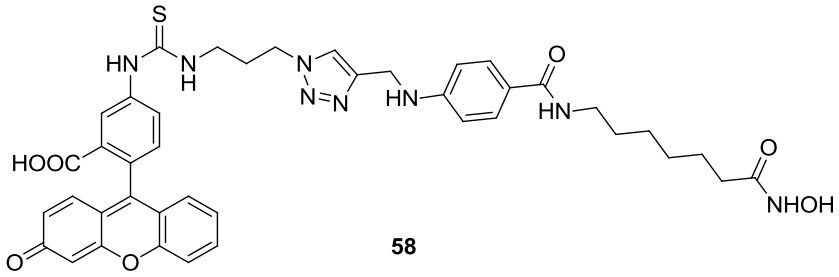

58

Figure 22. Fluorescently labeled SAHA derivative for fluorescence polarization assay.

A fluorescence resonance energy transfer (FRET) assay presents another high throughput screening protocol for screening for evaluating potential inhibitors for HDACs. Figure 23 shows the structure of furylacryloyl hydroxamic acid (FAHA) used in the FRET assay [160].

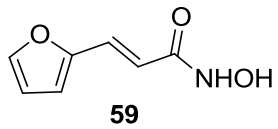

59

Furylacryloyl hydroxamic acid (FAHA)

Figure 23. Structure of furylacryloyl hydroxamic acid (FAHA)

Fluorescence resonance energy transfer takes place between the donor tryptophan residues of the HDAC protein and the acceptor furylacrloyl chromophore of the acceptor.

Binding of FAHA causes a decrease in fluorescence emission of the donor/protein. Displacement of FAHA by potential inhibitors in the assay leads to a decrease in FRET and reverses the initial decrease in fluorescence emission of the donor residues, which can be correlated to the affinity of the ligand.

The FP and FRET experiments described in the preceding paragraphs are binding assays, where a ligand of interest is titrated against fluorescently labeled ligand under equilibrium conditions and follow the basic premise that both ligands compete for the same site or the ligand binding to one site may cause a conformational change in protein that prevents binding to the labeled ligand, however may not differentiate between the two scenarios if the binding stoichiometry between the receptor and the ligand is 1:1. Binding assays also require the synthesis of a labeled ligand, which may or may not be economically feasible or time consuming in many cases. The synthesis of ligand **58**, requires 8 steps and is achieved in 40% overall yield. Binding of a ligand to a receptor may not necessarily alter its function on the biological landscape; hence assays which give information about the binding affinity and/or binding stoichiometry need to be coupled with functional assays to evaluate the full potential of a ligand of interest.

2.6. Choice of an assay to screen ligands for HDAC2

The choice of an assay to screen ligands for HDAC2 was primarily dictated by two factors, (1) economic feasibility and (2) assay time.

Assays based on radioactivity tend to be expensive and often require special efforts for handling and disposal and consequently limit throughput. Functional/binding assay based

fluorescence spectroscopy is often considered more sensitive than an assay based on absorption spectroscopy. The FP and FRET assays discussed in the preceding sections may shed insight into the binding affinity of the ligand but give limited information on the type and extent of enzymatic inhibition.

Another crucial factor dictating the choice of an assay is the time required for carrying out all the steps till measuring the read out signal on an instrument, this factor limits the throughput of screening of compounds in a drug discovery campaign. Amongst functional assays described in the preceding sections, homogenous assays require less time as compared to heterogeneous assays, due to the obvious circumvention of extraction steps. Amongst the homogenous assays, a two-step fluorogenic assay seemed more attractive than a three-step bioluminogenic assay. Cellular assays normally require additional time for growth and treatment of cells and immunoblotting, hence are not typically suited for screening a large number of compounds in a short amount of time.

Functional assays based using fluorogenic substrates, thus seemed to be an attractive option in screening for ligands for HDAC2. The choice of the fluorogenic substrate was Boc-Lys(Ac)-AMC as it is not cost prohibitive and available from multiple vendors. To the best of our knowledge, there are no reports of a fluorogenic screening protocol using human recombinant HDAC2 and Boc-Lys(Ac)-AMC, hence subsequent sections discuss the optimization of such a ligand screening protocol for HDAC2

2.7 Materials and Methods.

2.7.1 HDAC2 activity assays and enzyme kinetics.

Substrates BPS1 and BPS3 and HDAC2-His tag and HDAC2- Flag tag were purchased from BPS Biosciences. Substrate Boc-Lys(Ac)-AMC was purchased from Chem Impex Inc. All other chemicals/reagents were purchased from Sigma Aldrich unless otherwise stated. 96 well black opaque plates were purchased from Fischer Inc. Fluorescence measurements were conducted using Synergy H4 hybrid plate reader. All statistical calculations were done using Graph pad Prism.

A preliminary screening of potential enzyme-substrate pair was conducted by incubating 500 ng of each enzyme with 25 µM of each substrate in buffer 1 (25 mM Tris-HCl, pH 8.0, 137 mM NaCl, 2.7 mM KCl, 1 mM $MgCl_2$, 1 mg/mL BSA) at room temperature for 30 min in a 96 well plate opaque plate. Subsequently the enzymatic reaction was quenched by addition of 20 µl of buffer 3 (1 mg/ml trypsin in 25 mM Tris-HCl, pH 8.0, 137 mM NaCl, 5 µM TSA, 2.7 mM KCl, 1 mM $MgCl_2$) and the reaction mixture incubated at room temperature for 30 min. Fluorescence measurements were carried out at an excitation wavelength of 360 nm and emission wavelength of 460 nm. The fluorescence signal from the different enzyme-substrate pairs was compared with the signal from the substrate for the pair under analysis. An optimal enzyme-substrate pair is chosen based on signal/noise ratio, enzyme purity and economic constraints.

Steady state analysis for enzyme-substrate pair was carried out by incubating different amounts of enzyme (ranging from 0.5 ng to 1000 ng) with a fixed concentration of

substrate (25 µM) for 30 min in buffer 1 with a total reaction volume of 100 µl. Subsequently the reaction was quenched by addition of 50 µl of buffer 3and the reaction mixture incubated at room temperature for 30 min. Fluorescence measurements were carried out at an excitation wavelength of 360 nm and emission wavelength of 460 nm. The fluorescent signal is plotted against the amount of enzyme used to produce the signal and an optimal enzyme concentration is chosen such that it is in the initial linear region of the curve so as to be in the initial velocity conditions.

In the above mentioned experiments, the time for incubation for the enzyme-substrate pair was selected as 30 min based on reported assays for HDACs 3 and 8. However, the time for incubation can be further optimized by incubating an optimal concentration of enzyme as obtained from steady state analysis (as mentioned in the preceding paragraph) with a fixed amount of substrate for different time points. An optimal time point was chosen, such that it is in the linear portion of the curve of fluorescent signal vs. time and gives a Z factor above 0.5.

Enzyme kinetics experiments were performed to determine V_{max} and K_m values for the enzyme-substrate pair. Optimal enzyme concentration from steady state analysis was incubated with different amounts of substrate for the optimized time as per the incubation time test (as described in the preceding paragraph). The fluorescent signal obtained was plotted against the substrate concentration and the data fitted to Michealis-Menten curve using Graph pad.

Validation of the fluorogenic assay was performed using suberoylanilide hydroxamic acid and the IC_{50} and the K_i values calculated by evaluating the dose-response curves

using Graph pad Prism. A typical *in vitro* assay for HDAC2 follows a two-step procedure that can be carried out microtitration plates. The first step involves pre-incubating the enzyme and inhibitor at room temperature for a specified time.

The time for preincubation is decided based on the scaffold of the ligand, for example it is known that benzamide-based ligands exhibit a time dependent inhibition of HDAC2, however hydroxamate-based ligands do not exhibit any such time dependence. The maximum preincubation time was chosen as 24 h based on reported literature and experiments conducted to assess the changes in Z-factor for the assay as a function of time and temperature. In a typical experiment the enzyme (1 ng/uL) is diluted in buffer 1 and incubated in the presence or absence of a ligand at RT for the respective time points, before initiating the reaction by addition of the substrate (25 µM). After 1 h the reactions quenched by addition of developer/buffer 3 and the plate read after 30 min of incubation at room temperature. The fluorescence intensity was measured at λ_{exc} = 360 nm and λ_{ems} = 460 nm using a micro-titration plate reader.

2.8 Results and Discussion

2.8.1 Screening of commercially available HDAC2/substrate pairs.

Recombinant His tagged HDAC2 and Flag tagged HDAC2 were incubated with three commercially available fluorogenic substrates BPS 1, BPS 3 and Boc-Lys(Ac)-AMC. Figure 24 shows the fluorescent signal obtained from the enzyme-substrate pair in comparison to the background signal obtained from the substrate.

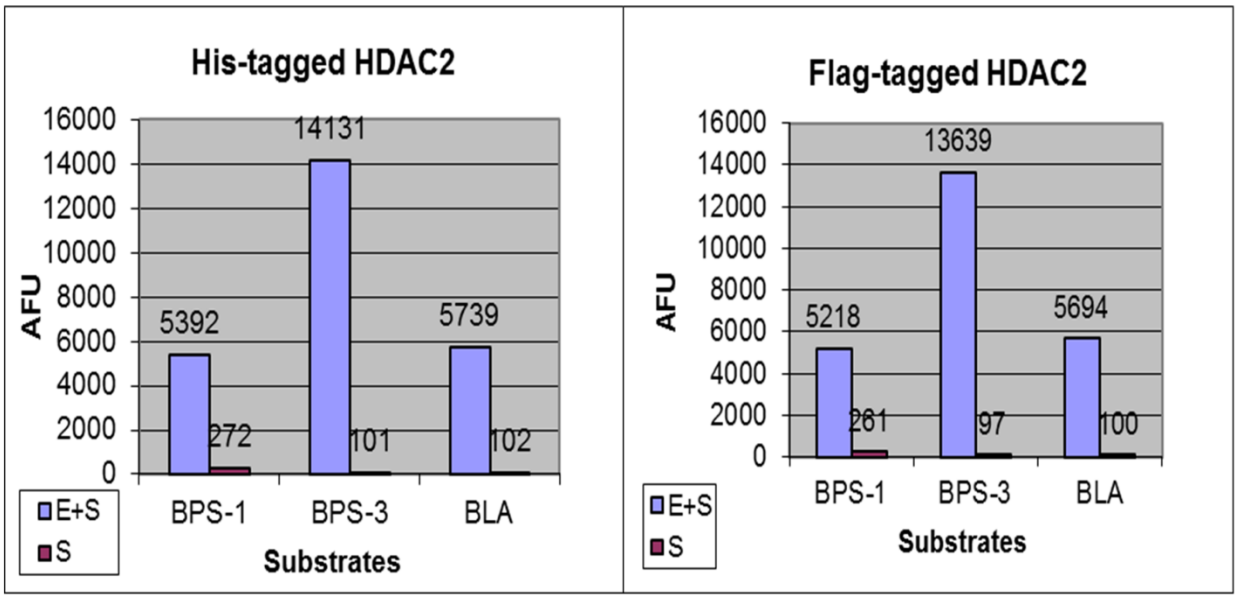

Figure 24. Comparison of fluorescent signal obtained from His-tagged and Flag-tagged HDAC2 with different commercially available substrates.

Amongst the three substrates BPS 1, 3 and Boc-Lys(Ac)-AMC (BLA), substrates BPS3 and BLA exhibited two-fold less background signal as compared to BPS-1 at the same concentration. The structures of the BPS substrates have not been revealed by the company, however presumably are peptidic in nature as other substrates for Class I histone deacetylases. Evaluation of the three substrates with His-tagged HDAC2 revealed that under the same concentration and time of incubation BPS-3 produced the highest signal/noise ratio. Similar trends were observed with Flag-tagged HDAC2, indicating the additional epitope did not affect substrate recognition at the active site. Although BPS-3

produced the higher signal/noise ratio, due to economic reasons Boc-Lys(Ac)-AMC was chosen as substrate for future assays.

Vendor specifications indicated His tagged HDAC2 had purity greater than 94% while Flag tagged HDAC2 was only 89% pure. To avoid nonspecific labeling of protein impurities, during photolabeling, His-tagged HDAC2 was carried forward for all photolabeling experiments and activity assays.

2.8.2 Optimization of amount of HDAC2 used per assay (steady state analysis).

Steady state analysis performed with recombinant His-tagged HDAC2 with Boc-Lys(Ac)-AMC revealed 50 ng of the enzyme was sufficient to produce a 6-fold signal/noise ratio after 30 min of incubation at room temperature. The final concentration of the enzyme was 1ng/µl and the substrate concentration was 25 µM. Figure 25 shows how the fluorescent signal changes with respect to amount of enzyme used in the assay.

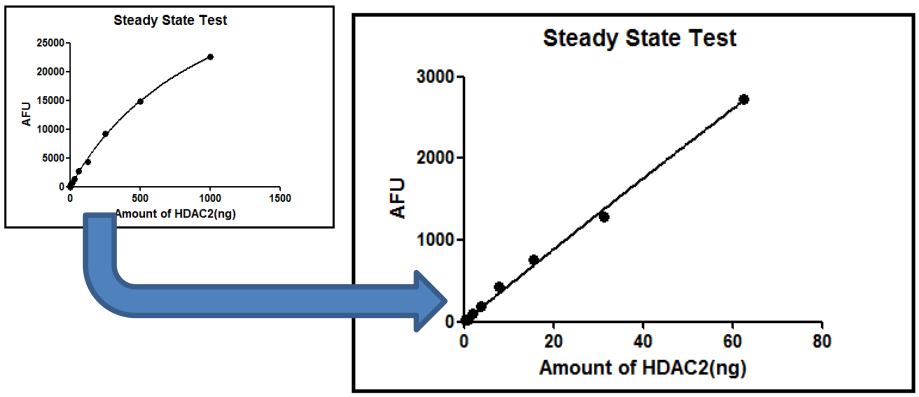

Figure 25. Steady state analysis of His-tagged HDAC2

1ng/µl of HDAC2 incubated with 25 µM of the substrate for 30 min produced signal that linearly increased with amount of enzyme indicating such conditions are in the initial velocity conditions. Using higher concentrations may result in aggregation of proteins in assay conditions and give misleading results during inhibitor screening campaigns. Besides use of higher concentrations of enzyme increases the cost of enzyme per assay.

2.8.3 Optimization of time of incubation of HDAC2 and substrate.

An incubation time test was performed with 1 ng/µl of His-tagged HDAC2 with 25 µM of the substrate by monitoring the fluorescent signal obtained over time. Figure 26 shows the change in the fluorescent signal with respect to time. A linear increase in the fluorescent signal is observed with respect to time indicating the enzyme kinetics under steady state conditions. An optimal time of 60 min was chosen as time for incubation based on signal/noise ratio and Z factor above 0.5

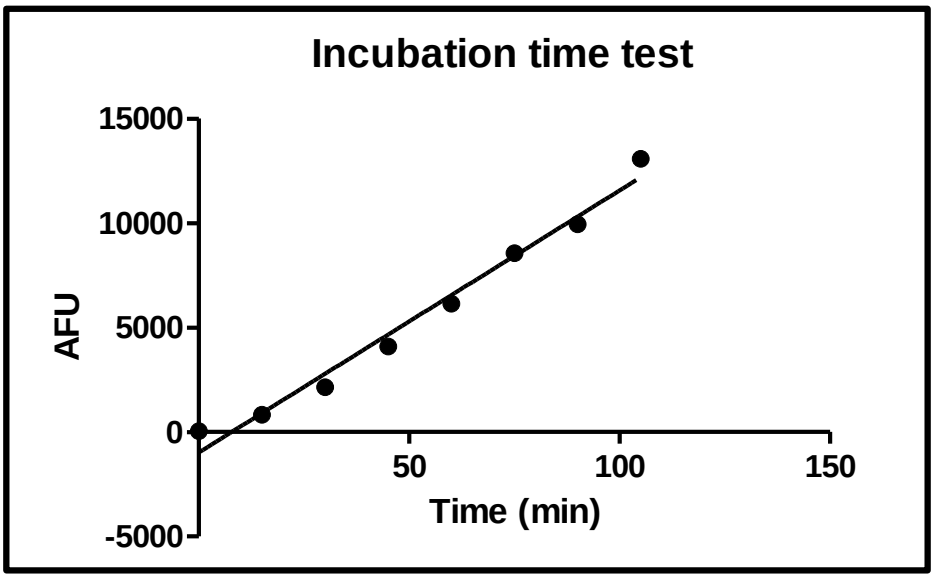

Figure 26. Temporal representation of deacetylation of Boc-Lys(Ac)-AMC by HDAC2.

2.8.4 Determination of V_{max} and K_m for the HDAC2

His-tagged HDAC2, at a final concentration of 1 ng/µl was incubated with varying concentrations of Boc-Lys(Ac)-AMC for 60 min and the fluorescent signal obtained plotted as a function of the substrate concentration. The data was fitted to a Michelis-Menten curve using Graph-pad Prism to calculate the V_{max} and K_m values. Figure 27 shows the Michelis- Menten curve obtained for the HDAC2, Boc-Lys(Ac)-AMC pair.

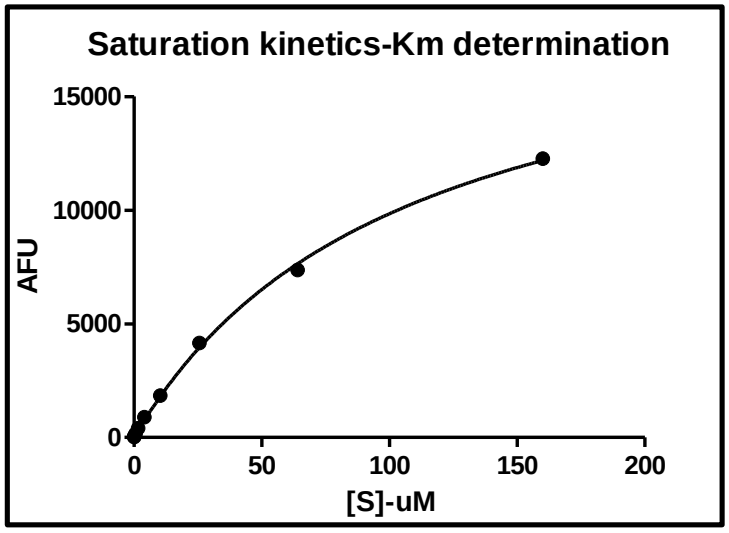

Figure 27. Saturation Kinetics of His-tagged HDAC2 with Boc-Lys(Ac)-AMC.

The kinetic parameters so obtained were, K_m = 105 µM, V_{max} = 674 AFU/min, K_2 = 13.5 AFU/min/ng.

2.8.5 Validation of the HDAC2 fluorogenic assay.

IC_{50} and K_i values of suberoylanilide hydroxamic acid (SAHA) were determined using the optimized fluorogenic assay and found comparable to values reported in the literature.[161] The IC_{50} of SAHA was found to be 200 ± 14 nM when it is preincubated with HDAC2 for 5 min at RT and 230 ± 4.3 nM when preincubated for 24 h. The IC_{50} for preincubation for 24 h at 4 °C is found to be 260 ± 9.2 nM. (Figure 28) Crystal structures have revealed that, hydroxamate-based ligands such as SAHA bind to the active site primarily through zinc chelation at the catalytic site and hydrophobic interactions with other residues in the protein and exhibit fast on-off binding, which may explain the

comparable IC_{50} values obtained with different preincubation times at the same temperature. The Z factor for the assays in different conditions were found to be above 0.8 (Figure 28 B), indicating the assay was robust in a variety of conditions and suitable for screening of ligands with different binding kinetics.

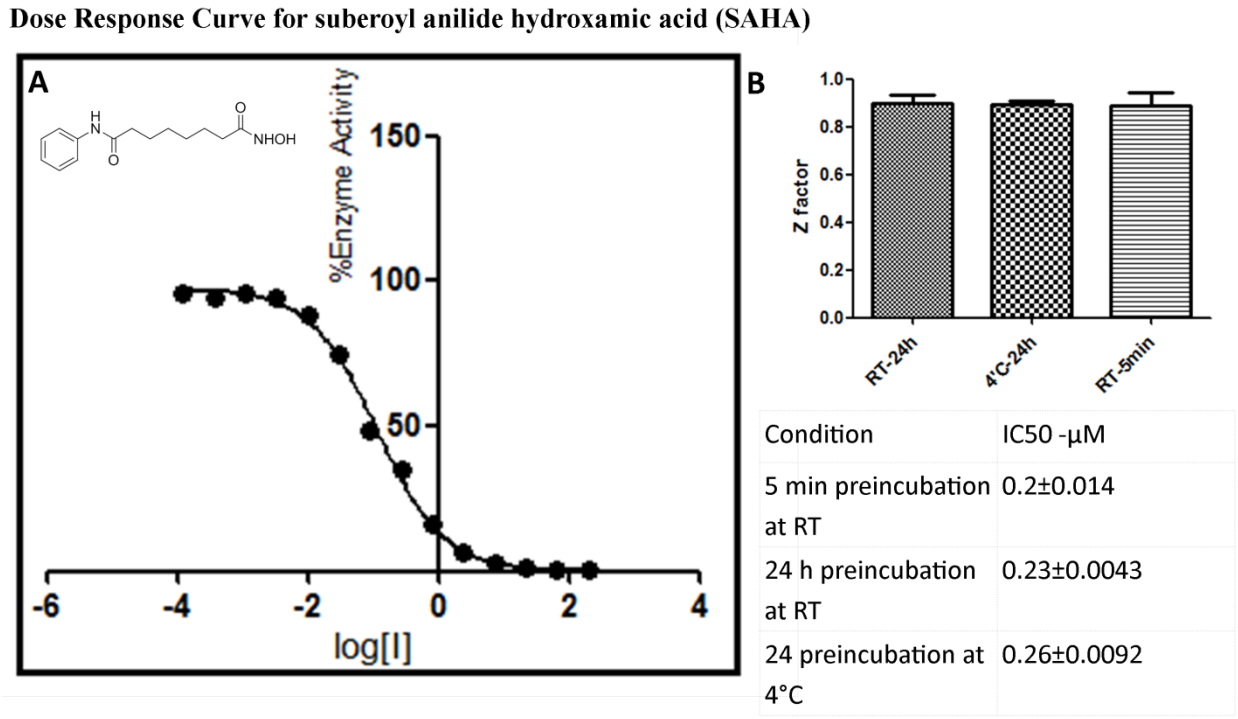

Condition	IC50 -µM
5 min preincubation at RT	0.2±0.014
24 h preincubation at RT	0.23±0.0043
24 preincubation at 4°C	0.26±0.0092

Figure 28. A. Dose response curve for SAHA. B. Z factors obtained in the fluorogenic assay for different preincubation times

2.9 Conclusions

The design of an optimized assay for screening of ligands/probes for HDACs is a prerequisite for photolabeling studies. In this chapter the methodology for optimization of a fluorogenic assay for HDAC2 is presented by considering several variables such as choice of enzyme and substrates, amount of enzyme used per assay, time for preincubation with ligands and incubation with substrates. 50 ng /assay of His-tagged HDAC2 is found to be optimal based on signal/noise ratio and Z-factor. The final concentration of enzyme and the substrate are found to be 1 ng/μL and the 25 μM respectively. The optimal time for incubation with substrate is found to be 1 h and the enzyme is found to be stable under the assay conditions for 24 h, allowing screening of ligands with different binding kinetics. The optimized assay discussed in this chapter has been used extensively to assess affinity of ligands/probes in successive chapters.

CHAPTER 3 NOVEL HISTONE DEACTYLASE 8 LIGANDS WITHOUT ZINC CHELATING GROUP: EXPLORING AN UPSIDE DOWN POSE

3.1 Introduction

The vast majority of the HDAC inhibitors contain a zinc chelating group (ZCG) as an essential part responsible for their binding affinity. The most commonly used ZCG in HDAC inhibitors is a hydroxamic acid group that shows poor metabolic stability *in vivo* and is rapidly hydrolyzed to carboxylic acid, a poor ZCG, and hydroxylamine.[162, 163] Compounds containing hydroxamic acid moieties are poorly absorbed *in vivo* and show extensive glucuronidation and sulfation.[164] The sulfate conjugates of hydroxamic acids may lead to formation of electrophiles such as isocyanates which may further react with nucleophiles in proteins and other biological macromolecules.[165-167] Non-hydroxamate ZCGs typically include carboxylic acids (sodium valproate), epoxy ketones (trapoxin), *o*-amino anilides (MS 275), electrophilic ketones, and thiols.[168-171] These non-hydroxamate ZCGs often suffer from poor potency,[172] redox activity,[173] general reactivity,[169] metabolic instability,[174] and poor aqueous solubility.[174] For life-long applications, e.g. as a potential treatment of Alzheimer's disease,[67, 175] these types of properties of HDAC inhibitors are highly undesirable. Clearly, there is an urgent need for development of HDAC inhibitors that may utilize novel binding modes that do not require a ZCG. A series of non-selective tetrapeptides likely not chelating to the active site Zn^{2+} of HDAC1-3 is the only example of the non-ZCG HDAC ligands we could find.[176] Figure 29 below shows different HDAC inhibitors and their therapeutic liabilities.

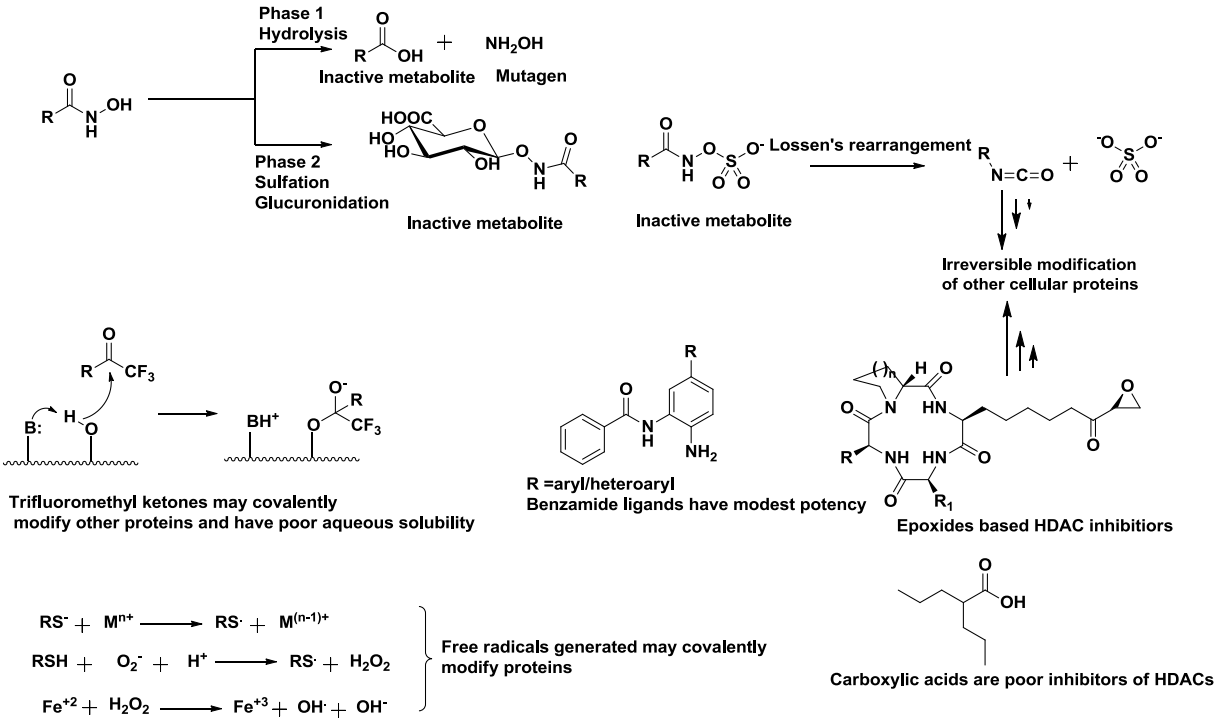

Figure 29. Therapeutic liabilities of HDAC inhibitors bearing zinc chelating groups.

Recently, we have published Binding Ensemble Profiling with Photoaffinity Labeling (BEProFL) approach that was used to map experimentally the multiple binding poses of the surface binding groups (SBG) of inhibitors of HDAC8,[177] a novel therapeutic target for neuroblastoma,[178-182] leukemia,[49] and cognitive disorders.[183] In our paper[177] we noted that some of the covalent modifications of HDAC8 may correspond to a novel "upside-down" pose of the diazide probe that was strikingly similar to that found in HDAC8 (PDB: 1T64)[25] for one of the two molecules of Trichostatin A bound to the secondary site proximal to the main catalytic site. *The main objective in this study was to design and synthesize a series of diazide-based probes/ligands lacking the hydroxamic acid moiety,*

test HDAC8 inhibition by these probes, and explore using photoaffinity labeling studies if they bind in an "upside-down" fashion in the secondary binding site in HDAC8.

3.2 Materials and methods

3.2.1 Synthesis

All chemicals and reagents were purchased from Sigma Aldrich (St. Louis, MO), TCI America and Fischer Scientific and used as received unless otherwise stated. All synthesized compounds were characterized by ^{1}H NMR, ^{13}C NMR and HRMS included for final compounds/probes. Full synthetic methodologies are described in Appendix A. Compound Characterization Spectra are presented in Appendix B.

3.2.2 HDAC activity assays

HDAC inhibition assay was performed in 96-well opaque half-area microplate (Corning). Human recombinant HDAC1, 2 and 3 (BPS Bioscience) and HDAC8(Biomol Inc.) were diluted with assay buffer 1 (25 mM Tris-HCl, pH 8.0, 137 mM NaCl, 2.7 mM KCl, 1 mM $MgCl_2$, and 1 mg/mL BSA), so as to have 4 ng/µl, 5 ng/µl and 1 ng/µl and 8.5 ng/µL stocks of each isoform respectively. Serial dilutions of the probes were made in assay buffer 2 (25 mM Tris-HCl, pH 8.0, 137 mM NaCl, 2.7 mM KCl, 1 mM $MgCl_2$).10 µL of the enzyme stock was added to 30 µL of the probes and preincubated for 5 min. After preincubation, 10 µL of 125 µM HDAC fluorescent substrate Boc-Lys(Ac)-AMC (Chem-Impex) in case of HDAC1, 2 and 3 and 10 µL of 25 µM BML-KI-178(Biomol Inc.) in case of HDAC8 was added, and the mixture incubated for 35 min (HDAC1, 3, 8), 60 min (HDAC2) at room temperature. The reaction was quenched with 50 µL of 1 mg/mL

trypsin and 5 μM trichostatin A in assay buffer 1 (25 mM Tris-HCl, pH 8.0, 137 mM NaCl, 2.7 mM KCl, 1 mM $MgCl_2$) and further incubated at room temperature for 35 min. The plate was read on Synergy 4 hybrid microplate reader (BioTeck) at excitation wavelength 360 nm and emission wavelength 460 nm. The IC_{50} values were determined using the GraphPad Prism 5 software (GraphPad Software Inc., La Jolla, CA). The IC_{50} determination for the upside down probes **52g** and **52h** for HDAC2 and 8 were conducted by myself, for HDAC1 and 3 were conducted by Dr. He Bai and Mr. Hazem Abdelkarim.

3.2.3 Photolabeling protocol

The probes or probe/competitor mixture was incubated with human recombinant HDAC8 (purified from E.coli) for 3 h in photolabelling buffer (25 mM Tris-HCl, pH 8.0, 137 mM NaCl, 2.7 mM KCl, 1 mM $MgCl_2$, 0.1% Triton-X), exposed to 254 nm UV light 3 × 1 min with 1 min resting. In case of denaturation experiments, post photocrosslinking, a solution of sodium dodecyl sulphate in water was added to attain final concentration of 2% w/v. Biotin tag BT was attached to HDAC8-probe adduct using the [3+2] cycloaddition reaction catalyzed by TBTA and Cu(I) produced in situ from $CuSO_4$ and TCEP. The final concentrations of BT, TCEP, TBTA and $CuSO_4$ are 50 μM, 0.5 mM, 0.1 mM, 1 mM respectively. After 60 min of incubation at rt, protein samples were analyzed by SDS-PAGE and western blot using an antibiotin primary antibody, streptavidin conjugated to horseradish peroxidase (Pierce, Rockford, IL), and ECL (Pierce, Rockford, IL). The membranes were then stripped in 0.2 M glycine, pH 2.6 for 10 min, and then in 0.2 M glycine, pH 2.3 for another 10 min, before being reblocked and

redecorated with an anti-HDAC primary antibody and an antirabbit-HRP secondary antibody.Western blotting was done with 0.5 µg of purified protein with 5X loading buffer containing 10% SDS, 0.05% bromophenol blue, 50% glycerol, and β-mercaptoethanol. Protein samples were boiled for 5 min and allowed to cool before loading on a denaturing 10% polyacrylamide gel electrophoresis (SDSPAGE). After electrophoresis, protein was transferred to a polyvinylidiene difluoride membrane (Imobilon-Millipore, Bedford, MA). The membrane was incubated for 1 h with 3 % albumin fraction V (USB, OH) and washed three times with 1X phosphate buffer saline supplemented with 0.1 % of Tween-20 (PBS-T). The membrane was then incubated with an anti-HDAC8 antibody (1:3000) for 1 h under rt with slight agitation. After three washes in PBS-T, the membranes were incubated with a secondary antibody antirabbit-HRP for 1 h at room temperature. The signals were detected using the enhanced chemiluminescence (ECL) kit from Pierce (Pierce Biotechnology, Rockford, IL). Under the mentorship of Dr. He Bai, I have conducted all the photolabeling experiments, discussed in the following sections.

3.2.4 Molecular modeling studies

The analysis of the SAR was facilitated by docking of the ligands to HDAC8 (PDB:1T64)[25] using GOLD v.5.1.[184] I thank, Ms. Emma Mendonca for conducting docking studies discussed in the subsequent sections.

3.2.5 Cell culture and western blot protocol

SH-SY5Y cells seeded at 1.0 x 10^5 cells/well in 6-plates and grown to 80% confluence in 1:1 DMEM:OPTI-MEM (Gibco) supplemented with 10% FBS (Gibco), 1% Antibiotic-Antimyctotic (Gibco) and 1% penicillin-streptomycin (Mediatech). Cells were treated with either vehicle, increasing concentrations of **52h**, or HDAC6-selective compound **73**. Cells were maintained at 37°C and 5% CO_2 for 24 h after treatment. Cells were lysed using 1X RIPA buffer (150mM NaCl, 1% Triton X-100, 0.5% sodium deoxycholate, 0.1% SDS, 50mM Tris, pH 8.0) containing 1:100 dilutions of protease inhibitor cocktail (Sigma) and 1:100 dilution of phosphatase inhibitor (Sigma) with shearing. Lysates were clarified through centrifugation at 13,000 rpm at 4°C. Total protein concentration was determined via the BCA Protein Assay Kit (Pierce). Lysates were stored at -20°C until later use. Sample vials were prepared by aliquoting 20 µg of total protein and adding 4X Sample Buffer with 10% β-mercaptoethanol. Sample vials were boiled for 5 min, cooled to room temperature, and separated by gel electrophoresis at 80 V. Proteins in the gel were transferred to PVDF membrane in 4 min using the Invitrogen iBlot system. Membranes were blocked using 5% Milk in PBST and probed using anti-GAPDH (1:5000), anti-acetyl α-tubulin, or anti-acetyl histone H4 (1:1000) overnight at 4 °C. Membranes were incubated with either anti-mouse (1:5000) or anti-rabbit (1:5000) in 5% Milk in PBST. Results were visualized using Femto chemiluminescent substrate (Pierce) in CCD camera. HRP-conjugated anti-rabbit IgG (H+L) was purchased from GE (Piscataway, NJ). Anti-acetyl α-tubulin was purchased from Santa Cruz Biotechnology (Santa Cruz, CA). All other antibodies (anti-GAPDH, anti-acetyl histone H4, HRP-

conjugated anti-mouse IgG (H+L)) were purchased from Millipore. I thank, Ms. Antonett Madriaga for conducting all the cell based studies discussed in the following sections.

3.3 Results and Discussion

3.3.1 Synthesis

The synthesis of the ligands/probes is outlined in Scheme 5. The synthesis of the probes/ligands in this section was a joint effort between myself and Dr. Raghupathi Neelarapu in our lab. My key contributions were in the synthesis of the upside down probes **52g** and **52h**.

Commercially available 4-benzyloxyaniline hydrochloride **60** was coupled with suberic acid monomethyl ester **61** or octanoic acid **62** using a facile carbodiimide-based coupling reaction using EDCI and HOBt in anhydrous dichloromethane in high yields. The benzylhydoxy group of **52d** and **63** was deprotected via catalytic hydrogenation to generate the corresponding phenol derivative that can subsequently utilized for O-alkylation reactions. Bromide **67** was commercially available whereas tosylates **66**[144] and **71** were synthesized in house.

Facile reduction of 3-amino-5-methoxy benzoic acid, **68** with lithium aluminium hydride resulted in generation of corresponding alcohol **69**. At first the conversion of aromatic amine into aromatic azide in intermediate **69** was attempted by using *t*-butyl nitrite and trimethylsilyl azide in acetonitrile from 0°C-rt, however the reaction did not go to completion even after prolonged stirring up to 48 h and yielded a complex mixture of products that was hard to separate. The *t*-butyl nitrite/ trimethylsilyl azide

methodology was tried to circumvent work up steps of extraction with ethyl acetate that are regularly encountered with conventional diazotization-azidation reactions with mineral acids, sodium nitrite and sodium azide. Conventional diazotization reactions also require the careful monitoring of temperature and pH without which unwanted diazo dyes are formed as tarry residues during the reaction. Figure 30 shows the mechanism of diazotization azidation reaction using sodium nitrite and *t*-butyl nitrite and possible side products that may form during the reaction. Surprisingly, conventional diazotization-azidation reaction with sodium nitrite, 10% hydrochloric acid and sodium azide gave the azide intermediate **70** in high yields without formation of by-products.

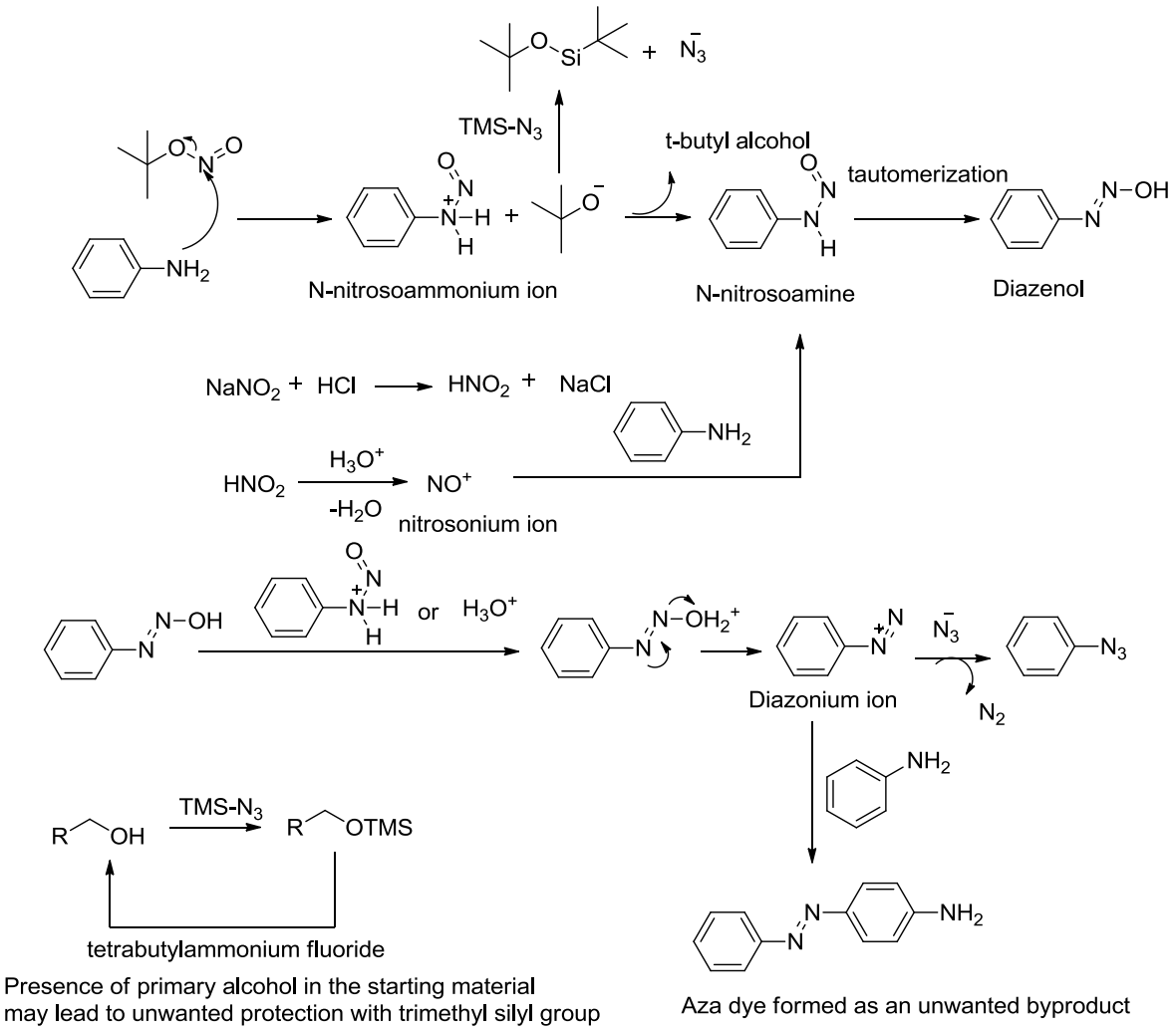

Figure 30. Mechanism of diazotization-azidation using *t*-butyl nitrite/trimethylsilyl azide and sodium nitrite/sodium azide.

The synthesis of tosylate **71** was straightforward and was achieved by portion wise addition of tosyl chloride to stirred cold solution of intermediate **70** and triethylamine in anhydrous dichloromethane. The tosylates/bromides **66** and **71** synthesized were used as alkylating agents for phenol derivatives **64** and **65** in presence of potassium carbonate as base in refluxing acetone to yield esters **52a**, **52e** and **72**.

Esters **52a**, **52e**, and **72** were subjected to basic hydrolysis to yield corresponding carboxylic acids that were used without further purification and subsequently re-esterified with appropriate alcohols using EDCI/HOBt coupling conditions or using corresponding commercially available acid chlorides, resulting in the formation of probes **52b**, **52f**, **52g** and **52h** respectively, in 20-65% overall yields. [4-(Azidomethyl)phenyl]methanol and 2-azidoethanol were synthesized by nucleophilic substitution reaction of sodium azide with commercially available [4-(bromomethyl)phenyl]methanol and 2-bromoethanol according to the reported methods and used without further purification.[185, 186] Synthetic procedures and data for compounds **52**, **52a**, **52d** and **64** and **53**, **53a**, **54**, **54a** and **66** were previously reported by us.[177, 187]

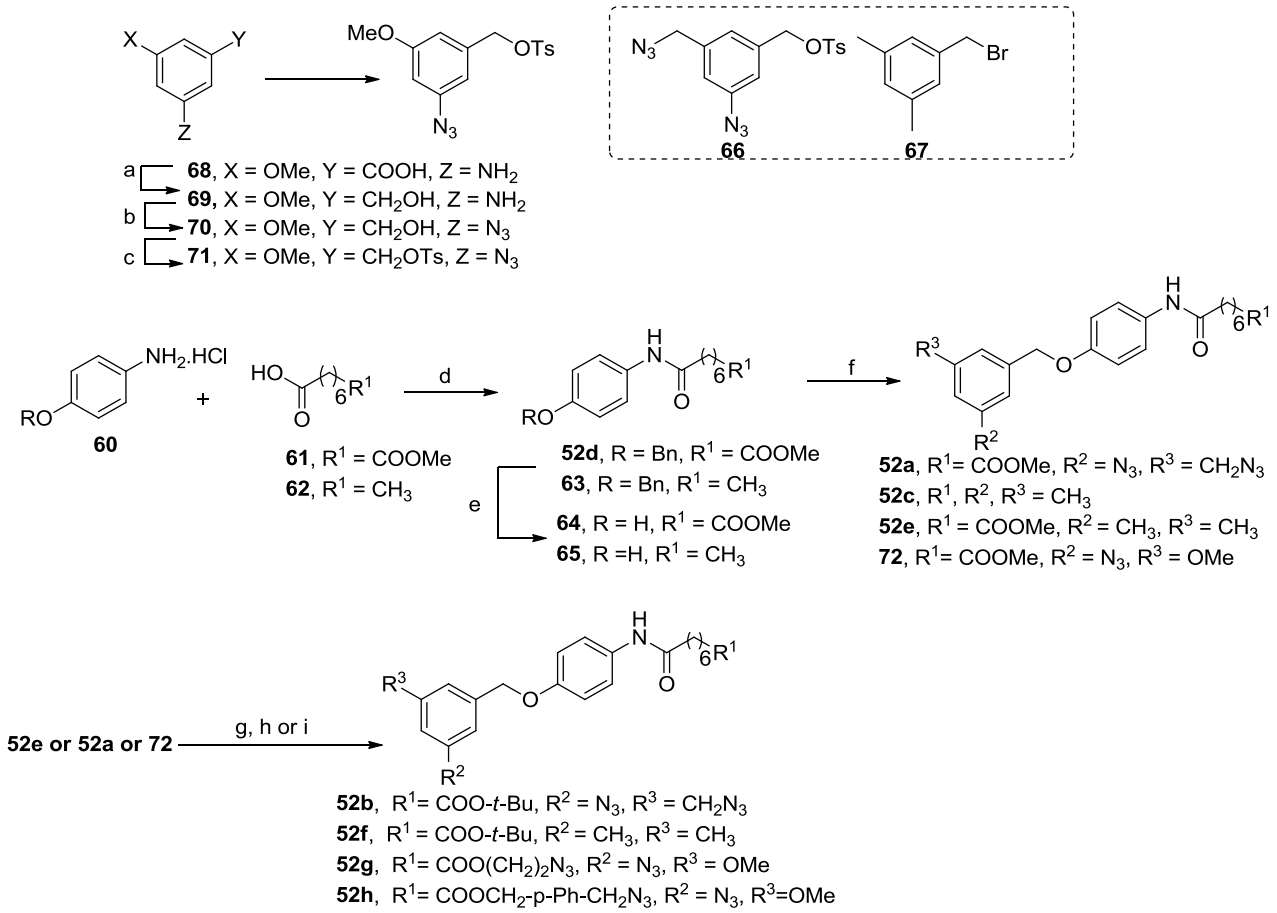

Scheme 5. . Synthesis of non ZCG ligands/probes.
Reagents and conditions (a) LAH, THF, 0 °C-rt; (b) $NaNO_2$, HCl(aq), NaN_3, 0 °C- rt; (c) TsCl, Et_3N, CH_2Cl_2, 0 °C; (d) suberic acid monomethyl ester or octanoic acid, EDCI, HOBt, DIPEA, CH_2Cl_2, 0 °C-rt; (e) Pd/C, MeOH, rt; (f) 66 or 67 or 71, K_2CO_3, acetone, reflux; (g) NaOH(aq) or KOH(aq), rt (h) $(COCl)_2$, t-BuOH, DMF, Et_3N, CH_2Cl_2; (i) [4-(azidomethyl)phenyl]methanol or 2-azidoethanol, EDCI, HOBt, CH_2Cl_2, 0 °C-rt.

3.3.2 Structure-activity trends and docking studies

Figure 31 and Table show the structures and activity trends observed for the probes/ligands synthesized for HDAC8.

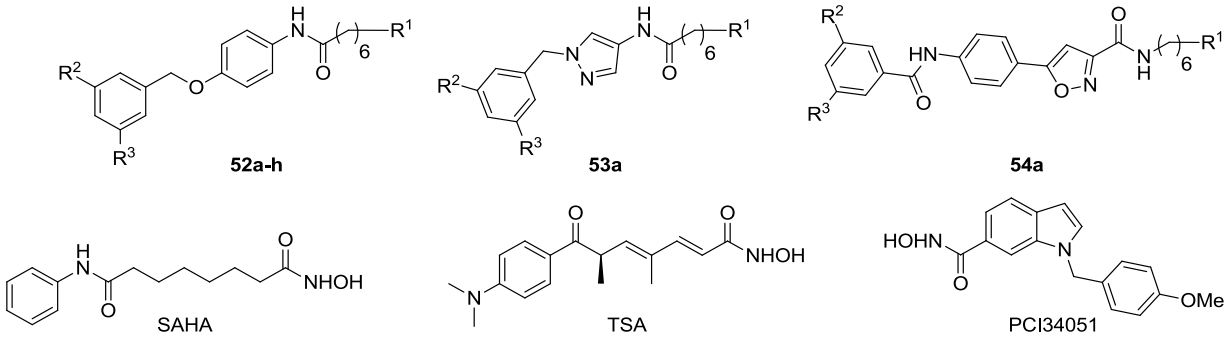

Figure 31. Structures of ligands/probes tested for HDAC8 inhibition

Cmpd #	R^1	R^2	R^3	HDAC8 IC_{50}(μM)
52[a]	CONHOH	N_3	CH_2N_3	7.34±0.22
52a	$COOCH_3$	N_3	CH_2N_3	37.4±2.34
52b	COO-*t*-Bu	N_3	CH_2N_3	42.6±1.81
52c	CH_3	CH_3	CH_3	NA
52d	$COOCH_3$	H	H	NA[d]
52e	$COOCH_3$	CH_3	CH_3	47.8±2.35
52f	COO-*t*-Bu	CH_3	CH_3	53.2±6.49
52g	$COOCH_2CH_2N_3$	N_3	OCH_3	67.5±4.79[e]
52h	$COOCH_2$-*p*-Ph-CH_2N_3	N_3	OCH_3	28.0±2.65[f]
53[b]	CONHOH	N_3	CH_2N_3	0.017±0.003
53a	$COOCH_3$	N_3	CH_2N_3	36.0±2.20

54[c]	CONHOH	N_3	CH_2N_3	0.651±0.12
54a	$COOCH_3$	N_3	CH_2N_3	47.1±1.76
SAHA	-	-	-	0.44±0.021[7]
TSA	-	-	-	0.39±0.018
PCI34051	-	-	-	0.01[49]

TABLE I HDAC8 IC_{50} VALUES FOR COMPOUNDS 52, 52A-H, 53, 53A, AND 54, 54A.

At first, we replaced the hydroxamic acid moiety in **52** with a methyl ester and found that ligand **52a** is able to maintain its HDAC8 inhibitory properties (IC_{50} of **52a** is 37.4 μM) despite the lack of a chemical moiety that can serve as a bidentate chelator to Zn^{2+} (Table). Although encouraging, this finding needed further proof that the ester group of ligand **52a** does not serve as a monodentate ZCG. Our preliminary modeling studies have shown that a *t*-butyl ester moiety instead of the methyl ester in **52a** would not be able to fit the binding site of HDAC8 because it is too bulky. The corresponding *t*-butyl ester **52b** was found to inhibit HDAC8 with an IC_{50} of 42.6 μM, which is similar to that of ligand **52a**. Docking showed that ligand **52b** can only fit the binding site by adopting an "upside-down" pose shown in Figure 32.

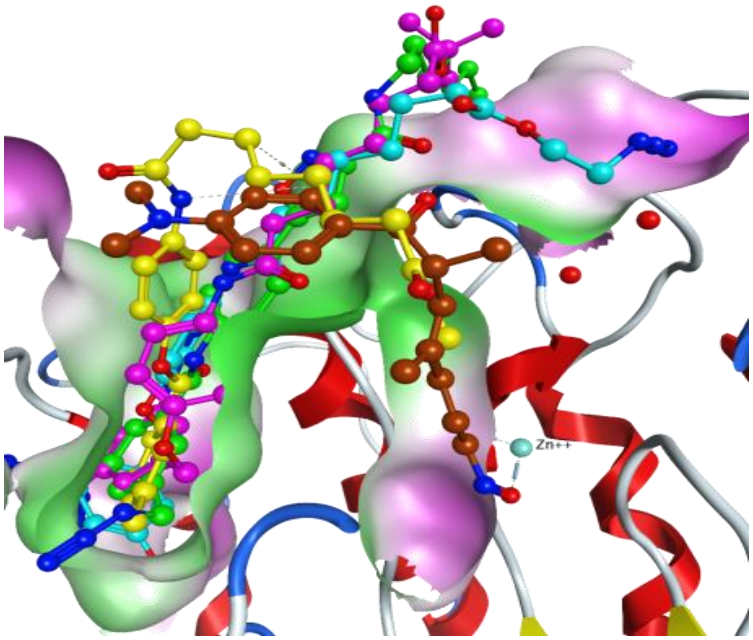

Figure 32. Upside down binding pose proposed for HDAC inhibitors.
52b (magenta), **52e** (yellow), **52g** (cyan) and **54a** (green). TSA bound to the main catalytic site (PDB: 1T64) is rendered brown. The binding site is rendered by solvent accessible surface, green – lipophilic, magenta – hydrophilic

Next, we removed the ester group in **52a**. The resulting ligand **52c** with a rather flexible unsubstituted alkyl chain was found to be inactive. If the binding mode of **52c** is similar to that of **52b**, its long alkyl chain substituent would be solvent exposed and may not contribute to the binding. Thus, lack of potency comparable to that of **52a** appears to be in line in the proposed binding mode.

To explore if the presence of the two lipophilic azide groups is required, we synthesized compound **52d** where hydrogen atoms were placed in both the meta positions in the terminal phenyl ring. Compound **52d** was found to be inactive up to 66 µM. The analysis of the binding site available to the ligands in those HDAC8 X-ray structures

where the second copy or an empty binding site adjacent to the catalytic site is present showed that the second pocket is relatively large and there are two additional lipophilic sub-pockets at the bottom. Our docking experiments suggested that in the case of ligands **52, 52a-b** their meta-azido and meta-methylene azido moieties can occupy these two lipophilic sub-pockets and form extensive hydrophobic interactions with the binding site. In the case of **52d** such interactions were missing. Next, to further verify if the presence of meta substituents is required, we synthesized compound **52e** that has two meta-methyl substituents in the terminal phenyl ring. The HDAC8 inhibitory potency of **52e** was restored to the level of ligands **52**, **52a-c**. The strong dependence on the presence of additional substituents in the terminal phenyl ring is consistent with the "upside-down" pose where extended interactions with the binding site would be necessary to compensate for the missing interactions between the ZCG and the active site Zn^{2+}. In agreement with the proposed "upside-down" binding pose and the data for esters **52a** and **52b**, potency of the substantially bulkier *t*-butyl ester **52f** is only marginally lower than that of the corresponding methyl ester **52e**. Comparable potency of diazides **52a** and **52b** with dimethyl-substituted **52f** and **52e** indicates that the azide moieties do not form an R-N_3···Zn^{2+} complex if the ligands bind "upside-down"

To confirm that the scaffold containing the terminal phenyl ring with two lipophilic meta substituents is, indeed, a universal feature responsible for activity, we synthesized and tested methyl ester derivatives of the diazide probes **53** and **54**.[7] Both **53** and **54** are nanomolar inhibitors of HDAC8. In these ligands the SBG contains a pyrazole or an isoxazole moiety, respectively, as well as the *meta*-azido and *meta*-methyleneazido

substituted phenyl ring. Consistently with the "upside-down" hypothesis, both esters **53a** and **54a** were found to inhibit HDAC8 with IC_{50} of 36.0 μM and 47.1 μM, respectively, which is comparable to the potency of compounds in series **52**. Relatively small difference in potency of **53a** and **54a** and similar compounds in series **52** is consistent with the binding pose of the ligands without ZCG (Figure 31). The terminal phenyl ring of **53a** and **54a** is completely immersed in the binding site whereas the pyrazole and the isoxazole portions of **53a** and **54a**, respectively, are only partially enclosed in the binding site but otherwise are solvent exposed.

3.3.3 Photoaffinity labeling studies

Next, we performed a series of photolabeling experiments with purified recombinant HDAC8 to further delineate the putative binding modes of the probes. In all the photolabeling experiments, the concentration of purified HDAC8 used was 0.5 μM, and all the experiments were performed in non-denaturing conditions unless otherwise stated. The probe or probe/competitor mixtures were preincubated with purified recombinant HDAC8 from E.coli[188], in photolabeling buffer for 3 h at room temperature, exposed to 254 nm UV light for 3×1 min with 1 min resting. In case of denaturation experiments, after photo irradiation a solution of sodium dodecyl sulphate was added to attain a final concentration of 2% w/v and the mixture incubated at 37 °C for 30 min. In all photolabeling experiments an alkyne containing biotin tag[177] was attached to the HDAC8-probe adduct using Cu(I) catalyzed (3+2) cycloaddition reaction carried out at room temperature for 1 h. The biotinylated HDAC8 was visualized by streptavidin-HRP

and western blot and the loading was confirmed by using anti-HDAC8 antibody. The control wells contained purified HDAC8, a mixture of HDAC8 and the biotin tag, or a mixture of HDAC8 and the probes used in the photolabeling experiments with click reagents. The click reagents in all the experiments are TCEP (500 μM), TBTA (100 μM), $CuSO_4$ (1000 μM).[177]

Our photolabeling studies required probes able to differentiate between the "normal" and the hypothesized "upside-down" poses leading us to design and synthesis of two additional probes **52g** and **52h**. We envisioned that after crosslinking both the probes **52g** and **52h** would still be detectable by the Strep-HRP antibody if they bind "upside-down" and their alkyl azide groups point toward the solvent and can react with the alkyne-containing biotin tag via (3+2) cycloaddition (Figure 33) If **52g** and **52h** bind with their ester group near the zinc atom of HDAC8 then the alkyl-azido ester group would be hidden in the binding site, and these ligands are not expected to react with the alkyne moiety of the biotin tag and the resulting adducts should not be recognized by the Strep-HRP antibody.

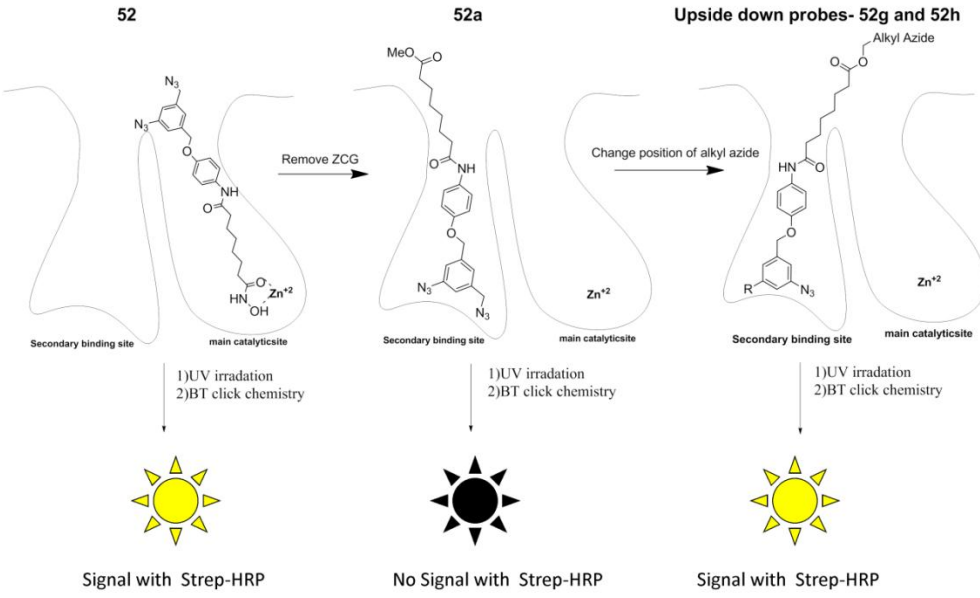

Figure 33. Proposed binding mode of probes **52**, **52a**, **52g** and **52h** in the HDAC8 binding site.

In agreement with the already established SAR, the effect of different ester groups on potency was marginal, and **52g** and **52h** inhibited HDAC8 with IC_{50} of 67.4 and 28.9 uM, respectively. We found that similarly to the probe **52**,[177] probes **52g** (not shown) and **52h** produce a dose-dependent increase in biotinylation of HDAC8 (Figure 34A). Next, we compared the dose-dependent increase in biotinylation for ligands **52**, **52a**, and **52g** (Figure 34B). It was expected that ligands **52** and **52g** would produce a pronounced dose-dependent biotinylation increase, whereas **52a** would not. Consistently with the binding mode proposed, probe **52a** gave only a very low non-specific biotinylation, whereas **52** and **52g** gave the pronounced dose-dependent biotinylation of HDAC8. To rule out the possibility of probe **52a** binding to the main catalytic site, a competition experiment was

carried out at equimolar concentration of 85-fold more potent SAHA. The presence of an equimolar concentration of SAHA did not result in decrease in the biotinylation signal produced by **52a** (Figure 34C), suggesting **52a** does not bind to the main catalytic site and produces only non-specific biotinylation under non-denaturing conditions. A comparison of the biotinylated bands corresponding to the HDAC8 adducts with **52** and **52g** provided further evidence for a novel binding mode of our non-ZCG probes. Specifically, probe **52g**, which is at least 9-fold less potent than probe **52**, gave much higher biotinylation than **52** at the same concentrations of both these probes (Figure 34B). Although the efficiency of the (3+2) cycloaddition and the biotinylation response may depend on the geometry of the moiety bearing the azido group and its accessibility, this observation clearly indicates that the preferable binding mode of **52g** is such that its azido group is exposed to the solvent, is accessible for the (3+2) cycloaddition reaction, and the resulting biotin-containing adduct is available for recognition by the Strep-HRP.

We envisioned that denaturing the protein prior to initiating the (3+2) cycloaddition reaction in case of probe **52a** may expose the alkyl azide, which was previously buried inside the secondary binding site, thus making it more accessible for the (3+2) cycloaddition reaction. Photolabeling of HDAC8 with probe **52a** followed by reaction with the biotin tag resulted in much higher biotinylation under denaturing conditions as compared to non-denaturing conditions as shown in Figure 34D. To further confirm that the biotinylation produced **52a** under denaturing conditions is primarily due to interaction of the probe with the binding site of HDAC8, we performed a series of competition experiments between probe **52a** and potent inhibitors SAHA, TSA, PCI34051 and ligand

52e (Figure 34E). All of the competitors exhibited a pronounced decrease in biotinylation of HDAC8 by **52a**. Interestingly, despite 100-1000 fold difference in potency (Table), the competing ligands completely decreased the biotinylation of HDAC8 only at very high concentrations (low concentrations are not shown), suggesting that the binding of SAHA, TSA and PCI34051 to the main catalytic site only partially obstructs the binding of probe **52a** to the secondary binding site. We observed that at 50-fold molar excess **52e** also decreased the biotinylation of HDAC8 produced by **52a** in a manner comparable to competition with SAHA, TSA, and PCI34051. Considering the remarkable difference in potency between **52e** and the latter HDAC inhibitors, the outcome of this photolabeling experiment appears to strongly indicate that the binding mode of **52a** and **52e** differs from that of the ligands that have ZCG.

Next, we investigated if probe **52h** can be competed by SAHA, TSA, PCI34051, and **52e** under non denaturing conditions. We observed that similar to probe **52a**, probe **52h** could be competed out by SAHA, TSA or PCI34051 at 25-50-fold molar excess concentrations as indicated in Figure 34F. The decrease in biotinylation of HDAC8 observed with **52** and SAHA at 0.25 μM and 2.5 μM (Figure 34G) is strikingly more pronounced than that observed for **52h**: SAHA/TSA/PCI34051 for both 37.5 μM and 75 μM of these ligands. These observations suggest that unlike the hydroxamate containing probe **52**, which probably binds primarily to the main catalytic site, probe **52h** is likely to bind to a secondary binding site where it's binding is only partially obstructed by the ligands binding to the main catalytic site such as SAHA, TSA or PCI34051. This is consistent with the experiments conducted with **52a** under denaturing conditions. We also

observed that ligand **52e** is able to compete out probe **52h** (Figure 34H). Due to relatively low potency of **52e** and low solubility the competition is less pronounced than in the case of SAHA, TSA, and PCI34051. These results further support our hypothesis that the binding of **52h** and other non-hydroxamate inhibitors in Table occurs to the secondary binding site as shown in Figure 32. With **52h** and other probes in this series, we could only conduct the photolabeling studies since the kinetics experiments would require concentrations of the inhibitors at which they were not soluble.

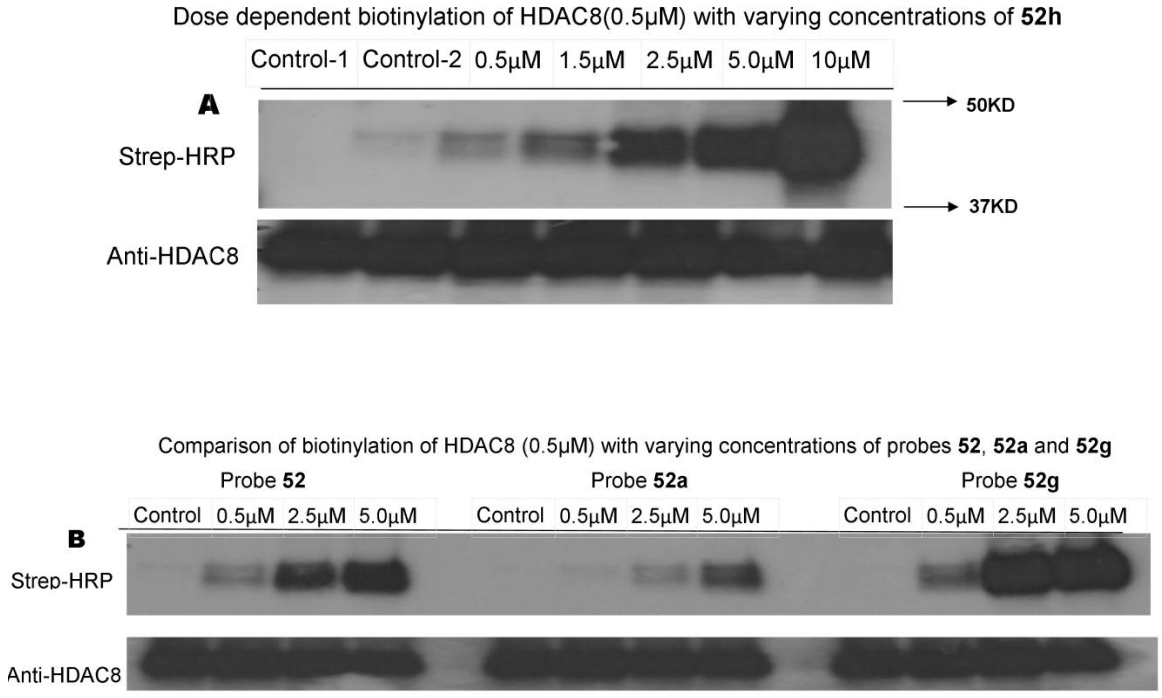

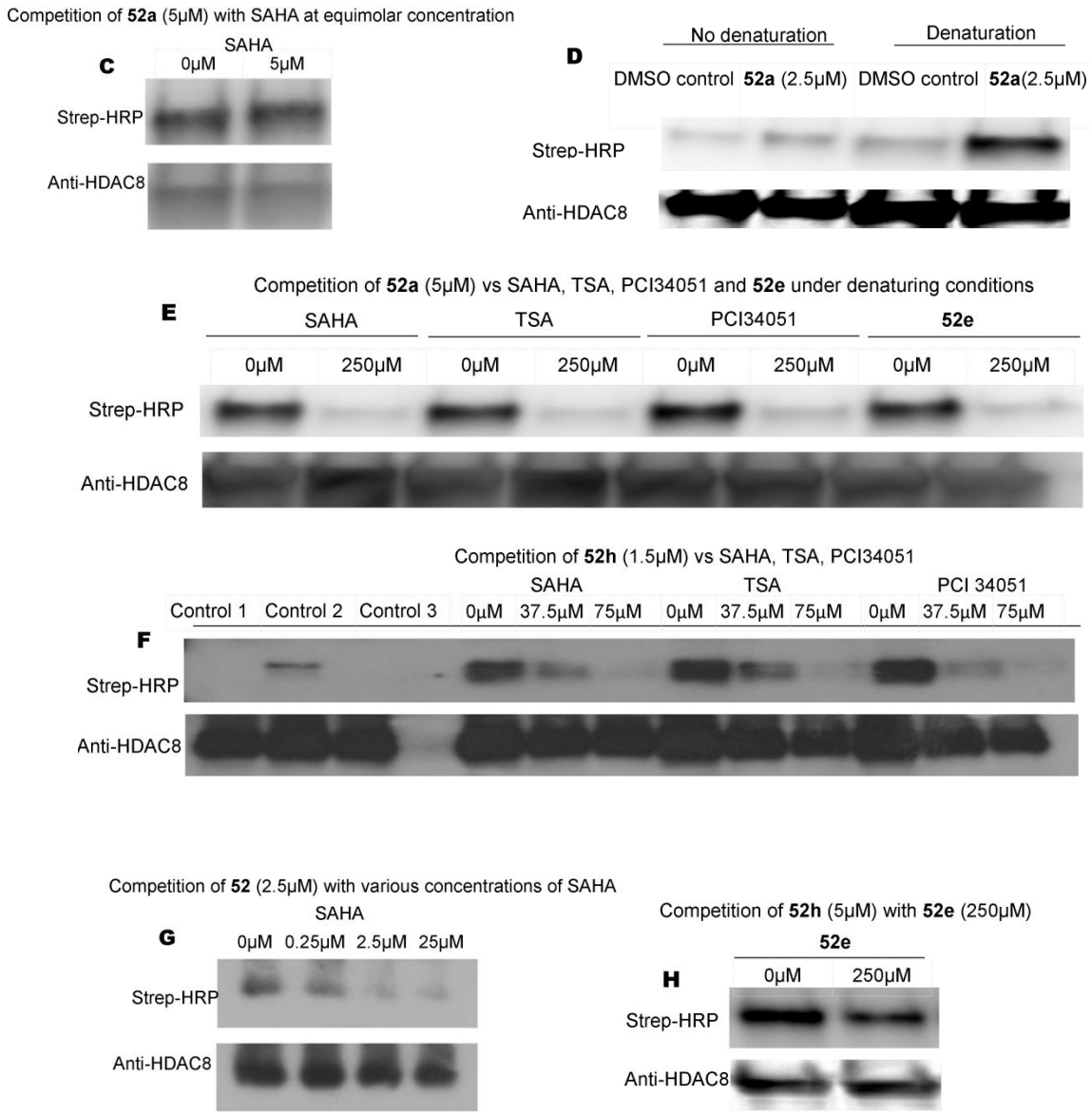

Figure 34. Photoaffinity labeling studies with the upside down probes with HDAC8. Characterization of biotinylated HDAC8 protein and total HDAC8 protein. (A) Western blot analysis of probe 52h binding to HDAC8 using Strep-HRP and anti-HDAC8 antibodies, control 1-HDAC8 (0.5 μM), click reagents, control 2-HDAC8 (0.5 μM), biotin tag (50 μM), click reagents, all other lanes contain different concentration (indicated) of 52h, biotin tag (50 μM), click reagents. (B) Western blot analysis of probes 52, 52a, 52g binding to HDAC8 using Strep-HRP and anti-HDAC8 antibodies, control - HDAC8 (0.5 μM), biotin tag (50 μM), click reagents, all other lanes contain different probes at concentrations indicated, biotin tag (50 μM), click reagents. (C) Western blot analysis of probe 52a binding to HDAC8 in presence and absence of equimolar concentration of SAHA. (D) Western blot analysis of probe 52a binding to HDAC8 under denaturing conditions and non-denaturing conditions. (E) Western blot analysis of probe 52a binding to HDAC8 in presence and absence of an excess of HDAC8 inhibitors

SAHA, TSA, PCI34051 and ligand 52e. (F) Western blot analysis of probe 52h binding to HDAC8 in presence and absence of an excess of HDAC8 inhibitors SAHA, TSA and PCI34051, control 1-HDAC8 (0.5 μM), click reagents, control 2-HDAC8 (0.5 μM), biotin tag (50 μM), click reagents, control 3-HDAC8 (0.5 μM), probe (1.5 μM), click reagents, all other lanes contain different inhibitors of HDAC8 at concentrations indicated, probe 52h (1.5 μM), biotin tag (50 μM), click reagents. (G) Western blot analysis of binding of probe 52 in presence of varying concentrations of SAHA. (H) Western blot analysis of binding of probe 52h in presence and absence of excess of ligand 52e. Click reagents in all experiments are TCEP (500 μM), TBTA (100 μM), $CuSO_4$ (1000 μM). Shown are representative blots of two or more independent experiments.

3.3.4 Monitoring H4 and α-tubulin acetylation in SH-SY5Y cells.

To obtain a preliminary selectivity profile for other HDAC class I isoform, we measured the inhibition of recombinant HDAC1, 2, and 3 by probes **52g** and **52h.** We also assessed inhibitory effect of probe **52h** on the cytoplasmic HDAC6, a representative class II HDAC isoform, vs. nuclear class I HDACs by monitoring the acetylation status of α-tubulin and histone H4 in SH-SY5Y cells, respectively. Neither **52g** nor **52h** inhibited HDAC3 at concentrations up to 66 μM, whereas HDAC1 and HDAC2 were inhibited by these ligands with IC_{50} of 111 and 72 μM and 86 and 79 μM, respectively. The binding modes of these ligands in HDAC1 and 2 are currently being investigated. Probe **52h** showed a dose dependent increase in acetylation status of histone H4 after a 24 h treatment (Figure 35A). Unlike the HDAC6 selective compound **73**,[189] probe **52h** did not inhibit the deacetylation of α-tubulin, suggesting that **52h** targets only nuclear class I HDACs.(Figure 35B)

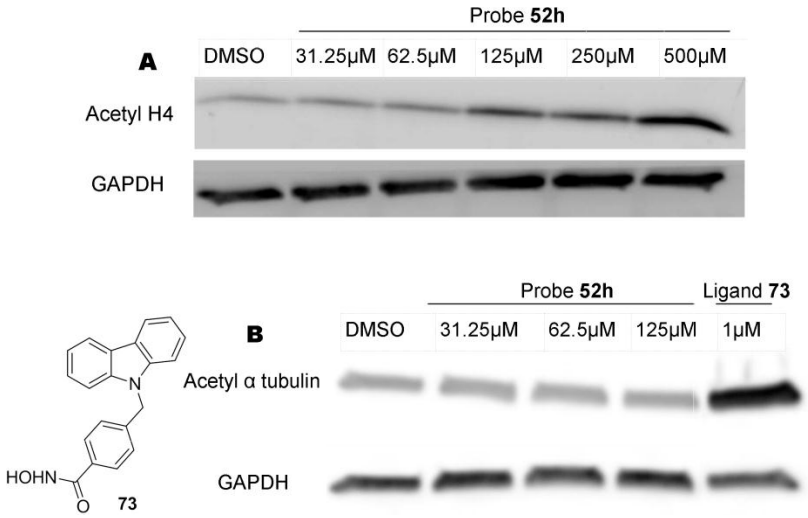

Figure 35 Monitoring acetylation status of H4 and alpha tubulin in SH-SY5Y cells upon treatment with probe **52h** and ligand **73**
(A) Western blot detection of acetylation of histone H4 following a 24 h treatment with probe **52h** in SH-SY5Y cells.(B) Western blot detection of acetylation of α tubulin following a 24 h treatment with probe **52h** and ligand **73** in SH-SY5Y cells Shown is a representative blot of two or more independent experiments.

3.4 Conclusions.

In summary, we demonstrated that HDAC8 enzymatic activity can be inhibited by compounds that lack an active site Zn^{2+} bidentate chelating group. Although the structure and activity require further optimization, multiple lines of evidence presented in the study indicate that the ligands **52a**, **52b**, **52e-52h**, **53a**, and **54a** have binding modes different from those of the parent compounds **52**, **53**, and **54** and are likely to be positioned "upside-down" in the secondary binding site proximal to the main catalytic site. One of the most potent "upside-down" inhibitors **52h** was shown to increase acetylation of H4

but not α tubulin in SH-SY5Y cells. Studies to expand the SAR presented in the paper, to elucidate the key pharmacophore and auxophore portions, to improve the HDAC8 inhibition and selectivity, and to co-crystallize HDAC8 with the “upside-down” ligands are now in progress.

CHAPTER 4. DESIGN, SYNTHESIS, MODELING, BIOLOGICAL EVALUATION AND PHOTOAFFINITY LABELING STUDIES OF NOVEL SERIES OF PHOTOREACTIVE BENZAMIDE PROBES FOR HISTONE DEACETYLASE 2

4.1 Introduction

Recently, Cravatt et al.[120] and Gottesfeld et al.[141] described the design and applications of photoaffinity probes for profiling HDACs in native proteomes and live cells.[120, 141] The scaffold of the probes included a portion of a pan HDAC inhibitor suberoylanilide hydroxamic acid (SAHA), a benzophenone group as a photoreactive group, and an alkyne handle to attach an azide containing reporter tag via (3+2) cycloaddition. Attempts to use the same features based on HDAC1 and 2 selective benzamide scaffolds resulted in probes with HDAC potency above 180 μM in HeLa cell nuclear lysate.[140]

We have already established the Binding (E) nsemble (Pro) filing with (F) photoaffinity (L) abeling approach (BEProFL) where we have experimentally mapped the multiple binding modes of diazide-based photoreactive probes for HDACs.[144 144]The design of these probes included decoration of HDAC ligands with a 3-azido-5-azidomethylene moiety, a photoaffinity labeling group originally proposed by Suzuki et al.[143] for specific labeling of the catalytic portion of HMG-CoA reductase. The aromatic azido moiety was used as a photoreactive group and the aliphatic azide was well suited for (3+2) cycloaddition with an alkyne moiety of the biotin-containing reporter group. Based on these features, we have successfully designed and synthesized highly potent and selective probes for HDAC3 and HDAC8 and demonstrated they are cell permeable and exhibit excellent antiproliferative activity against several cancer cell lines.[48] *The*

main purpose of this study was to design photoreactive benzamide probes for HDAC2 and evaluate their activity/selectivity profile for other class I HDAC isoforms.

We hypothesized that a set of potent and selective benzamide-based probes capable of crosslinking with HDAC2 can be designed by appropriately decorating benzamides **8** and **75** (Figure 36) with a combination of the aryl and alkyl azides. Both **8** and **75** and their derivatives were reported by Delorme[190], Miller[43], Gangloff[21], and their colleagues to be active and selective inhibitors of HDACs1 and 2.

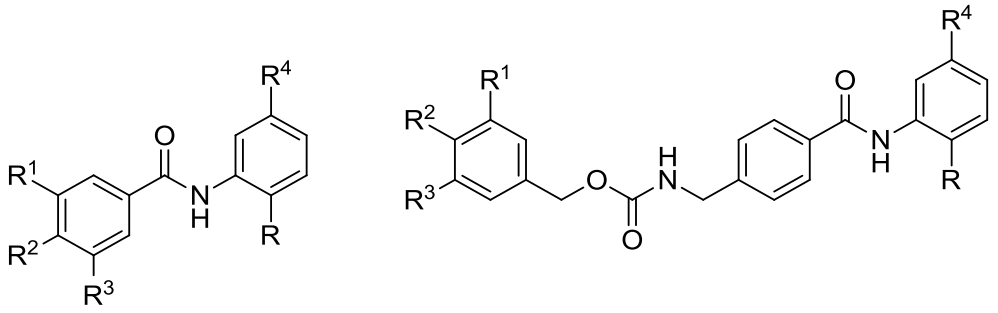

8, R^1 = H, R^2 =H, R^3 =H, R^4 =Ph, R=NH_2 **75**, R^1 = H, R^2 =H, R^3 =H, R^4 =Ph, R=NH_2

Figure 36. Benzamide inhibitors of HDAC1 and 2

4.2 Materials and methods

4.2.1 Synthesis

All chemicals and reagents were purchased from Sigma Aldrich (St. Louis, MO), TCI America and Fischer Scientific and used as received unless otherwise stated. All synthesized compounds were characterized by ^{1}H NMR, ^{13}C NMR and HRMS included for final compounds/probes. Full synthetic methodologies are described in Appendix A. Compound Characterization Spectra are presented in Appendix B.

4.2.2 HDAC activity assays

HDAC inhibition assay was performed in 96-well opaque half-area microplate (Corning). Human recombinant HDAC1, 2 and 3 (BPS Bioscience) and HDAC8(Biomol Inc.) were diluted with assay buffer 1 (25 mM Tris-HCl, pH 8.0, 137 mM NaCl, 2.7 mM KCl, 1 mM $MgCl_2$, and 1 mg/mL BSA), so as to have 4 ng/µl, 5 ng/µl and 1 ng/µl and 8.5 ng/µL stocks of each isoform respectively. Serial dilutions of the probes were made in assay buffer 2 (25 mM Tris-HCl, pH 8.0, 137 mM NaCl, 2.7 mM KCl, 1 mM $MgCl_2$).10 µL of the enzyme stock was added to 30 µL of the probes and preincubated for different times. It was observed the Z-factor for the assays remained above 0.7 up to 3 h for HDAC1, 3 and 8 and up to 24 h for HDAC2, hence these preincubation times were chosen for the assays. After preincubation, 10 µL of 125 µM HDAC fluorescent substrate Boc-L-Lys (Ac)-AMC (Chem-Impex) in case of HDAC1, 2 and 3 and 10 µL of 25 µM BML-KI-178(Biomol Inc.) in case of HDAC8 was added, and the mixture incubated for 35 min (HDAC1, 3, 8), 60 min (HDAC2) at room temperature. The reaction was quenched with

50 μL of 1 mg/mL trypsin and 5 μM trichostatin A in assay buffer 1 (25 mM Tris-HCl, pH 8.0, 137 mM NaCl, 2.7 mM KCl, 1 mM $MgCl_2$) and further incubated at room temperature for 35 min. The plate was read on Synergy 4 hybrid microplate reader (BioTeck) at excitation wavelength 360 nm and emission wavelength 460 nm. The IC_{50} values were determined using the GraphPad Prism 5 software (GraphPad Software Inc., La Jolla, CA). The IC_{50} determination of the probes for HDAC2 were conducted by myself, for HDAC1 and 3 were conducted by and Mr. Hazem Abdelkarim and for HDAC8 by Ms. Antonett Madriaga.

4.2.3 Photolabeling protocol

Diazide probe (25 μM) or probe-TSA (25 μM-probe and 125 μM-TSA) mixture was incubated with HDAC2 (1.25 μM) for 24 h in photolabelling buffer (25 mM Tris-HCl, pH 8.0, 137 mM NaCl, 2.7 mM KCl, 1 mM $MgCl_2$, 0.1% Triton-X), exposed to 254 nm UV light 3×1 min with 1 min resting. 500 μM of DBCO-PEG4-biotin conjugate(Click Chemistry tools) in photolabeling buffer was added to initiate the [3+2] cycloaddition reaction with HDAC2-probe adduct.The cycloaddition reaction was carried out for 3 h at room temperature. Western blotting was done with 1.5 μg of purified protein with 5X loading buffer containing 10% SDS, 0.05% bromophenol blue, 50% glycerol, and β-mercaptoethanol. Protein samples were boiled for 5 min and allowed to cool before loading on a denaturing 4-15% polyacrylamide gel electrophoresis (SDS PAGE). After electrophoresis, protein was transferred to a polyvinylidiene difluoride membrane (Iblot-Invitrogen).The membrane was incubated for 12 h with 5% albumin fraction V (Sigma-

aldrich) in 1X Tris-based saline supplemented with 0.1% Tween-20 (TBS-T). The membrane was washed three times with TBST and then incubated with Ni-HRP (1:2000) in TBST for 1 h under room temperature with slight agitation. After three washes in TBS-T, the chemilumiscent signal was detected using the enhanced chemiluminescence (ECL) kit from Pierce (Pierce Biotechnology, Rockford, IL). The membrane was washed three times with 1X phosphate buffer saline supplemented 0.1% Tween-20 (PBS-T), and stripped of Ni-HRP by incubating with 5% BSA, 2M Imidazole in PBST for 1h at room temperature. After three washes of PBST, the membrane was incubated with Streptavidin-HRP (1:5000) in PBST for 1h. After three washes in PBST and water, the chemilumiscent signal was detected using the enhanced chemiluminescence (ECL) kit from Pierce (Pierce Biotechnology, Rockford, IL)

4.2.4 Molecular modeling studies

The analysis of SAR was facilitated by docking all the probes to HDAC2 (PDB:3MAX),[191] HDAC3 (PDB:4A69),[192] and HDAC8 (PDB: 1T69)[25] using GOLD v.5.1.[184, 193]

4.2.5 Cell culture and western blot protocol

MDA-MB-231 cells seeded at 1.0 x 10^5 cells/well in 6-plates and grown to 90% confluence in DMEM (Gibco) supplemented with 10% FBS (Gibco) and 1% penicillin-streptomycin (Mediatech). Cells were treated with either DMSO or benzamide probes at a final concentration of 50 μM and maintained at 37°C and 5% CO_2 for 24 h. Cells were lysed using 1X RIPA buffer (150 mM NaCl, 1% Triton X-100, 0.5% sodium

deoxycholate, 0.1% SDS, 50 mM Tris, pH 8.0) containing protease inhibitor cocktail (Roche) and 1:100 dilution of phosphatase inhibitor (Sigma) with shearing. Lysates were clarified through centrifugation at 13,000 rpm at 4°C. Total protein concentration was determined via the BCA Protein Assay Kit (Pierce). Lysates were stored at -20°C until later use. Sample vials were prepared by aliquoting 25 µg of total protein and adding 5X Sample Buffer. Sample vials were boiled for 5 min, cooled to room temperature, and proteins separated by gel electrophoresis at 80 V. Proteins in the gel were transferred to PVDF membrane in 4 min using the Invitrogen iBlot system. Membranes were blocked using 5% Milk in PBST and probed using anti-GAPDH (1:5000) or anti-acetyl histone H4 (1:1000) overnight at 4 °C. Membranes were incubated with either anti-mouse (1:5000) or anti-rabbit (1:5000) in 5% Milk in PBST. Results were visualized using Femto chemiluminescent substrate (Pierce) in CCD camera.

4.3 Results and Discussion

4.3.1 Synthesis

Substituted benzoic acids **76-81**, mono-N-Boc protected phenylenediamines **82**, **83** and azidoaniline **84** shown in Figure 37 were chosen as precursors for the synthesis of the photoreactive probes.

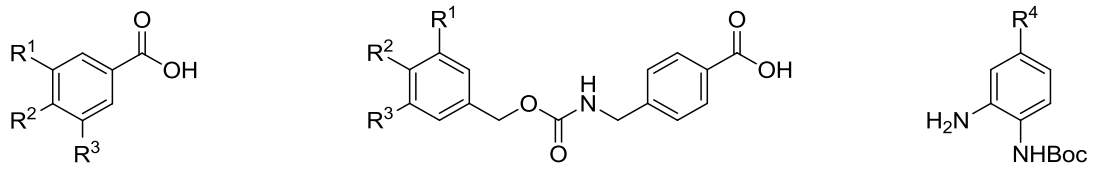

76, R^1 = H, R^2 = N_3, R^3 = H
77, R^1 = N_3, R^2 = H, R^3 = CH_2N_3
78, R^1 = N_3, R^2 = -$O(CH_2)_2N_3$ H, R^3 = H
79, R^1 = H, R^2 = $NHCO(CH_2)_2N_3$, R^3 = H

80, R^1 = N_3, R^2 = H, R^3 = H
81, R^1 = N_3, R^2 = H, R^3 = CH_2N_3

82, R^4 = Ph
83, R^4 = 2-thiophenyl
84, R^4 = N_3

Figure 37. Amine and acid precursors used for synthesis of photoreactive probes

The synthesis of diazide acid **77** and diazide alcohol **92** was a joint effort between myself and Dr. Raghupathi Neelarapu and is outlined in scheme 6 below. Dimethyl 5-aminoisopthalate, **93** was a common precursor for both intermediates **77** and **92**. Regioselective reduction of ester, **93** to alcohol, **96** was carried out with lithium borohydride in THF at refluxing temperature, while lithium aluminum hydride was used to reduce the ester to the diol **94**. The aryl amine functionality in intermediate **96** and **94** was converted into corresponding azides with the help of *t*-buONO and $TMSN_3$ at low temperatures in acetonitrile. The advantage of using *t*-buONO and $TMSN_3$ combination over sodium nitrite and sodium azide in aqueous acidic conditions is the circumvention of aqueous workup. Due to the high polarity of intermediates like **95** or **97**, aqueous extraction may be particularly tedious and may lead to losses while extraction from the aqueous phase, hence reaction strategies that circumvent aqueous work up may be particularly useful. A one pot, two step strategy allowed the facile conversion of **97** to **98** and **95** to **92** using bis (2,4 dichlorophenyl) chlorophosphate, which activates the alcohol

precursors in situ via formation a phosphate ester intermediate, which subsequently undergoes a nucleophilic substitution reaction in presence of sodium azide. The final step in the synthesis of acid **77** is the basic hydrolysis of ester **98**. Detailed procedures and characterization of the above mentioned intermediates are reported by us previously.[48]

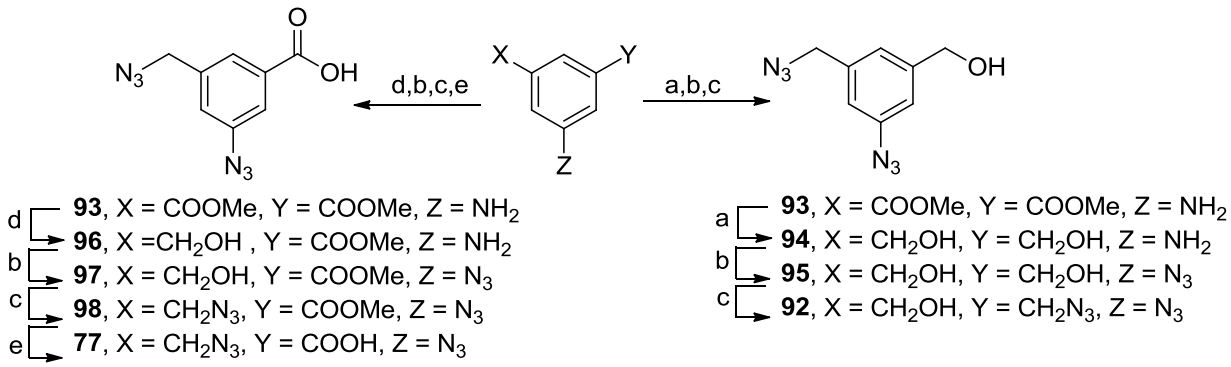

Scheme 6. Synthesis of diazide intermediates 77 and 92
Reagents and Conditions.(a) $LiAlH_4$, THF, 5 h, 0 °C- rt, 90%; (b) t-BuONO,$TMSN_3$, 8 h, 0 °C - rt, 90%; (c) Bis (2,4 dichlorophenyl) chlorophosphate, DMAP, NaN_3, THF 5 h, rt, 80-90%; (d) $LiBH_4$, THF, 5 h, 0 °C- rt, 70%; (e) THF/H2O (1:1), KOH, 10 h, 70 °C, 88%.

The N-boc protected phenylenediamines **82** and **83** were synthesized according to Scheme 7. Commercially available 4-bromo-2-nitro-aniline was subjected to Boc protection with stoichiometric quantities of Boc anhydride and sodium hydride in anhydrous DMF at low temperatures to get quantitative yields of Boc protected intermediate **99**. It was observed that excess equivalents of sodium hydride, Boc

anhydride or higher temperatures lead to exclusive formation of a diboc protected product **100** instead of a required mono-Boc protected intermediate **99**. In the event of formation of a diboc product **100**, it was also observed that the required intermediate **99** could be obtained by treatment of **100** with an aqueous solution of 2N sodium hydroxide at 65°C overnight.[194] Intermediate **99** was subjected to Suzuki coupling conditions with 2-thienyl boronic acid or phenyl boronic acid with tetrakis triphenyl phosphine palladium zero as a catalyst in presence of potassium carbonate as base, with anhydrous tetrahydrofuran as a solvent in a sealed pressure vessel at 85 °C to afford intermediates **101** and **102** in high yields. The nitro derivatives **101** and **102** were reduced into the required amino derivatives **82** and **83** using zinc, ammonium formate as a reducing agent. Zinc/ammonium formate reduction offers several advantages over Pt or Pd catalyzed hydrogenation reactions namely (1) economic feasibility; (2) prevents use of high pressure apparatus such as a parr shaker; (3) Fast reaction times; (4) minimum workup and (5) compatible with several reducible functionalities such as halogens, nitriles, amides.[195] The carbamate linkage in acids **80** and **81** was installed using carbonyl diimidazole as a coupling agent, 1,8 diazabicycloundec-7-ene as base and intermediates **91**, **92** and 4-(aminomethyl) benzoic acid. [196]Detailed synthetic procedures and characterization can be found in Appendix A and B.

Azido intermediate, **91** was synthesized by diazotization-azidation of aryl amine **103** using sodium nitrite, sodium azide in acidic conditions as per published procedures.[197] The intermediate **91** was used in further reactions without any purification.

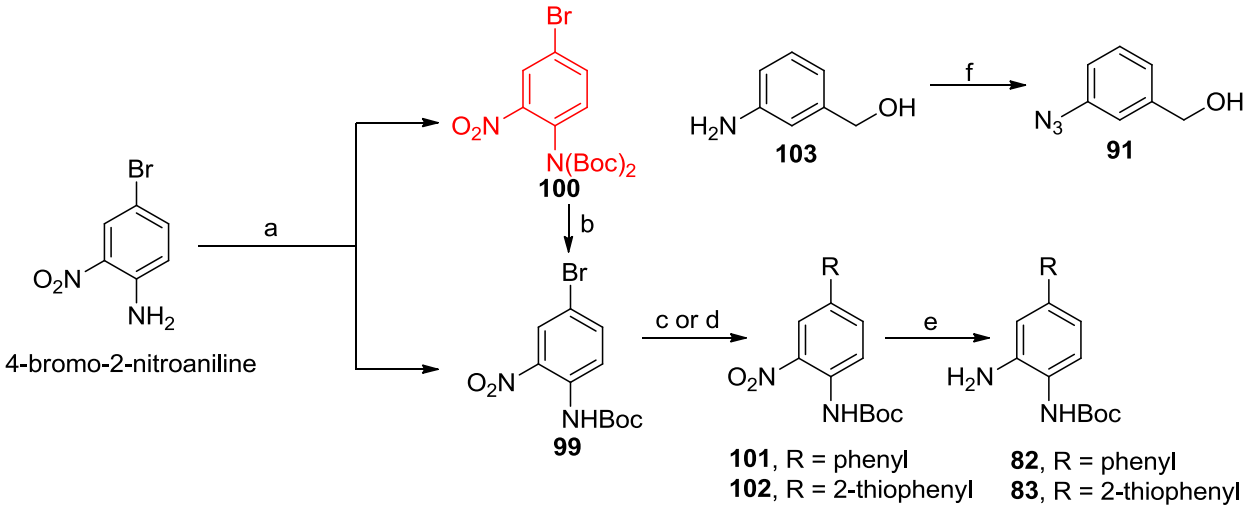

Scheme 7. Synthesis of mono-Boc protected phenylendiaamines
Reagents and Conditions (a) $Boc_2(O)$, NaH, DMF, 12 h, 0°C-rt, 95%; (b) 2N NaOH, ,12 h, 65°C quantitative yield; (c) phenyl boronic acid, $Pd(PPh_3)_4$, K_2CO_3, THF, 12 h, reflux, 92%; (d)) 2-thiophenyl boronic acid, $Pd(PPh_3)_4$, K_2CO_3, THF, 12 h, reflux, 95%; (e) Zinc dust, ammonium formate, MeOH, 15 min, rt, 90%; (f) $NaNO_2$, NaN_3, 10% HCl, 3 h, 0-rt, 92%.

The synthesis of acid probe **78** is outlined in Scheme 8. Commercially available 3-amino-4-hydroxy benzoic acid, **85** was subjected to diazotization azidation using sodium nitrite, sodium azide in acidic aqueous conditions to yield azido intermediate **86** in high yields. Intermediate **86** was subjected to esterification using thionyl chloride and methanol to yield the methyl ester **87**. Intermediate **87** was subjected to O-alkylation using 2-azidoethyl-4-methylbenzene sulphonate as an alkylating agent and potassium carbonate as a base in refluxing acetone to yield intermediate **88**. The final step towards the synthesis of acid **78** was the basic hydrolysis of ester, **88** using aqueous potassium hydroxide. Detailed procedures and compound characterization are provided in Appendix

A and B. The synthesis of intermediates **84**, **79** and probe **8g** was carried out by Dr. Bhargava Karumudi and is outlined in Scheme 8 shown in subsequent sections.

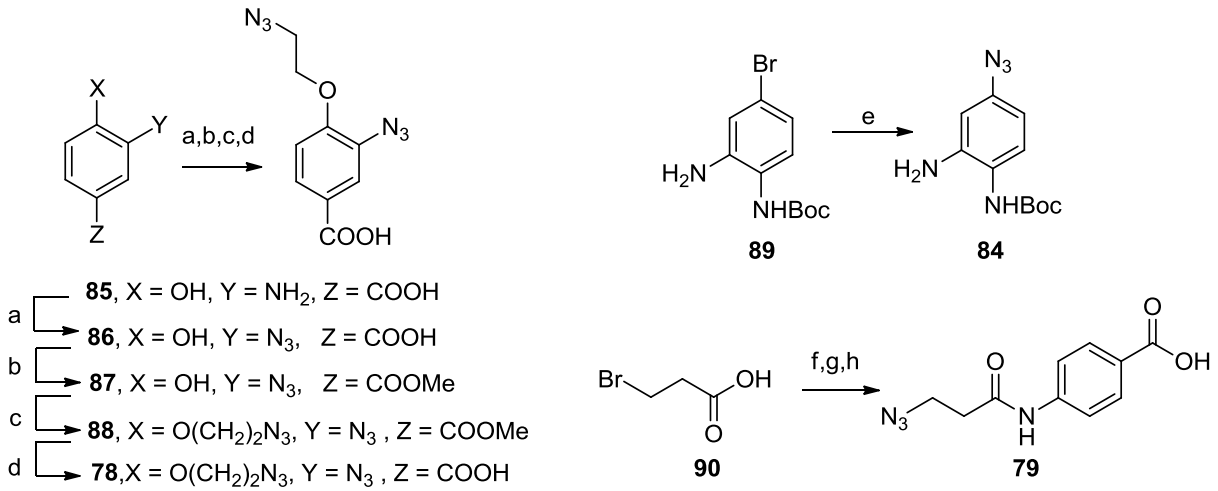

Scheme 8. Synthesis of diazide intermediate 78 and monoazide intermediates 84 and 79 Reagents and conditions: (a) $NaNO_2$, HCl, NaN_3, 5 h, 0 °C- rt, 85%; (b) $SOCl_2$, MeOH, 8 h, 0 °C - rt, 87%; (c) K_2CO_3, 2-azidoethyl-4-methylbenzene sulphonate, acetone, 5 h, reflux, 77%; (d) THF/H_2O (1:1), KOH, 10 h, 70 °C, 92%; (e) NaN_3, Sod. ascorbate, CuI, N,N-dimethylethane-1,2-diamine, EtOH/H_2O, reflux, 92%; (f) i: NaN_3, CH_3CN, reflux, 80% ; ii: oxalyl chloride, DCM, 6 h; (g) methyl 4-aminobenzoate, Pyridine, DCM, 0 °C-rt, 86% ; (h) 2N NaOH, THF/H_2O (8:2), 2 h, rt, 93%.

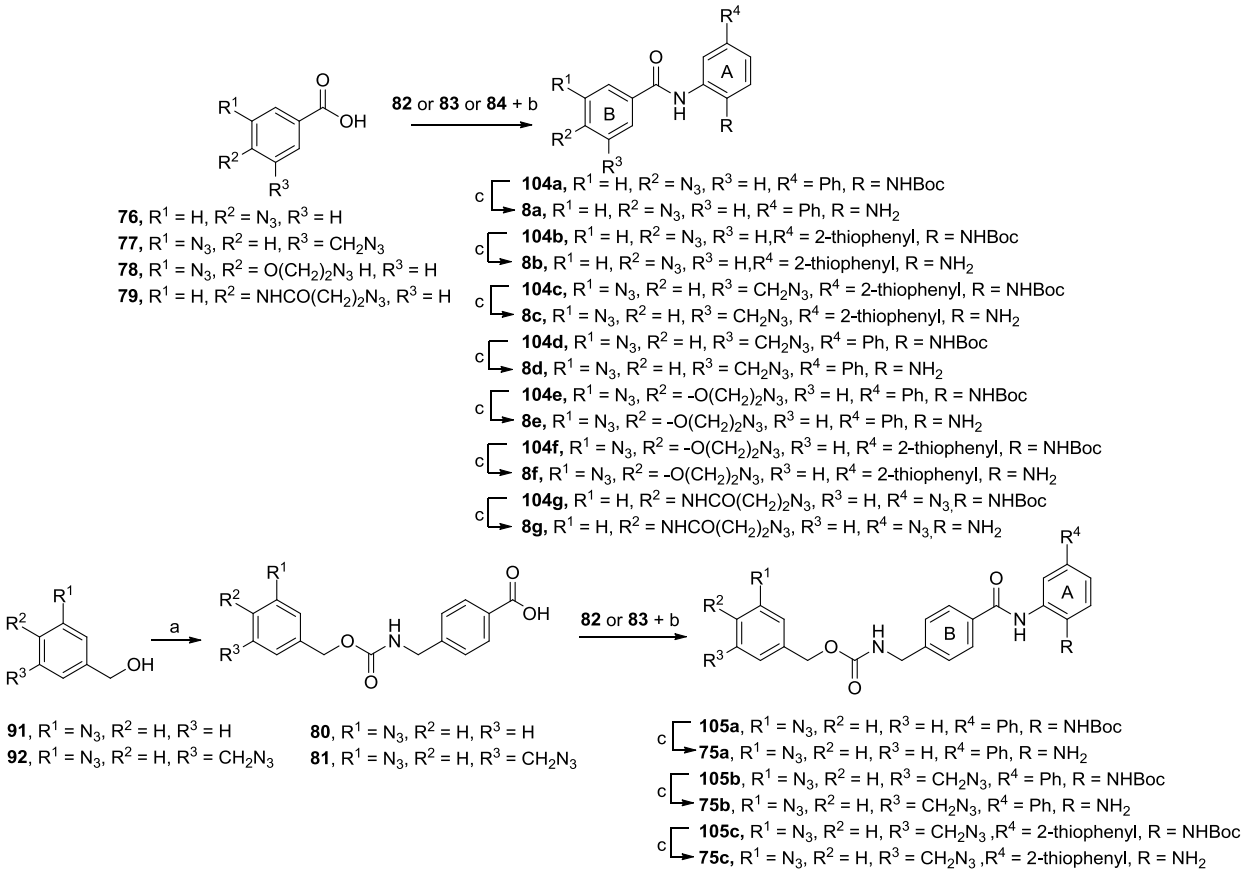

Scheme 9. Synthesis of monoazide and diazide-based benzamide probes.
Reagents and conditions: (a) CDI, DBU, TEA, 4-(aminomethyl)benzoic acid, THF, 10 h, 0 °C - rt, 90-92%; (b) EDCI, HOBt, DMF, 12 h, 80 °C, 80-90%; (c) TFA/DCM, 0.5 h, rt, 90-95%.

The synthesis of the probes **8a-g** and **75a-c** proceeded through an efficient carbodiimide - based coupling reaction between mono-N-Boc protected phenylendiamines **82-84** and benzoic acids **76-81** followed by deprotection of the resulting N-Boc products to give the final probes in 70-80% overall yield (Scheme 9).

4.3.2 Structure activity trends and docking studies

The inhibitory profile of the probes against class I HDAC isoforms was determined using a fluorogenic assay and the results are given in Table 2. The inhibition of HDAC8 was measured using the fluorogenic acetylated substrate Fluor de Lys and purified recombinant human HDAC8 from E.coli,[188] whereas the inhibition of HDAC1-3 was measured using fluorogenic acetylated substrate Boc- L-Lys(Ac)-AMC and commercially available recombinant human HDAC1-3. We also explored the effect of preincubation with HDAC1, 2, 3, and 8 as it was previously observed that the potency of the benzamide-based HDAC inhibitors increased with preincubation with HDAC1-3.[21, 198] The maximum incubation time was chosen on the basis of stability of HDAC proteins in the conditions used to determine IC_{50} values. We found that for HDAC1, 3, and 8 the maximum incubation time was 3 hours, whereas HDAC2 protein was stable for 24 hours. The IC_{50} values of ligands **8** and **75** determined in this study vary from those reported previously.[21, 43] We attribute this discrepancy to the differences in the assay conditions, the protein sources, substrates, and preincubation times.

All the newly synthesized benzamide-based probes had activity ranging between 70 nM and 55 μM and 110 nM and 77 μM for HDAC1 and HDAC2, respectively. All of the probes demonstrated a robust 2-40-fold increase in inhibition of HDAC1 and 2 upon preincubation with the enzymes for 3 h and 24 h, respectively (Table 3).

#	HDAC1 IC_{50} (nM)		HDAC2 IC_{50} (nM)			HDAC3 %Inhibition (10μM)		HDAC8 %Inhibition (10μM)	
	Preincubation time		Preincubation time			Preincubation time		Preincubation time	
	5 min	3 h	5 min	3 h	24 h	5 min	3 h	5 min	3 h
8a	2100 ± 44	140 ± 34	5130 ± 470	1050 ± 81	210 ± 17	6.6	35	NA	NA
8b	1200 ± 85	70 ± 5.3	3200 ± 260	690 ± 57	110 ± 36	8.7	56	NA	4.7
8c	5600 ± 520	1400 ± 160	18000 ± 910	5200 ± 400	2400 ± 74	2.2	27	NA	11
8d	21000 ± 100	13000 ± 320	32000 ± 1700	21000 ± 720	10000 ± 490	NA	24	NA	14
8e	23000 ± 1400	2700 ± 69	34000 ± 2300	6500 ± 120	830 ± 28	4.3	16	NA	22
8f	18000 ± 130	3800 ± 54	17000 ± 4400	6600 ± 140	750 ± 81	7.6	12	NA	6.6
8g	96000 ± 1600	55000 ± 1300	120000 ± 4900	94000 ± 530	77000 ± 4100	2.0	6.5	NA	26
75a	3800 ± 120	780 ± 22	3800 ± 540	1000 ± 70	320 ± 32	7.8	48	NA	NA
75b	2500 ± 280	990 ± 53	7000 ± 250	1100 ± 25	350 ± 16	11	46	NA	25
75c	2800 ± 240	1210 ± 68	7100 ± 220	1000 ± 50	300 ± 77	21	47	NA	22
8	410 ± 16	52 ± 4.3	1200 ± 93	350 ± 15	140 ± 8	26	96	NA	24
75	14500 ± 1300	1880 ± 5.2	38000 ± 2000	14000 ± 1030	740 ± 49	8.8	40	NA	3.0
SAHA	29 ± 1.6	34 ± 3.2	200 ± 14	ND	260 ± 4.3	100	100	100	100

TABLE II. INHIBITORY PROFILE OF BENZAMIDE PROBES AGAINST CLASS I HDACS. NA- NO INHIBITION UP TO 10 μM, ND- NOT DETERMINED. DATA ARE MEAN± SD OF THREE INDEPENDENT EXPERIMENTS

#	HDAC1 IC_{50} ratio 3 h/5 min	HDAC2 IC_{50} ratio 3 h/5 min	HDAC2 IC_{50} ratio 24 h/5 min	HDAC3 %inhibition ratio 3 h/ 5 min	HDAC2/HDAC1 IC_{50} ratio 3 h/ 3 h	HDAC2/HDAC1 IC_{50} ratio 24 h/ 3 h
8a	15	4.9	24	5.3	7.5	1.5
8b	17	4.6	29	6.4	9.9	1.6
8c	4.0	3.5	7.5	12	3.7	1.7
8d	1.6	1.5	3.2	-	1.6	0.77
8e	8.5	5.2	41	3.7	2.4	0.31
8f	4.7	2.6	23	1.6	1.7	0.20
8g	1.7	1.3	1.6	3.3	1.7	1.4
75a	4.9	3.8	12	6.2	1.3	0.41
75b	2.5	6.4	20	4.2	1.1	0.35
75c	2.3	7.1	24	2.2	0.82	0.25
8	7.9	3.4	8.6	3.7	6.7	2.7
75	7.8	2.7	52	4.5	7.5	0.39
SAHA	0.85	ND	0.77	1.0	ND	7.7

TABLE III. RATIOS OF IC_{50} OF BENZAMIDE PROBES FOR HDAC1, 2 AND 3 WITH RESPECT TO PREINCUBATION TIME AND SELECTIVITY.

Consistent with the previously reported observation,[191] SAHA, a hydroxamate-based inhibitor, did not exhibit time-dependent inhibition. Similar trends were observed with HDAC3 and HDAC8. In the discussion below we will use only IC_{50}'s obtained at the maximum preincubation time, unless specified otherwise.

In general, the probes exhibited better activity and selectivity for HDAC1 and 2 as compared to HDAC3 and HDAC8 (Table 2). The most HDAC1 and 2 potent probe **8b** had an estimated 100- and 1000-fold selectivity for HDAC1 and 2 as compared to HDAC3 and HDAC8, respectively. In the case of HDAC8, no inhibition was observed

after 5 min, whereas inhibition of HDAC3 varied from 2% for **8g** to 21% for **8c** at 10μM After preincubation for 3 h, inhibition of HDAC3 and HDAC8 by the probes varied from 6.5 % for **8g** to 56 % for **8b** and from 4.7% for **8b** to 26 % for **8g**, respectively. Similarly to the probes, ligand **8** showed pronounced inhibition of HDAC3 and HDAC8, 96% and 24%, respectively, and ligand **75** inhibited 40% of activity of HDAC3 and only 3% of activity of HDAC8. Despite the similarity of probes **75a-c**, **75a** did not inhibit HDAC8 at 10 μM, whereas both **75b** and **75c** inhibited 25% and 22% of activity of HDAC8, respectively.

Gangloff et al.[191] suggested that the time-dependent inhibition in the case of HDAC2 may be explained by the gradual disruption of the internal hydrogen bond between the aniline hydrogen and carbonyl oxygen in the unbound form of the ligand so as to form a bidentate complex with Zn^{2+} ion in the bound form. After a preincubation 3 h, increase in inhibition of HDAC1 and HDAC2 by the probes varied from 1.6-fold for **8d** to 17-fold for **8b** and from 1.3-fold for **8g** to 7.1-fold for **75c** respectively (Table 3). After preincubation for 24 h, inhibition of HDAC2 further improved to 1.6-fold for **8g** to 41-fold for **8e**. A comparison of the IC_{50} ratios for 3 h vs. 5 min and 24 h vs. 5 min for HDAC2 (Table 3) shows that the weakest inhibitors **8c**, **8d**, and **8g** exhibit the least pronounced change in their IC_{50} with time. A somewhat similar but less pronounced trend is observed in the case of HDAC1. In general, the trends observed in our case seem to be consistent with the explanation for the time-dependent inhibition given by Gangloff et al.[191] The difference in the time-dependent inhibition by the probes that have the same substituent binding to the "foot pocket", e.g. **8a**, **8d**, **8e, 8a**, and **8b**, at 3 h vs. 5 min and

24 h vs. 5 min suggests that additional factors should be taken into account. Overall ability of the ligands to adopt the necessary conformation for induced fit may play a role in addition to the conformational flexibility of the benzamide portion of the ligands. HDAC1 is highly homologous to HDAC2, and, therefore, its time-dependent inhibition may be explained in a similar fashion. However, neither HDAC3 nor HDAC8 were reported to have crystal structures that would contain a binding pocket similar to the "foot pocket" of HDAC2. The docking of the probes to HDAC2 showed that their binding poses are essentially the same as that of ligand **8**, i.e. the aniline nitrogen and the amide oxygen form a bi-dentate chelate with Zn^{2+}, whereas the bi-aryl portion occupies the "foot pocket"

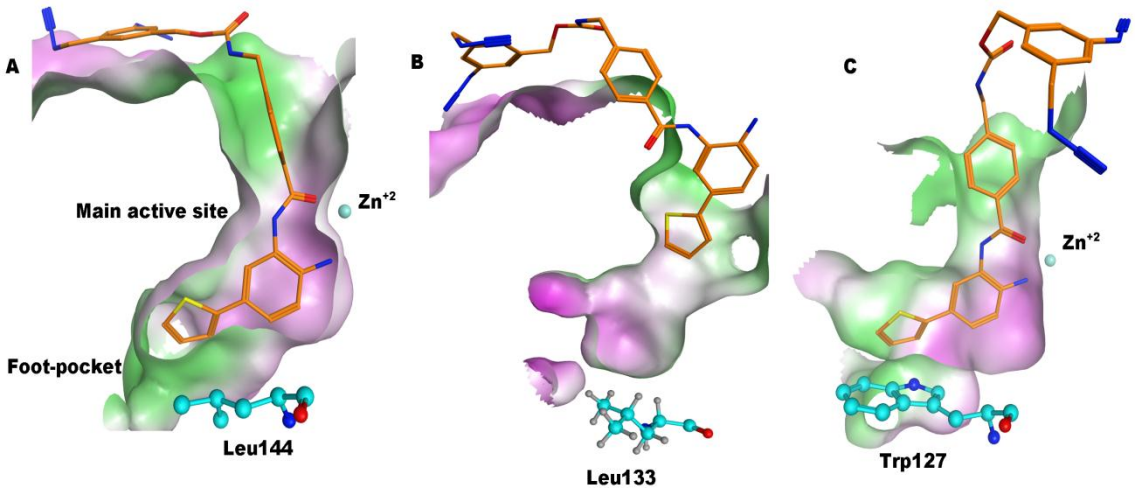

Figure 38. Probe **75c** docked into the active site of (A) HDAC2, (B) HDAC3, and (C) HDAC8.

A comparison of the docking pose of probe **75c** in HDAC2, HDAC3, and HDAC8 shows that, unlike HDAC2 (Figure 38A), HDAC3 (Figure 38B) and HDAC8 (Figure 38C) cannot accommodate **75c** such that it can form a bi-dentate complex with Zn^{2+} in the catalytic site. The binding site of HDAC3 in 4A69 is too small for **75c** and the probe is mostly resides outside the binding site. In HDAC8 in 1T69, the binding site is too short and has a somewhat different shape compared to HDAC2. None of the docking poses of **75c** coordinates with Zn^{2+} despite the proximity of the groups necessary for coordination. After a co-minimization of **75c** with the HDAC8, only coordination between the carbonyl oxygen of **75c** and Zn^{2+} was observed. Interestingly, although the residues in the foot pocket of HDAC2 and the corresponding residues in HDAC3 (according to sequence alignment) are the same, the recent X-ray apo-structure of HDAC3[192] did not contain a "foot pocket". Schwabe et al.[192] noted that the HDAC3 structure was crystallized in the absence of the ligand and, therefore, may not be representative of the actual protein-ligand complex interactions. In our opinion, the similarity of the time-dependent inhibition of HDAC2 and HDAC3 and HDAC8 suggests that the latter two isoforms may also adopt the conformation with a "foot pocket" that can accommodate the benzamide--based ligands. The relatively low inhibition of HDAC8 compared to HDAC1-3 may be rationalized by the difference in the residues at the entrance to the "foot-pocket" that imposes different steric and electrostatic requirements on the R^4 substituent. In HDAC8, the opening to the putative "foot pocket" is hindered by the presence of bulky side chain of Trp127 as shown in Figure 38, whereas in HDAC1, 2 and 3 the corresponding residue Leu144 is less bulky and more flexible and makes the "foot pocket" more accessible to

the ligands. This is also indirectly supported by the SAR - probe **8g** is consistently the least active against HDAC1-3 but its inhibition of HDAC8 is comparable to that of **8**, **8e**, **75b**, and **75c**.

Cravatt et.al[199] attributed the low potency of benzophenone-based benzamide probes to the positioning of the photoreactive group. Based on their observations, we decided to carry out a small SAR study to explore how the positioning of the aryl azide and aliphatic azide affects the potency and selectivity of the probes. Despite the presence of additional azido groups, probes **8a** and **8b** were comparable in potency to ligand **8** and probes **75a-c** were more than 2-2.5-fold more potent than ligand **75** for HDAC1 and 2. Probes **8c-g** were 27-1000 and 5-550-fold less potent than ligand **8** for HDAC1 and 2 respectively. In general, probes **8a-g** were found to be less potent than ligand **8** for both HDAC3 and 8, whereas compounds **75a-c** and ligand **75** demonstrated comparable potency against HDAC3. In HDAC8, the diazide probes **75b** and **75c** appear to be more potent than ligand **75** and the monoazide probe **75a** was inactive. To gain insights into the plausible explanations for the difference in potency we compared the docking poses of the probes with that of ligand **8**. We observed that the meta-substituents R^1 and R^3 are too close to the residues Phe210, Gly154, Phe155, Leu276, and Asp104 (Figure 39).

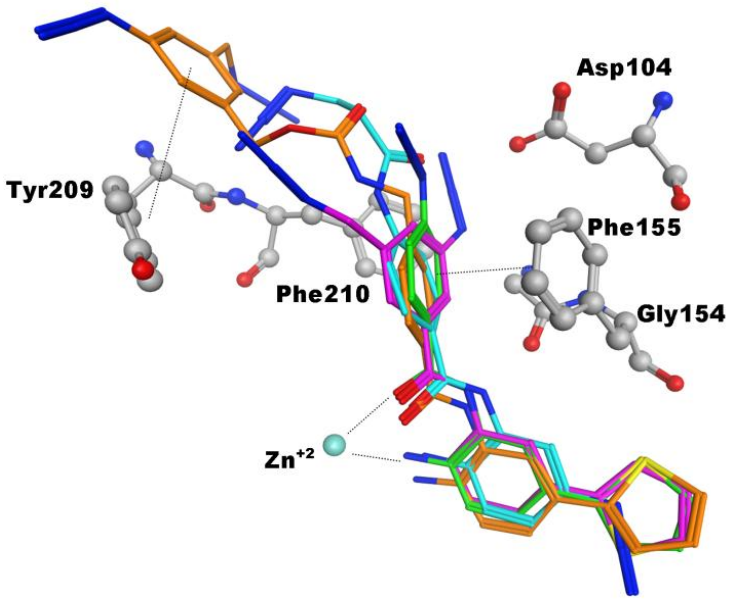

Figure 39.Overlay of compounds **8b** (green), **8c** (magenta), **8g** (cyan) and **75c** (gold) in the active site of HDAC2.

As a result of this steric interference, the probes are forced to adopt a conformation where the face-to-face π-π stacking between ring B of the probes and Phe155 is disrupted. The loss of these π-π stacking interactions may explain relatively poor potency of mono meta-substituted probes **8e** and **8f**, 830 and 750 nM respectively, and especially 3,5-disubstituted probes **8c** and **8d**, 2.4 μM and 10 μM respectively, compared to probes with no meta substituents **8a** and **8b**, 210 and 110 nM, respectively. The width and shape of the gorge region appears to be important to gain potency and isoform selectivity as demonstrated by Kozikowski et al.[189] in design of tubastatin A, a selective inhibitor of HDAC6. Placement of the aromatic azido group in the "foot-pocket" in **8g** led to poor potency for HDAC1 and 2, 55 μM and 77 μM respectively, slightly less pronounced

decrease in inhibition of HDAC3 but not HDAC8. The docking showed that the R^4 azido substituent fits well in the "foot pocket" and occupies the same space as the R^4 phenyl and 2-thiophenyl substituents in **8a-f**. This observation appears to be consistent with the SAR found by Methot et al.[200] where non-polar aromatic substituents were found to be preferable compared to polar and/or relatively small substituents R^4. The additional interactions between the carbamate appendage in probes **75a**, **75b** and **75c** and Tyr209 of HDAC2 identified by docking did not contribute to potency of these ligands, suggesting that this appendage is likely to remain solvent exposed.

4.3.3 Photolabeling studies

Photoaffinity labeling studies were conducted with the probes using commercially available recombinant His-tagged HDAC2. The probes (25 μM) were preincubated with HDAC2 (1.25 μM) for 24 h in photolabeling buffer, exposed to 254 nm UV light for 3×1 min with 1 min resting. A commercially available strained cyclooctyne-based biotin tag (BT) was attached to the HDAC2-probe adduct using (3+2) cycloaddition reaction and the biotinylated HDAC2 was visualized by streptavidin-HRP and western blot analysis (Figure 40). Photolabeling indicated that hydroxamate-based probes **52**, **53** and **54** gave comparable biotinylation as benzamide probes **8c-f**, **75b** and **75c**. The weakly potent ligand gave less pronounced biotinylation as compared to other diazide-based probes. The strained cyclooctyne-based biotin tag was used primarily to allow extension of the protocol in cells, where the copper catalyst may cause unwanted toxicity. The loading

was confirmed by using nickel-HRP, which recognized the His-tag on the recombinant HDAC2 protein.

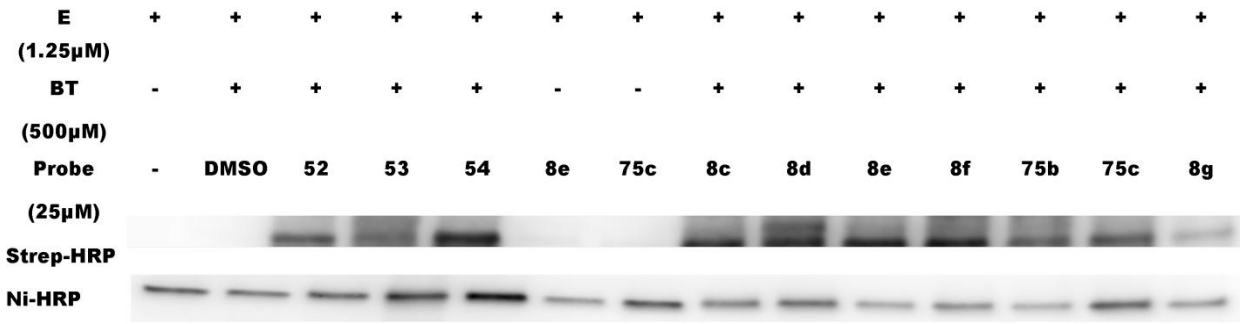

Figure 40. Western blot analysis of probes **52**, **53**, **54**, **8c**, **8d**, **8e**, **8f**, **75b**, **75c** and **8g** (25 μM) photocrosslinked to HDAC2 (1.25 μM) using streptavidin-HRP and nickel-HRP

To ensure that the biotinylation was primarily driven through interactions of the probes with the binding site of HDAC2, we performed competition experiments of the probes with a known potent HDAC inhibitor Trichostatin A (125 μM), which has an IC_{50} of 68 nM for HDAC2.[187] All of the diazide probes showed a pronounced decrease in biotinylation in the presence of 5-fold molar excess of the competing ligand. The decrease was slightly less pronounced in the case of weakly potent probe **8g**.

Figure 41 shows a western blot for a competition experiment between various diazide probes and Trichostatin A.

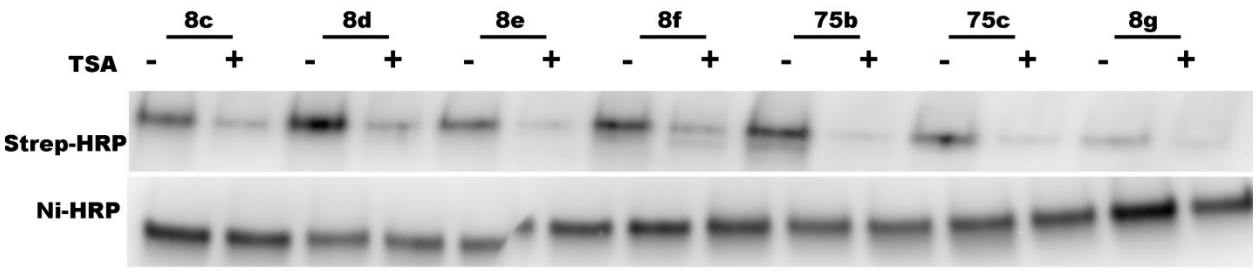

Figure 41. Western blot analysis of diazide probes **8c**, **8d**, **8e**, **8f**, **75b**, **75c** and **8g** (25 μM) photocrosslinked to HDAC2 (1.25 μM) in the presence or absence of 125 μM of Trichostatin A using streptavidin-HRP and nickel-HRP
Shown is the representative western blot of two independent experiments

4.3.4 Monitoring H4 acetylation in MDA-MB-231 cells.

We also confirmed that our probes **8a-f** and **75a-c** are cell permeable and capable of inhibiting nuclear HDACs by monitoring the acetylation status of histone H4 in MDA-MB-231 breast cancer cell line. H4 is a known nuclear target for HDAC1 and HDAC2 in this cell line.[201] All of the probes inhibited deacetylation of histone H4 at 50 μM concentration after a 24 h treatment (Figure 42).

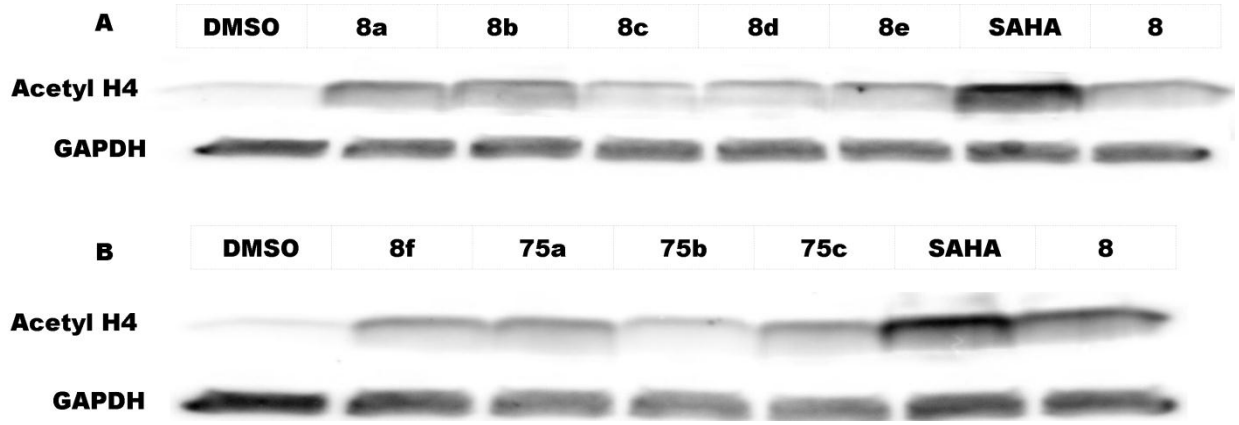

Figure 42. Western blot detection of acetyl H4 in MDA-MB-231 cell lines following a 24h treatment with various diazide and monoazide-based benzamide probes at 50 μM (A) Treatment of cells with probes **8a**, **8b**, **8c**, **8d**, **8e**, suberoylanilide hydroxamic acid(SAHA) and parent ligand 8.(B) Treatment of cells with probes **8f**, **75a**, **75b**, **75c**, suberoylanilide hydroxamic acid (SAHA) and parent ligand **8**. Shown is a representative blot of three independent experiments.

4.4 Conclusions

In conclusion, two benzamide scaffolds were successfully explored for design of novel HDAC2 nanomolar potent and selective photoreactive probes suitable for further BEProFL experiments. A total of 10 monoazide and diazide containing benzamide probes were synthesized and tested for their inhibitory activity against class I HDAC isoforms. All the probes are readily accessible in few synthetic steps carried out in a convergent manner. The inhibition was measured at two time points for HDAC1, 3, and 8 and three points for HDAC2. The probes exhibited a 2-40-fold increase in inhibition with respect to time for HDAC1 and 2 and modest increase was observed for HDAC3 and 8. Time-

dependent inhibition of HDAC1, 3, and 8 suggests that these isoforms may also adopt the "foot pocket" conformation similar to that of HDAC2 to accommodate the benzamide ligands. The most potent probes exhibit nanomolar activity against HDAC1 and 2. Probe **8b** has an IC_{50} of 70 nM and 110 nM for HDAC1 and 2, respectively, and shows an estimated 100-1000-fold selectivity for HDAC1 and 2 as compared to HDAC3 and 8. The most active diazide probes **75b** and **75c** have an IC_{50} of 0.9 and 1.2 μM and 300 and 350 nM for HDAC1 and 2 respectively and show approximately 30-fold selectivity for HDAC1 and 2 as compared to HDAC3 and 8. Docking studies with HDAC2 indicated that the placement of the azido groups meta but not para to the benzamide group in ring B leads to unfavorable for π-π stacking between ring B and Phe155 orientation of the ligand. Consistent with earlier reports, the presence of the bi-aryl moiety in the "foot-pocket" was found to be essential for maintaining potency for HDAC1-3. On the other hand, **8g**, a probe that lacks the bi-aryl portion found in **8a-f** and **75a-c**, was found to be superior to the biaryl-containing probes in inhibiting of HDAC8. As demonstrated by our photolabeling experiments, all the diazide probes efficiently photocrosslinked with recombinant HDAC2. Cell-based studies show that the benzamide probes are able to enter the cell nucleus and trigger accumulation of acetylated H4. Presently, the probes are being extensively used in mapping the binding site of HDAC2 via proteomics experiments. Cell-based photolabeling experiments are currently underway to understand how these probes bind to HDAC complexes in cells.

CHAPTER 5. CONCLUSIONS AND FUTURE DIRECTIONS

Majority of drug discovery campaigns undertaken by the pharmaceutical industries and academia involve important stages of target identification, validation and lead optimization in a variety of *in vitro* and *in vivo* studies, before ligands of interest are pushed towards clinical evaluation. Photoaffinity labeling studies are an integral of target identification and help in mapping the binding sites of putative targets so as to provide insights into conformational changes in proteins during binding of ligands, protein-protein interactions and identify novel binding sites. All these efforts ultimately assist in harnessing the chemical space of molecules more efficiently so as to yield drug candidates with improved pharmacodyanamic and pharmacokinetic properties. The studies described in this thesis describe the design, synthesis, photoaffinity labeling and biological evaluation of a series of probes for histone deacetylase 2 and 8 which are attractive targets for neurodegenerative conditions.

In the first part of this study we have explored the binding modes of novel ligands for HDAC8 that likely bind to a secondary binding site, proximal to the main catalytic site. Exploration of secondary binding sites in HDAC8 was performed by combining multidisciplinary techniques such as affinity-based protein profiling, computational studies. To the best of our knowledge ligands reported in Chapter 3 remain to be the first series of active HDAC8 ligands without a zinc chelating group, which are cell permeable and inhibit deacetylation of H4 in SYSY5Y cells. Extensive SAR studies are now underway to improve potency/selectivity of ligands for HDAC8 and further delineate

ligand binding by orthogonal techniques such as mass spectrometry, X-ray crystallography.

In the second part of this study, we have established a fluorogenic protocol for screening of ligands for HDAC2 which was used extensively to evaluate inhibitory potential of ligands in a time dependent and concentration dependent fashion. In subsequent sections/chapters we have discussed the design and synthesis of 10 monoazide and diazide probes-based on two benzamide scaffolds for profiling HDAC2. Benzamide photoaffinity probes discussed, exhibited time dependent inhibition, have low nM potency and are selective for HDAC1 and 2. Time dependent inhibition of other Class I HDAC isoforms suggested that these isoforms may also adopt a novel foot-pocket like conformation in solution as observed in the HDAC2 crystal structure. Molecular modeling studies revealed the positioning of the photoreactive group- aryl azide and the image tag attachment group-alkyl azide was crucial for maintaining potency and selectivity for HDAC2. Photolabeling experiments indicated the probes are efficient in crosslinking to HDAC2. The probes are able to inhibit the deacetylation of H4 in MDA-MB-231 cells indicating they are cell permeable and target the nuclear HDACs.

Future studies include profiling of HDAC2 binding site in a time dependent fashion to understand the conformational changes taking place in the active site during ligand binding. Extension of the BEProFL approach in cells is also underway to identify protein partners within HDAC2 containing complexes and other proteins that may be targets for the benzamide class of ligands.

APPENDICES

APPENDIX A. SYNTHETIC EXPERIMENTAL PROCEDURES AND COMPOUND CHARACTERIZATION

General Methods:

Unless stated otherwise, all reactions were carried out under an atmosphere of nitrogen in oven-dried glassware. Indicated reaction temperatures refer to those of the reaction bath, while room temperature (rt) is noted as 25 °C. All other solvents were of anhydrous quality purchased from Aldrich Chemical Co. and used as received. Pure reaction products were typically dried under high vacuum .Commercially available starting materials and reagents were purchased from Aldrich, TCI and Fisher Scientific and were used as received unless specified otherwise. Analytical thin layer chromatography (TLC) was performed with (5 x20 cm, 60 Å, 250 μm). Visualization was accomplished using a 254 nm UV lamp. ^{1}H and ^{13}C NMR spectra were recorded on Bruker DPX 400 MHz spectrophotometer. Chemical shifts are reported in ppm with the solvent resonance as internal standard ([$CDCl_3$ 7.27 ppm, 77.23 ppm] [DMSO-d_6 2.5 ppm, 39.51 ppm] and [MeODd_4 4.78, 49.0] for ^{1}H, ^{13}C respectively). Data are reported as follows: chemical shift, multiplicity (s= singlet, d = doublet, dd = doublet of doublet, t = triplet, q = quartet, br = broad, m = multiplet, abq = ab quartet), number of protons, and coupling constants. Low-resolution mass spectra (LRMS) were acquired on an Shimadzu 2020 LC/MS. High resolution mass spectrometric data was collected using Waters SYNAPT QTOF and Shimadzu LCMS IT-TOF. All compounds submitted for biological testing were found to be $\geq$ 95 % pure.

APPENDIX A (CONTINUED)

The following experimental section shall only discuss the synthesis of novel ligands **52g** and **52i**. discussed in Chapter 3.

The synthesis of intermediates **69**, **70**, **71**, **72** will be discussed in detail while. the synthesis of intermediates **52d** and **64** was carried out using published synthetic procedures[144] and the crude products used in further steps used without further purification.

(3-Amino-5-methoxyphenyl)methanol (**69**). To a solution of **68** (5 g, 0.03 mol) in anhydrous THF (100 mL) was added $LiALH_4$ (2.3 g, 0.06 mol) in portions at 0 °C. The reaction mixture was stirred overnight, cooled to 0 °C, and quenched by slow addition of aqueous KOH solution (20%, 5 mL) followed by ethyl acetate (50 mL). The mixture was filtered through a pad of Celite and rinsed with ethyl acetate. The filtrate was dried over Na_2SO_4, filtered, and concentrated under reduced pressure. The crude was purified by flash chromatography (60:40 → 40:60, hexanes:EtOAc) to give compound **69** as a pale yellow solid (2.75 g, 60%). ^{1}H NMR (400 MHz, $CDCl_3$): δ 6.38 (s, 1H), 6.34 (s, 1H), 6.31 (s, 1H), 4.39 (s, 2H), 3.79 (s, 3H), 3.77 (s, 1H). ^{13}C NMR (100 MHz, $CDCl_3$): δ 160.61, 147.49, 143.13, 105.90, 102.04, 99.87, 64.98, 54.78.

(3-Azido-5-methoxyphenyl)methanol (**70**). To a solution of **69** (1.75 g, 11.46 mmol) in glacial acetic acid $AcOH/H_2SO_4$ (98% w/v)/water (4:1:5) (15 mL) was added $NaNO_2$ (1.58 g, 22.93 mmol) in portions at 0 °C and stirred for 10 min. NaN_3 (2.24 g, 34.4 mmol) was then added portion wise at 0 °C and the resulting mixture was stirred for 5 h

APPENDIX A (CONTINUED)

at rt. The reaction was quenched with saturated aqueous $NaHCO_3$ solution and extracted with EtOAc (3 × 30 mL). The combined organic extracts were washed with brine, dried (Na_2SO_4), filtered, and concentrated under reduced pressure. The crude was purified by flash chromatography (70:30 → 50:50, hexanes:EtOAc) to a give compound **70** as a pale yellow oil (1.88 g, 90%). ^{1}H NMR (400 MHz, $CDCl_3$): δ 6.69 (s, 1H), 6.65 (s, 1H), 6.47 (s, 1H), 4.64 (s, 2H), 3.81 (s, 3H), 2.26 (bs, 1H). ^{13}C NMR (100 MHz, $CDCl_3$): δ 160.93, 144.02, 141.43, 109.46, 108.85, 104.02, 64.68, 55.45.

Toluene-4-sulfonic acid 3-azido-5-methoxybenzyl ester (**71**). To a solution of **70** (1.88 g, 10.49 mmol) in anhydrous dichloromethane was added triethylamine (2.92 mL, 20.98 mmol) followed by tosyl chloride (2.20 g, 11.54 mmol) at 0 °C portion wise. The reaction mixture was stirred for 30 min at the same temperature. After completion of the reaction, the mixture was concentrated under reduced pressure and the residue was immediately purified by flash chromatography (90:10 → 80:20, hexanes:EtOAc) to give **71** as white solid (1.75 g, 70%). The compound **71** was observed to be hygroscopic and was used in subsequent reactions almost immediately after purification.^{1}H NMR (400 MHz, $CDCl_3$): δ 7.82(d, *J* = 8.2 Hz, 2H), 7.36 (d, *J* = 8.2 Hz, 2H), 6.58 (s, 1H), 6.50 (s, 1H), 6.47 (s, 1H), 5.01 (s, 2H), 3.78 (s, 3H), 2.47 (s, 3H). ^{13}C NMR (100 MHz, $CDCl_3$): δ 160.91, 145.04, 141.68, 136.24, 133.09, 129.90(2C), 127.99(2C), 110.95, 110.39, 105.40, 71.05, 55.52, 21.66.

7-[4-(3-Azido-5-methoxybenzyloxy)phenylcarbamoyl]heptanoic acid methyl ester (**72**). To a solution of **71** (0.72 g, 2.15 mmol) and **64** (0.50 g, 1.79 mmol) in dry acetone

APPENDIX A (CONTINUED)

(8 mL) was added K_2CO_3 (1.48 g, 10.74 mmol) at ambient temperature, and the reaction mixture was refluxed for 12 h. The mixture was poured into water and extracted with EtOAc (3 × 30 mL). The organic layer was washed with water, dried over Na_2SO_4, and evaporated under reduced pressure. The residue was purified by flash chromatography (90:10 → 70:30, hexanes:EtOAc) to afford **61** as white solid (0.56 g, 75%). ^{1}H NMR (400 MHz, $CDCl_3$): δ (ppm) 7.43 (d, *J* = 8.8 Hz, 2H), 7.24 (s, 1H), 6.92 (d, *J* = 8.8 Hz, 2H), 6.76 (s, 1H), 6.72 (s, 1H), 6.51 (s, 1H), 5.01 (s, 2H), 3.82 (s, 3H), 3.68 (s, 3H), 2.32 (m, 4H) ,1.69 (m, 4H), 1.35 (m, 4H). ^{13}C NMR (100 MHz, $CDCl_3$): δ 174.25, 171.11, 160.99, 155.15, 141.56, 140.18, 131.57, 121.65(2C), 115.18(2C), 110.01, 109.51, 104.32, 69.69, 55.49, 51.51, 37.42, 33.95, 28.77, 28.31, 25.39, 24.69.

7-[4-(3-Azido-5-methoxybenzyloxy)phenylcarbamoyl]heptanoic acid (**74**). To a solution of **72** (0.26 g, 0.59 mmol) in THF/MeOH (1:1, 5 mL) was added 4N KOH (0.43 mL, 1.78 mmol) at rt, and stirred for 24 h. The mixture was neutralized with 2N HCl and extracted with EtOAc. The combined organic extracts were washed with brine, dried (Na_2SO_4), filtered, and concentrated under reduced pressure. The crude **74** obtained as a yellow solid (0.24 mg, 98%) was used for next reaction without any further purification.

7-[4-(3-Azido-5-methoxybenzyloxy)phenylcarbamoyl]heptanoicacid-4-azidomethylbenzyl ester (**52h**). To an ice cooled solution of **74** (0.05 g, 0.18 mmol) in anhydrous dichloromethane was added EDCI (0.038 g, 0.18 mmol) followed by HOBt (0.024 g, 0.18 mmol) and stirred for 1 h. To this, was then added a solution of [4-(Azidomethyl)phenyl]methanol (0.023 g, 0.14 mmol) and DIPEA (61.3 µL, 0.35 mmol)

APPENDIX A (CONTINUED)

in anhydrous dichloromethane at 0 °C and stirred for 12 h. Saturated aqueous $NaHCO_3$ solution was added to the reaction mixture and extracted with EtOAc. The organic layer was washed with water, dried over Na_2SO_4, and evaporated under reduced pressure. The residue was purified by flash chromatography (90:10 → 70:30, hexanes:EtOAc) to afford **52h** as a white solid (0.02 g, 68%). ^{1}H NMR (400 MHz, $CDCl_3$): δ 7.43 (d, J = 8.8 Hz, 2H), 7.38 (d, *J* = 8.8 Hz, 2H), 7.34 (d, *J* = 8.0 Hz, 2H), 7.15 (s, 1H), 6.93 (d, *J* = 8.0 Hz, 2H), 6.77 (s, 1H), 6.72 (s, 1H), 6.51 (s, 1H), 5.14 (s, 2H), 5.01 (s, 2H), 4.36 (s, 2H), 3.83 (s, 3H), 2.38 (t, *J* = 7.6 Hz ,2H), 2.31 (t, *J* = 7.6 Hz ,2H), 1.69 (m, 4H), 1.38 (m ,4H). ^{13}C NMR (100 MHz, $CDCl_3$) δ 173.53, 171.03, 160.99, 155.16, 141.57, 140.18, 136.25, 135.38, 131.54, 128.65(2C), 128.40(2C), 121.63(2C), 115.19(2C), 110.01, 109.51, 104.32, 69.69, 65.66, 55.49, 55.46, 37.41, 34.15, 28.69 (2C), 25.38, 24.27. HRMS (ESI) m/z [M + H]+ calcd for $C_{30}H_{34}N_7O_5$ 572.2621, found 572.2625.

7-[4-(3-Azido-5-methoxybenzyloxy)phenylcarbamoyl]heptanoicacid-2-azidoethyl ester (**52g**). Compound **52g** was prepared by a coupling reaction between acid **74** and 2-azido ethanol following the same procedure described for probe **52h**. White solid, 65% yield. ^{1}H NMR (400 MHz, $CDCl_3$) δ 7.43(d, *J* = 8.8 Hz, 2H), 6.93 (d, *J* = 8.8 Hz, 2H), 6.75 (s, 1H), 6.71 (s, 1H), 6.50 (s, 1H), 5.00 (s, 2H), 4.25 (t, *J* = 4.8 Hz, 2H), 3.82 (s, 3H), 3.48 (t, *J* = 4.8 Hz, 2H), 2.38 (m, 4H), 1.69 (m, 4H), 1.40 (m, 4H). ^{13}C NMR (100 MHz,) $CDCl_3$): δ 173.40, 171.11, 160.99, 155.15, 141.55, 140.18, 131.57, 121.67(2C), 115.17(2C), 110.01, 109.51, 104.31, 69.69, 62.83, 55.48, 49.80, 37.39, 33.95, 28.69,

APPENDIX A (CONTINUED

28.69, 25.38, 24.57. HRMS (ESI) m/z [M + H]+ calcd for $C_{24}H_{30}N_7O_5$ 496.2308, found 496.2318.

APPENDIX A (CONTINUED)

The following experimental section deals with procedures followed for synthesis of intermediates and final compounds mentioned in Chapter 4.

***Tert*-butyl (4-bromo-2-nitrophenyl)carbamate** (**99**) To an ice cooled solution of 4-bromo-2-nitroaniline (1 g; 4.61 mmol) in anhydrous DMF (25 ml) was added sodium hydride (0.2 g, 5.53 mmol) portion wise and stirred at 0°C for 30 min. A solution of Boc_2 (O) (1 g, 4.61 mmol) in anhydrous DMF (10 ml) is added drop wise using a syringe over a period of 30 min and the reaction allowed to reach room temperature overnight. The reaction is quenched by addition of cold water (50 ml) and extracted with ethyl acetate (3 × 30 ml). The organic layer washed with brine and dried over anhydrous sodium sulphate and the concentrated in vacuo. The residue is purified using flash chromatography (100:0 → 90:10, hexanes:EtOAc) to yield a yellow solid (1.38 g, 95 %). ^{1}H NMR (400 MHz, $CDCl_3$) δ ppm 1.54 (s, 9H) 7.68 (dd, J=9.22, 2.40 Hz, 1H) 8.31 (d, J=2.27 Hz, 1H) 8.50 (d, J=9.09 Hz, 1H) 9.59 (br. s., 1H).

***Tert*-butyl (3-nitrobiphenyl-4-yl)carbamate** (**101**). To an oven dried pressure vessel was added 25 ml anhydrous THF, 99 (1 g, 3.16 mmol), phenyl boronic acid (0.58 g, 4.75 mmol), potassium carbonate (1.3 g, 9.5 mmol) and tetrkistiphenylphosphine palladium (0) (0.37, 0.32 mmol). The vessel was screwed tightly and the reaction mixture heated at 85 °C for 12 h. After the completion of reaction as confirmed by TLC, brine (50 ml) was added to the reaction mixture and extracted with ethyl acetate (3 × 30 ml). The organic layer washed with brine again and dried over anhydrous sodium sulfate and concentrated in vacuo. The residue is purified by flash chromatography (100:0 → 90:10,

APPENDIX A (CONTINUED)

hexanes:EtOAc) to yield a yellow solid (0.91 g, 92%). ^{1}H NMR (400MHz, $CDCl_3$) δ ppm = 9.69 (s, 1H), 8.65 (d, J = 8.8 Hz, 1 H), 8.43 (d, J = 2.3 Hz, 1H), 7.86 (dd, J = 2.3, 8.8 Hz, 1H), 7.63 - 7.57 (m, 2H), 7.48 (m, 2H), 7.41 (d, J = 7.3 Hz, 1H), 1.59 (s, 9H). ^{13}C NMR (100 MHz, $CDCl_3$) δ ppm = 152.1, 141.3, 136.0, 134.8, 132.8, 128.7(2C), 128.3(2C), 125.6, 123.9, 122.3, 121.1, 82.0, 28.2

***Tert*-butyl [2-nitro-4-(thiophen-2-yl)phenyl]carbamate** (**102**). Compound **102** was prepared by a Suzuki coupling reaction between aryl bromide **99** and 2-thienyl boronic acid following the same procedure described for intermediate **101**, yellow solid (0.94 g, 93%) ^{1}H NMR (400 MHz , $CDCl_3$) δ ppm = 9.66 (s, 1 H), 8.59 (d, J = 9.1 Hz, 1 H), 8.38 (d, J = 2.3 Hz, 1 H), 7.80 (dd, J = 2.1, 9.0 Hz, 1 H), 7.33 (d, J = 4.0 Hz, 2 H), 7.14 - 7.06 (m, 1 H), 1.58 (s, 9 H). ^{13}C NMR (100MHz, $CDCl_3$) δ ppm = 152.2, 138.1, 136.2, 134.9, 134.1, 129.1, 128.1, 126.7, 123.7, 121.1, 81.9, 28.2

***Tert*-butyl (3-aminobiphenyl-4-yl)carbamate**. (**82**). Intermediate **101** (0.5 g, 1.59 mmol), was dissolved in methanol (50 ml) and ammonium formate (0.5 g, 7.96 mmol) was added to it. Thereafter zinc dust (0.52 g, 7.96 mmol) was added to the reaction and the mixture stirred vigorously at rt for 15 min. The completion of the reaction is confirmed by TLC as well as change in the reaction mixture from yellow to colorless. The reaction mixture is filtered through a pad of celite and concentrated in vacuo. The residue purified by flash chromatography (100:0 → 90:30, hexanes:EtOAc) to yield an off white solid. (0.41 g, 90 %).^{1}H NMR (400MHz, $CDCl_3$) δ ppm = 7.59 - 7.53 (m, 2H), 7.46 - 7.31 (m, 4H), 7.08 - 6.99 (m, 2H), 3.84 (br. s., 2H), 1.56 (s, 9H) ^{13}C NMR

APPENDIX A (CONTINUED)

(100MHz, $CDCl_3$) δ ppm = 153.9, 140.9, 140.0, 139.2, 128.7(2C), 127.1(2C), 126.9, 124.9, 124.2, 118.6, 116.3, 80.7, 28.4

***Tert*-butyl [2-amino-4-(thiophen-2-yl)phenyl]carbamate** (**83**). Compound **83** was prepared by reduction of nitro derivative **102** using zinc dust and ammonium formate following the same procedure described for intermediate **82**, yellow solid (0.42 g, 90 %) ^{1}H NMR (400 MHz, $CDCl_3$) δ ppm = 7.22 - 7.37 (m, 3H), 6.98 - 7.10 (m, 3H), 6.28 (m, 1H) 3.82 (br. s., 2H) 1.54 (s, 9H) ^{13}C NMR (100MHz , $CDCl_3$) δ ppm = 153.8, 144.1, 140.0, 132.2, 127.9, 124.9, 124.4, 122.8, 117.5, 115.0, 80.7, 28.3

3-Azido-4-hydroxybenzoic acid. (**86**) 3.3 mL of 10 M HCl was added drop wise to 10 mL of water/acetonitrile (6:4 v/v) mixture and cooled to 0°C. Thereafter 3-amino-4-hydroxybenzoic acid (2.5 g, 16.3 mmol) was added portion wise to the cold solution of HCl in water/acetonitrile. A cold solution of sodium nitrite (2.25 g, 32.7 mmol) in 5 mL water was added to reaction mixture drop wise. The reaction mixture was stirred for 20 min at 0°C, before the addition of sodium azide (3.2 g, 49 mmol) in small quantities. A dark red solution is formed with vigorous effervescence due to the liberation of nitrogen gas. The reaction mixture was further stirred for 5 h at 0-5°C. Thereafter concentrated HCl was added to the reaction mixture drop wise to aid the precipitation of the product. The precipitate formed was filtered and dried to yield the final product (2.5 g, 85%) as red solid. ^{1}H NMR (400 MHz, DMSO-d_6) δ ppm = 11.00, (s, 1H), 7.62 (dd, *J*=8.46, 2.15

APPENDIX A (CONTINUED)

Hz, 1H), 7.46 (d, *J*=2.02 Hz, 1H), 6.95 (d, *J*=8.34 Hz, 1H) ^{13}C NMR (100 MHz, DMSO-d_6) 166.96, 154.92, 128.26, 126.25, 122.77, 122.39, 116.51.

Methyl 3-azido-4-hydroxybenzoate (**87**) Thionyl chloride (1.4 mL, 18.9 mmol) was added drop wise to a cold solution of **86** (1.7 g, 9.5 mmol) in 20 mL methanol. A dark brown solution is formed, which is further stirred at room temperature for 8 h. Excess thionyl chloride and methanol were removed in vacuo and the residue left was adsorbed onto silica. The compound **87** was purified using flash chromatography (100:0 → 90:30, hexanes:EtOAc) as an off white powder. (1.6g, 87%). ^{1}H NMR (400 MHz, $CDCl_3$) δ ppm = 7.74 - 7.85 (m, 2H), 6.98 (d, *J*=8.34 Hz, 1H), 5.94 (br. s., 1H), 3.93 (s, 3H).^{13}C NMR (100 MHz, $CDCl_3$) δ ppm = 166.13, 151.29, 128.11, 126.39, 123.29, 119.91, 115.68, 52.21.

Methyl 3-azido-4-(2-azidoethoxy)benzoate (**88**) To a solution of **87** (1 g, 5.2 mmol) in dry acetone (20 mL) was added calcined potassium carbonate (2.1 g, 15.5 mmol) to yield a cloudy suspension. Thereafter a solution of 2-azidoethyl 4-methylbenzenesulfonate (1.5 g, 6.2 mmol) in 5 mL acetone was added drop wise to the above suspension. A yellow solution is obtained which slowly turns brown as it is refluxed for 5 h. Thereafter the solvent is removed in vacuo and the residue directly adsorbed onto silica. The compound **15** is purified by flash chromatography (100:0 → 90:20, hexanes:EtOAc) as a white solid (1.05 g, 77%). ^{1}H NMR (400 MHz, $CDCl_3$) δ ppm 7.83 (dd, *J*=8.59, 2.02 Hz, 1H), 7.72 (d, *J*=2.02 Hz, 1H), 6.93 (d, *J*=8.59 Hz, 1H), 4.25 (t, *J*=5.05 Hz, 2H), 3.92 (s, 3H), 3.73

APPENDIX A (CONTINUED)

(t, *J*=5.05 Hz, 2H) ^{13}C NMR (100 MHz , $CDCl_3$) δ ppm = 166.0, 154.2, 128.9, 127.6, 124.1, 122.1, 112.2, 77.3, 77.0, 76.7, 67.8, 52.2, 49.9.

3-Azido-4-(2-azidoethoxy)benzoic acid (**78**). To a solution of **88** (1.0 g, 5.1 mmol) in 10 mL of THF/water (1:1 v/v) was added potassium hydroxide (1.07 g, 19 mmol) portion wise and heated for 70°C overnight. The reaction mixture was cooled and neutralized by the slow addition of concentrated HCl. A white solid precipitate is formed which is filtered and dried to yield the final product (0.87 g, 92%). ^{1}H NMR (400 MHz, DMSO-d_6) δ ppm =7.75 (dd, *J*=8.59, 2.02 Hz, 1H), 7.52 (d, *J*=2.02 Hz, 1H), 7.21 (d, *J*=8.59 Hz, 1H), 4.31 (t, *J*=4.67 Hz, 2 H), 3.69 (t, *J*=4.67 Hz, 2 H) ^{13}C NMR (100MHz, DMSO-d_6) δ ppm = 166.8, 154.7, 128.2, 127.9, 124.6, 122.0, 113.6, 68.4, 50.0.

4-[({[(3-Azidobenzyl)oxy]carbonyl amino)methyl]benzoic acid (**80**)

To a suspension of 1,1'-carbonyldiimidazole (1.08 g, 6.7 mmol) in THF (20 mL) was added (3-azidophenyl)methanol (1 g, 6.7 mmol) in THF (10 mL) at 10°C, and the mixture stirred for 1 h at room temperature. The resulting solution was added to a suspension of 4-(aminomethyl)benzoic acid (1.01 g, 6.7 mmol), DBU (1.02 g, 6.7 mmol) and triethylamine (0.94 mL, 6.7 mmol) in THF (10 mL). After stirring for 10 h at room temperature, the mixture was evaporated to remove THF and then dissolved in water (50 mL). The solution was acidified with hydrochloric acid (pH 5) to precipitate a white solid which was collected by filtration, washed with water (100 mL) and dried to give **5** as white solid (1.96 g, 90%). 1H NMR (400 MHz, DMSO-d_6) δ ppm = ^{1}H NMR 7.38-7.91

APPENDIX A (CONTINUED)

(m., 3H), 7.09-7.18 (m., 5H), 5.08 (br. s., 2H), 4.29 (br. s., 2H). ^{13}C NMR (100MHz , DMSO-d_6) δ ppm = 167.7, 156.8, 145.3, 139.9, 130.5, 129.9(2C), 127.4(2C), 124.7, 118.9, 118.3, 65.3, 44.1

4-{[({[3-Azido-5-(azidomethyl)benzyl]oxy}carbonyl)amino]methyl}benzoic acid (**81**)

The synthesis was similar to that of **80**. ^{1}H NMR (400 MHz, DMSO-d_6) δ ppm =7.99 (br. s., 1H) 7.90 (d, *J*=8.08 Hz, 2H) 7.37 (d, *J*=8.08 Hz, 2H) 7.17 (s, 1H) 7.04 - 7.15 (m, 2H) 5.08 (s, 2H) 4.49 (s, 2H) 4.28 (d, *J*=5.56 Hz, 2H) ^{13}C NMR (100MHz, DMSO-d_6) δ ppm = 167.6, 156.7, 145.3, 140.8, 140.4, 138.6, 129.8(2C), 127.4(2C), 124.3, 118.6, 118.0, 65.1, 53.4, 44.1.

General procedure for synthesis of probes

Peptide coupling protocol

To a solution of substituted benzoic acid **76-81** (1.1 equiv) in anhydrous DMF (5 mL/mmol of amine) was added EDCI (1.2 equiv) followed by HOBt (1.2 equiv) and stirred at room temperature for 1 h. Thereafter substituted aniline **82-84** (1 equiv) was added and the mixture heated at 78°C overnight. After completion of the reaction as confirmed by TLC, saturated sodium bicarbonate solution (20 mL/mmoL of amine) was added and the mixture was extracted with ethyl acetate (30 mL/mmol of amine). The organic layer was washed with water (30 mL/mmol of amine), dried over anhydrous sodium sulphate and evaporated in vacuo. The residue was purified using flash

APPENDIX A (CONTINUED)

chromatography (silica gel, hexane/ethyl acetate gradient) to yield the N-boc protected probes **104a-g** and **105a-c** in 60-80% yields as off white solids

Boc deprotection protocol

The Boc group in intermediates **104a-g** and **105a-c** was removed by treating N-boc protected compound with a mixture of TFA/DCM (1:1 v/v) at room temperature for half an hour. Saturated bicarbonate solution was added to the reaction mixture after the completion of the reaction, as confirmed by TLC and the reaction extracted with DCM (3 × 30 mL) and the organic layer washed with brine. The solvent was removed in vacuo and the residue purified using flash chromatography (silica gel, hexane/ethyl acetate gradient) to yield the final probes **8a-g** and **75a-c** as light yellow solids in 70-80% over all yield.

Tert-butyl (3-(4-azidobenzamido)-[1,1'-biphenyl]-4-yl)carbamate, **104(a)**

^{1}H NMR (400MHz, $CDCl_3$) δ ppm = 9.44 (br. s., 1H), 7.98 (d, *J* = 8.1 Hz, 2H), 7.90 (br. s., 1H), 7.48 (d, *J* = 6.8 Hz, 2H), 7.42 - 7.25 (m, 5H), 7.10 -7.01 (m, 3 H), 1.53 (s, 9H). ^{13}C NMR (100MHz, $CDCl_3$) δ ppm = 164.9, 154.7, 143.7, 139.7, 138.6, 130.7, 130.3, 129.5, 129.2(2C), 128.7(2C), 127.3, 126.9(2C), 124.8, 124.5, 124.4, 119.0(2C), 81.3, 28.3

Tert-butyl (2-(4-azidobenzamido)-4-(thiophen-2-yl)phenyl)carbamate, **104(b)**

^{1}H NMR (400MHz, $CDCl_3$) δ ppm = 8.06 - 7.96 (m, 3H), 7.61 - 7.53 (m, 2H), 7.44 - 7.27 (m, 5H), 7.13 - 7.06 (m, 2H), 6.87 (m, 1H), 1.53 (s, 9 H). ^{13}C NMR (100MHz, $CDCl_3$)

APPENDIX A (CONTINUED)

δ ppm = 164.7, 154.7, 143.8, 139.9, 139.1, 131.1, 130.6, 129.2(2C), 128.9(2C), 128.7, 127.4, 127.0, 124.7, 124.5, 119.0, 81.6, 28.3

Tert-butyl (2-(3-azido-5-(azidomethyl)benzamido)-4-(thiophen-2-yl)phenyl)carbamate, **104(c)**

^{1}H NMR (400MHz, $CDCl_3$) δ ppm = 7.99 (s, 1H), 7.65 (s, 1H), 7.68 (s, 1 H), 7.36 (d, *J* = 8.3 Hz, 1H), 7.32 - 7.18 (m, 4H), 7.15 (s, 1H), 7.04 (m, 1H), 6.95 (s, 1 H), 4.41 (s, 2 H), 1.53 (s, 9 H) ^{13}C NMR (100MHz, $CDCl_3$) δ ppm = 164.3, 154.7, 143.0, 141.5, 138.1, 136.4, 132.3, 130.6, 129.1, 128.0, 125.0, 124.8, 123.6, 123.4, 123.1, 122.9, 121.5, 118.1, 81.7, 54.0, 28.3

Tert-butyl (3-(3-azido-5-(azidomethyl)benzamido)-[1,1'-biphenyl]-4-yl)carbamate, **104(d)**

^{1}H NMR (400MHz, $CDCl_3$) δ ppm = 7.90 (s, 1H), 7.65 (s, 1H), 7.68 (s, 1H), 7.49 (d, *J* = 7.1 Hz, 2H), 7.42 - 7.23 (m, 5H), 7.12 (s, 1H), 7.03 (s, 1H), 4.37 (s, 2H), 1.57 (s, 9 H) ^{13}C NMR (100MHz, $CDCl_3$) δ ppm = 164.3, 154.8, 141.5, 139.7, 138.8, 138.1, 136.3, 130.4, 129.3, 128.7(2C), 127.4, 126.9(2C), 126.9, 124.7, 124.3, 123.1, 121.4, 118.0, 81.6, 54.0, 53.9, 28.3

Tert-butyl(3-(3-azido-4-(2-azidoethoxy)benzamido)-[1,1'-biphenyl]-4-yl)carbamate, 104(e)

^{1}H NMR (400MHz, $CDCl_3$) δ ppm = 8.01-7.93 (m, 1H), 7.77-7.67 (m, 2H), 7.54 (d, *J* = 7.3 Hz, 2H), 7.44-7.26 (m, 6H), 6.96-6.85 (m, 2H), 4.23 (t, *J* = 5.1 Hz, 2H), 3.74 (t, *J* =

APPENDIX A (CONTINUED)

4.9 Hz, 2H), 1.57(s, 9 H) ^{13}C NMR (100MHz, $CDCl_3$) δ ppm = 164.4, 154.7, 153.6, 139.8, 138.9, 130.9, 129.1(2C), 128.7(2C), 127.9, 127.4, 127.0, 125.1, 124.7, 124.5, 124.3, 120.4, 112.4, 81.6, 67.8, 50.0, 28.3

Tert-butyl (2-(3-azido-4-(2-azidoethoxy)benzamido)-4-(thiophen-2-yl)phenyl)carbamate, 104(f)

^{1}H NMR (400MHz, $CDCl_3$) δ ppm = 7.97 (d, *J* = 1.8 Hz, 1H), 7.72 (dd, *J* = 2.0, 8.6 Hz, 1H), 7.68 (d, *J* = 2.0 Hz, 1H), 7.36 (dd, *J* = 2.0, 8.3 Hz, 1H), 7.27 - 7.22 (m, 3H), 7.05 (dd, *J* = 3.5, 5.1 Hz, 1H), 6.95 (s, 1H), 6.88 (d, *J* = 8.6 Hz, 1H), 4.24 (t, *J* = 5.1 Hz, 2H), 3.74 (t, *J* = 5.1 Hz, 2H), 1.54 (s, 9 H) ^{13}C NMR (100MHz, $CDCl_3$) δ ppm = 164.4, 154.7, 153.6, 143.2, 132.2, 130.9, 129.2, 129.1, 128.0, 127.9, 125.1, 124.9, 124.8, 123.4, 122.9(2C), 120.5, 112.4, 81.6, 67.8, 50.0, 28.3

Tert-butyl(3-(4-(((((3-azidobenzyl)oxy)carbonyl)amino)methyl)benzamido)-[1,1'-biphenyl]-4-yl)carbamate, **105(a)**

^{1}H NMR (400MHz, $CDCl_3$) δ ppm = 7.99 (s, 1H), 7.94 (d, *J* = 8.1 Hz, 2H), 7.55 (d, *J* = 7.3 Hz, 2H), 7.43 - 7.30 (m, 9H), 7.15 (d, *J* = 7.1 Hz, 1H), 7.07 - 6.96 (m, 3H), 5.15 (s, 2 H), 4.44 (d, *J* = 5.8 Hz, 2H), 1.53 (s, 9H) ^{13}C NMR (100MHz, $CDCl_3$) δ ppm = 165.5, 154.6, 142.5, 140.4, 139.9, 138.8, 133.3, 130.9, 130.0, 129.3, 129.3, 128.7(2C), 127.8(2C), 127.5(2C), 127.4, 127.0(2C), 124.8, 124.6, 124.3, 124.3, 124.3, 118.7, 118.4, 81.4, 66.3, 44.7, 28.3.

APPENDIX A (CONTINUED)

Tert-butyl(3-(4-(((((3-azido-5-(azidomethyl)benzyl)oxy)carbonyl)amino)methyl) benzamido)-[1,1'-biphenyl]-4-yl)carbamate, **105(b)**

^{1}H NMR (400MHz, $CDCl_3$) δ ppm = 8.07 - 8.04 (m, 1H), 7.97 (d, *J* = 8.3 Hz, 2H), 7.60 (d, *J* = 7.1 Hz, 2H), 7.46 - 7.32 (m, 8H), 7.11 (s, 1H), 7.02 (s., 1H), 6.95 (s, 1H), 6.87 (s, 1H), 5.16 (s, 2H), 4.48 (d, *J* = 6.1 Hz, 2H), 4.37 (s, 2H), 1.55 (s, 9H) ^{13}C NMR (100MHz , $CDCl_3$) δ ppm = 165.3, 156.1, 154.6, 142.4, 141.1, 140.0, 139.2, 139.1, 137.9, 133.5, 131.0, 129.1, 128.74(2C), 128.72(2C), 127.8(2C), 127.6, 127.4, 127.1(2C), 124.8, 124.6, 124.3, 123.7, 118.2, 81.5, 77.3, 77.2, 77.0, 76.7, 66.0, 54.2, 44.8, 28.3

Tert-butyl(2-(4-(((((3-azido-5-(azidomethyl)benzyl)oxy)carbonyl)amino)methyl) benzamido)-4-(thiophen-2-yl)phenyl)carbamate, 105(c)

^{1}H NMR (400MHz, $CDCl_3$) δ ppm = 8.09 - 8.03 (m, 1H), 7.97 (d, *J* = 8.1 Hz, 2H), 7.60 (d, *J* = 7.3 Hz, 2H), 7.47 - 7.31 (m, 7H), 7.11 (s, 1H), 7.02 (s, 1H), 6.95 (s, 1H), 6.85 (s, 1H), 5.16 (s, 2H), 4.48 (d, *J* = 6.1 Hz, 2H), 4.37 (s, 2H), 1.55 (s, 9H) ^{13}C NMR (100 MHz, $CDCl_3$) δ ppm = 165.2, 156.1, 154.6, 142.4, 141.1, 140.0, 139.2, 139.1, 139.1, 137.9, 133.5, 131.0, 129.0, 128.7(2C), 127.8, 127.6, 127.4, 127.1(2C), 124.8, 124.6, 124.3, 123.7, 118.2, 81.6, 66.0, 54.2, 44.8, 28.3

N-(4-amino-[1,1'-biphenyl]-3-yl)-4-azidobenzamide, **8(a)**

^{1}H NMR (400MHz, Med/DMSO-d_6) δ ppm = 9.85 (s, 1H), 8.07 (d, *J* = 8.6 Hz, 2H), 7.59 - 7.52 (m, 3H), 7.43 - 7.36 (m, 3H), 7.30 - 7.23 (m, 3H), 6.93 (d, *J* = 8.3 Hz, 2H). ^{13}C NMR (100 MHz ,DMSO-d_6) δ ppm = 165.5, 143.5, 142.4, 140.8, 131.8, 130.6(2C),

APPENDIX A (CONTINUED)

130.0(2C), 129.7, 127.1(2C), 126.4, 125.7, 125.7, 124.9, 119.8(2C), 118.0, HRMS (ESI) m/z [M + H]+ calcd for $C_{19}H_{15}N_5O$ 330.1355, found 330.1356.

N-(2-amino-5-(thiophen-2-yl)phenyl)-4-azidobenzamide, **8(b)**

^{1}H NMR (400MHz, Med/DMSO-d_6) δ ppm = 9.84 (s, 1H), 8.07 (d, *J* = 8.6 Hz, 2H), 7.48 (d, *J* = 2.0 Hz, 1H), 7.40 - 7.32 (m, 2H), 7.29 - 7.25 (m, 3H), 7.09 - 7.04 (m, 1H), 6.88 (d, *J* = 8.3 Hz, 1H) ^{13}C NMR (100MHz, Med/DMSO-d_6) δ ppm = 165.1, 144.4, 143.1, 143.1, 131.3, 130.3(2C), 128.7, 124.5, 124.4, 124.3, 123.9, 123.6, 121.8, 119.3(2C), 117.5. HRMS (ESI) m/z [M + H]+ calcd for $C_{17}H_{13}N_5OS$ 336.0919, found 336.0912.

N-(2-amino-5-(thiophen-2-yl)phenyl)-3-azido-5-(azidomethyl)benzamide (8c)

^{1}H NMR (400MHz, DMSO-d_6) δ ppm = 10.09 (s, 1H), 7.83 (s, 1H), 7.76 (s, 1H), 7.66 (s, 1H), 7.60 - 7.55 (m, 2H), 7.46 (dd, *J* = 1.4, 4.9 Hz, 2H), 7.36 (s, 1H), 6.96 (d, *J* = 8.3 Hz, 2H), 4.60 (s, 2H). ^{13}C NMR (100MHz, DMSO-d_6) δ ppm = 164.8, 158.4, 141.6, 140.6, 138.7, 136.9, 127.3, 126.7, 126.2, 125.3, 125.2, 125.1, 125.09, 125.06, 122.2, 119.1, 118.5, 53.3 HRMS (ESI) m/z [M + H]+ calcd for $C_{18}H_{14}N_8OS$ 391.1090, found 391.1092

N-(4-amino-[1,1'-biphenyl]-3-yl)-3-azido-5-(azidomethyl)benzamide, **8(d)**

^{1}H NMR (400MHz, DMSO-d_6) δ ppm = 10.04 (br. s., 1H), 7.83 (s, 1H), 7.76 (s, 1H), 7.62 - 7.52 (m, 3H), 7.44-7.40 (m, 3 H), 7.36 (s, 1H), 7.30 - 7.24 (m, 1H), 6.98 (d, *J* = 8.1 Hz, 2H), 4.60 (s, 2H). ^{13}C NMR (100MHz, DMSO-d_6) δ ppm = 165.3, 141.0, 140.5, 140.2, 139.1, 137.3, 131.7, 129.8(2C), 127.4, 126.6(2C), 126.0, 125.9, 125.8, 125.4,

APPENDIX A (CONTINUED)

122.6, 119.2, 118.9, 53.7. HRMS (ESI) m/z [M + H]+ calcd for $C_{20}H_{16}N_8O$ 385.1525, found 385.1531

N-(4-amino-[1,1'-biphenyl]-3-yl)-3-azido-4-(2-azidoethoxy)benzamide, **8(e)**

^{1}H NMR (400MHz, DMSO-d_6) δ ppm = 9.81 (br. s., 1H), 7.86 (d, *J* = 6.6 Hz, 1H), 7.77 - 7.71 (m, 1H), 7.58-7.51 (m, 3 H), 7.45 - 7.34 (m, 3H), 7.27 (d, *J* = 8.3 Hz, 1H), 6.93 (d, *J* = 8.1 Hz, 1H), 4.42 - 4.30 (t, *J* = 5Hz, 2H), 3.80 - 3.67 (t, *J* = 5Hz, 2H). ^{13}C NMR (100MHz, DMSO-d_6) δ ppm = 164.6, 153.6, 140.5, 129.4, 129.3(2C), 128.2, 127.7, 127.4, 126.7, 126.6, 126.0(2C), 125.4, 125.3, 124.4, 121.0, 117.5, 113.5, 68.3, 50.0. HRMS (ESI) m/z [M + H]+ calcd for $C_{21}H_{18}N_8O_2$ 415.1631, found 415.1637.

N-(2-amino-5-(thiophen-2-yl)phenyl)-3-azido-4-(2-azidoethoxy)benzamide, **8(f)**

^{1}H NMR (400MHz ,DMSO-d_6) δ ppm = 9.73 (s, 1H), 7.85 (dd, *J* = 2.1, 8.7 Hz, 1H), 7.74 (d, *J* = 2.3 Hz, 1H), 7.44 (d, *J* = 1.8 Hz, 1H), 7.36 (dd, *J* = 1.1, 5.2 Hz, 1H), 7.31 (dd, *J* = 2.0, 8.3 Hz, 1H), 7.28 - 7.24 (m, 2H), 7.06 (dd, *J* = 3.5, 5.1 Hz, 1H), 6.83 (d, *J* = 8.3 Hz, 1H), 4.36 - 4.32 (t, *J* = 5 Hz, 2H)), 3.76 - 3.72 (t, *J* = 5 Hz, 2H). ^{13}C NMR (100MHz, DMSO-d_6) δ ppm = 165.5, 153.6, 144.6, 143.4, 128.7, 128.1, 127.7, 126.7, 124.6, 124.5, 123.8, 123.7, 122.9, 121.5, 121.0, 116.9, 113.5, 68.3, 50.0 HRMS (ESI) m/z [M + H]+ calcd for $C_{19}H_{16}N_8O_2S$ 421.1195, found 421.1211.

3-Azidobenzyl (4-((4-amino-[1,1'-biphenyl]-3-yl)carbamoyl)benzyl)carbamate, **75(a)**

^{1}H NMR (400MHz, DMSO-d_6) δ ppm = 9.73 (s, 1H), 7.99 - 7.95 (m, 3H), 7.50 - 7.34 (m, 7H), 7.31 (dd, *J* = 2.0, 8.3 Hz, 1H), 7.26 (dd, *J* = 1.0, 3.5 Hz, 1H), 7.19 (d, *J* = 7.3 Hz,

APPENDIX A (CONTINUED)

1H), 7.12 - 7.05 (m, 3H), 6.84 (d, *J* = 8.3 Hz, 1H), 5.08 (s, 2H), 4.30 (d, *J* = 6.1 Hz, 2H). ^{13}C NMR (100MHz, DMSO-d_6) δ ppm = 166.2, 157.2, 145.0, 144.2, 143.3, 140.4, 140.3, 133.9, 131.0, 129.1, 128.8(4C), 127.6(4C), 125.1, 124.8, 124.7, 124.5, 124.2, 123.5, 122.0, 119.3, 118.7, 117.5, 65.6, 44.5. HRMS (ESI) m/z [M + H]+ calcd for $C_{28}H_{24}N_6O_3$ 493.1988, found 493.2002.

3-Azido-5-(azidomethyl)benzyl(4-((4-amino-[1,1'-biphenyl]-3-yl)carbamoyl)benzyl)carbamate, **75(b)**

^{1}H NMR (400MHz, DMSO-d_6) δ ppm = 9.88 (s, 1H), 7.98 (m, 3 H), 7.58 (d, *J* = 7.8 Hz, 3H), 7.44 - 7.38 (m, 5H), 7.28 (s, 1H), 7.18 (s, 1H), 7.10 (s, 2H), 6.99 (d, *J* = 8.3 Hz, 1H), 5.09 (s, 2H), 4.50 (s, 2H), 4.31 (d, *J* = 6.1 Hz, 2H). ^{13}C NMR (100MHz, DMSO-d_6) δ ppm = 165.9, 156.7, 143.9, 140.4, 140.4, 140.3, 138.6, 133.4, 129.3(2C), 128.4(2C), 127.2(2C), 126.9, 126.2(2C), 125.5, 125.5, 125.2, 124.9, 124.3, 118.6, 118.4, 118.4, 118.0, 65.1, 53.4, 44.1, 41.5. HRMS (ESI) m/z [M + H]+ calcd for $C_{29}H_{25}N_9O_3$ 548.2159, found 548.2135.

3-Azido-5-(azidomethyl)benzyl(4-((2-amino-5-(thiophen-2-yl)phenyl)carbamoyl)benzyl)carbamate, **75(c)**

^{1}H NMR (400MHz ,DMSO-d_6) δ ppm = 9.76 (br. s., 1H), 8.05 - 7.95 (m, 3H), 7.60 - 7.52 (m, 3H), 7.44 - 7.33 (m, 4H), 7.26 (d, *J* = 7.3 Hz, 1H), 7.19 (br. s., 1H), 7.10 (br. s., 1H), 6.91 (d, *J* = 8.6 Hz, 1H), 5.09 (br. s., 2H), 4.50 (s, 2H), 4.30 (d, *J* = 5.8 Hz, 2H). ^{13}C NMR (100MHz, DMSO-d_6) δ ppm = 167.3, 156.7, 143.5, 140.5, 140.4, 140.4, 140.0,

APPENDIX A (CONTINUED)

138.6, 133.6, 129.3(2C), 128.3, 127.2, 126.6, 126.0(2C), 125.7, 125.2, 125.2, 124.4, 124.3, 118.6, 118.0, 117.3, 65.1, 53.4, 44.1. HRMS (ESI) m/z [M + H]+ calcd for $C_{27}H_{23}N_9O_3S$ 554.1723, found 554.1725.

APPENDIX B. COMPOUND CHARACTERIZATION SPECTRA

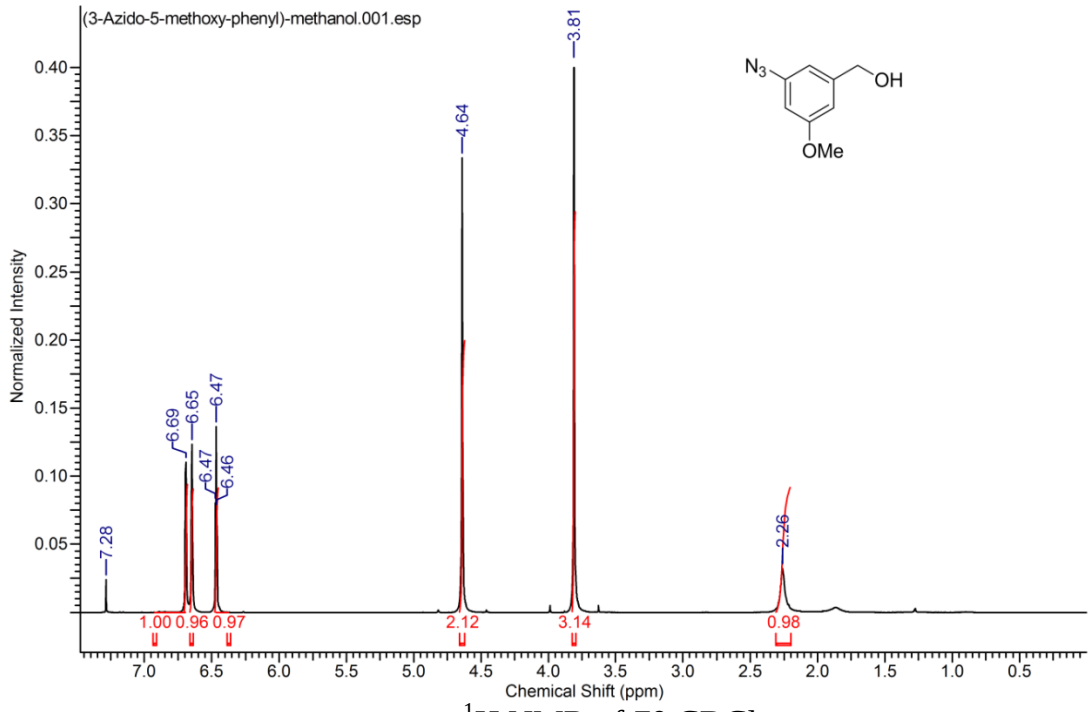

^{1}H NMR of **70** $CDCl_3$

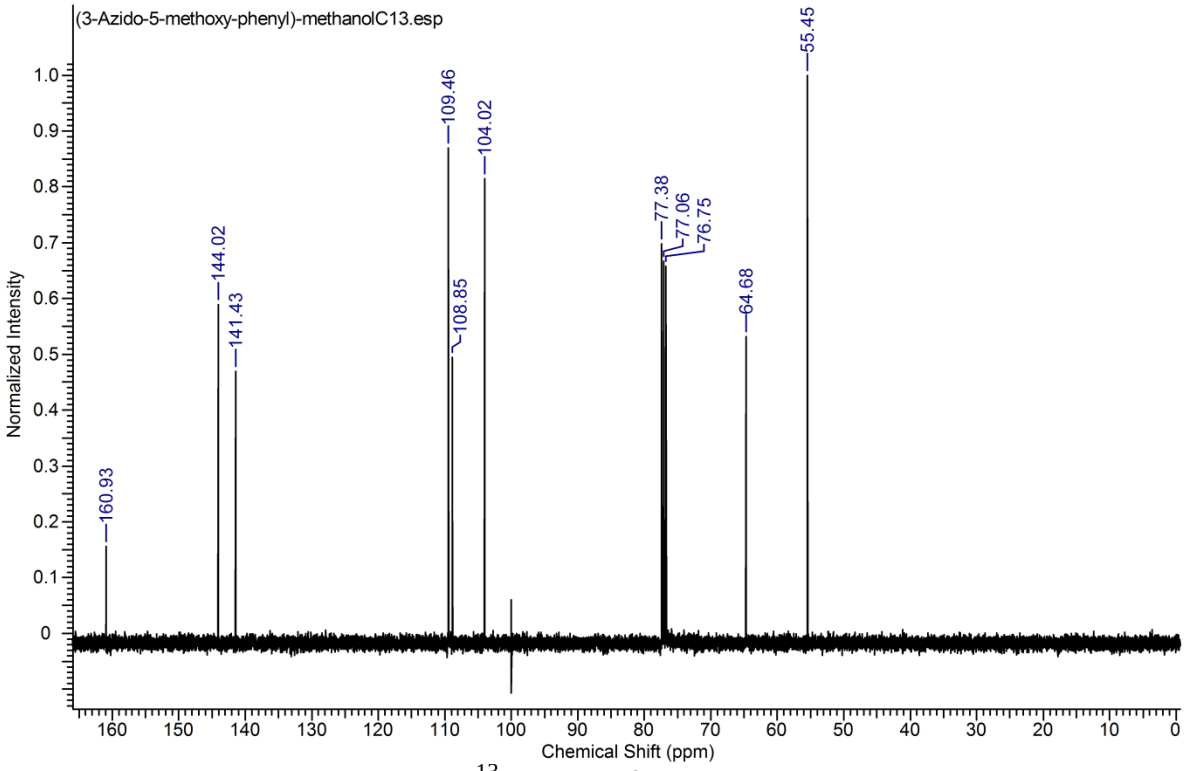

^{13}CNMR of **70** $CDCl_3$

APPENDIX B (CONTINUED)

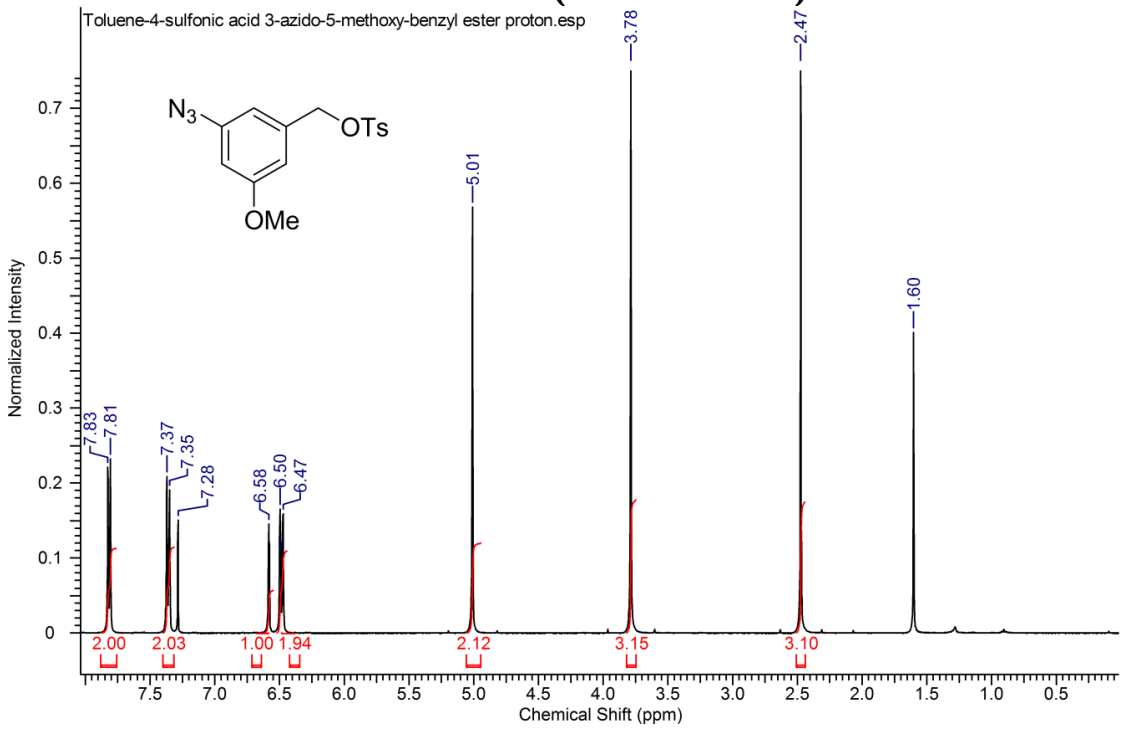

^{1}H NMR of **71** $CDCl_3$

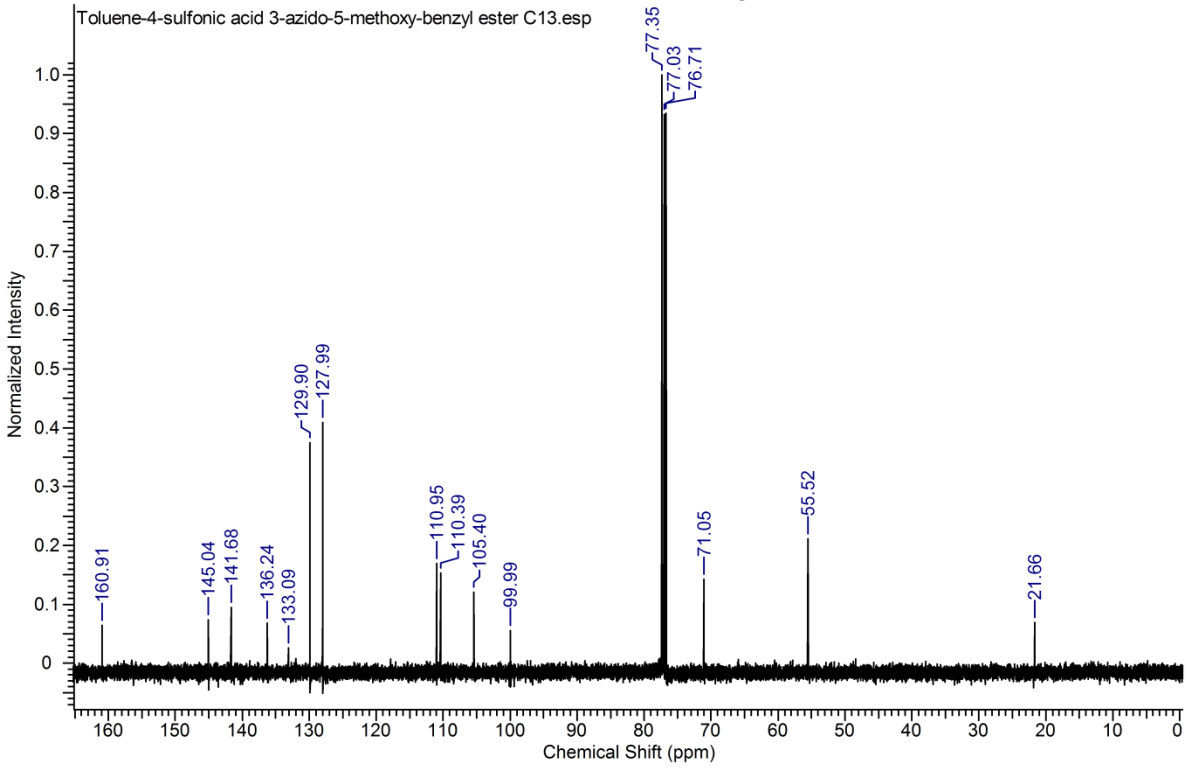

^{13}C NMR of **71** $CDCl_3$

APPENDIX B (CONTINUED)

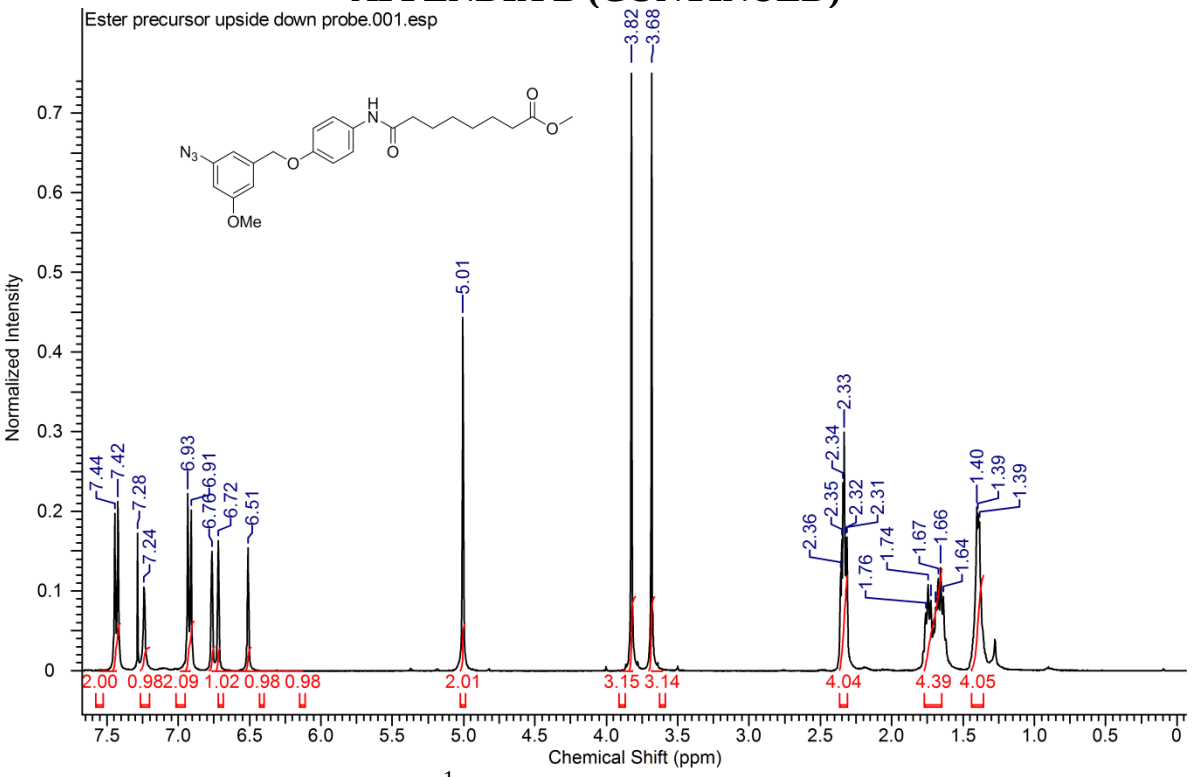

^{1}H NMR of **72** $CDCl_3$

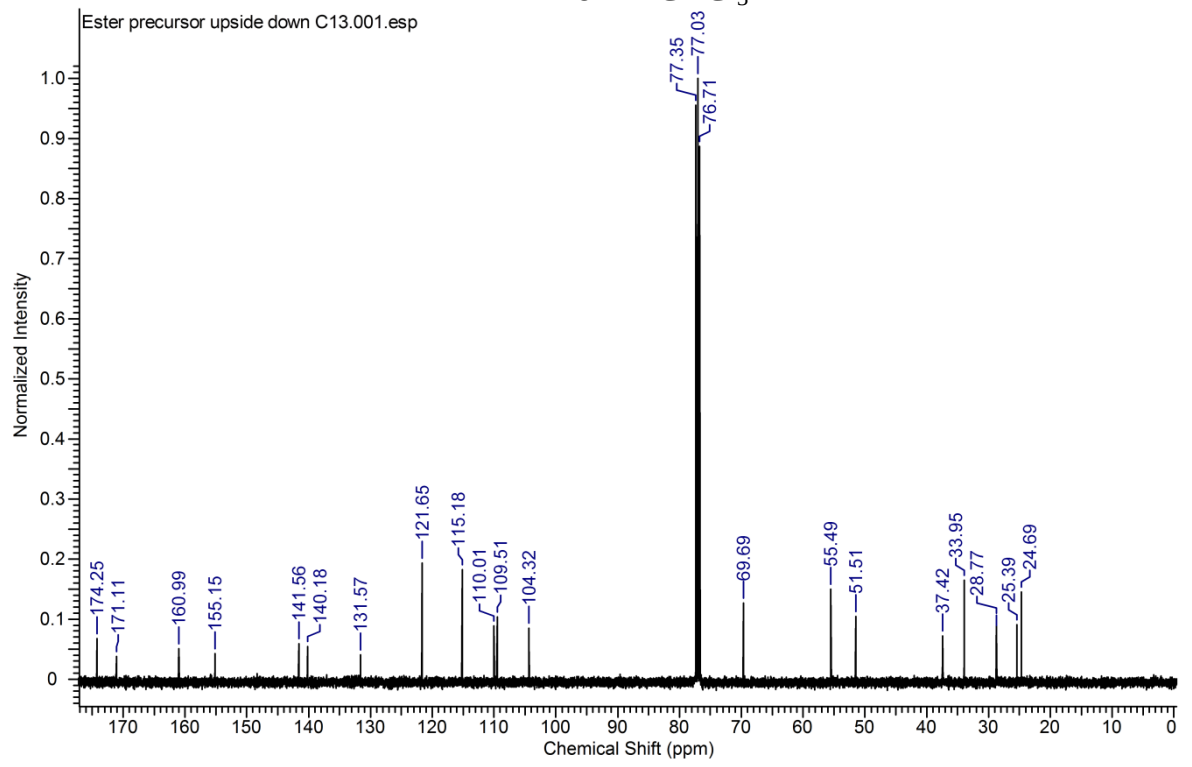

^{13}C NMR of **72** $CDCl_3$

APPENDIX B (CONTINUED)

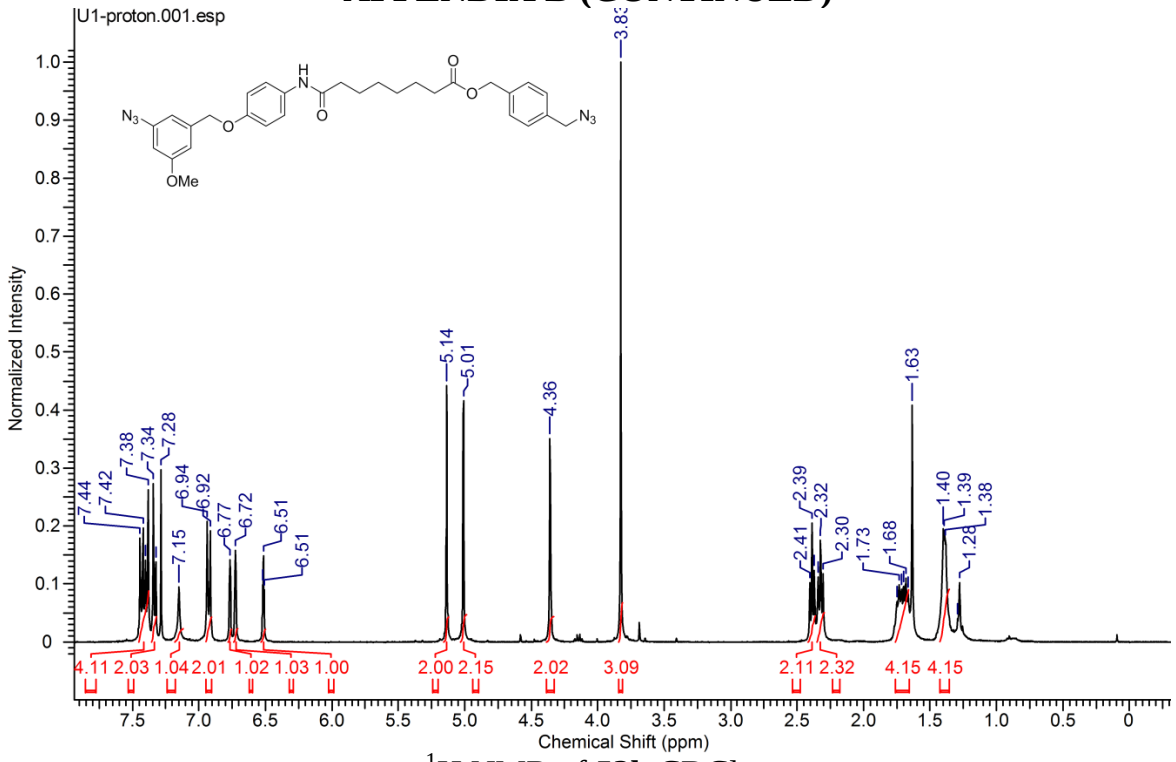

^{1}H NMR of **52h** $CDCl_3$

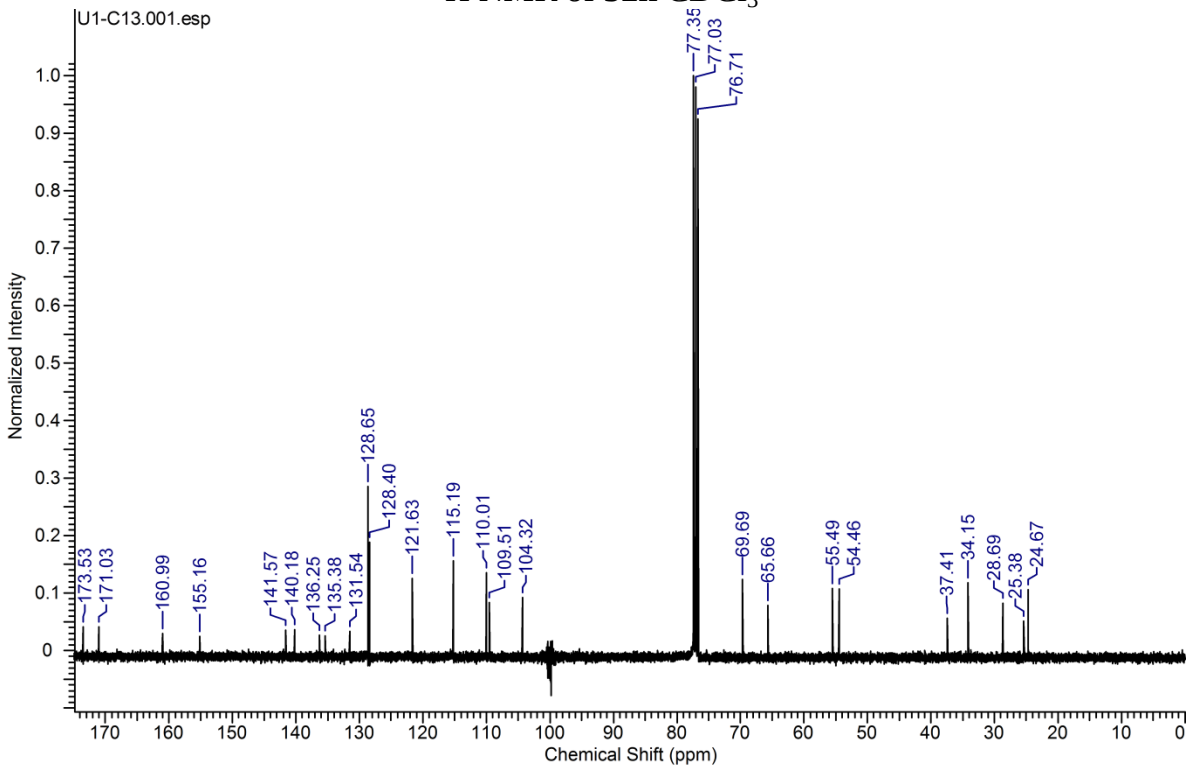

^{13}C NMR of **52h** $CDCl_3$

APPENDIX B (CONTINUED)

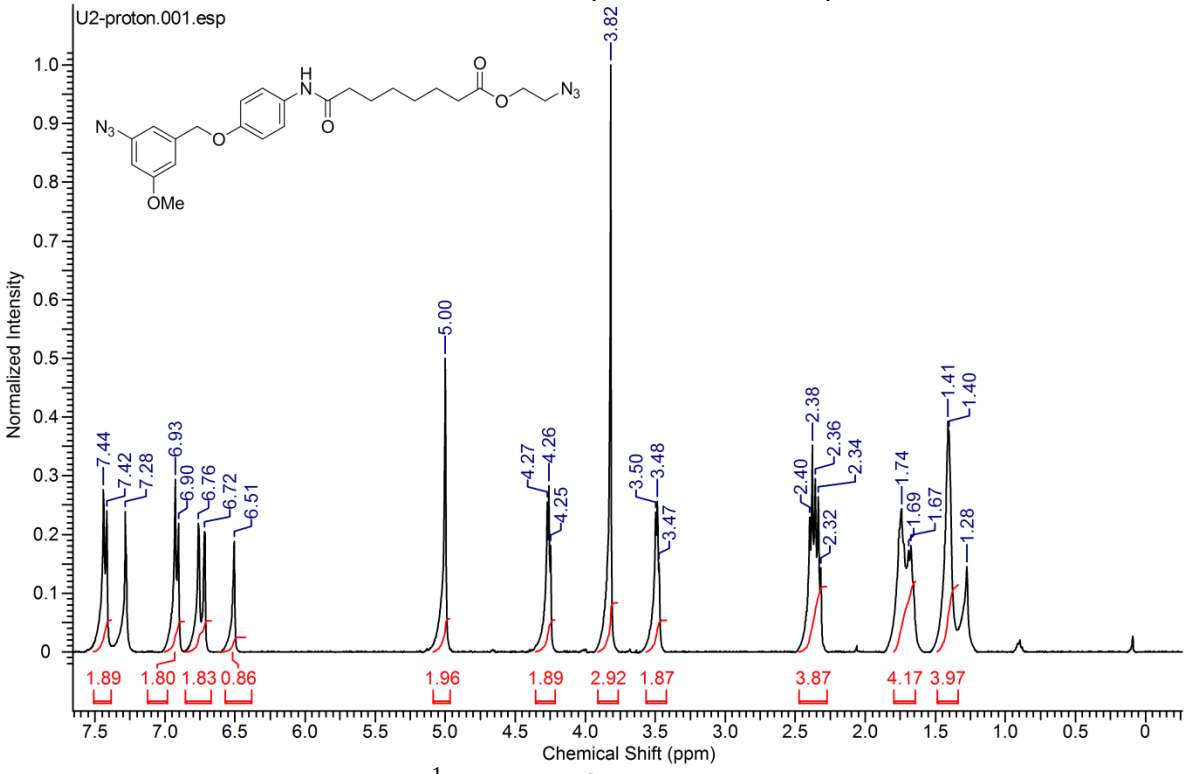

^{1}H NMR of **52g** $CDCl_3$

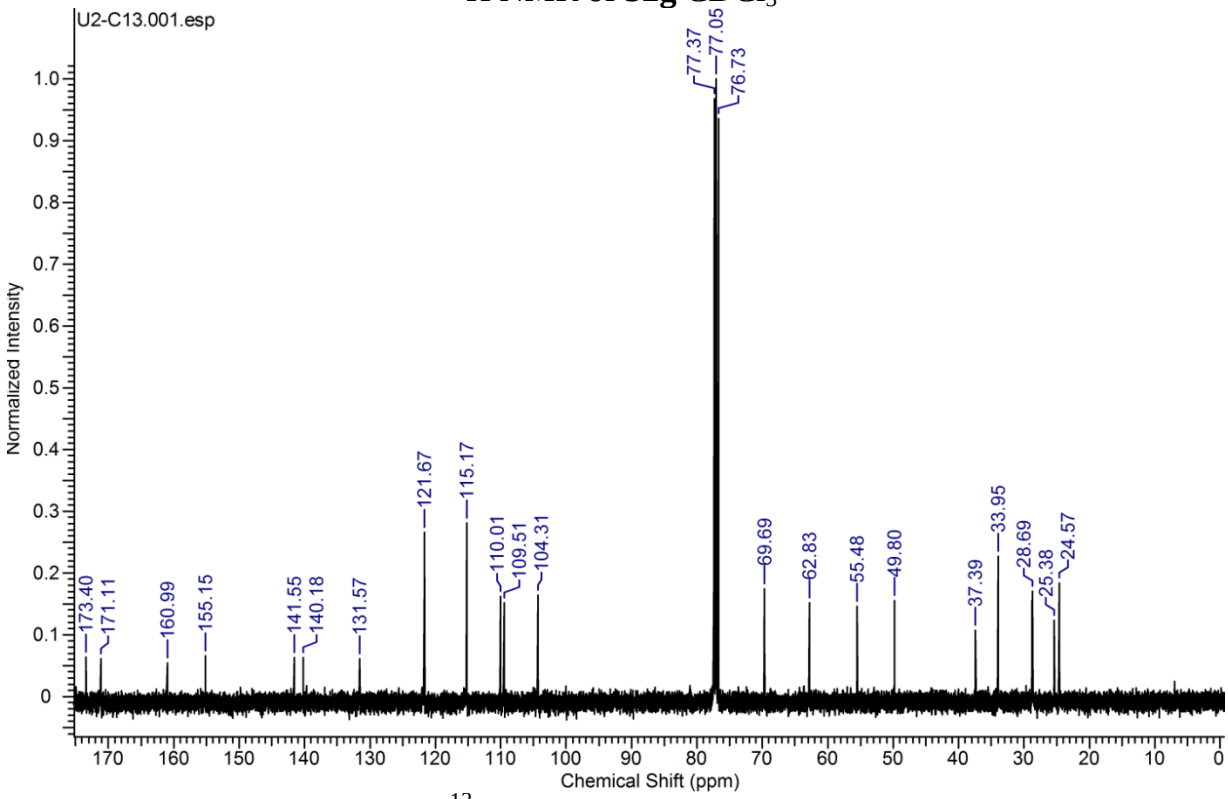

^{13}C NMR of **52g** $CDCl_3$

APPENDIX B (CONTINUED)

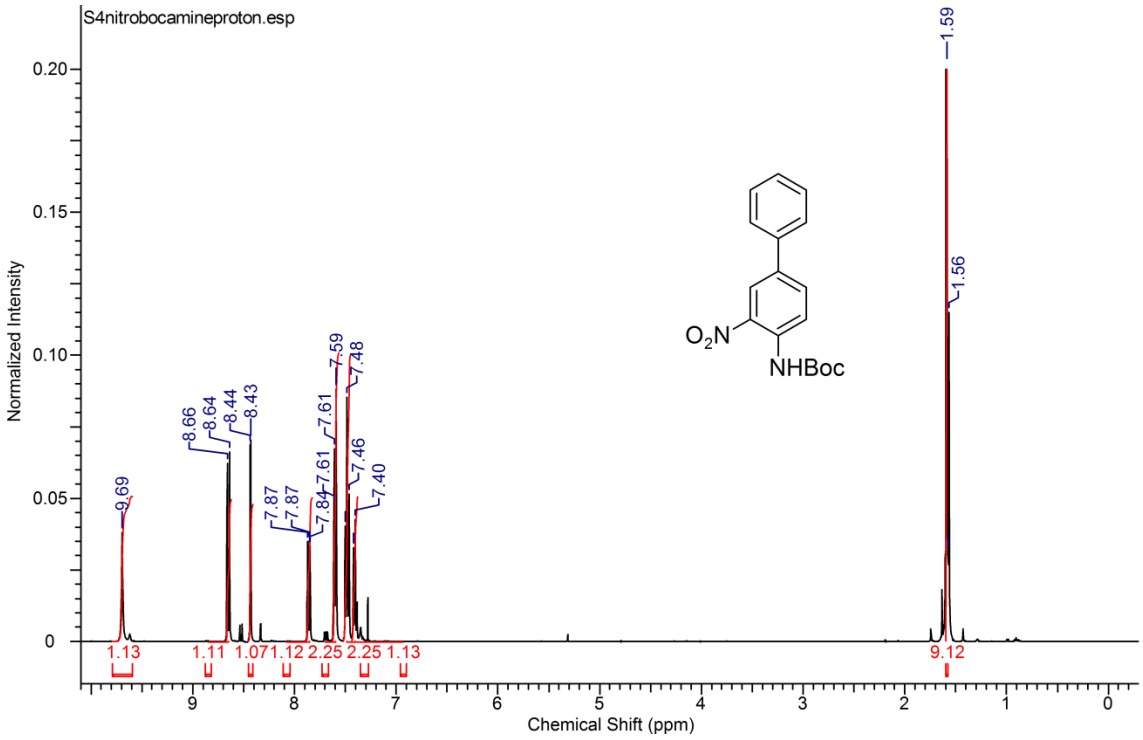

^{1}H NMR of **101** $CDCl_3$

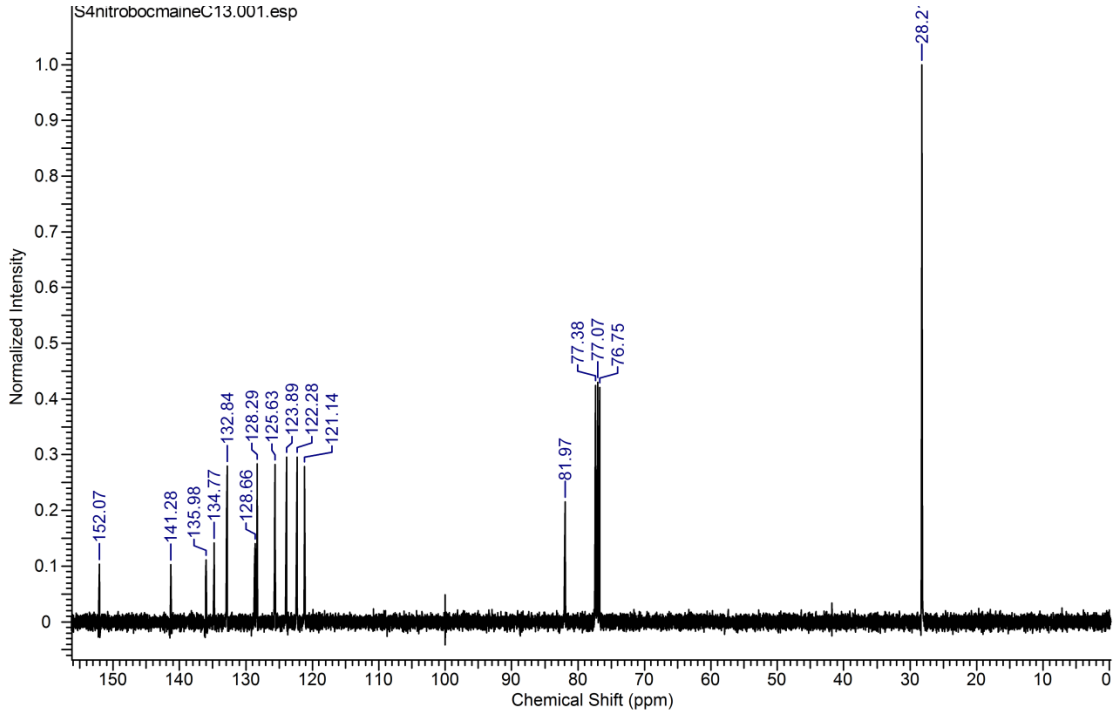

^{13}C NMR of **101** $CDCl_3$

APPENDIX B (CONTINUED)

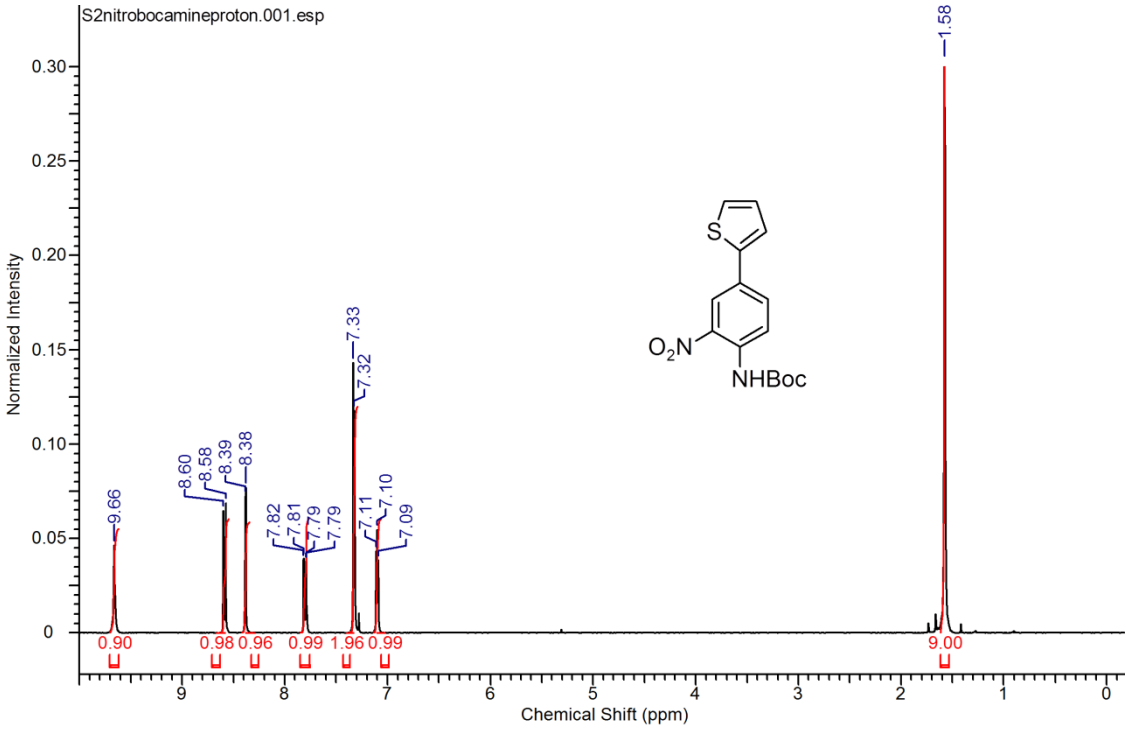

^{1}H NMR of **102** $CDCl_3$

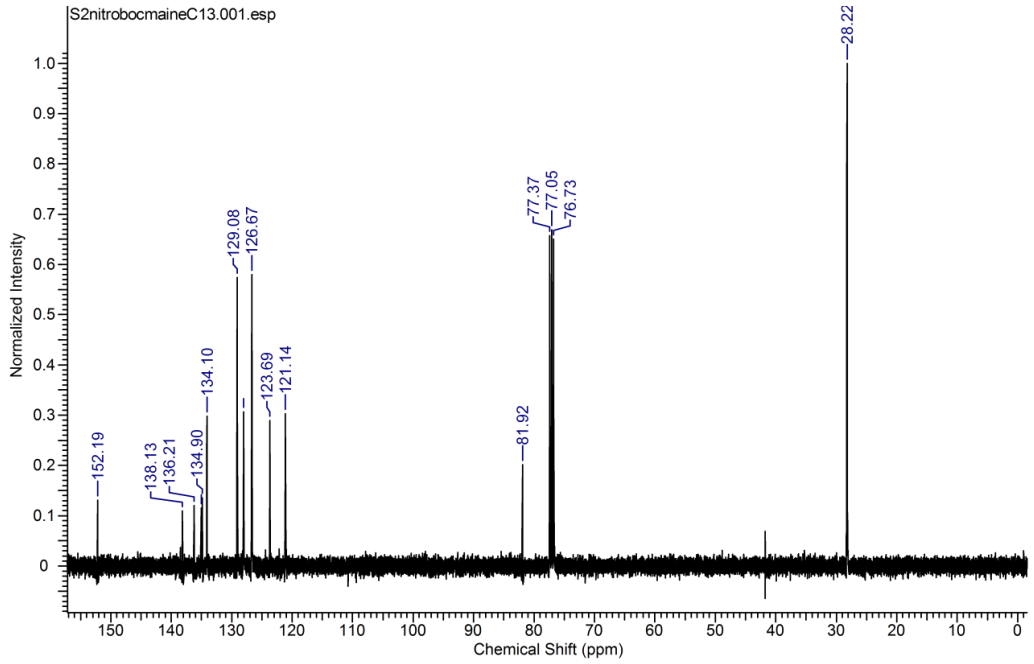

^{13}C NMR of **102** $CDCl_3$

APPENDIX B (CONTINUED)

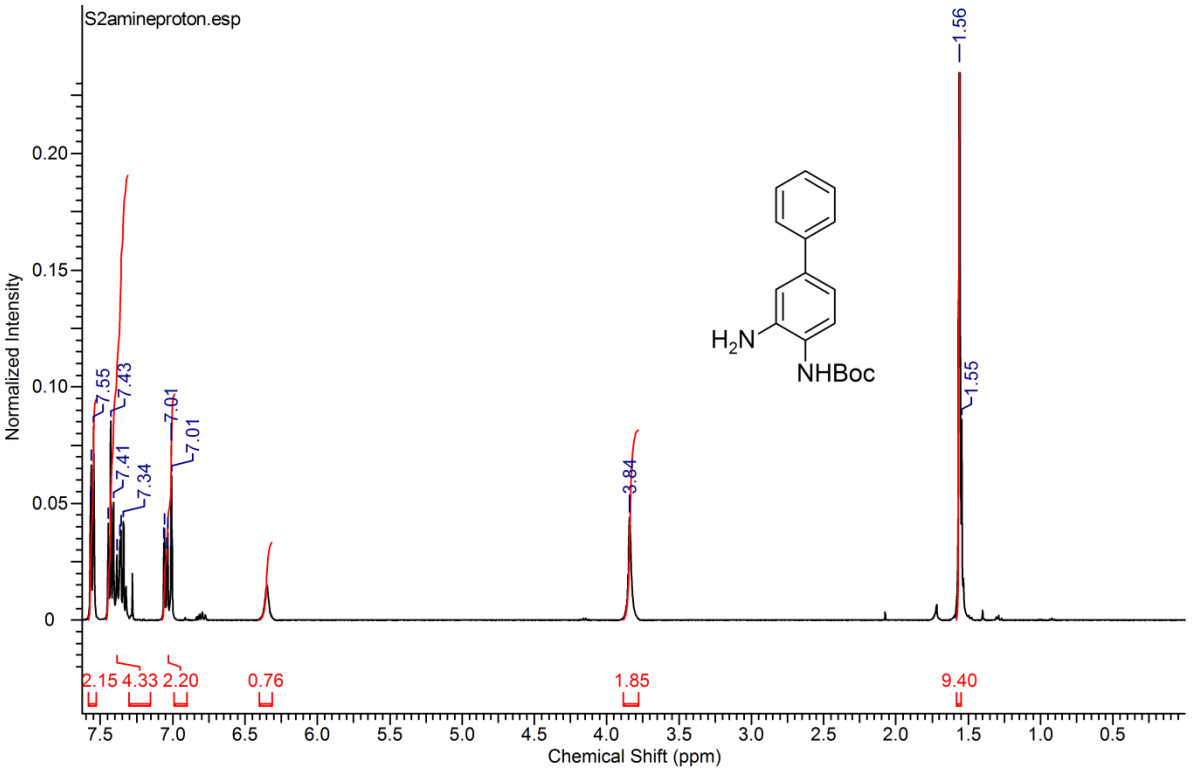

^{1}H NMR of **82** $CDCl_3$

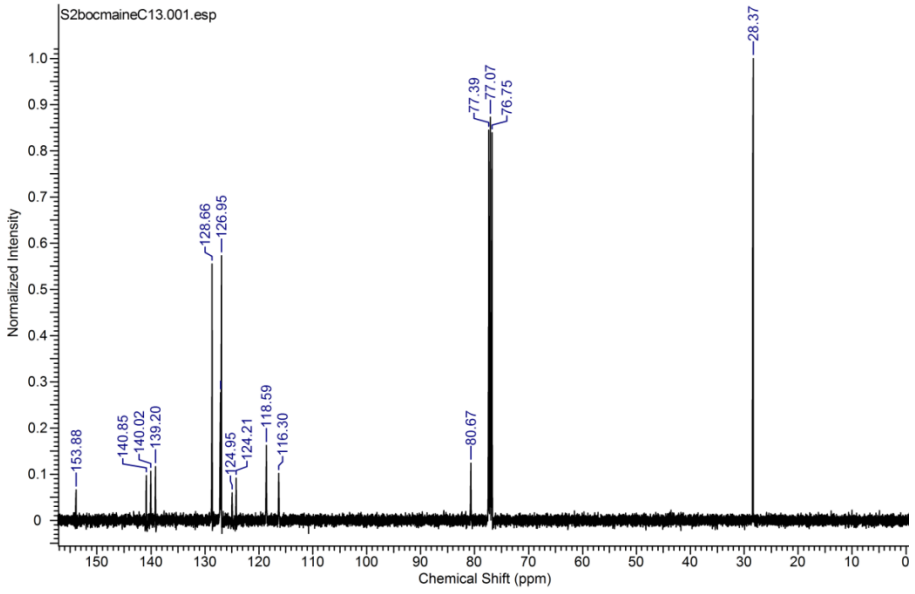

^{13}C NMR of **82** $CDCl_3$

APPENDIX B (CONTINUED)

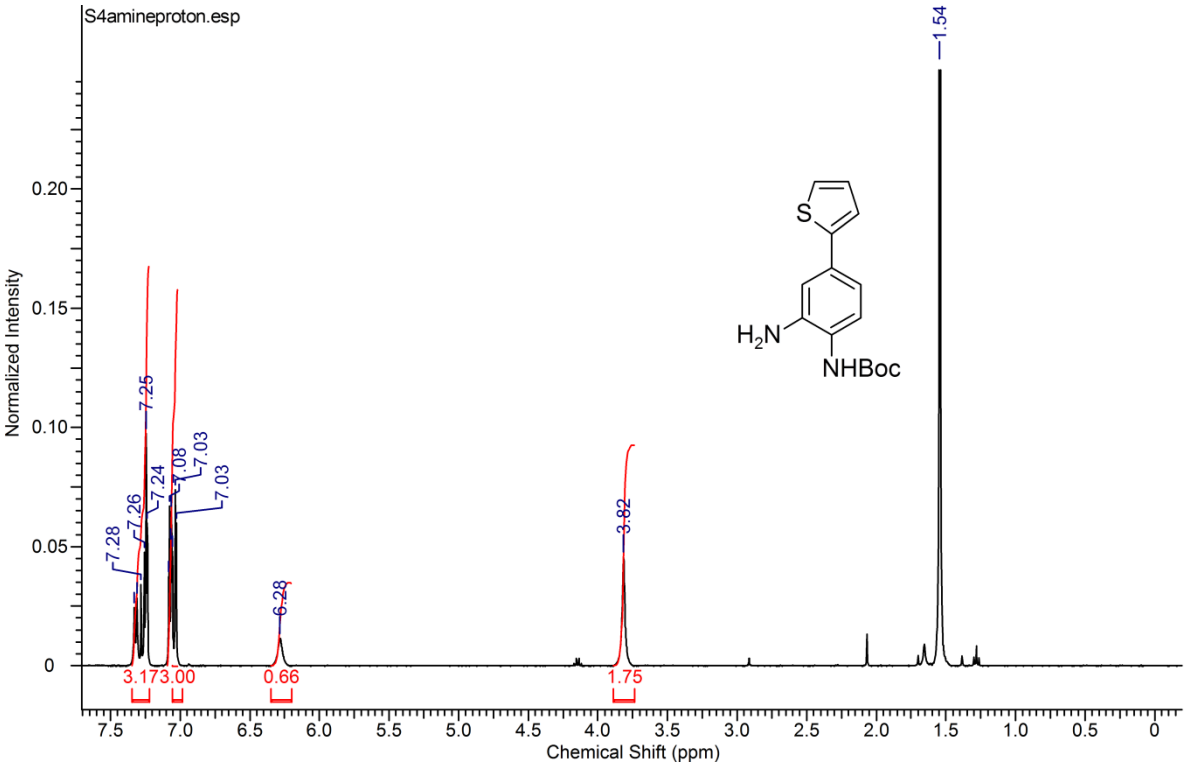

^{1}H NMR of **83** $CDCl_3$

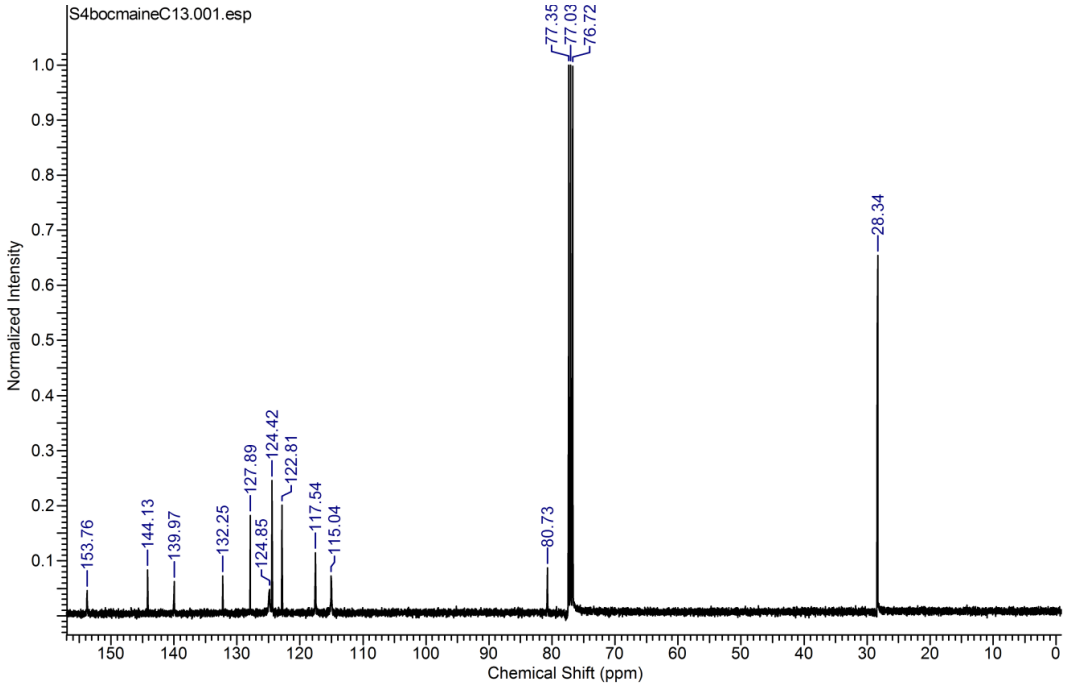

^{13}C NMR of **83** $CDCl_3$

APPENDIX B (CONTINUED)

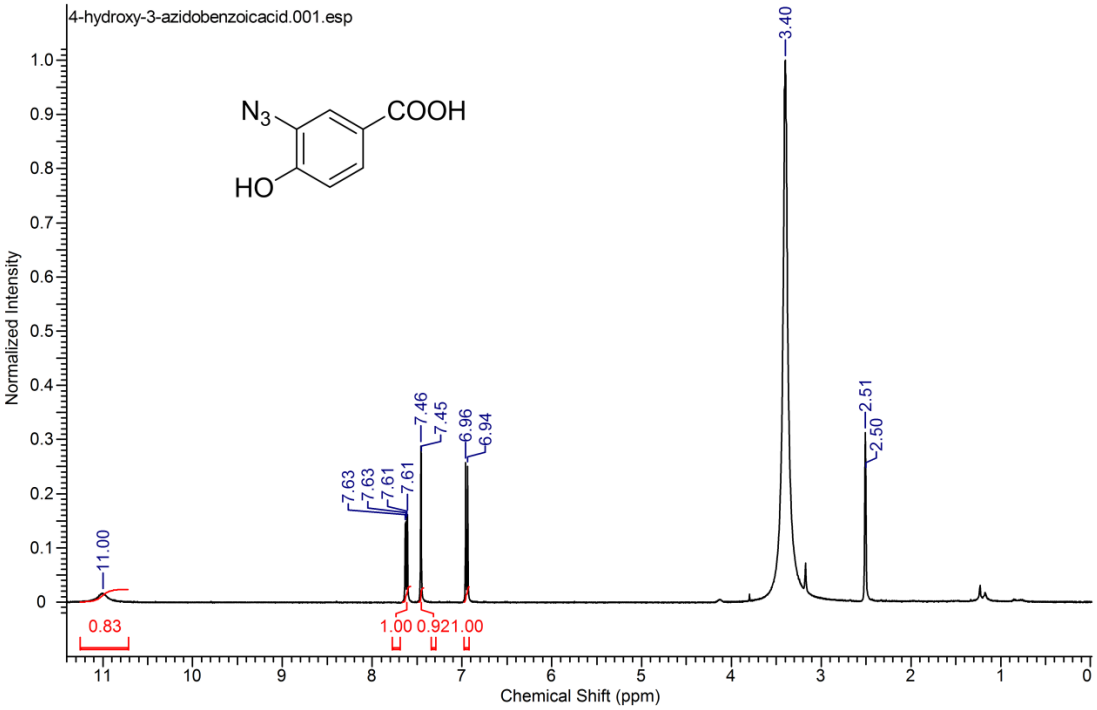

^{1}H NMR of **86** DMSO-d_6

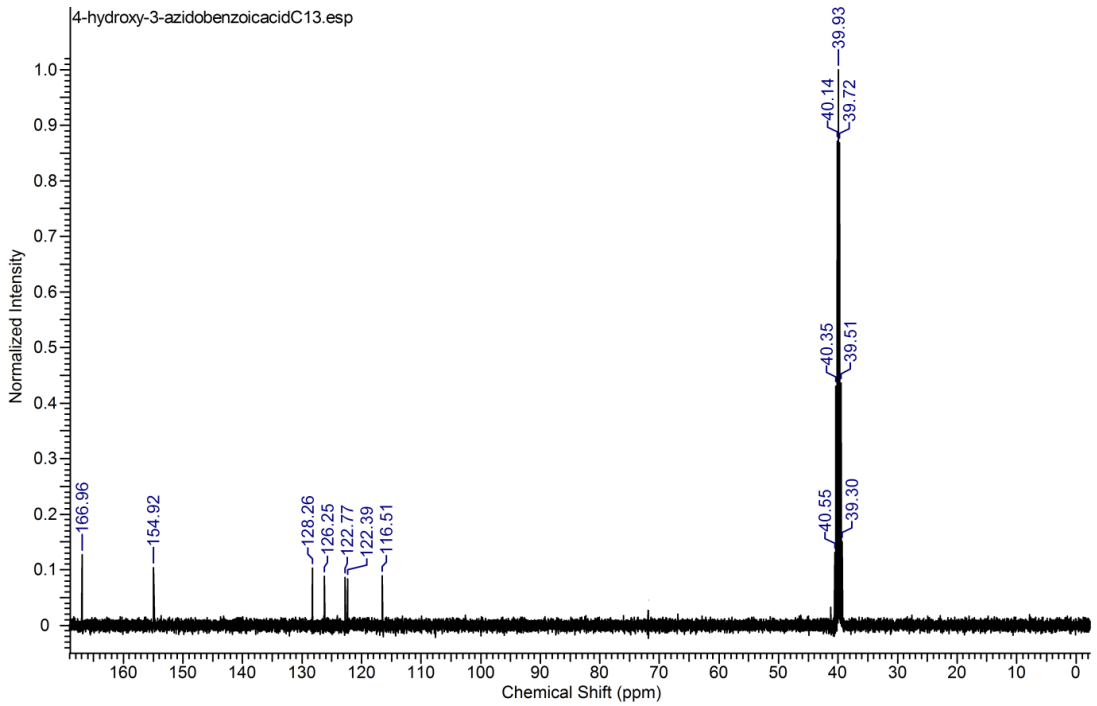

^{13}C NMR of **86** DMSO-d_6

APPENDIX B (CONTINUED)

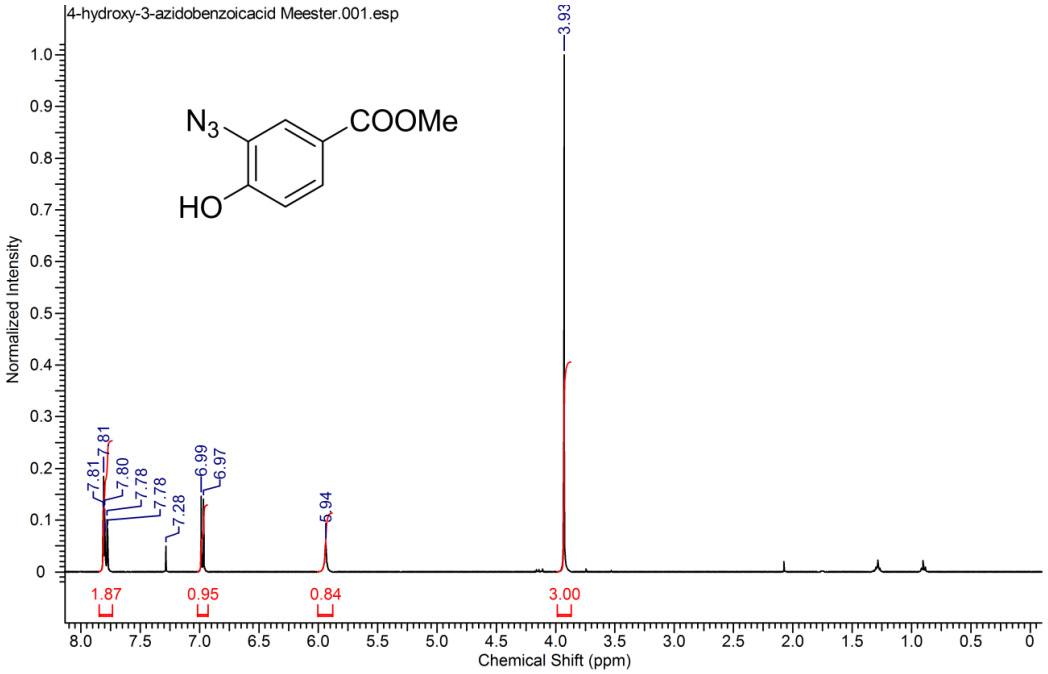

^{1}H NMR of **87** $CDCl_3$

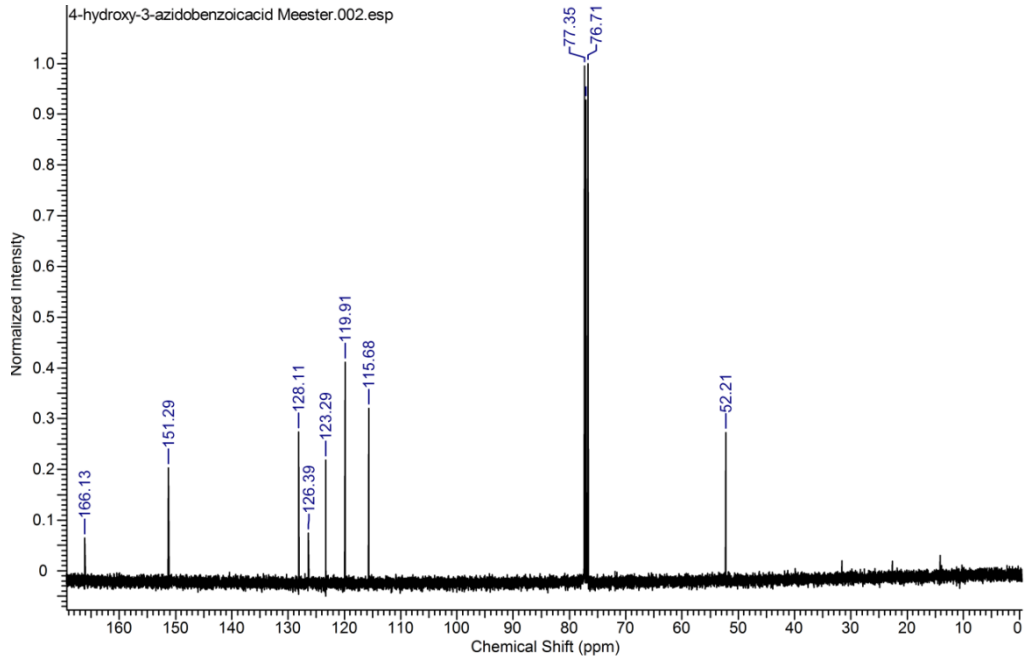

^{13}C NMR of **87** $CDCl_3$

APPENDIX B (CONTINUED)

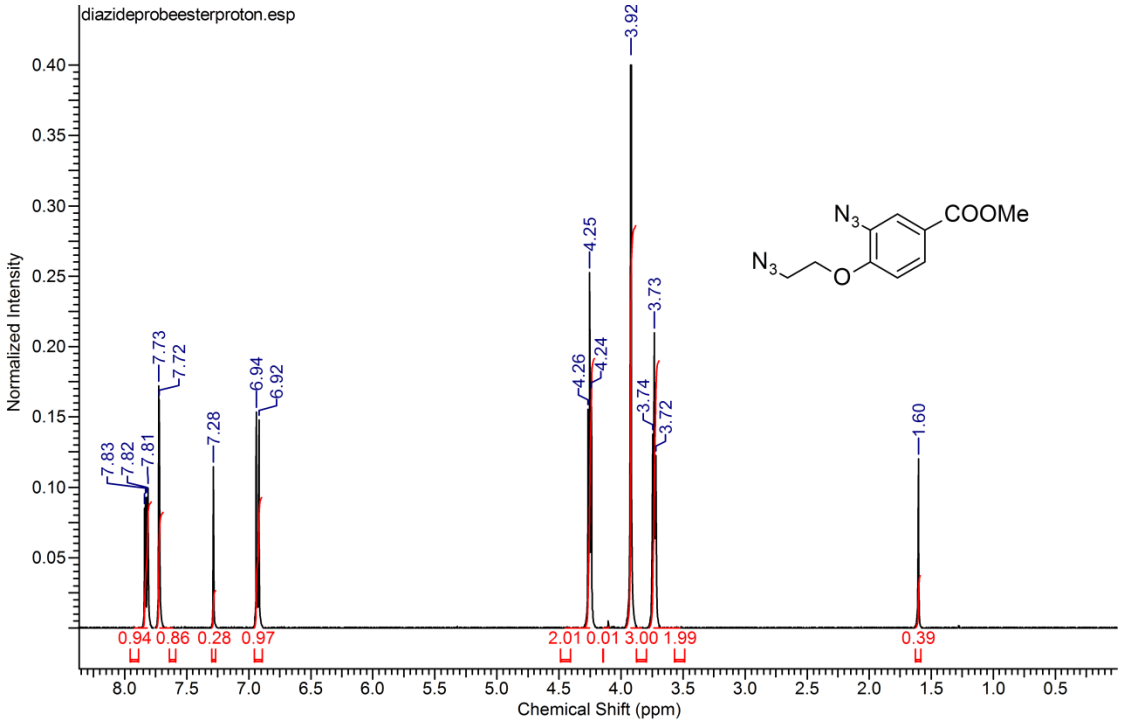

^{1}H NMR of **88** $CDCl_3$

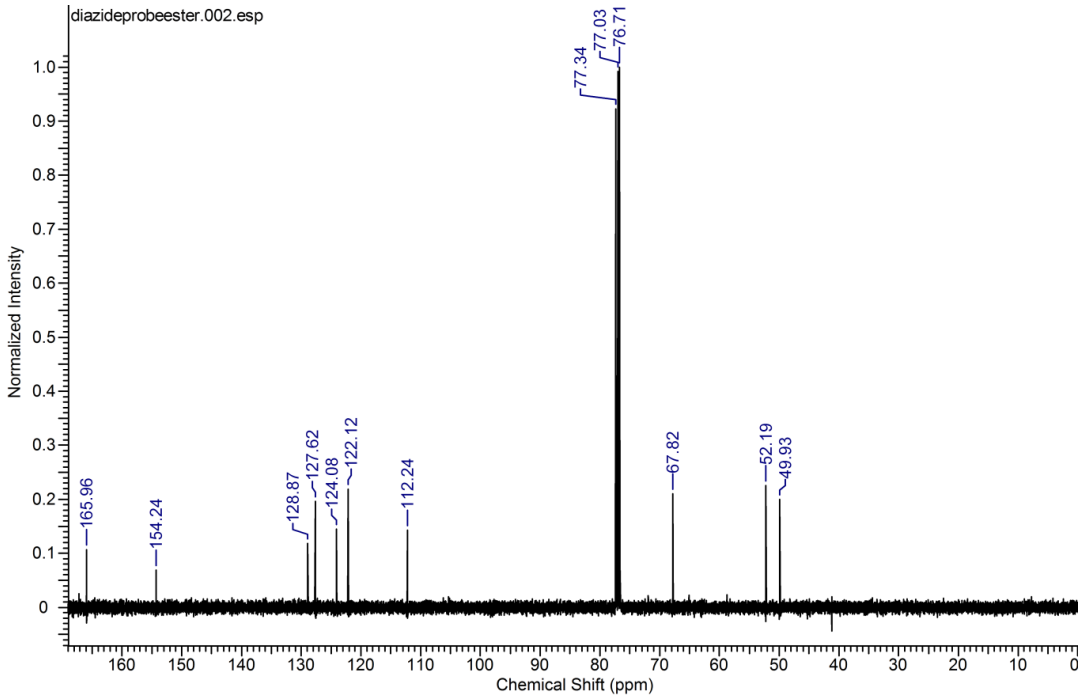

^{13}C NMR of **88** $CDCl_3$

APPENDIX B (CONTINUED)

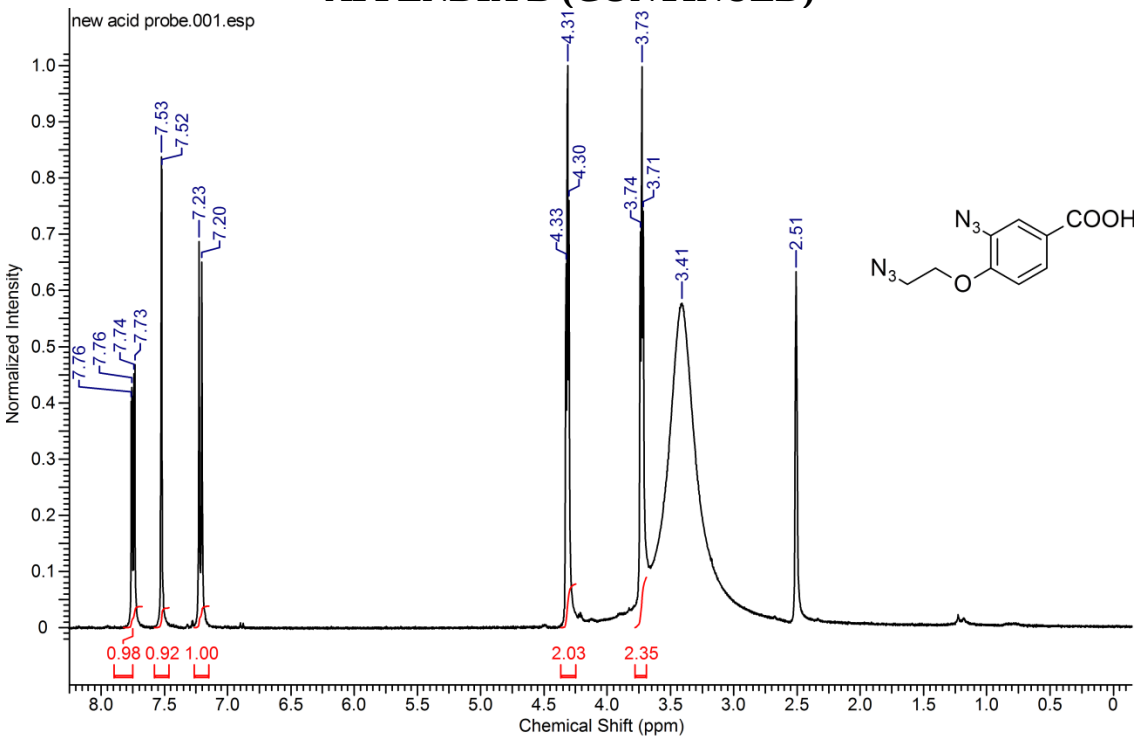

^{1}H NMR of **78** DMSO-d_6

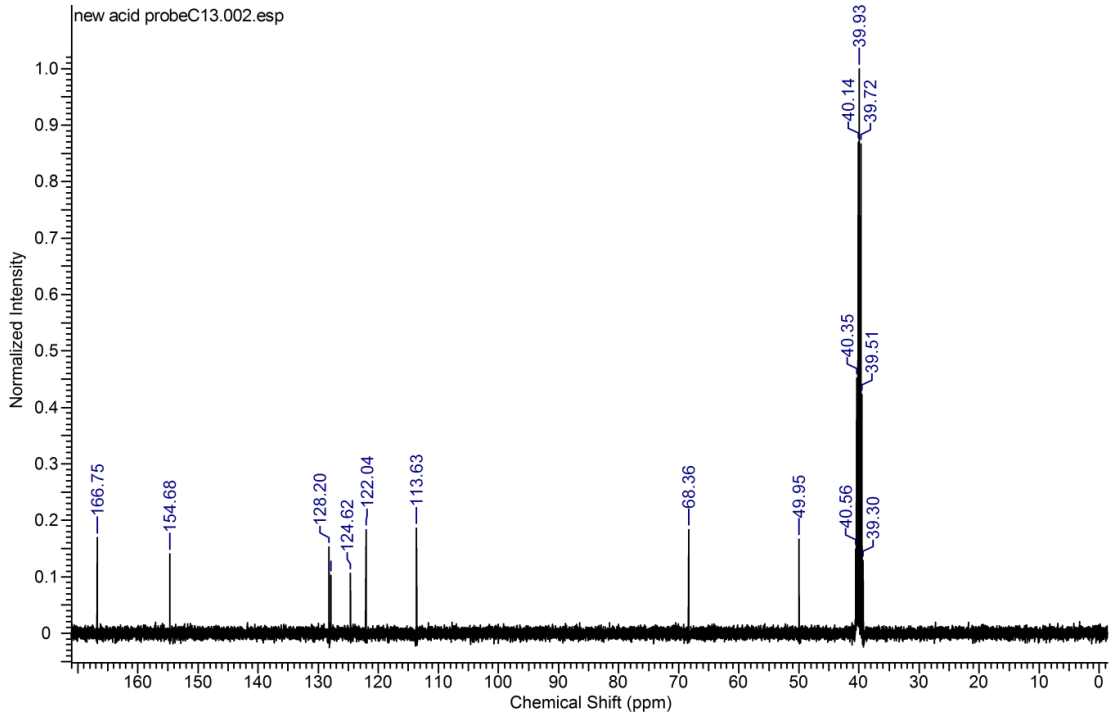

^{13}C NMR of **78** DMSO-d_6

APPENDIX B (CONTINUED)

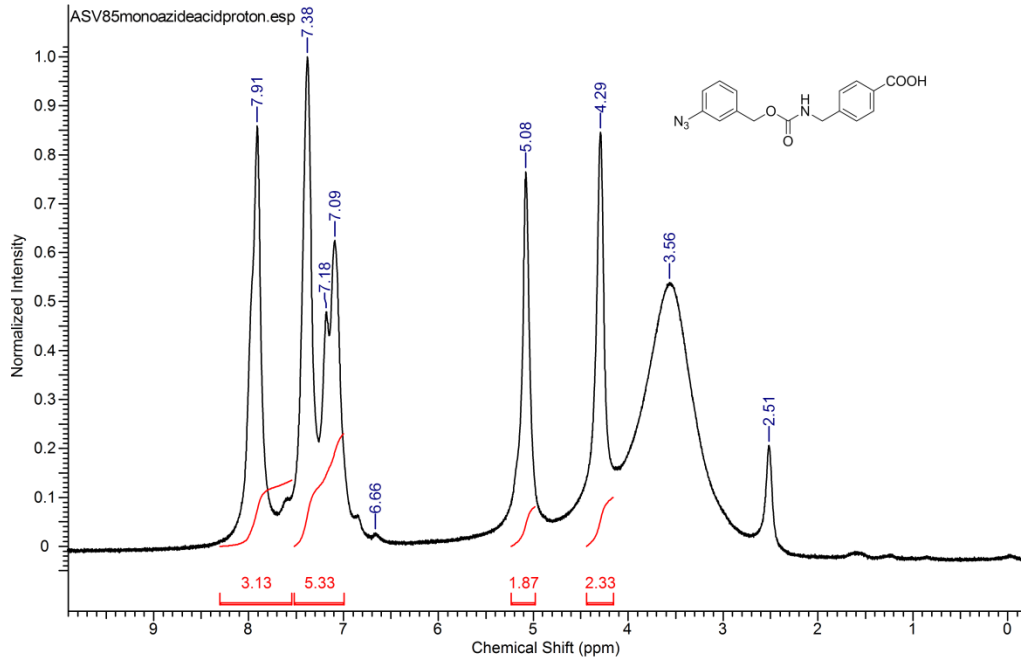

^{1}H NMR of **80** DMSO-d_6

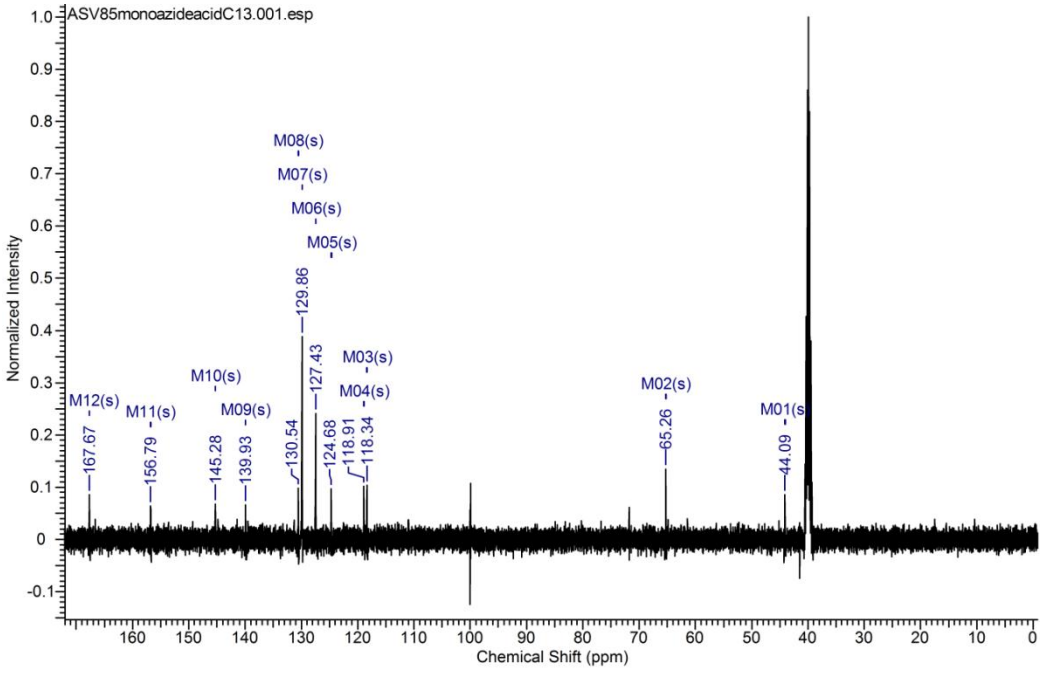

^{13}C NMR of **80** DMSO-d_6

APPENDIX B (CONTINUED)

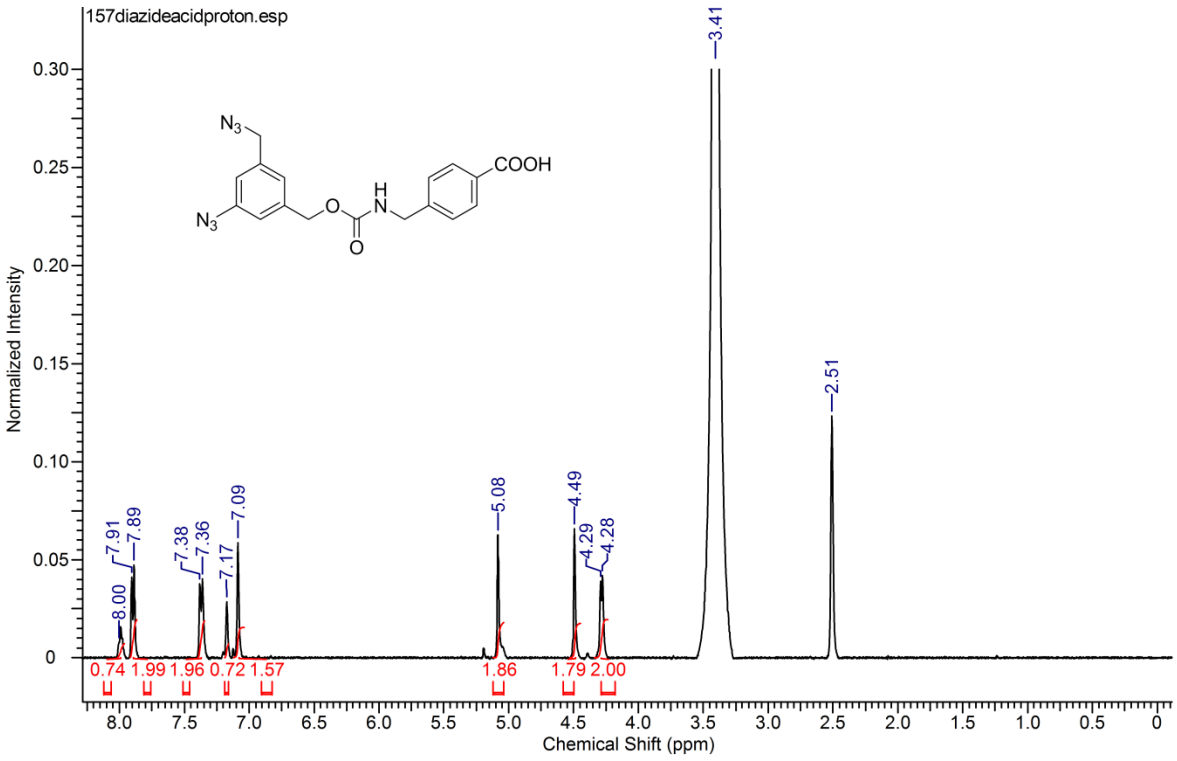

^{1}H NMR of **81** DMSO-d_6

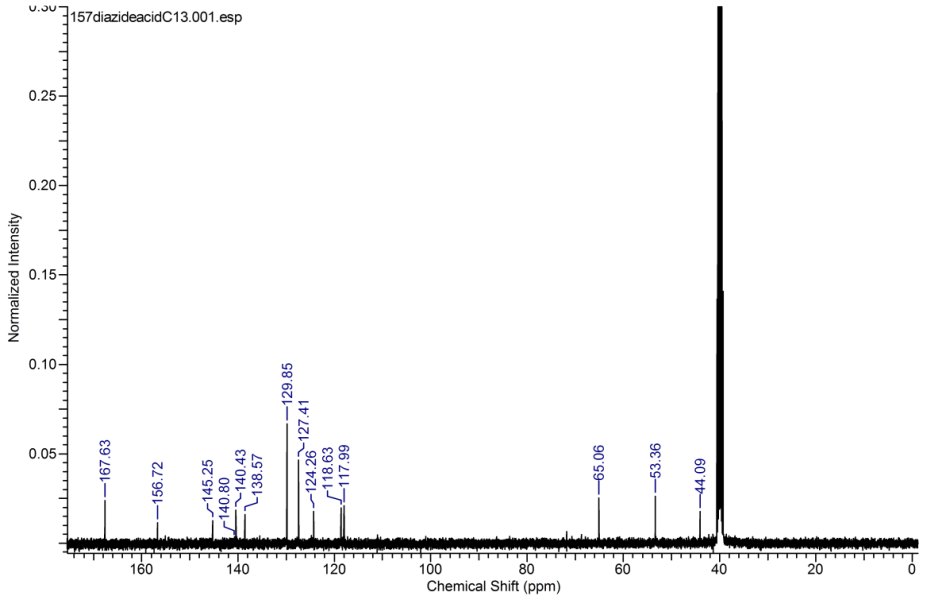

^{13}C NMR of **81** DMSO-d_6

APPENDIX B (CONTINUED)

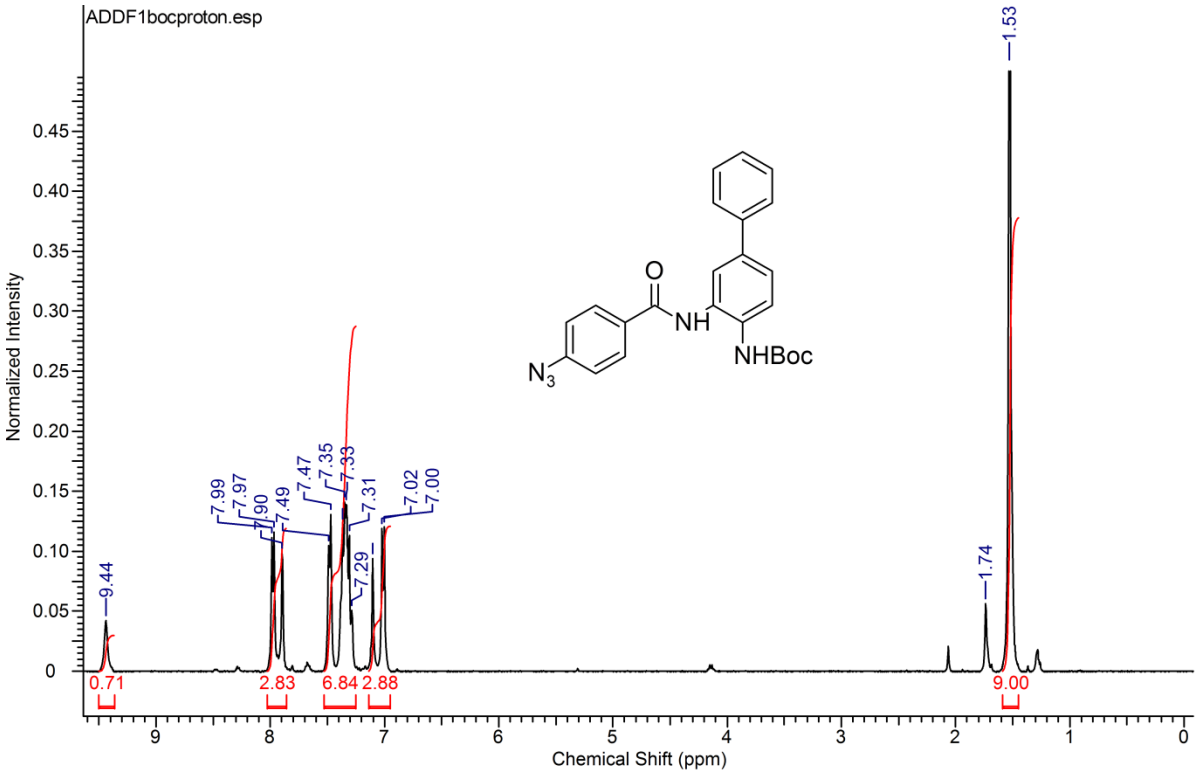

^{1}H NMR of **104a** $CDCl_3$

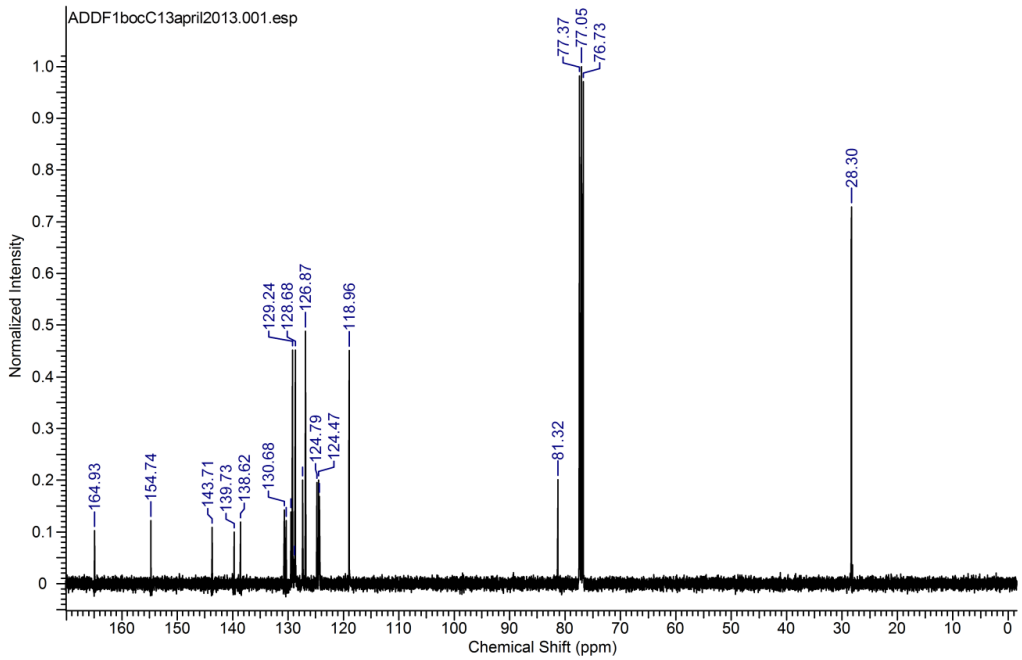

^{13}C NMR of **104a** $CDCl_3$

APPENDIX B (CONTINUED)

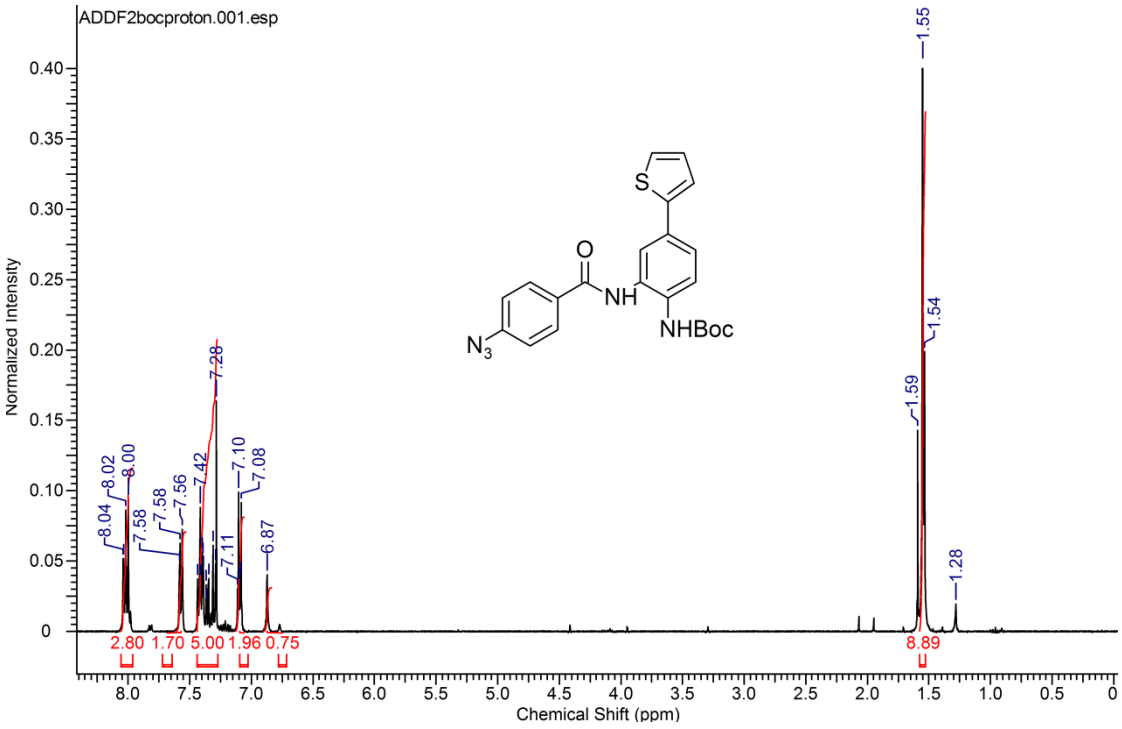

^{1}H NMR of **104b** $CDCl_3$

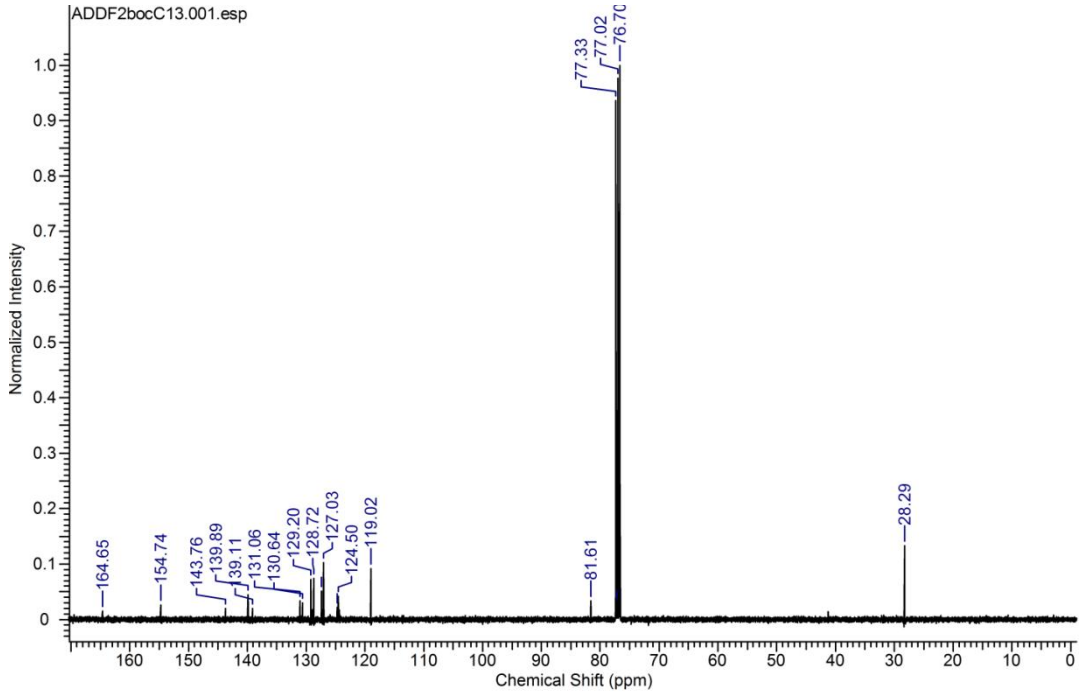

^{13}C NMR of **104b** $CDCl_3$

APPENDIX B (CONTINUED)

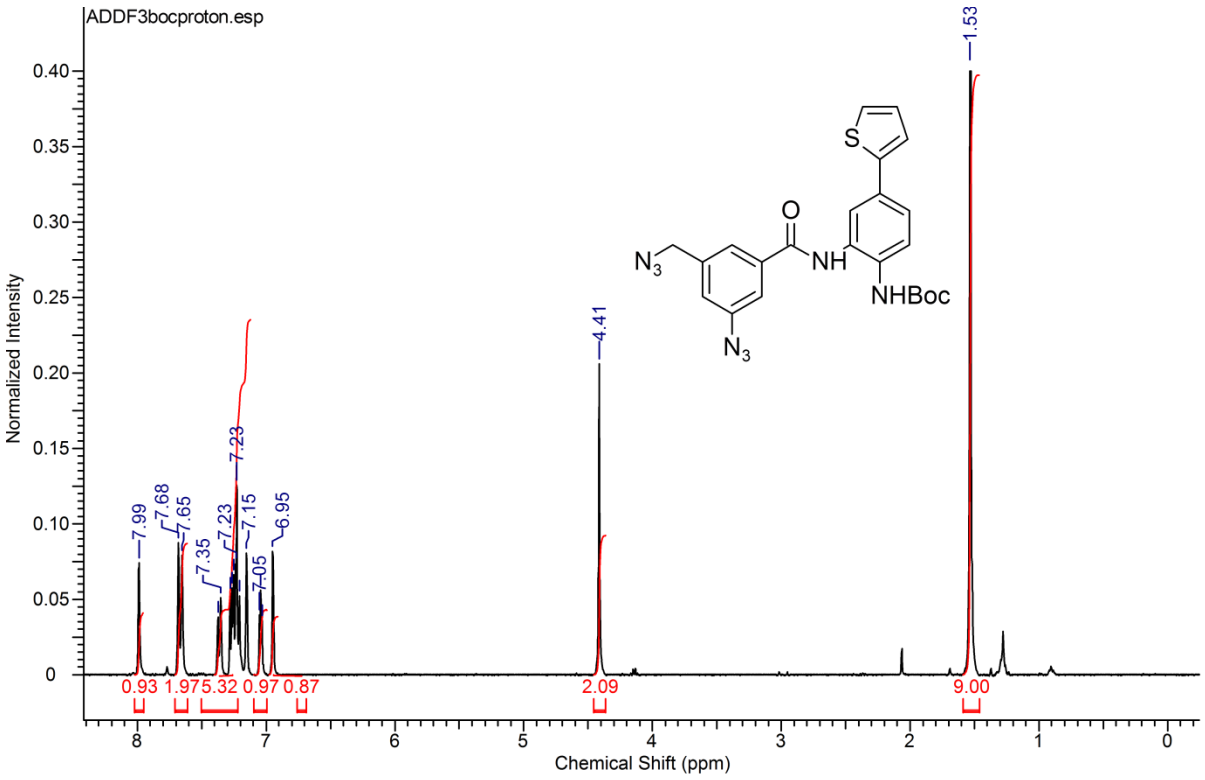

^{1}H NMR of **104c** $CDCl_3$

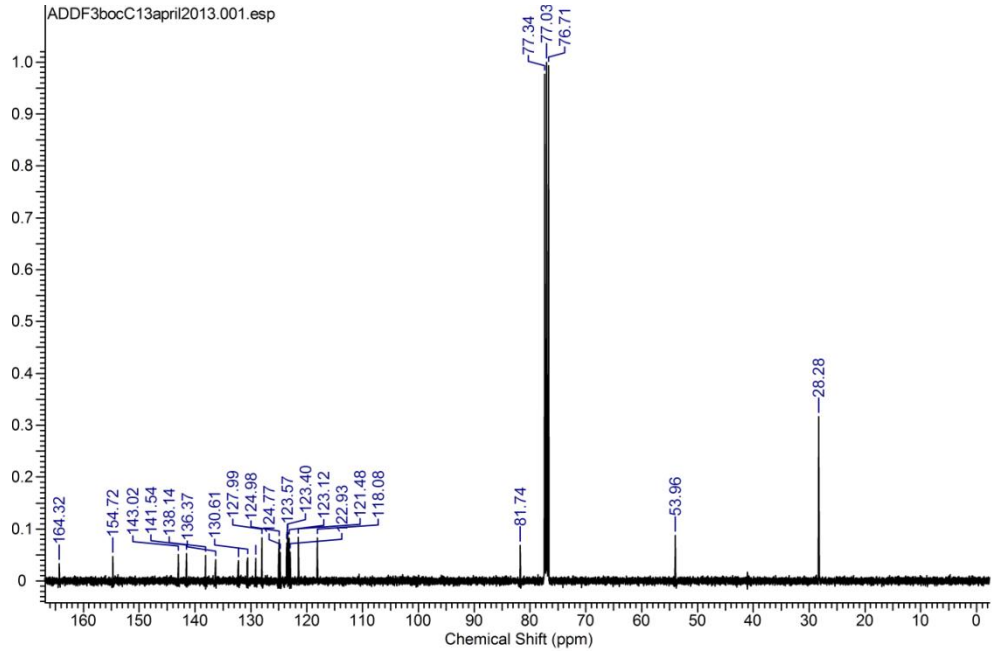

^{13}C NMR of **104c** $CDCl_3$

APPENDIX B (CONTINUED)

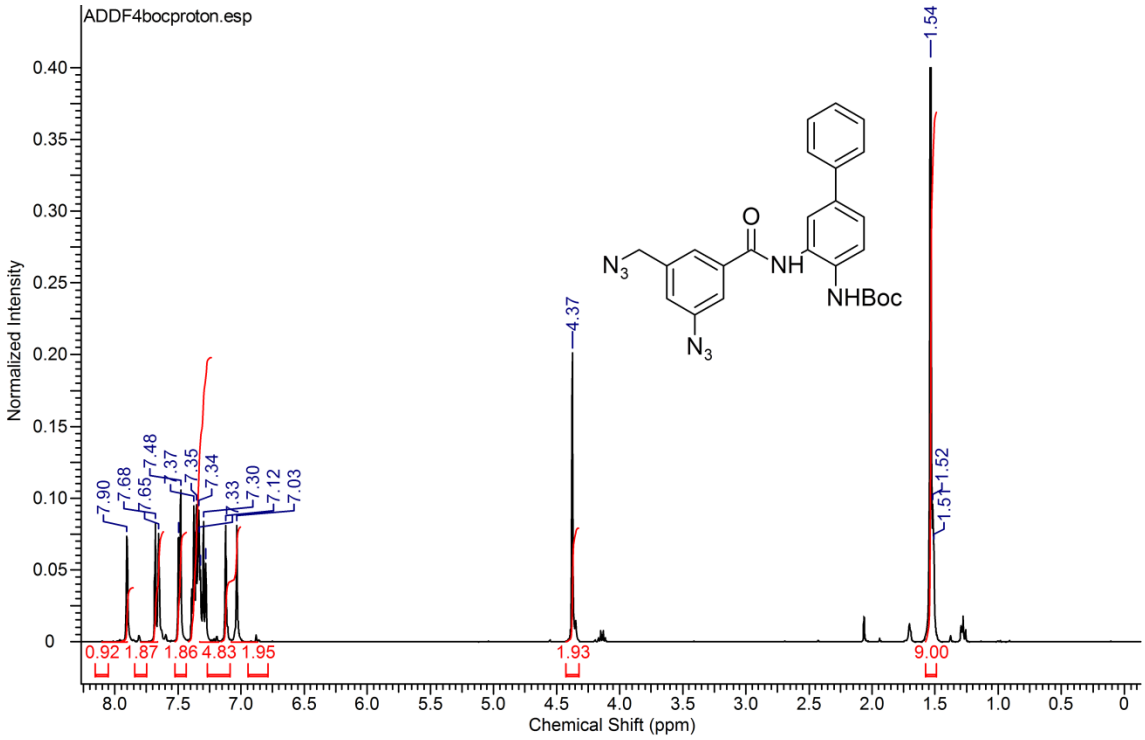

^{1}H NMR of **104d** $CDCl_3$

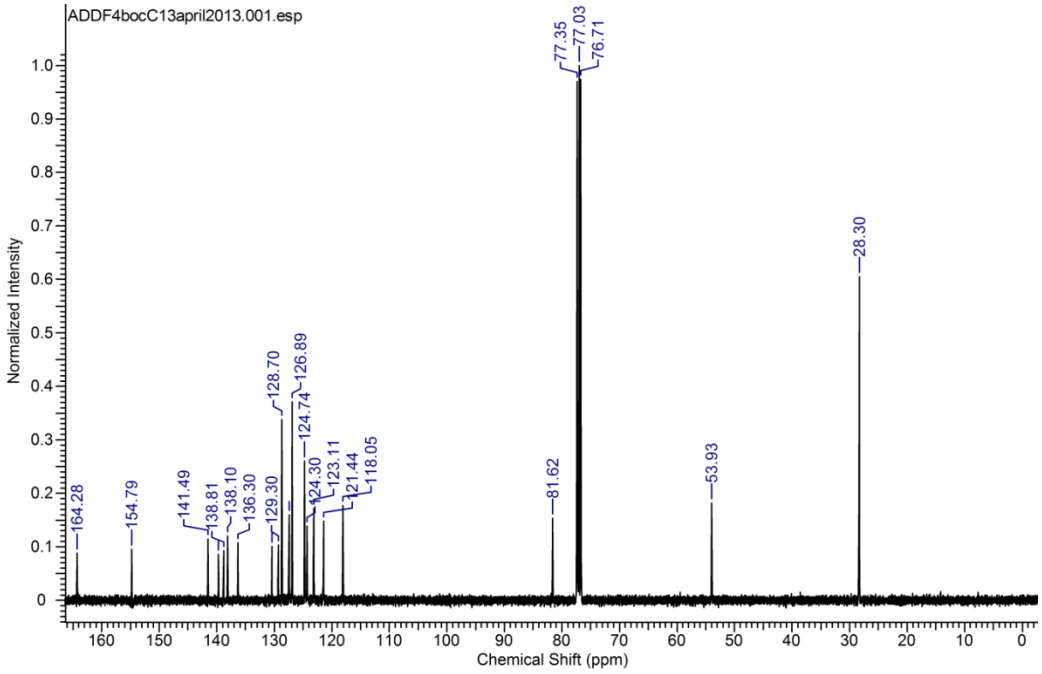

^{13}C NMR of **104d** $CDCl_3$

APPENDIX B (CONTINUED)

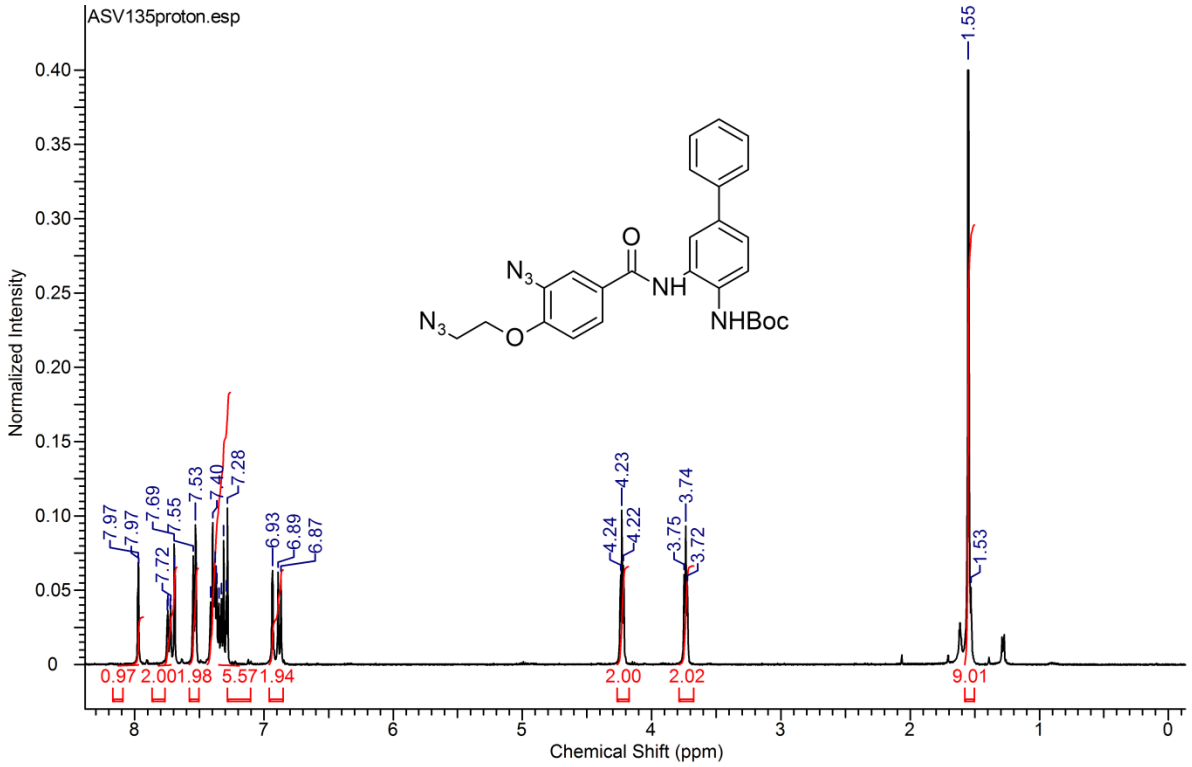

^{1}H NMR of **104e** $CDCl_3$

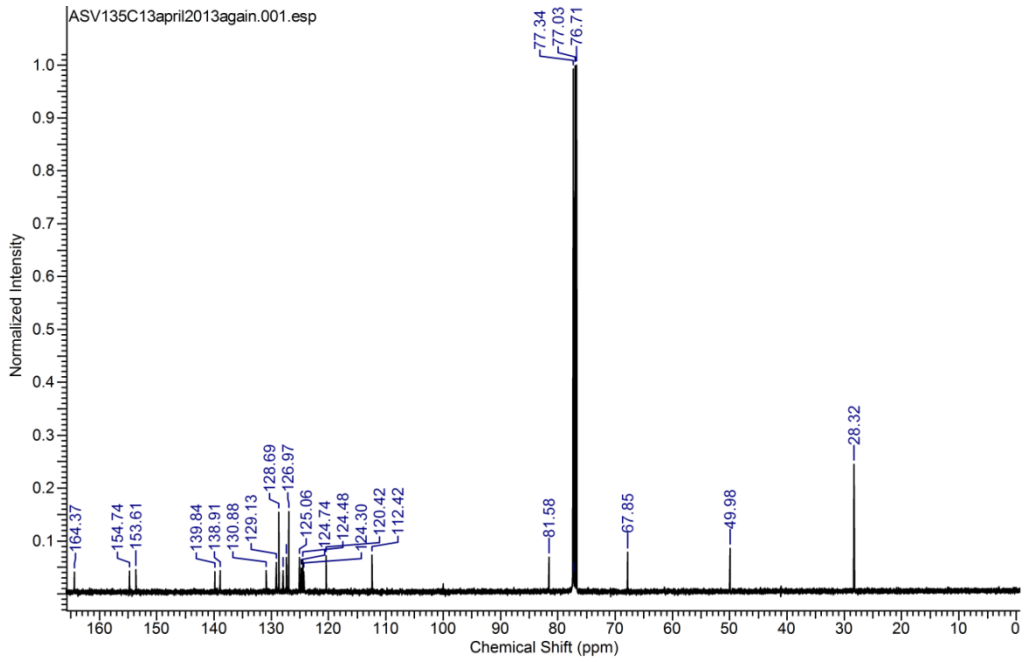

^{13}C NMR of **104e** $CDCl_3$

APPENDIX B (CONTINUED)

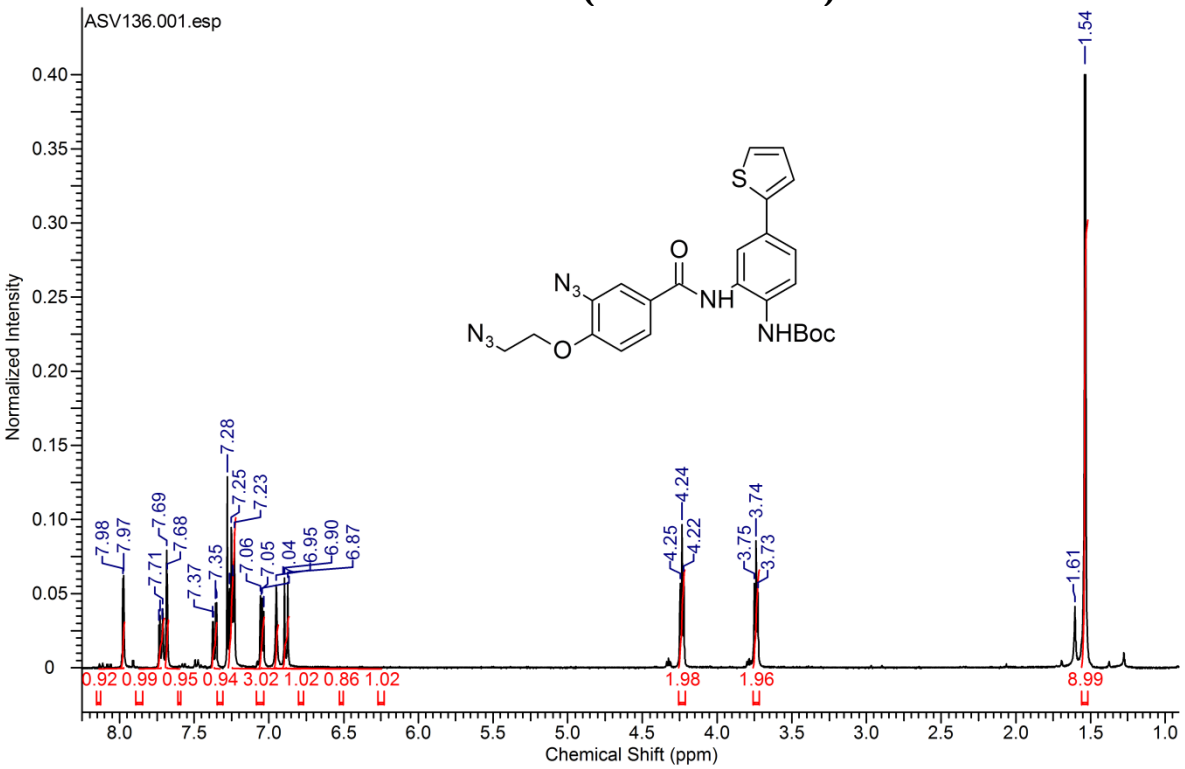

^{1}H NMR of **104f** $CDCl_3$

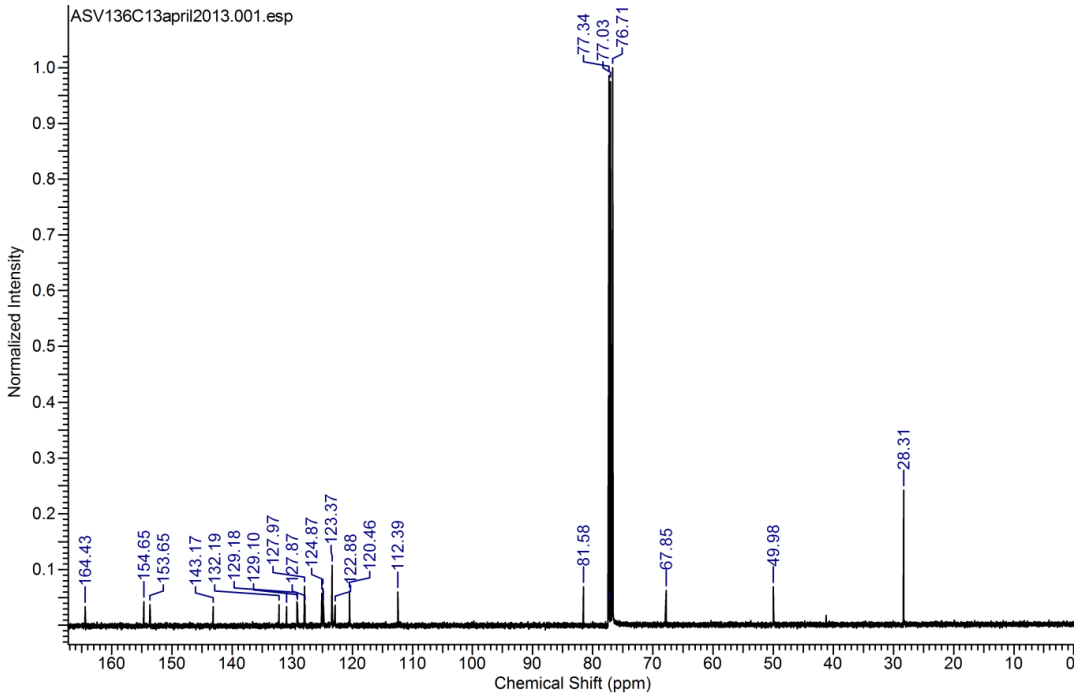

^{13}C NMR of **104f** $CDCl_3$

APPENDIX B (CONTINUED)

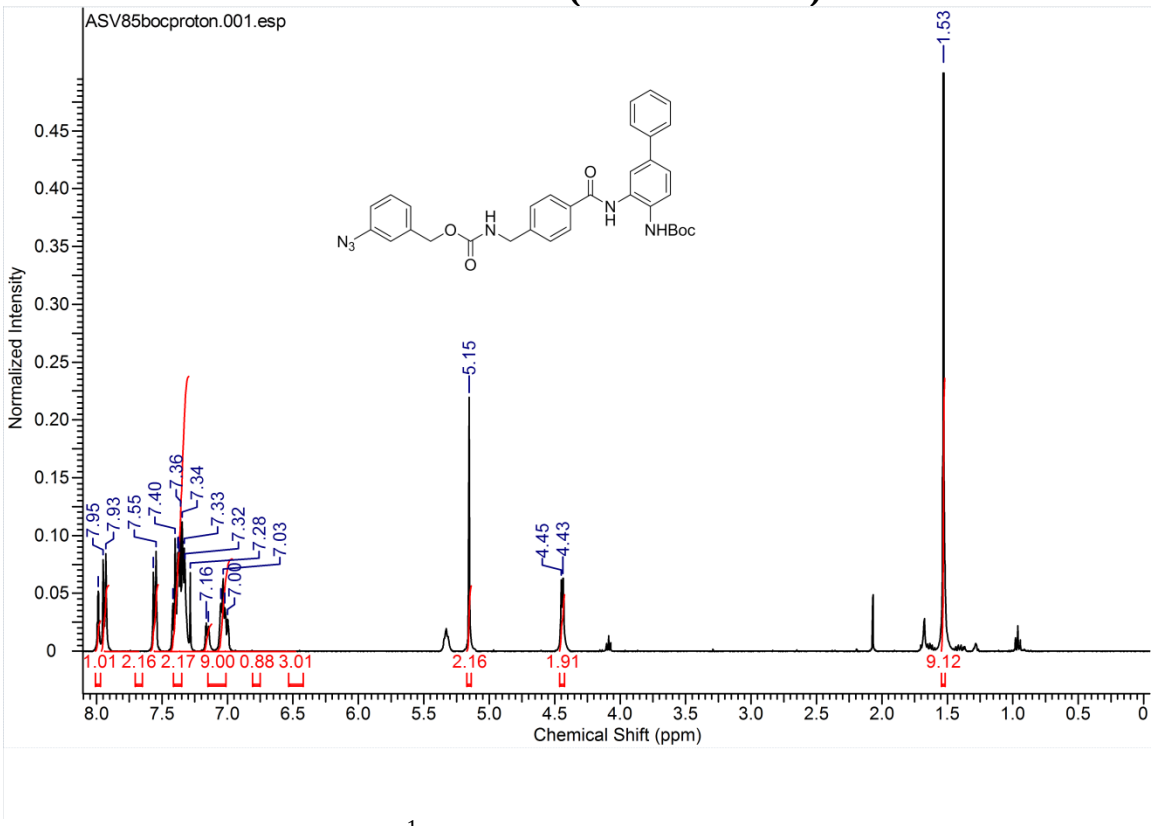

^{1}H NMR of **105a** $CDCl_3$

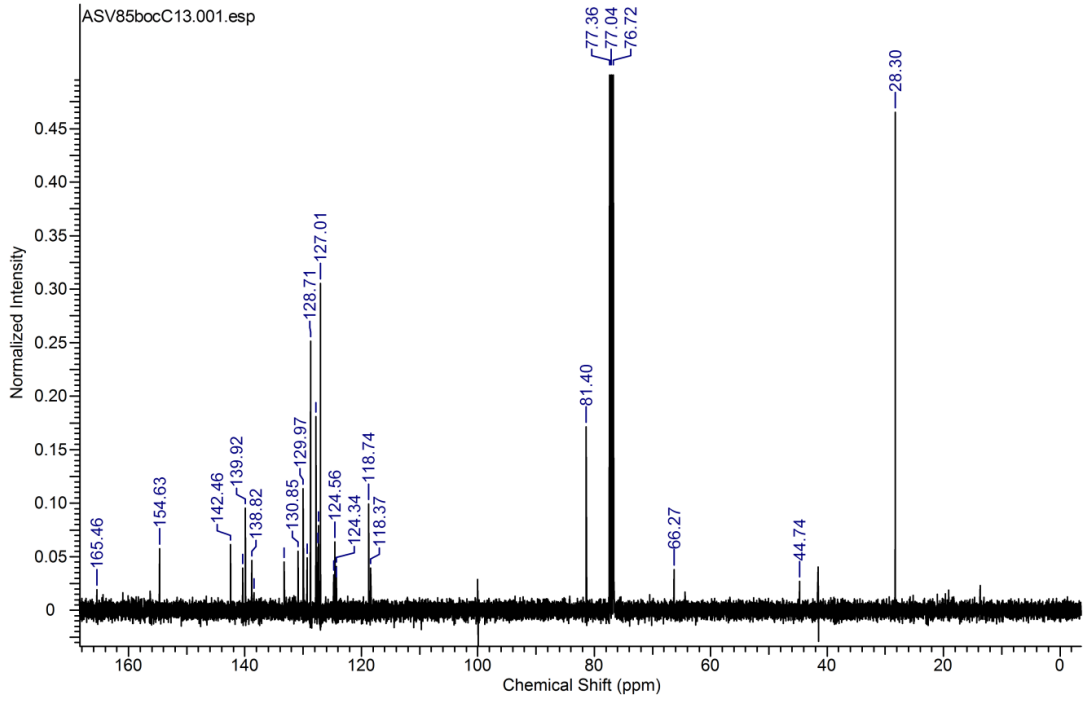

^{13}C NMR of **105a** $CDCl_3$

APPENDIX B (CONTINUED)

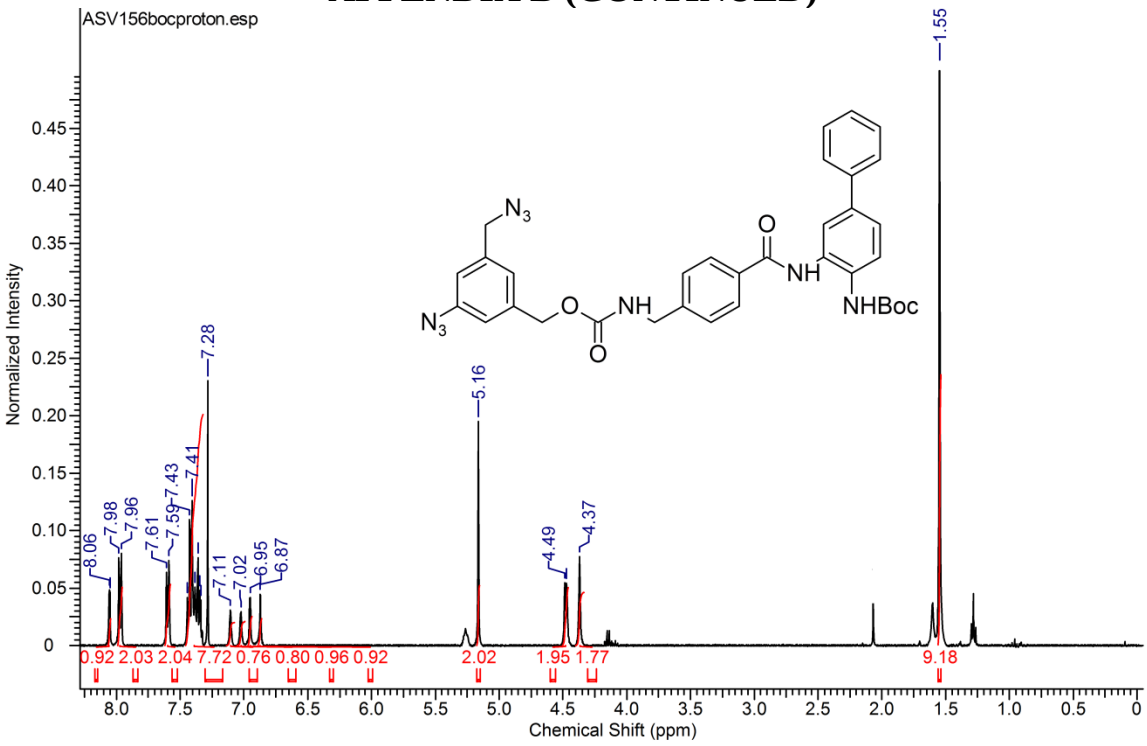

^{1}H NMR of **105b** $CDCl_3$

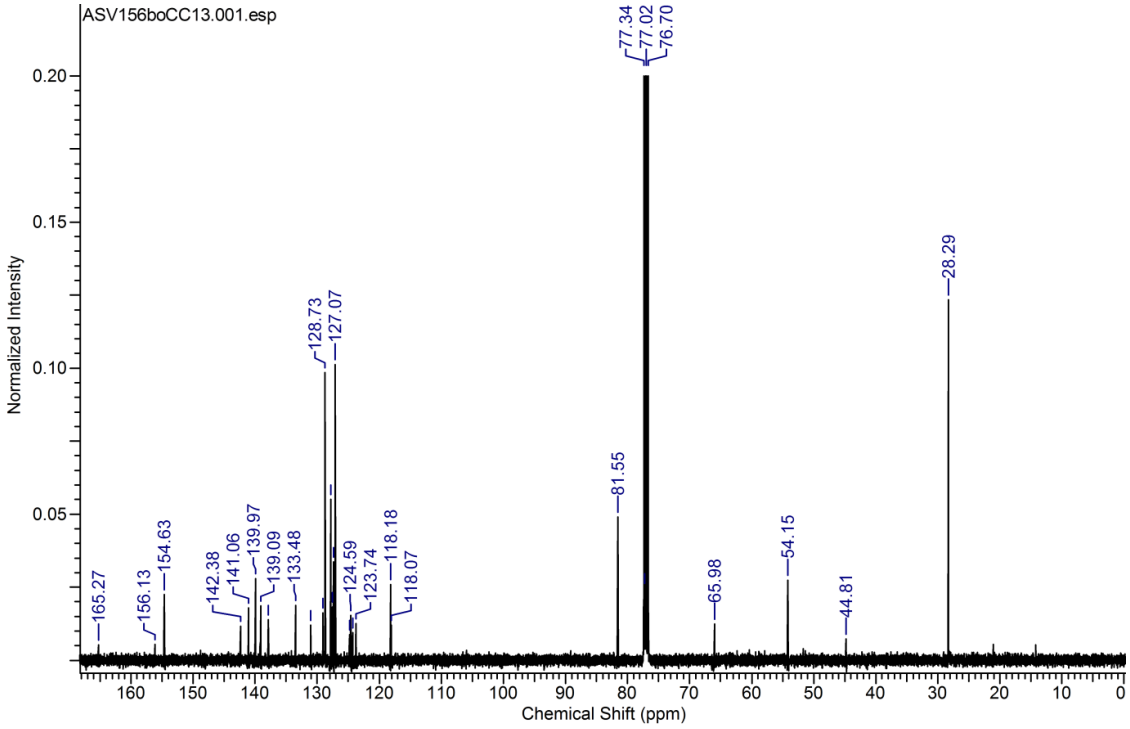

^{13}C NMR of **105b** $CDCl_3$

APPENDIX B (CONTINUED)

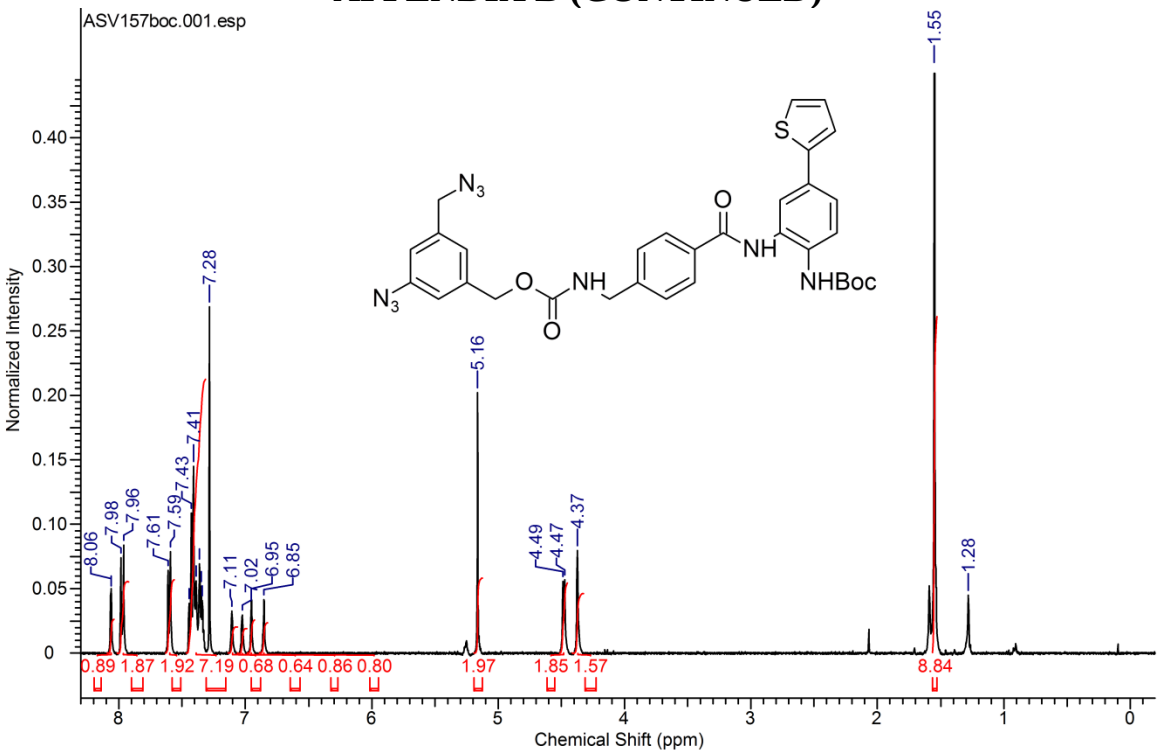

^{1}H NMR of **105c** $CDCl_3$

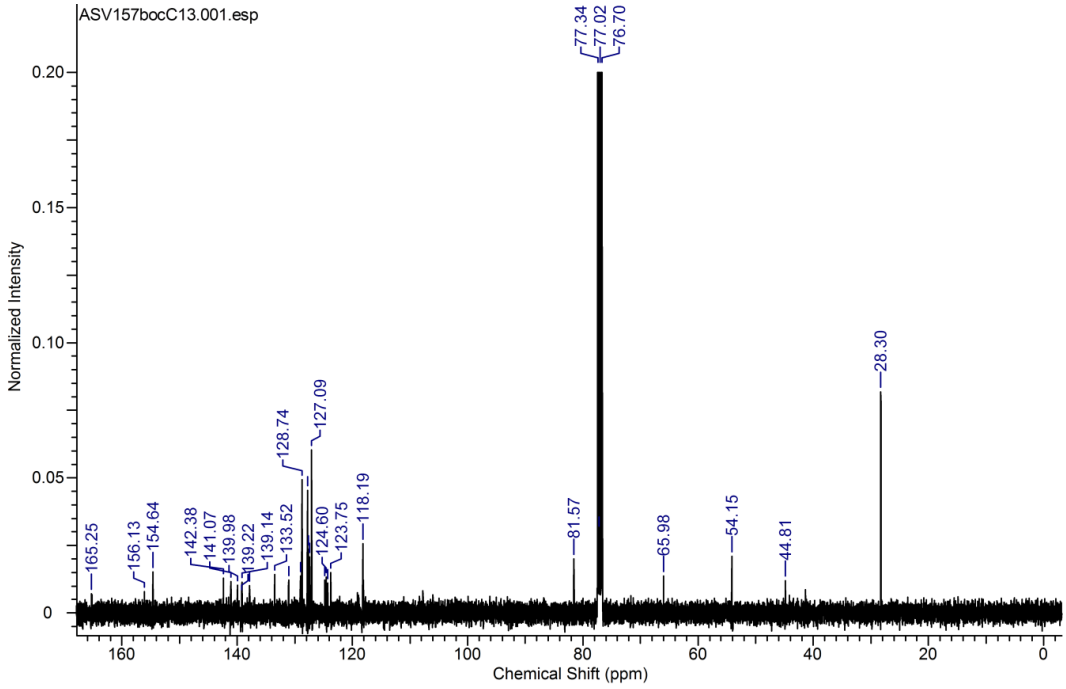

^{13}C NMR of **105c** $CDCl_3$

APPENDIX B (CONTINUED)

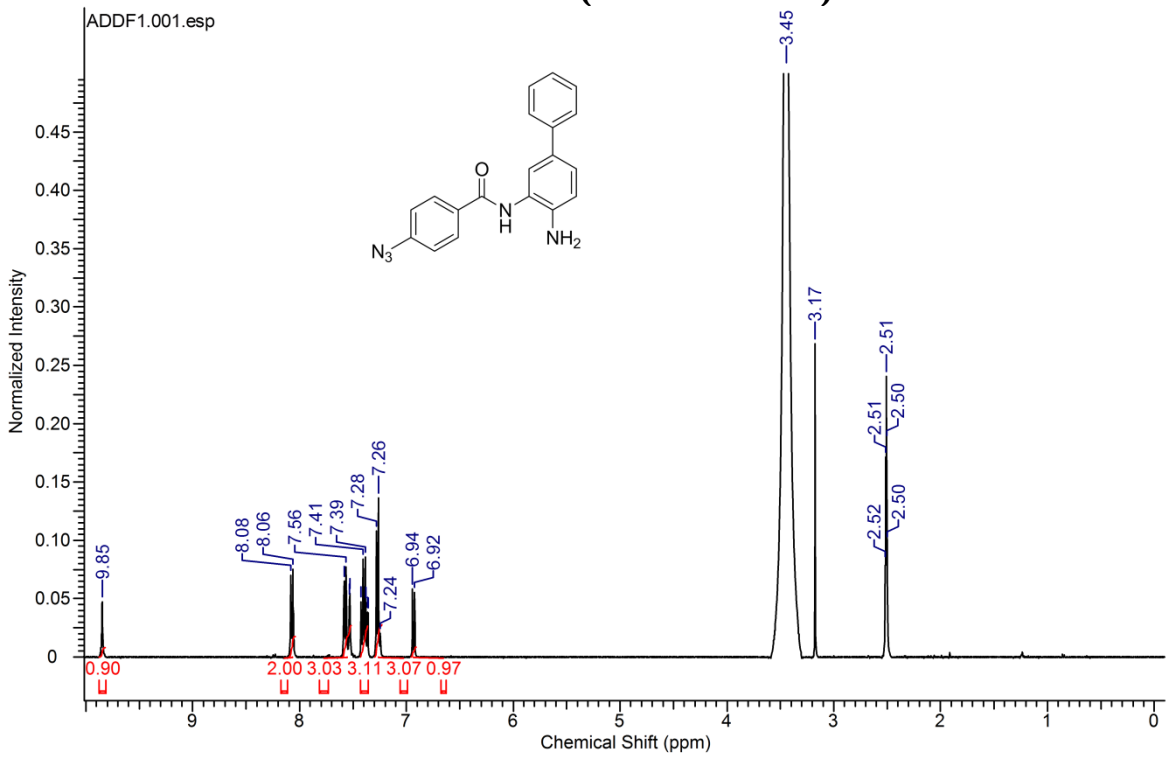

^{1}H NMR of **8a** Med/DMSO-d_6

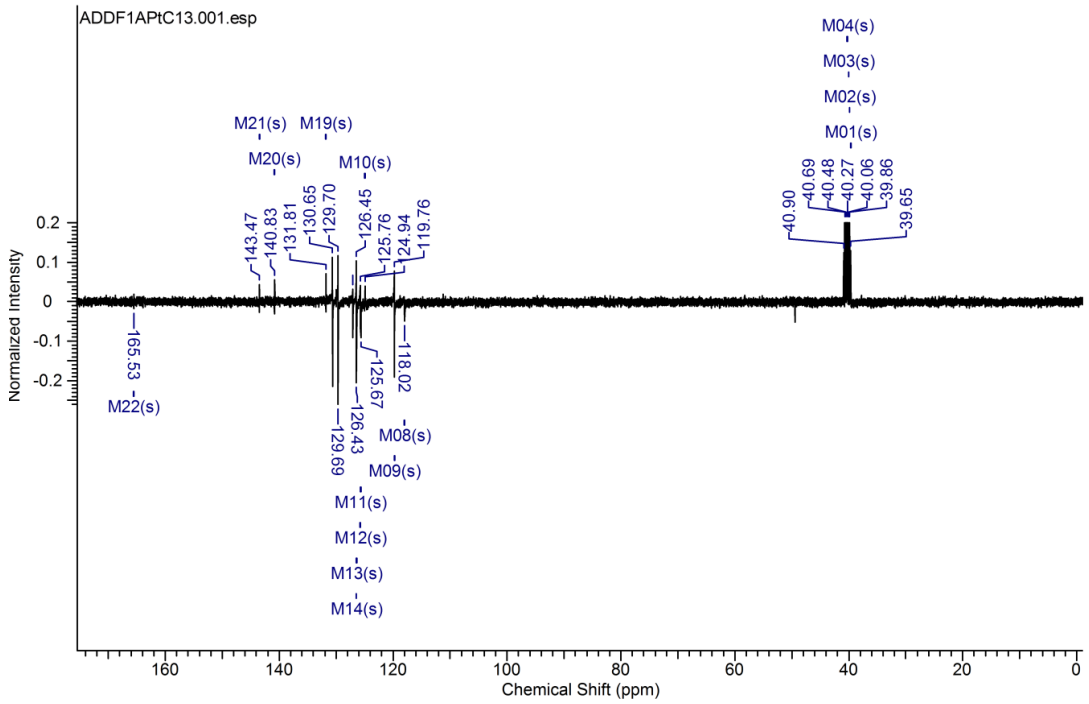

APT Spectra of **8a in DMSO-d_6**

APPENDIX B (CONTINUED)

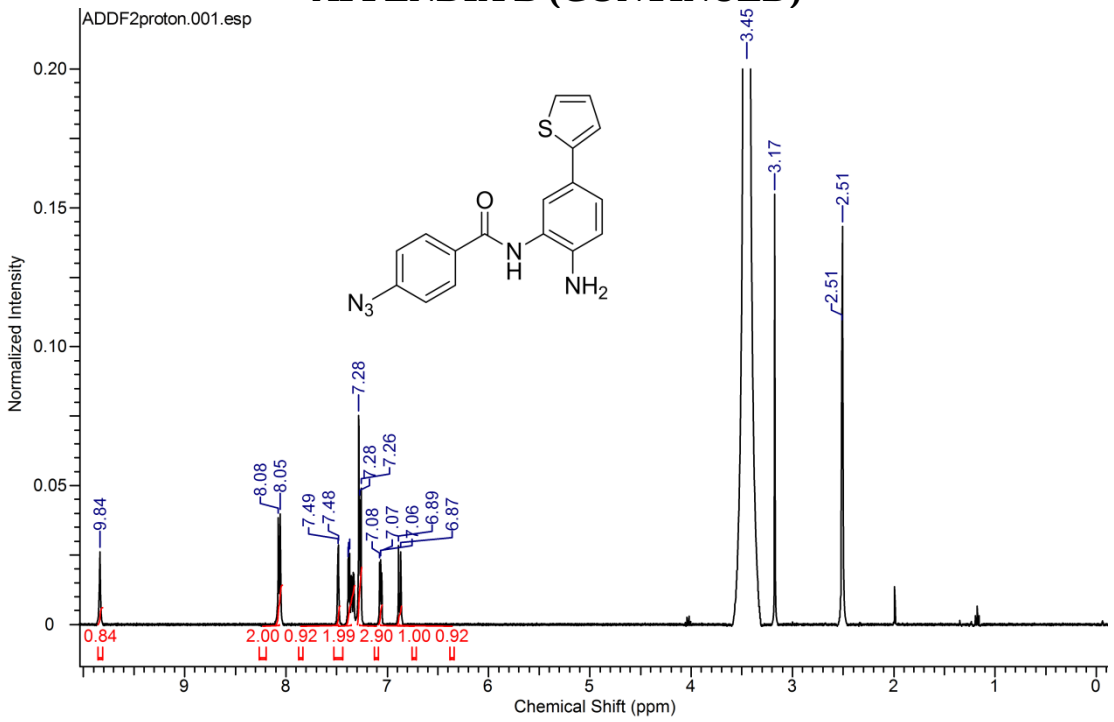

^{1}H NMR of **8b** Med/DMSO-d_6

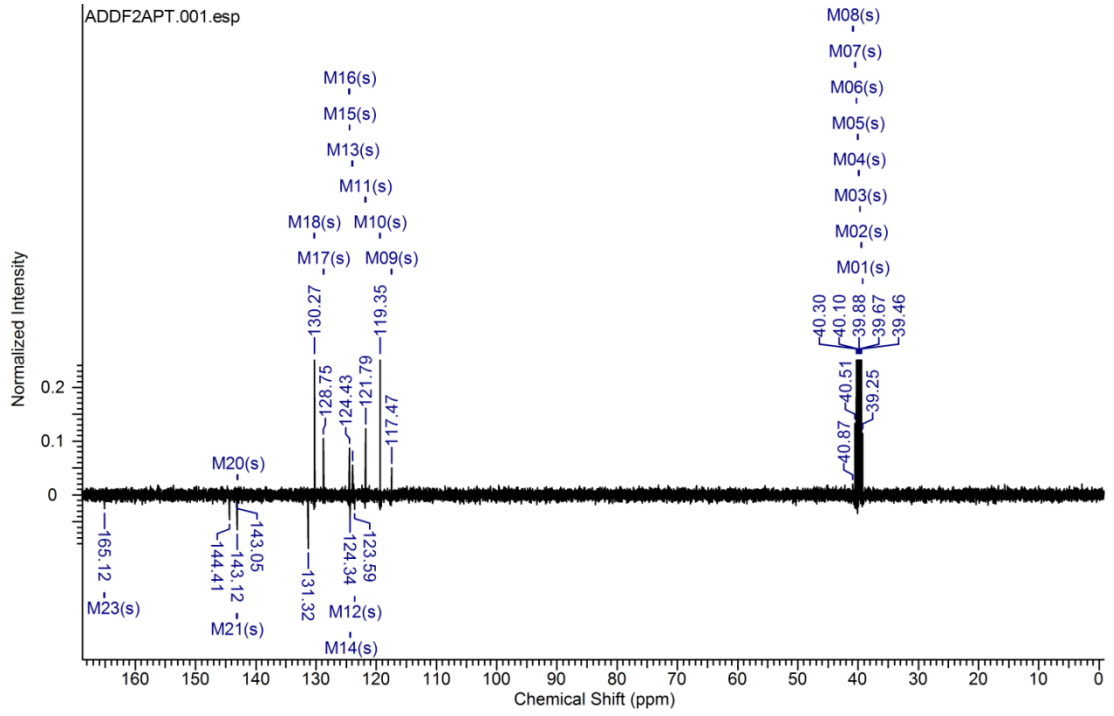

APT Spectra of **8b in DMSO-d_6**

APPENDIX B (CONTINUED)

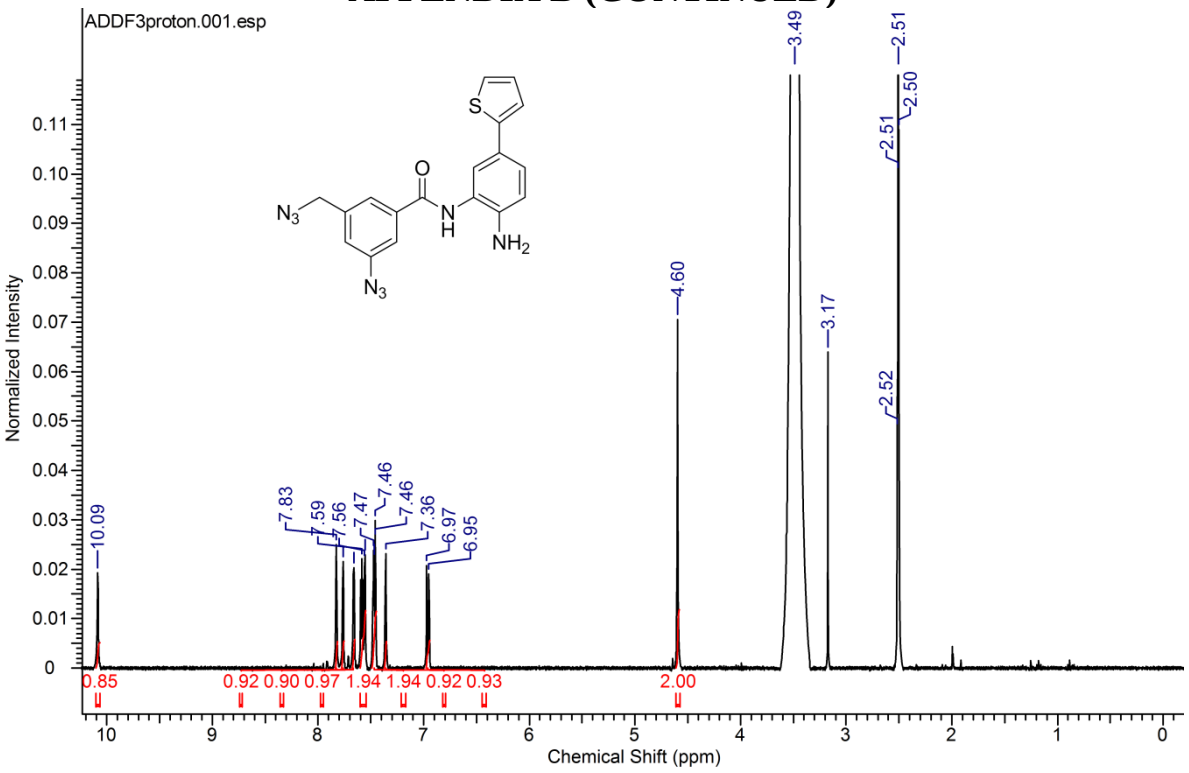

^{1}H NMR of **8c** Med/DMSO-d_6

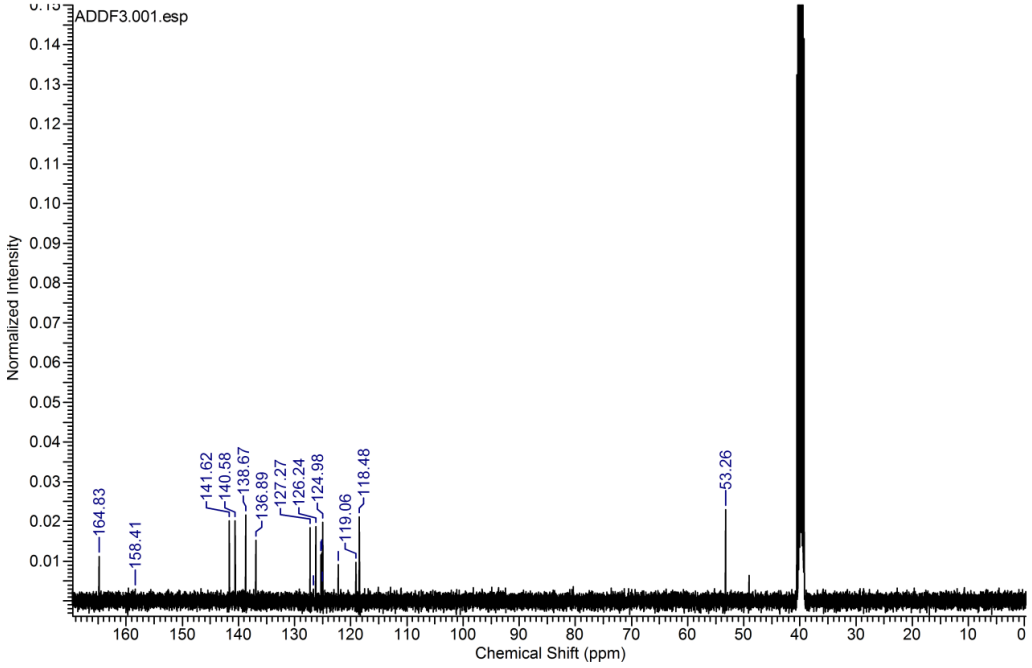

^{13}C NMR of **8c** DMSO-d_6

APPENDIX B (CONTINUED)

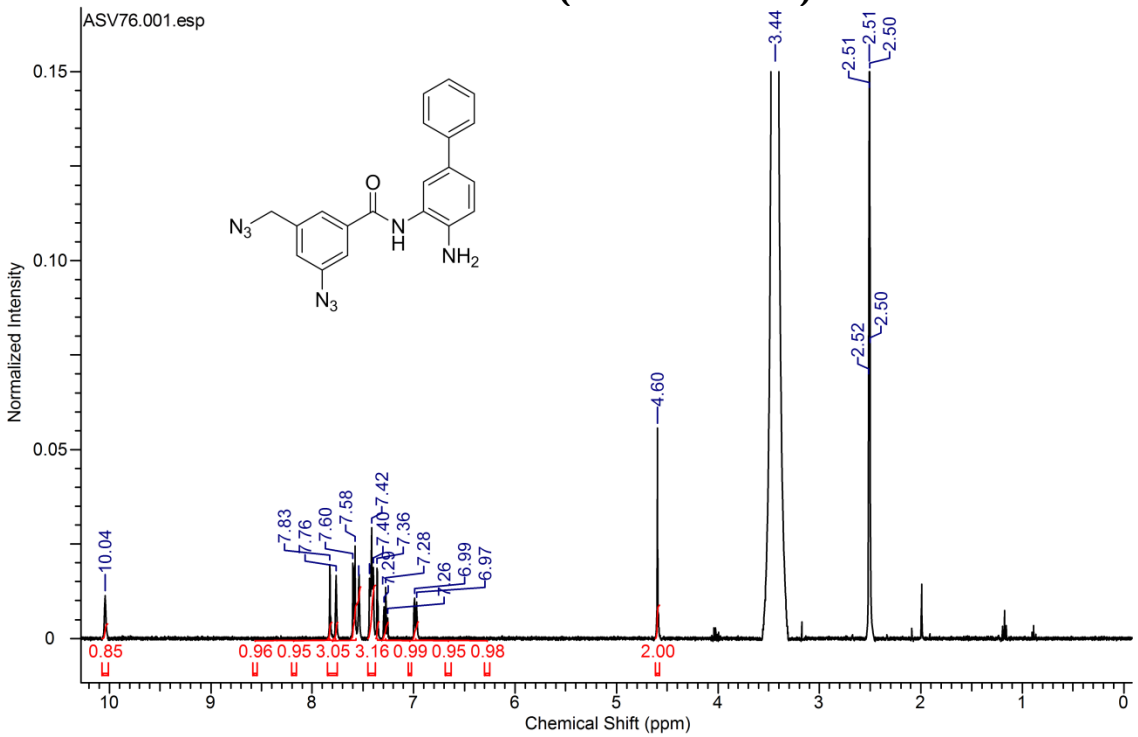

^{1}H NMR of **8d** Med/DMSO-d_6

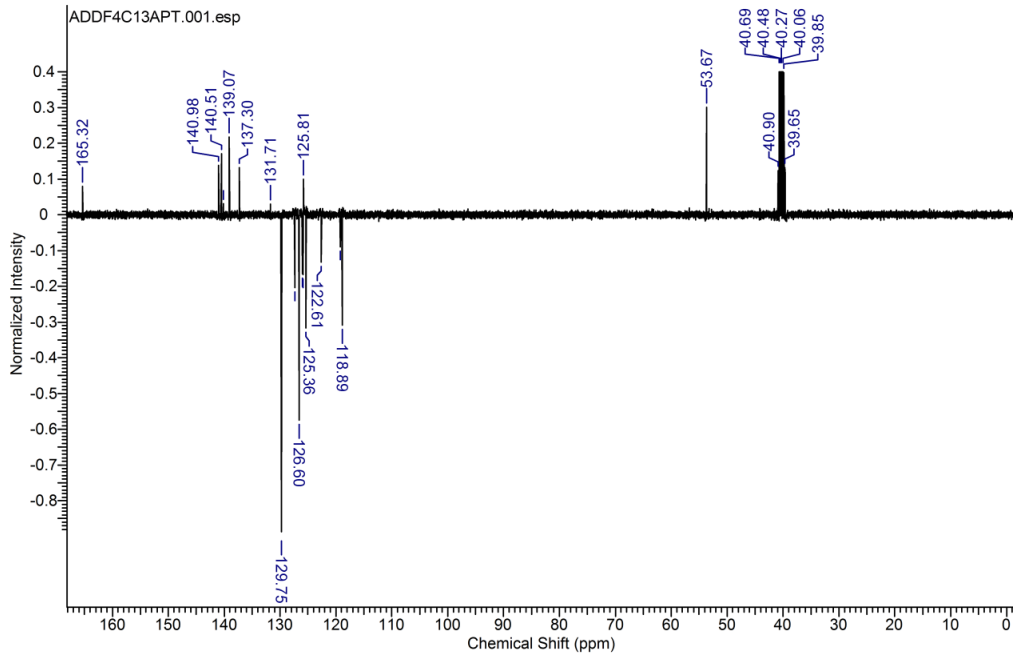

APT Spectra of **8d** in DMSO-d_6

APPENDIX B (CONTINUED)

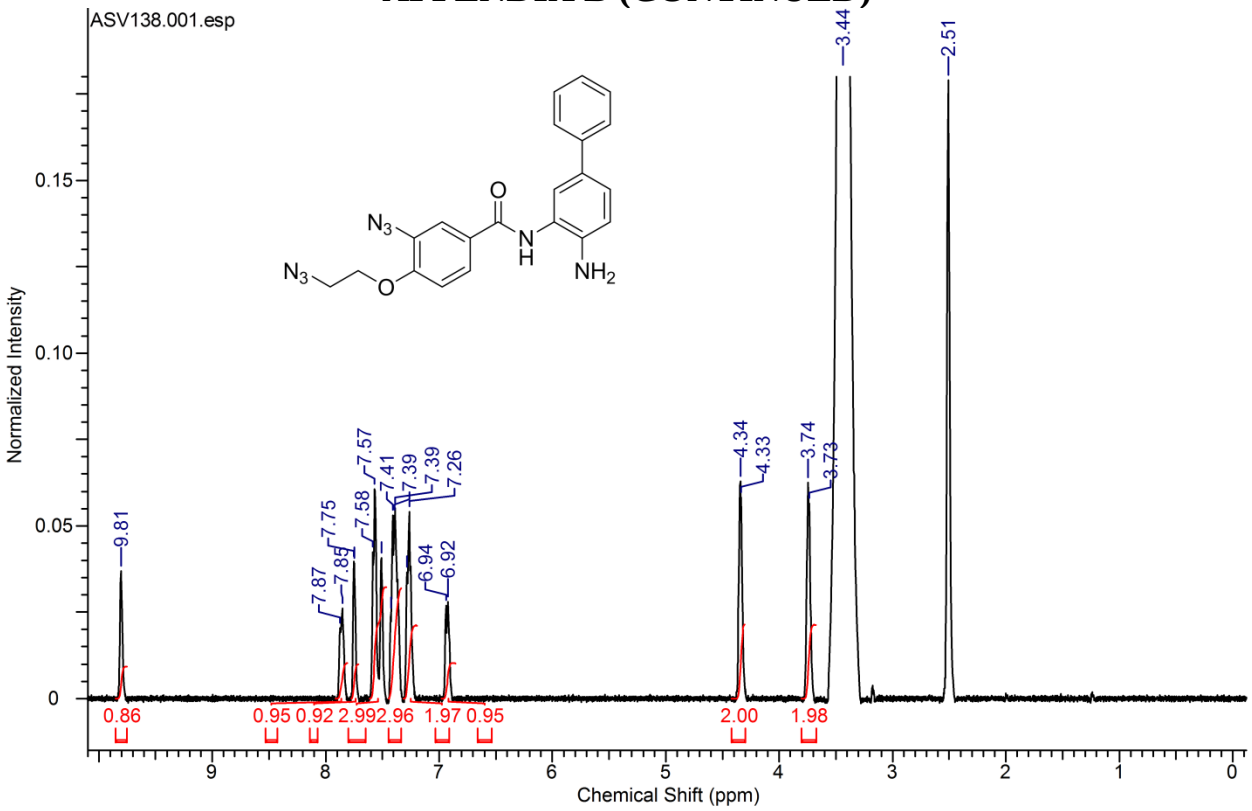

^{1}H NMR of **8e** DMSO-d_6

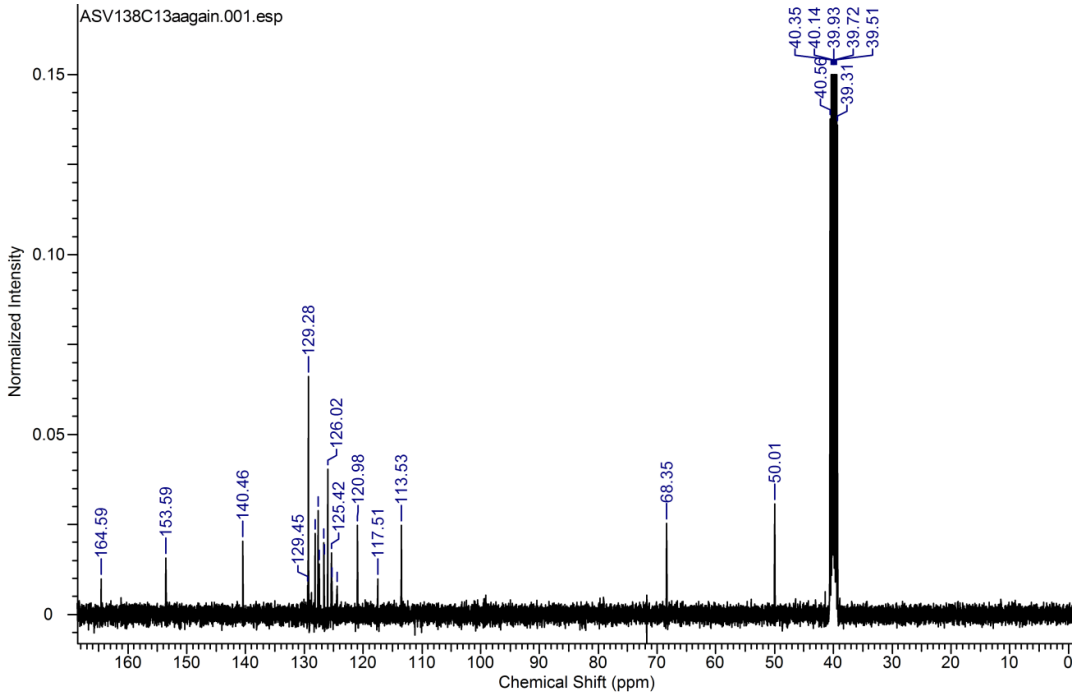

^{13}C NMR of **8e** DMSO-d_6

APPENDIX B (CONTINUED)

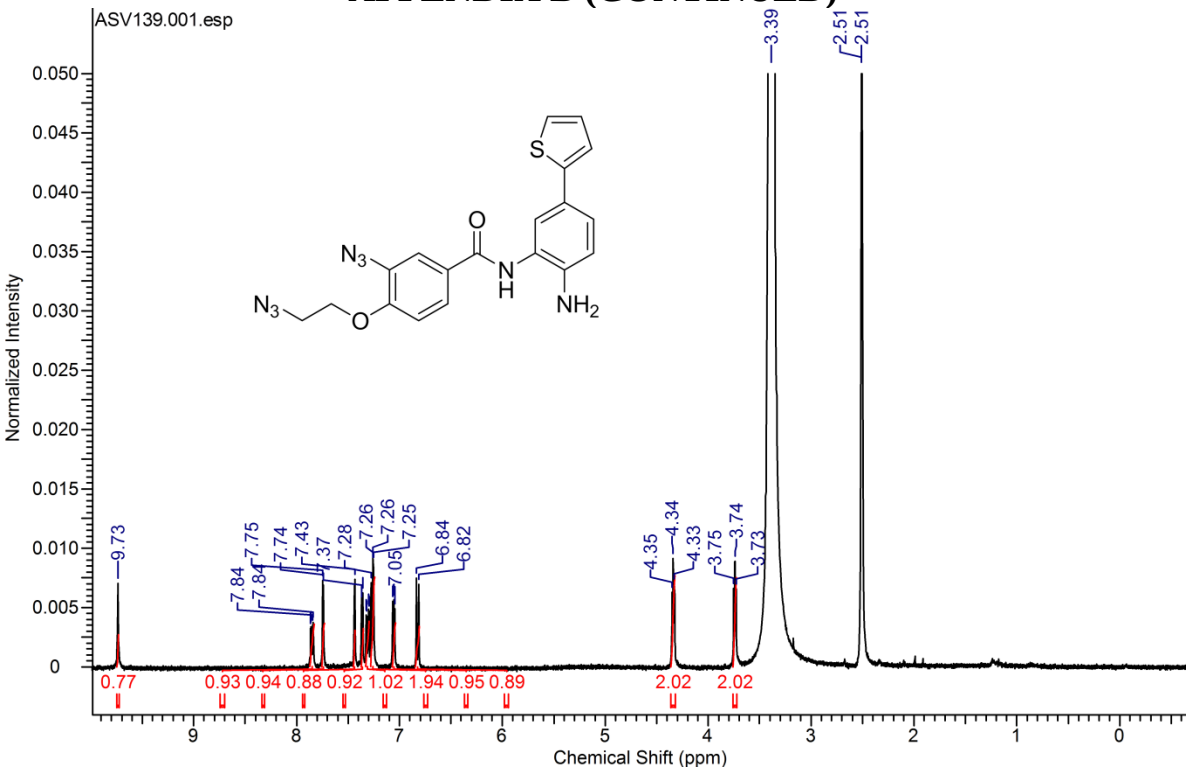

^{1}H NMR of **8f** DMSO-d_6

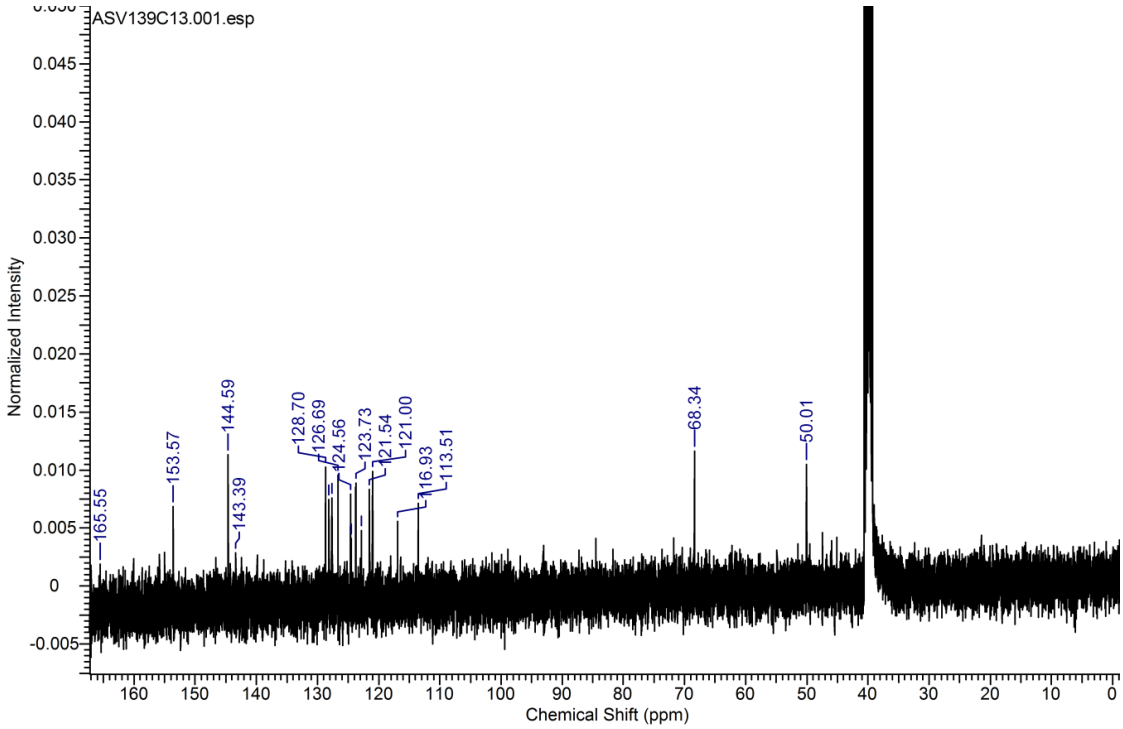

^{13}C NMR of **8f** DMSO-d_6

APPENDIX B (CONTINUED)

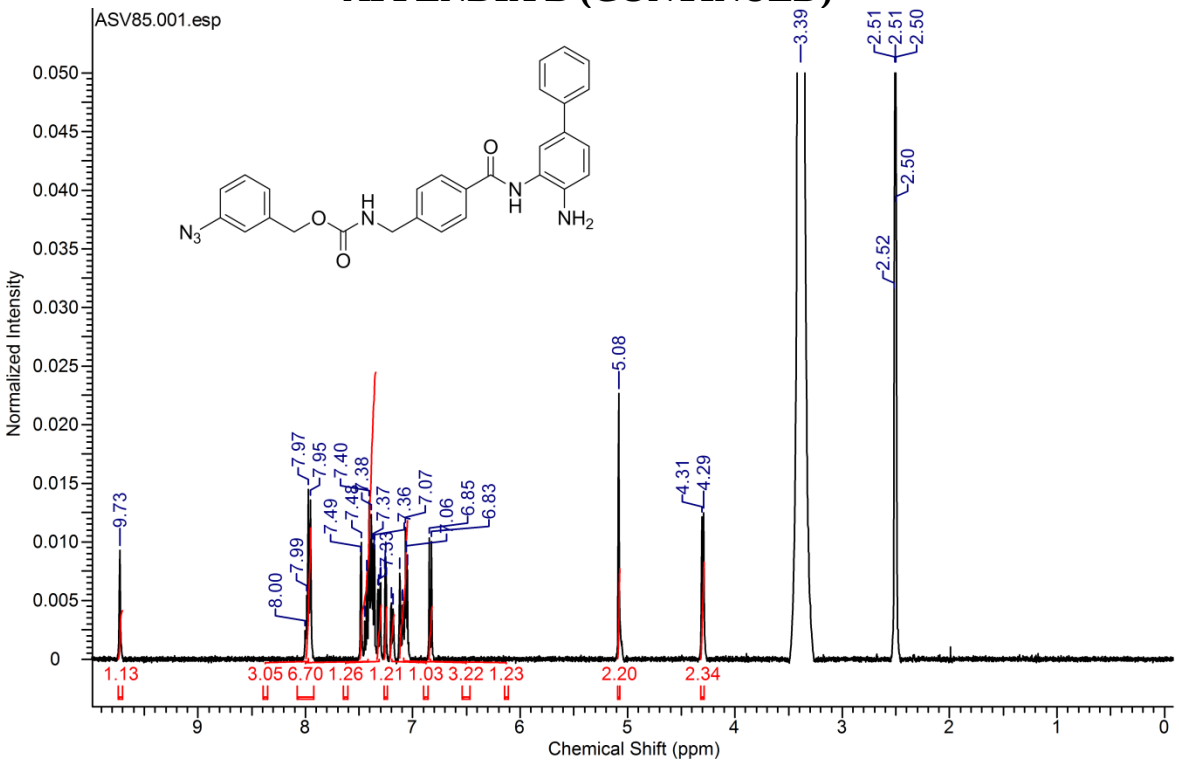

^{1}H NMR of **75a** DMSO-d_6

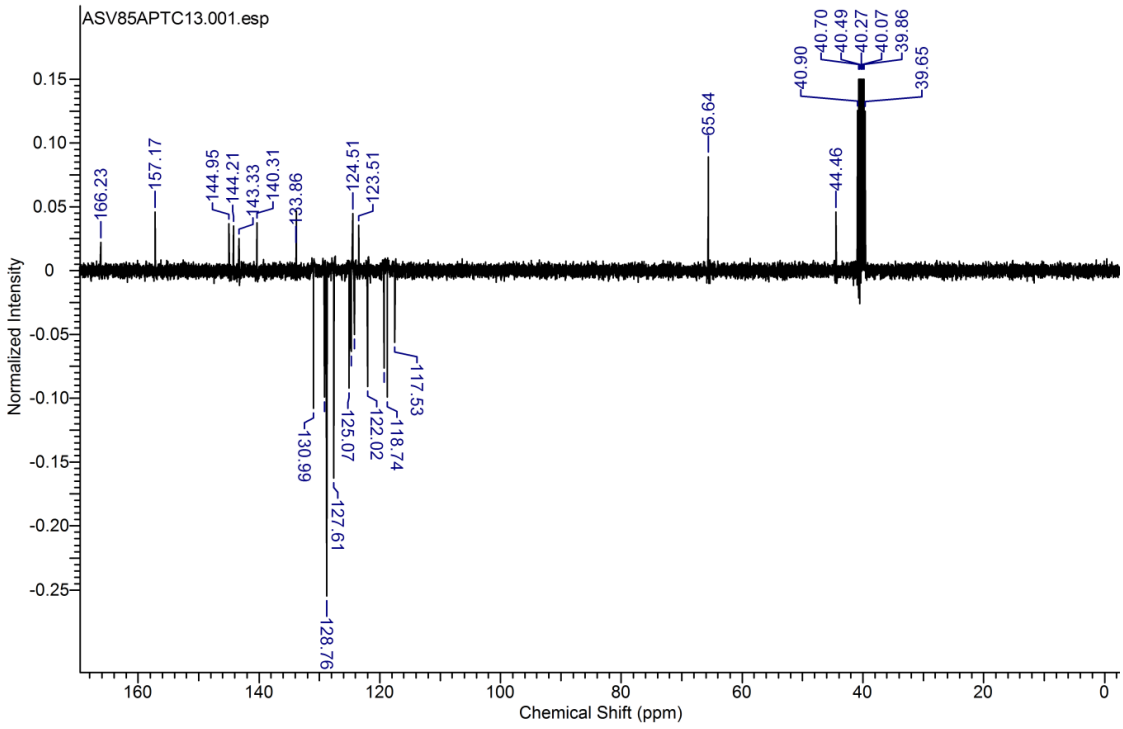

APT Spectra of **75a** in DMSO-d_6

APPENDIX B (CONTINUED)

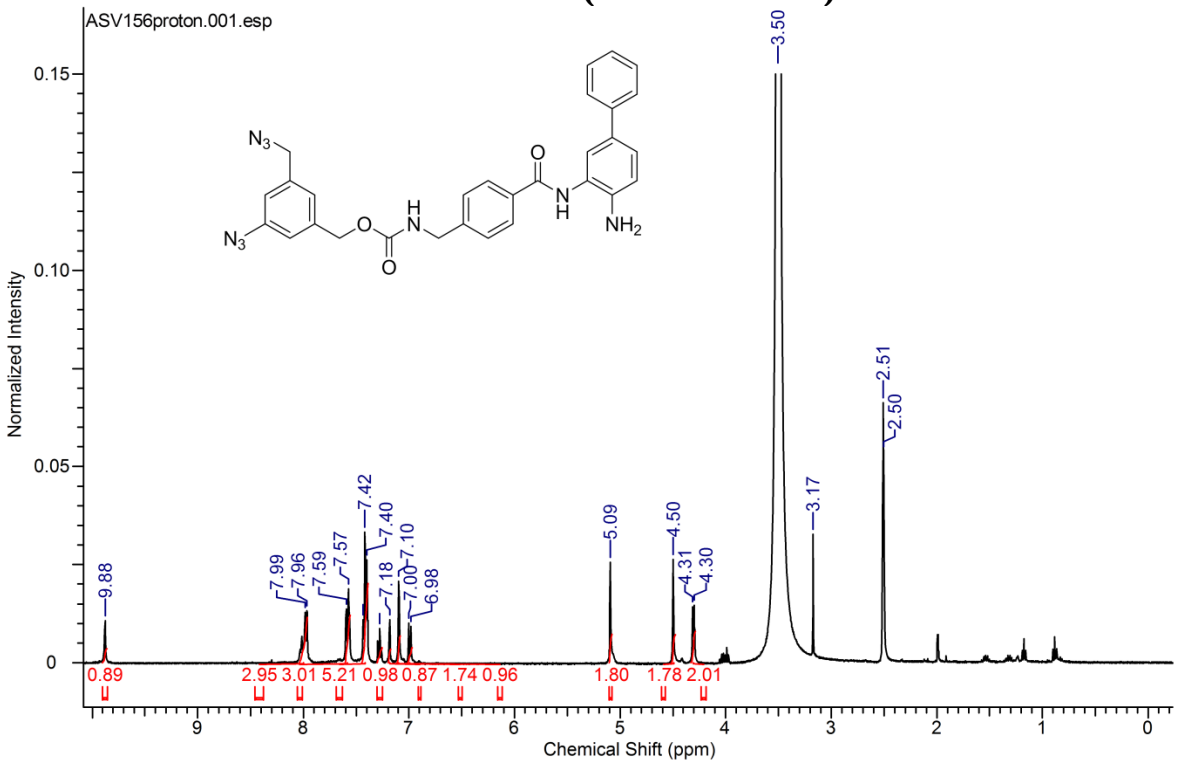

^{1}H NMR of **75b** DMSO-d_6

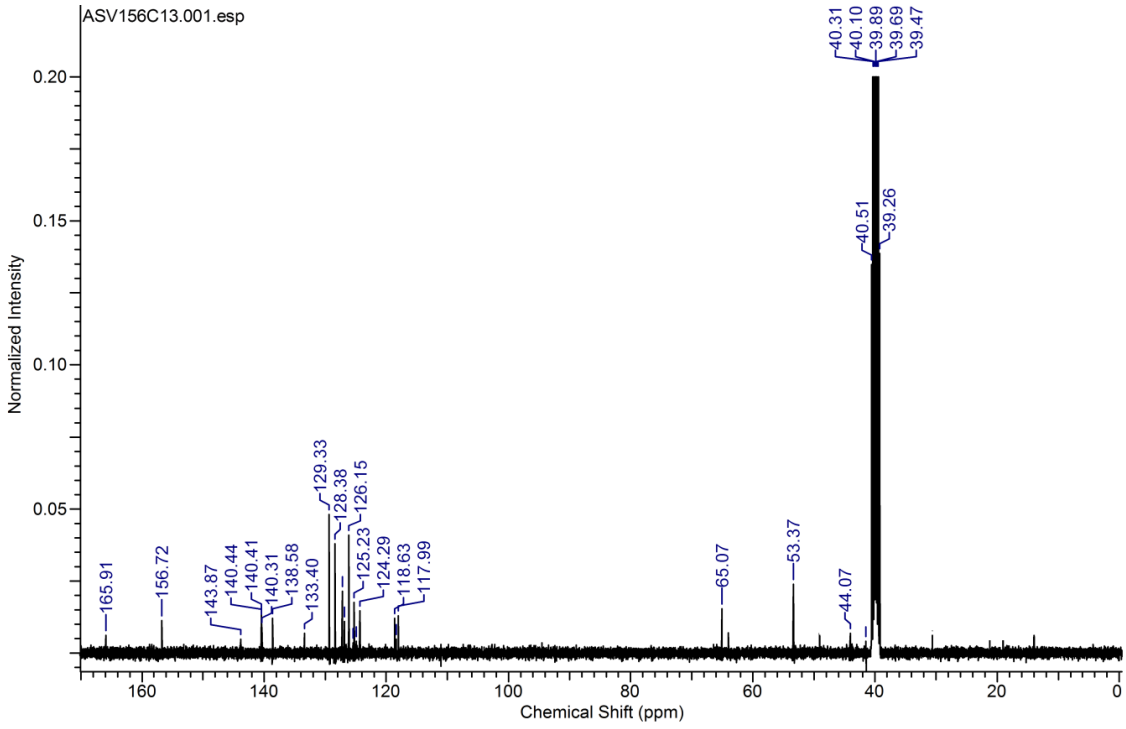

^{13}C NMR of **75b** DMSO-d_6

APPENDIX B (CONTINUED)

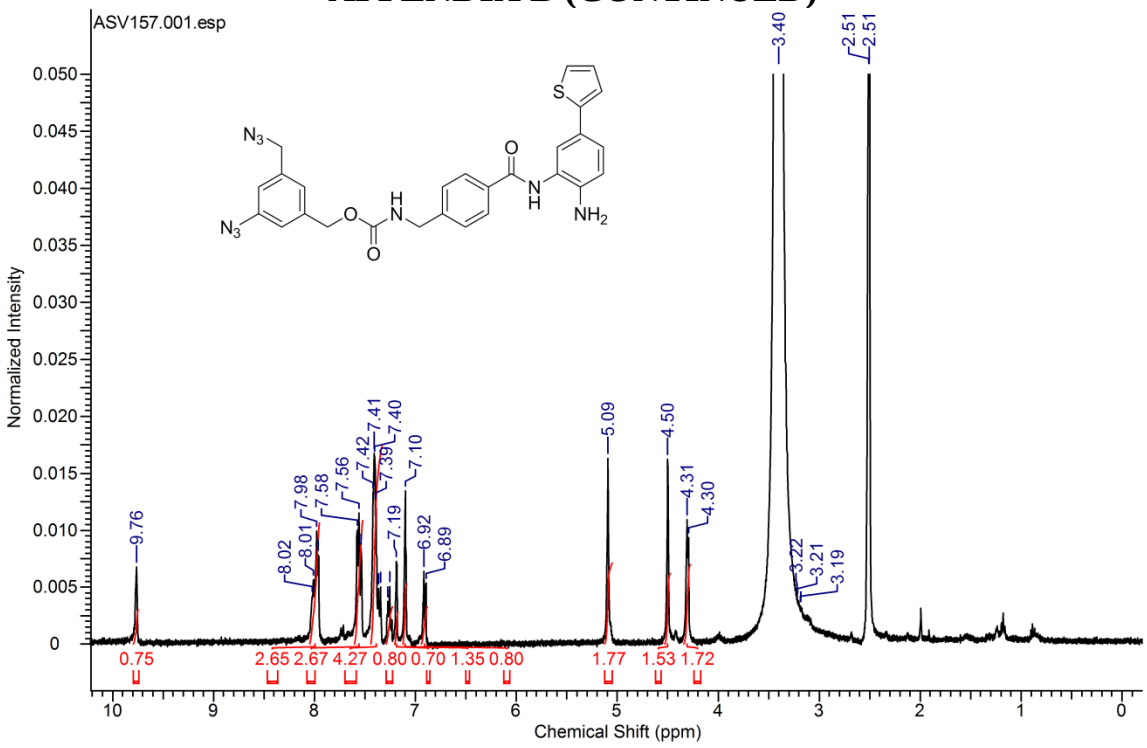

^{1}H NMR of **75c** DMSO-d_6

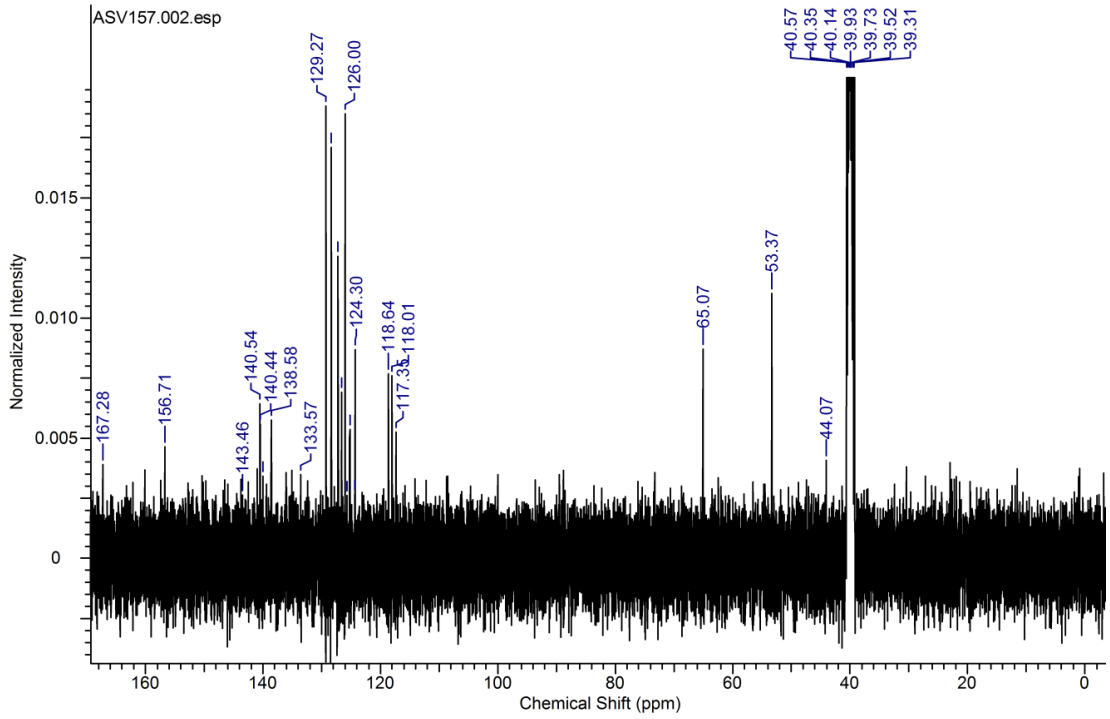

^{13}C NMR of **75c** DMSO-d_6

10/17/13 Rightslink Printable License

APPENDIX C: COPYRIGHT AGREEMENTS

ELSEVIER LICENSE
TERMS AND CONDITIONS

Oct 17, 2013

This is a License Agreement between Aditya S Vaidya ("You") and Elsevier ("Elsevier") provided by Copyright Clearance Center ("CCC"). The license consists of your order details, the terms and conditions provided by Elsevier, and the payment terms and conditions.

All payments must be made in full to CCC. For payment instructions, please see information listed at the bottom of this form.

Supplier	Elsevier Limited The Boulevard,Langford Lane Kidlington,Oxford,OX5 1GB,UK
Registered Company Number	1982084
Customer name	Aditya S Vaidya
Customer address	246 W Big Springs Rd RIVERSIDE, CA 92507
License number	3251531400221
License date	Oct 17, 2013
Licensed content publisher	Elsevier
Licensed content publication	Bioorganic & Medicinal Chemistry Letters
Licensed content title	Design, synthesis, modeling, biological evaluation and photoaffinity labeling studies of novel series of photoreactive benzamide probes for histone deacetylase 2
Licensed content author	Aditya Sudheer Vaidya,Bhargava Karumudi,Emma Mendonca,Antonett Madriaga,Hazem Abdelkarim,Richard B. van Breemen,Pavel A. Petukhov
Licensed content date	1 August 2012
Licensed content volume number	22
Licensed content issue number	15
Number of pages	6
Start Page	5025
End Page	5030
Type of Use	reuse in a thesis/dissertation
Portion	full article
Format	both print and electronic
Are you the author of this Elsevier article?	Yes
Will you be translating?	No
Order reference number	
Title of your thesis/dissertation	Design, Synthesis, Biological Evaluation and Photoaffinity labeling studies of novel photoreactive probes for histone deacetylase 2 and 8
Expected completion date	Oct 2013
Estimated size (number of pages)	200
Elsevier VAT number	GB 494 6272 12
Permissions price	0.00 USD
VAT/Local Sales Tax	0.0 USD / 0.0 GBP
Total	0.00 USD

APPENDIX C (CONTINUED)

ELSEVIER LICENSE
TERMS AND CONDITIONS

Oct 17, 2013

This is a License Agreement between Aditya S Vaidya ("You") and Elsevier ("Elsevier") provided by Copyright Clearance Center ("CCC"). The license consists of your order details, the terms and conditions provided by Elsevier, and the payment terms and conditions.

All payments must be made in full to CCC. For payment instructions, please see information listed at the bottom of this form.

Supplier	Elsevier Limited The Boulevard,Langford Lane Kidlington,Oxford,OX5 1GB,UK
Registered Company Number	1982084
Customer name	Aditya S Vaidya
Customer address	246 W Big Springs Rd RIVERSIDE, CA 92507
License number	3251540698466
License date	Oct 17, 2013
Licensed content publisher	Elsevier
Licensed content publication	Bioorganic & Medicinal Chemistry Letters
Licensed content title	Novel histone deacetylase 8 ligands without a zinc chelating group: Exploring an 'upside-down' binding pose
Licensed content author	Aditya Sudheer Vaidya,Raghupathi Neelarapu,Antonett Madriaga,He Bai,Emma Mendonca,Hazem Abdelkarim,Richard B. van Breemen,Sylvie Y. Blond,Pavel A. Petukhov
Licensed content date	1 November 2012
Licensed content volume number	22
Licensed content issue number	21
Number of pages	7
Start Page	6621
End Page	6627
Type of Use	reuse in a thesis/dissertation
Intended publisher of new work	other
Are you the author of this Elsevier article?	Yes
Will you be translating?	No
Order reference number	
Title of your thesis/dissertation	Design, Synthesis, Biological Evaluation and Photoaffinity labeling studies of novel photoreactive probes for histone deacetylase 2 and 8
Expected completion date	Oct 2013
Estimated size (number of pages)	200
Elsevier VAT number	GB 494 6272 12
Permissions price	0.00 USD
VAT/Local Sales Tax	0.0 USD / 0.0 GBP
Total	0.00 USD

REFERENCES

1. Henikoff, S. *Curr Biol* **2012,** *22*, R106.

2. Jablonka, E. *Clin Pharmacol Ther* **2012,** *92*, 683.

3. Suva, M. L.; Riggi, N.; Bernstein, B. E. *Science* **2013,** *339*, 1567.

4. Gapp, K.; Woldemichael, B. T.; Bohacek, J.; Mansuy, I. M. *Neuroscience* **2012**.

5. Wolffe, A. P.; Guschin, D. *J Struct Biol* **2000,** *129*, 102.

6. Moudrianakis, E. N.; Arents, G. *Cold Spring Harb Symp Quant Biol* **1993,** *58*, 273.

7. Evertts, A. G.; Coller, H. A. *Genes Cancer* **2012,** *3*, 678.

8. Inbar-Feigenberg, M.; Choufani, S.; Butcher, D. T.; Roifman, M.; Weksberg, R. *Fertil Steril* **2013**.

9. Janzen, W. P.; Wigle, T. J.; Jin, J.; Frye, S. V. *Drug Discov Today Technol* **2010,** *7*, e59.

10. Marmorstein, R.; Roth, S. Y. *Curr Opin Genet Dev* **2001,** *11*, 155.

11. Sanchez, R.; Zhou, M. M. *Curr Opin Drug Discov Devel* **2009,** *12*, 659.

12. Cosgrove, M. S. *Nat Struct Mol Biol* **2012,** *19*, 739.

13. Wilson, B. J.; Tremblay, A. M.; Deblois, G.; Sylvain-Drolet, G.; Giguere, V. *Mol Endocrinol* **2010,** *24*, 1349.

14. Mal, A.; Sturniolo, M.; Schiltz, R. L.; Ghosh, M. K.; Harter, M. L. *Embo J* **2001,** *20*, 1739.

15. Ai, J.; Wang, Y.; Dar, J. A.; Liu, J.; Liu, L.; Nelson, J. B.; Wang, Z. *Mol Endocrinol* **2009,** *23*, 1963.

16. Zhang, Y.; Li, N.; Caron, C.; Matthias, G.; Hess, D.; Khochbin, S.; Matthias, P. *Embo J* **2003,** *22*, 1168.

17. Wurtele, H.; Li, Q.; Zhou, H.; Zhang, Z.; Verreault, A. *Med Sci (Paris)* **2009,** *25*, 121.

18. van Holde, K.; Zlatanova, J. *Proc Natl Acad Sci U S A* **1996,** *93*, 10548.

19. Millard, C. J.; Watson, P. J.; Celardo, I.; Gordiyenko, Y.; Cowley, S. M.; Robinson, C. V.; Fairall, L.; Schwabe, J. W. *Mol Cell* **2013,** *51*, 57.

20. Lauffer, B. E.; Mintzer, R.; Fong, R.; Mukund, S.; Tam, C.; Zilberleyb, I.; Flicke, B.; Ritscher, A.; Fedorowicz, G.; Vallero, R.; Ortwine, D. F.; Gunzner, J.; Modrusan, Z.; Neumann, L.; Koth, C. M.; Lupardus, P. J.; Kaminker, J. S.; Heise, C. E.; Steiner, P. *J Biol Chem* **2013,** *288*, 26926.

21. Bressi, J. C.; Jennings, A. J.; Skene, R.; Wu, Y.; Melkus, R.; De Jong, R.; O'Connell, S.; Grimshaw, C. E.; Navre, M.; Gangloff, A. R. *Bioorg Med Chem Lett* **2010,** *20*, 3142.

22. Arrar, M.; Turnham, R.; Pierce, L.; de Oliveira, C. A.; McCammon, J. A. *Protein Sci* **2013,** *22*, 83.

23. Vannini, A.; Volpari, C.; Gallinari, P.; Jones, P.; Mattu, M.; Carfi, A.; De Francesco, R.; Steinkuhler, C.; Di Marco, S. *EMBO Rep* **2007,** *8*, 879.

24. Ficner, R. *Curr Top Med Chem* **2009,** *9*, 235.

25. Somoza, J. R.; Skene, R. J.; Katz, B. A.; Mol, C.; Ho, J. D.; Jennings, A. J.; Luong, C.; Arvai, A.; Buggy, J. J.; Chi, E.; Tang, J.; Sang, B. C.; Verner, E.; Wynands, R.; Leahy, E. M.; Dougan, D. R.; Snell, G.; Navre, M.; Knuth, M. W.; Swanson, R. V.; McRee, D. E.; Tari, L. W. *Structure* **2004,** *12*, 1325.

26. Finnin, M. S.; Donigian, J. R.; Cohen, A.; Richon, V. M.; Rifkind, R. A.; Marks, P. A.; Breslow, R.; Pavletich, N. P. *Nature* **1999,** *401*, 188.

27. Lombardi, P. M.; Cole, K. E.; Dowling, D. P.; Christianson, D. W. *Curr Opin Struct Biol* **2011,** *21*, 735.

28. Whitehead, L.; Dobler, M. R.; Radetich, B.; Zhu, Y.; Atadja, P. W.; Claiborne, T.; Grob, J. E.; McRiner, A.; Pancost, M. R.; Patnaik, A.; Shao, W.; Shultz, M.; Tichkule, R.; Tommasi, R. A.; Vash, B.; Wang, P.; Stams, T. *Bioorg Med Chem* **2011,** *19*, 4626.

29. Vermeulen, M.; Walter, W.; Le Guezennec, X.; Kim, J.; Edayathumangalam, R. S.; Lasonder, E.; Luger, K.; Roeder, R. G.; Logie, C.; Berger, S. L.; Stunnenberg, H. G. *Mol Cell Biol* **2006,** *26*, 5226.

30. Butler, K. V.; Kozikowski, A. P. *Curr Pharm Des* **2008,** *14*, 505.

31. Thangapandian, S.; John, S.; Lee, K. W. *J Biomol Struct Dyn* **2012,** *29*, 677.

32. Wang, D. F.; Helquist, P.; Wiech, N. L.; Wiest, O. *J Med Chem* **2005,** *48*, 6936.

33. Hildmann, C.; Wegener, D.; Riester, D.; Hempel, R.; Schober, A.; Merana, J.; Giurato, L.; Guccione, S.; Nielsen, T. K.; Ficner, R.; Schwienhorst, A. *J Biotechnol* **2006,** *124*, 258.

34. Furumai, R.; Komatsu, Y.; Nishino, N.; Khochbin, S.; Yoshida, M.; Horinouchi, S. *Proc Natl Acad Sci U S A* **2001,** *98*, 87.

35. Furumai, R.; Matsuyama, A.; Kobashi, N.; Lee, K. H.; Nishiyama, M.; Nakajima, H.; Tanaka, A.; Komatsu, Y.; Nishino, N.; Yoshida, M.; Horinouchi, S. *Cancer Res* **2002,** *62*, 4916.

36. Montero, A.; Beierle, J. M.; Olsen, C. A.; Ghadiri, M. R. *J Am Chem Soc* **2009,** *131*, 3033.

37. Olsen, C. A.; Ghadiri, M. R. *J Med Chem* **2009,** *52*, 7836.

38. Di Micco, S.; Terracciano, S.; Bruno, I.; Rodriquez, M.; Riccio, R.; Taddei, M.; Bifulco, G. *Bioorg Med Chem* **2008,** *16*, 8635.

39. Xiao, J. J.; Byrd, J.; Marcucci, G.; Grever, M.; Chan, K. K. *Rapid Commun Mass Spectrom* **2003,** *17*, 757.

40. Rajendran, P.; Williams, D. E.; Ho, E.; Dashwood, R. H. *Crit Rev Biochem Mol Biol* **2011,** *46*, 181.

41. Kattar, S. D.; Surdi, L. M.; Zabierek, A.; Methot, J. L.; Middleton, R. E.; Hughes, B.; Szewczak, A. A.; Dahlberg, W. K.; Kral, A. M.; Ozerova, N.; Fleming, J. C.; Wang, H.; Secrist, P.; Harsch, A.; Hamill, J. E.; Cruz, J. C.; Kenific, C. M.; Chenard, M.; Miller, T. A.; Berk, S. C.; Tempest, P. *Bioorg Med Chem Lett* **2009,** *19*, 1168.

42. Methot, J. L.; Hamblett, C. L.; Mampreian, D. M.; Jung, J.; Harsch, A.; Szewczak, A. A.; Dahlberg, W. K.; Middleton, R. E.; Hughes, B.; Fleming, J. C.; Wang, H.; Kral, A. M.; Ozerova, N.; Cruz, J. C.; Haines, B.; Chenard, M.; Kenific, C. M.; Secrist, J. P.; Miller, T. A. *Bioorg Med Chem Lett* **2008,** *18*, 6104.

43. Witter, D. J.; Harrington, P.; Wilson, K. J.; Chenard, M.; Fleming, J. C.; Haines, B.; Kral, A. M.; Secrist, J. P.; Miller, T. A. *Bioorg Med Chem Lett* **2008,** *18*, 726.

44. Wilson, K. J.; Witter, D. J.; Grimm, J. B.; Siliphaivanh, P.; Otte, K. M.; Kral, A. M.; Fleming, J. C.; Harsch, A.; Hamill, J. E.; Cruz, J. C.; Chenard, M.; Szewczak, A. A.; Middleton, R. E.; Hughes, B. L.; Dahlberg, W. K.; Secrist, J. P.; Miller, T. A. *Bioorg Med Chem Lett* **2008,** *18*, 1859.

45. Suzuki, T.; Kasuya, Y.; Itoh, Y.; Ota, Y.; Zhan, P.; Asamitsu, K.; Nakagawa, H.; Okamoto, T.; Miyata, N. *PLoS One* **2013,** *8*, e68669.

46. Marson, C. M.; Matthews, C. J.; Yiannaki, E.; Atkinson, S. J.; Soden, P. E.; Shukla, L.; Lamadema, N.; Thomas, N. S. *J Med Chem* **2013,** *56*, 6156.

47. Kozikowski, A. P.; Tapadar, S.; Luchini, D. N.; Kim, K. H.; Billadeau, D. D. *J Med Chem* **2008,** *51*, 4370.

48. Neelarapu, R.; Holzle, D. L.; Velaparthi, S.; Bai, H.; Brunsteiner, M.; Blond, S. Y.; Petukhov, P. A. *J Med Chem* **2011,** *54*, 4350.

49. Balasubramanian, S.; Ramos, J.; Luo, W.; Sirisawad, M.; Verner, E.; Buggy, J. J. *Leukemia* **2008,** *22*, 1026.

50. Suzuki, T.; Ota, Y.; Ri, M.; Bando, M.; Gotoh, A.; Itoh, Y.; Tsumoto, H.; Tatum, P. R.; Mizukami, T.; Nakagawa, H.; Iida, S.; Ueda, R.; Shirahige, K.; Miyata, N. *J Med Chem* **2012,** *55*, 9562.

51. Gottlicher, M. *Ann Hematol* **2004,** *83 Suppl 1*, S91.

52. Butler, K. V.; He, R.; McLaughlin, K.; Vistoli, G.; Langley, B.; Kozikowski, A. P. *ChemMedChem* **2009,** *4*, 1292.

53. Suzuki, T.; Kouketsu, A.; Matsuura, A.; Kohara, A.; Ninomiya, S.; Kohda, K.; Miyata, N. *Bioorg Med Chem Lett* **2004,** *14*, 3313.

54. Anandan, S. K.; Ward, J. S.; Brokx, R. D.; Bray, M. R.; Patel, D. V.; Xiao, X. X. *Bioorg Med Chem Lett* **2005,** *15*, 1969.

55. Pescatore, G.; Kinzel, O.; Attenni, B.; Cecchetti, O.; Fiore, F.; Fonsi, M.; Rowley, M.; Schultz-Fademrecht, C.; Serafini, S.; Steinkuhler, C.; Jones, P. *Bioorg Med Chem Lett* **2008,** *18*, 5528.

56. Jones, P.; Steinkuhler, C. *Curr Pharm Des* **2008,** *14*, 545.

57. Vasudevan, A.; Ji, Z.; Frey, R. R.; Wada, C. K.; Steinman, D.; Heyman, H. R.; Guo, Y.; Curtin, M. L.; Guo, J.; Li, J.; Pease, L.; Glaser, K. B.; Marcotte, P. A.; Bouska, J. J.; Davidsen, S. K.; Michaelides, M. R. *Bioorg Med Chem Lett* **2003,** *13*, 3909.

58. Galletti, P.; Quintavalla, A.; Ventrici, C.; Giannini, G.; Cabri, W.; Penco, S.; Gallo, G.; Vincenti, S.; Giacomini, D. *ChemMedChem* **2009,** *4*, 1991.

59. Grunstein, M. *Nature* **1997,** *389*, 349.

60. Chuang, D. M.; Leng, Y.; Marinova, Z.; Kim, H. J.; Chiu, C. T. *Trends Neurosci* **2009,** *32*, 591.

61. Mattson, M. P. *Nature* **2004,** *430*, 631.

62. Kilgore, M.; Miller, C. A.; Fass, D. M.; Hennig, K. M.; Haggarty, S. J.; Sweatt, J. D.; Rumbaugh, G. *Neuropsychopharmacology* **2010,** *35*, 870.

63. Stefanko, D. P.; Barrett, R. M.; Ly, A. R.; Reolon, G. K.; Wood, M. A. *Proc Natl Acad Sci U S A* **2009,** *106*, 9447.

64. Green, K. N.; Steffan, J. S.; Martinez-Coria, H.; Sun, X.; Schreiber, S. S.; Thompson, L. M.; LaFerla, F. M. *J Neurosci* **2008,** *28*, 11500.

65. Fischer, A.; Sananbenesi, F.; Wang, X.; Dobbin, M.; Tsai, L. H. *Nature* **2007,** *447*, 178.

66. Vecsey, C. G.; Hawk, J. D.; Lattal, K. M.; Stein, J. M.; Fabian, S. A.; Attner, M. A.; Cabrera, S. M.; McDonough, C. B.; Brindle, P. K.; Abel, T.; Wood, M. A. *J Neurosci* **2007,** *27*, 6128.

67. Guan, J. S.; Haggarty, S. J.; Giacometti, E.; Dannenberg, J. H.; Joseph, N.; Gao, J.; Nieland, T. J.; Zhou, Y.; Wang, X.; Mazitschek, R.; Bradner, J. E.; DePinho, R. A.; Jaenisch, R.; Tsai, L. H. *Nature* **2009,** *459*, 55.

68. Ballas, N.; Grunseich, C.; Lu, D. D.; Speh, J. C.; Mandel, G. *Cell* **2005,** *121*, 645.

69. Lunyak, V. V.; Burgess, R.; Prefontaine, G. G.; Nelson, C.; Sze, S. H.; Chenoweth, J.; Schwartz, P.; Pevzner, P. A.; Glass, C.; Mandel, G.; Rosenfeld, M. G. *Science* **2002,** *298*, 1747.

70. Nott, A.; Watson, P. M.; Robinson, J. D.; Crepaldi, L.; Riccio, A. *Nature* **2008,** *455*, 411.

71. Yeh, S. H.; Lin, C. H.; Gean, P. W. *Mol Pharmacol* **2004,** *65*, 1286.

72. Lubin, F. D.; Sweatt, J. D. *Neuron* **2007,** *55*, 942.

73. Grissom, N. M.; Lubin, F. D. *Cellscience* **2009,** *6*, 44.

74. Gao, J.; Siddoway, B.; Huang, Q.; Xia, H. *Biochem Biophys Res Commun* **2009,** *379*, 1.

75. Fass, D. M.; Reis, S. A.; Ghosh, B.; Hennig, K. M.; Joseph, N. F.; Zhao, W. N.; Nieland, T. J.; Guan, J. S.; Kuhnle, C. E.; Tang, W.; Barker, D. D.; Mazitschek, R.; Schreiber, S. L.; Tsai, L. H.; Haggarty, S. J. *Neuropharmacology* **2013,** *64*, 81.

76. McQuown, S. C.; Barrett, R. M.; Matheos, D. P.; Post, R. J.; Rogge, G. A.; Alenghat, T.; Mullican, S. E.; Jones, S.; Rusche, J. R.; Lazar, M. A.; Wood, M. A. *The Journal of neuroscience : the official journal of the Society for Neuroscience* **2011,** *31*, 764.

77. McKinsey, T. A.; Zhang, C. L.; Olson, E. N. *Curr Opin Genet Dev* **2001,** *11*, 497.

78. Colussi, C.; Mozzetta, C.; Gurtner, A.; Illi, B.; Rosati, J.; Straino, S.; Ragone, G.; Pescatori, M.; Zaccagnini, G.; Antonini, A.; Minetti, G.; Martelli, F.; Piaggio, G.; Gallinari, P.; Steinkuhler, C.; Clementi, E.; Dell'Aversana, C.; Altucci, L.; Mai, A.; Capogrossi, M. C.; Puri, P. L.; Gaetano, C. *Proc Natl Acad Sci U S A* **2008,** *105*, 19183.

79. Mal, A.; Sturniolo, M.; Schiltz, R. L.; Ghosh, M. K.; Harter, M. L. *EMBO J* **2001,** *20*, 1739.

80. Lee, S. J.; McPherron, A. C. *Proc Natl Acad Sci U S A* **2001,** *98*, 9306.

81. McCroskery, S.; Thomas, M.; Maxwell, L.; Sharma, M.; Kambadur, R. *J Cell Biol* **2003,** *162*, 1135.

82. Rios, R.; Carneiro, I.; Arce, V. M.; Devesa, J. *Am J Physiol Cell Physiol* **2002,** *282*, C993.

83. Langley, B.; Thomas, M.; Bishop, A.; Sharma, M.; Gilmour, S.; Kambadur, R. *J Biol Chem* **2002,** *277*, 49831.

84. Oehme, I.; Deubzer, H. E.; Wegener, D.; Pickert, D.; Linke, J. P.; Hero, B.; Kopp-Schneider, A.; Westermann, F.; Ulrich, S. M.; von Deimling, A.; Fischer, M.; Witt, O. *Clin Cancer Res* **2009,** *15*, 91.

85. Oehme, I.; Deubzer, H. E.; Lodrini, M.; Milde, T.; Witt, O. *Expert Opin Investig Drugs* **2009,** *18*, 1605.

86. Bruserud, O.; Stapnes, C.; Ersvaer, E.; Gjertsen, B. T.; Ryningen, A. *Current pharmaceutical biotechnology* **2007,** *8*, 388.

87. Whittaker, M.; Floyd, C. D.; Brown, P.; Gearing, A. J. *Chemical reviews* **2001,** *101*, 2205.

88. Vassiliou, S.; Mucha, A.; Cuniasse, P.; Georgiadis, D.; Lucet-Levannier, K.; Beau, F.; Kannan, R.; Murphy, G.; Knauper, V.; Rio, M. C.; Basset, P.; Yiotakis, A.; Dive, V. *J Med Chem* **1999,** *42*, 2610.

89. Mulder, G. J.; Meerman, J. H. *Environmental health perspectives* **1983,** *49*, 27.

90. Kelly, W. K.; Richon, V. M.; O'Connor, O.; Curley, T.; MacGregor-Curtelli, B.; Tong, W.; Klang, M.; Schwartz, L.; Richardson, S.; Rosa, E.; Drobnjak, M.; Cordon-Cordo, C.; Chiao, J. H.; Rifkind, R.; Marks, P. A.; Scher, H. *Clin Cancer Res* **2003,** *9*, 3578.

91. Qiu, L.; Kelso, M. J.; Hansen, C.; West, M. L.; Fairlie, D. P.; Parsons, P. G. *British journal of cancer* **1999,** *80*, 1252.

92. Suzuki, T.; Miyata, N. *Current medicinal chemistry* **2005,** *12*, 2867.

93. Suzuki, T.; Miyata, N. *Mini reviews in medicinal chemistry* **2006,** *6*, 515.

94. Khan, N.; Jeffers, M.; Kumar, S.; Hackett, C.; Boldog, F.; Khramtsov, N.; Qian, X.; Mills, E.; Berghs, S. C.; Carey, N.; Finn, P. W.; Collins, L. S.; Tumber, A.;

Ritchie, J. W.; Jensen, P. B.; Lichenstein, H. S.; Sehested, M. *The Biochemical journal* **2008,** *409*, 581.

95. Beconi, M.; Aziz, O.; Matthews, K.; Moumne, L.; O'Connell, C.; Yates, D.; Clifton, S.; Pett, H.; Vann, J.; Crowley, L.; Haughan, A. F.; Smith, D. L.; Woodman, B.; Bates, G. P.; Brookfield, F.; Burli, R. W.; McAllister, G.; Dominguez, C.; Munoz-Sanjuan, I.; Beaumont, V. *PLoS One* **2012,** *7*, e44498.

96. Frey, R. R.; Wada, C. K.; Garland, R. B.; Curtin, M. L.; Michaelides, M. R.; Li, J.; Pease, L. J.; Glaser, K. B.; Marcotte, P. A.; Bouska, J. J.; Murphy, S. S.; Davidsen, S. K. *Bioorg Med Chem Lett* **2002,** *12*, 3443.

97. Domingo, J. L. *Reproductive toxicology (Elmsford, N.Y* **1998,** *12*, 499.

98. Ndinguri, M. W.; Bhowmick, M.; Tokmina-Roszyk, D.; Robichaud, T. K.; Fields, G. B. *Molecules* **2012,** *17*, 14230.

99. Estiu, G.; West, N.; Mazitschek, R.; Greenberg, E.; Bradner, J. E.; Wiest, O. *Bioorg Med Chem* **2010,** *18*, 4103.

100. Brunsteiner, M.; Petukhov, P. A. *J Mol Model* **2012,** *18*, 3927.

101. Wang, D. F.; Helquist, P.; Wiech, N. L.; Wiest, O. *J Med Chem* **2005,** *48*, 6936.

102. Methot, J. L.; Chakravarty, P. K.; Chenard, M.; Close, J.; Cruz, J. C.; Dahlberg, W. K.; Fleming, J.; Hamblett, C. L.; Hamill, J. E.; Harrington, P.; Harsch, A.; Heidebrecht, R.; Hughes, B.; Jung, J.; Kenific, C. M.; Kral, A. M.; Meinke, P. T.; Middleton, R. E.; Ozerova, N.; Sloman, D. L.; Stanton, M. G.; Szewczak, A. A.; Tyagarajan, S.; Witter, D. J.; Secrist, J. P.; Miller, T. A. *Bioorg Med Chem Lett* **2008,** *18*, 973.

103. He, B.; Velaparthi, S.; Pieffet, G.; Pennington, C.; Mahesh, A.; Holzle, D. L.; Brunsteiner, M.; van Breemen, R.; Blond, S. Y.; Petukhov, P. A. *J Med Chem* **2009,** *52*, 7003.

104. Singh, A.; Thornton, E. R.; Westheimer, F. H. *J Biol Chem* **1962,** *237*, 3006.

105. G. W. J. FLEET, R. R. P. J. R. K. *Nature* **1969,** *224*, 511.

106. Galardy, R. E.; Craig, L. C.; Printz, M. P. *Nat New Biol* **1973,** *242*, 127.

107. Smith, R. A.; Knowles, J. R. *J Am Chem Soc* **1973,** *95*, 5072.

108. Kapfer, I.; Jacques, P.; Toubal, H.; Goeldner, M. P. *Bioconjug Chem* **1995,** *6*, 109.

109. Tsao, M. L.; Platz, M. S. *J Am Chem Soc* **2003,** *125*, 12014.

110. Charles J. Shields , D. E. F., Gary B. Schuster , Ole Buchardt , Peter E. Nielsen. *J.Org.Chem.* **1988,** *53*, 3501.

111. K. Barral, A. D. M., J. E. Moses. *Org. Lett.* **2007,** *9*, 1809.

112. Q. Liu, Y. T. *Org. Lett.* **2003,** *5*, 2571.

113. E. D. Goddard-Borger, R. V. S. *Org. Lett.* **2007,** *9*, 3797

114. Crocker, P. J.; Imai, N.; Rajagopalan, K.; Boggess, M. A.; Kwiatkowski, S.; Dwyer, L. D.; Vanaman, T. C.; Watt, D. S. *Bioconjug Chem* **1990,** *1*, 419.

115. Staros, J. V.; Bayley, H.; Standring, D. N.; Knowles, J. R. *Biochem Biophys Res Commun* **1978,** *80*, 568.

116. R. J. Bergeron, J. B. D., M. J. Ingeno,. *J.Org.Chem.* **1987,** *52*, 144.

117. Brunner, J.; Senn, H.; Richards, F. M. *J Biol Chem* **1980,** *255*, 3313.

118. Fleming, S. A. *Tetrahedron* **1995,** *51*, 12479.

119. Dorman, G.; Prestwich, G. D. *Biochemistry* **1994,** *33*, 5661.

120. Salisbury, C. M.; Cravatt, B. F. *Proc Natl Acad Sci U S A* **2007,** *104*, 1171.

121. Thirumurugan, P.; Matosiuk, D.; Jozwiak, K. *Chemical reviews* **2013**.

122. Massi, A.; Nanni, D. *Org Biomol Chem* **2012,** *10*, 3791.

123. van Geel, R.; Pruijn, G. J.; van Delft, F. L.; Boelens, W. C. *Bioconjug Chem* **2012,** *23*, 392.

124. Kohn, M.; Breinbauer, R. *Angew Chem Int Ed Engl* **2004,** *43*, 3106.

125. Ning, X.; Temming, R. P.; Dommerholt, J.; Guo, J.; Ania, D. B.; Debets, M. F.; Wolfert, M. A.; Boons, G. J.; van Delft, F. L. *Angew Chem Int Ed Engl* **2010,** *49*, 3065.

126. Singh, I.; Heaney, F. *Chem Commun (Camb)* **2011,** *47*, 2706.

127. Debets, M. F.; van Berkel, S. S.; Dommerholt, J.; Dirks, A. T.; Rutjes, F. P.; van Delft, F. L. *Acc Chem Res* **2011,** *44*, 805.

128. Haun, M.; Wasi, S. *Anal Biochem* **1990,** *191*, 337.

129. Panchuk-Voloshina, N.; Haugland, R. P.; Bishop-Stewart, J.; Bhalgat, M. K.; Millard, P. J.; Mao, F.; Leung, W. Y. *J Histochem Cytochem* **1999,** *47*, 1179.

130. Naganathan, S.; Ye, S.; Sakmar, T. P.; Huber, T. *Biochemistry* **2013,** *52*, 1028.

131. Zhao, C.; Hellman, L. M.; Zhan, X.; Bowman, W. S.; Whiteheart, S. W.; Fried, M. G. *Anal Biochem* **2010,** *399*, 237.

132. Long, M. J.; Hedstrom, L. *Chembiochem* **2012,** *13*, 1818.

133. Huisgen, R. *Proc. Chem. Soc.* **1961**, 357.

134. Vsevolod V. Rostovtsev, L. G. G., Valery V. Fokin, K. Barry Sharpless. *41* **2002,** *14*, 2596.

135. M., T. C. C. C. M. *J.Org.Chem.* **2002,** *67*, 3057.

136. F. Wolbers, P. t. B., S. Le Gac, R. Luttge, H. Andersson,; I. Vermes and A. van den Berg. *Electrophoresis* **2006,** *27*, 5073.

137. Schoenebeck, F.; Ess, D. H.; Jones, G. O.; Houk, K. N. *J Am Chem Soc* **2009,** *131*, 8121.

138. van Berkel, S. S.; van Eldijk, M. B.; van Hest, J. C. *Angew Chem Int Ed Engl* **2011,** *50*, 8806.

139. Agard, N. J.; Baskin, J. M.; Prescher, J. A.; Lo, A.; Bertozzi, C. R. *ACS Chem Biol* **2006,** *1*, 644.

140. Salisbury, C. M.; Cravatt, B. F. *J Am Chem Soc* **2008,** *130*, 2184.

141. Xu, C.; Soragni, E.; Chou, C. J.; Herman, D.; Plasterer, H. L.; Rusche, J. R.; Gottesfeld, J. M. *Chem Biol* **2009,** *16*, 980.

142. Fischer, J. J.; Michaelis, S.; Schrey, A. K.; Diehl, A.; Graebner, O. Y.; Ungewiss, J.; Horzowski, S.; Glinski, M.; Kroll, F.; Dreger, M.; Koester, H. *Proteomics* **2011,** *11*, 4096.

143. Hosoya, T.; Hiramatsu, T.; Ikemoto, T.; Nakanishi, M.; Aoyama, H.; Hosoya, A.; Iwata, T.; Maruyama, K.; Endo, M.; Suzuki, M. *Org Biomol Chem* **2004,** *2*, 637.

144. He, B.; Velaparthi, S.; Pieffet, G.; Pennington, C.; Mahesh, A.; Holzle, D. L.; Brunsteiner, M.; van Breemen, R.; Blond, S. Y.; Petukhov, P. A. *J Med Chem* **2009,** *52*, 7003.

145. Friend, C.; Scher, W.; Holland, J. G.; Sato, T. *Proc Natl Acad Sci U S A* **1971,** *68*, 378.

146. Richon, V. M.; Webb, Y.; Merger, R.; Sheppard, T.; Jursic, B.; Ngo, L.; Civoli, F.; Breslow, R.; Rifkind, R. A.; Marks, P. A. *Proc Natl Acad Sci U S A* **1996,** *93*, 5705.

147. Darkin-Rattray, S. J.; Gurnett, A. M.; Myers, R. W.; Dulski, P. M.; Crumley, T. M.; Allocco, J. J.; Cannova, C.; Meinke, P. T.; Colletti, S. L.; Bednarek, M. A.; Singh, S. B.; Goetz, M. A.; Dombrowski, A. W.; Polishook, J. D.; Schmatz, D. M. *Proc Natl Acad Sci U S A* **1996,** *93*, 13143.

148. Kolle, D.; Brosch, G.; Lechner, T.; Lusser, A.; Loidl, P. *Methods* **1998,** *15*, 323.

149. Nare, B.; Allocco, J. J.; Kuningas, R.; Galuska, S.; Myers, R. W.; Bednarek, M. A.; Schmatz, D. M. *Anal Biochem* **1999,** *267*, 390.

150. Fatkins, D. G.; Zheng, W. *Anal Biochem* **2008,** *372*, 82.

151. Hoffmann, K.; Brosch, G.; Loidl, P.; Jung, M. *Nucleic Acids Res* **1999,** *27*, 2057.

152. Heltweg, B.; Trapp, J.; Jung, M. *Methods* **2005,** *36*, 332.

153. Heltweg, B.; Dequiedt, F.; Marshall, B. L.; Brauch, C.; Yoshida, M.; Nishino, N.; Verdin, E.; Jung, M. *J Med Chem* **2004,** *47*, 5235.

154. Riester, D.; Wegener, D.; Hildmann, C.; Schwienhorst, A. *Biochem Biophys Res Commun* **2004,** *324*, 1116.

155. Riester, D.; Hildmann, C.; Grunewald, S.; Beckers, T.; Schwienhorst, A. *Biochem Biophys Res Commun* **2007,** *357*, 439.

156. Halley, F.; Reinshagen, J.; Ellinger, B.; Wolf, M.; Niles, A. L.; Evans, N. J.; Kirkland, T. A.; Wagner, J. M.; Jung, M.; Gribbon, P.; Gul, S. *J Biomol Screen* **2011,** *16*, 1227.

157. Richon, V. M.; Zhou, X.; Secrist, J. P.; Cordon-Cardo, C.; Kelly, W. K.; Drobnjak, M.; Marks, P. A. *Methods Enzymol* **2004,** *376*, 199.

158. Glaser, K. B.; Li, J.; Pease, L. J.; Staver, M. J.; Marcotte, P. A.; Guo, J.; Frey, R. R.; Garland, R. B.; Heyman, H. R.; Wada, C. K.; Vasudevan, A.; Michaelides, M. R.; Davidsen, S. K.; Curtin, M. L. *Biochem Biophys Res Commun* **2004,** *325*, 683.

159. Mazitschek, R.; Patel, V.; Wirth, D. F.; Clardy, J. *Bioorg Med Chem Lett* **2008,** *18*, 2809.

160. Riester, D.; Hildmann, C.; Schwienhorst, A.; Meyer-Almes, F. J. *Anal Biochem* **2007,** *362*, 136.

161. Khan, N.; Jeffers, M.; Kumar, S.; Hackett, C.; Boldog, F.; Khramtsov, N.; Qian, X.; Mills, E.; Berghs, S. C.; Carey, N.; Finn, P. W.; Collins, L. S.; Tumber, A.; Ritchie, J. W.; Jensen, P. B.; Lichenstein, H. S.; Sehested, M. *Biochem J* **2008,** *409*, 581.

162. Whittaker, M.; Floyd, C. D.; Brown, P.; Gearing, A. J. *Chem. Rev.* **2001,** *101*, 2205.

163. Weisburger, J. H.; Weisburger, E. K. *Pharmacol Rev* **1973,** *25*, 1.

164. Mulder, G. J.; Meerman, J. H. *Environ. Health. Perspect.* **1983,** *49*, 27.

165. Groutas, W. C.; Giri, P. K.; Crowley, J. P.; Castrisos, J. C.; Brubaker, M. J. *Biochem. Biophys. Res. Commun.* **1986,** *141*, 741.

166. Gilissen, R. A.; Bamforth, K. J.; Stavenuiter, J. F.; Coughtrie, M. W.; Meerman, J. H. *Carcinogenesis* **1994,** *15*, 39.

167. Meerman, J. H.; Ringer, D. P.; Coughtrie, M. W.; Bamforth, K. J.; Gilissen, R. A. *Chem Biol Interact* **1994,** *92*, 321.

168. Suzuki, T.; Miyata, N. *Mini. Rev. Med. Chem.* **2006,** *6*, 515.

169. Suzuki, T.; Miyata, N. *Curr. Med. Chem.* **2005,** *12*, 2867.

170. Suzuki, T.; Matsuura, A.; Kouketsu, A.; Hisakawa, S.; Nakagawa, H.; Miyata, N. *Bioorg. Med. Chem.* **2005,** *13*, 4332.

171. Curtin, M. L. *Curr. Opin. Drug. Discov. Devel.* **2004,** *7*, 848.

172. Khan, N.; Jeffers, M.; Kumar, S.; Hackett, C.; Boldog, F.; Khramtsov, N.; Qian, X.; Mills, E.; Berghs, S. C.; Carey, N.; Finn, P. W.; Collins, L. S.; Tumber, A.; Ritchie, J. W.; Jensen, P. B.; Lichenstein, H. S.; Sehested, M. *Biochem. J* **2008,** *409*, 581.

173. Munday, R. *Free Radical Biol. Med.* **1989,** *7*, 659.

174. Frey, R. R.; Wada, C. K.; Garland, R. B.; Curtin, M. L.; Michaelides, M. R.; Li, J.; Pease, L. J.; Glaser, K. B.; Marcotte, P. A.; Bouska, J. J.; Murphy, S. S.; Davidsen, S. K. *Bioorg. Med. Chem. Lett.* **2002,** *12*, 3443.

175. McQuown, S. C.; Barrett, R. M.; Matheos, D. P.; Post, R. J.; Rogge, G. A.; Alenghat, T.; Mullican, S. E.; Jones, S.; Rusche, J. R.; Lazar, M. A.; Wood, M. A. *J. Neurosci.* **2011,** *31*, 764.

176. Chris J. Vickers, C. A. O., Luke J. Leman, and M. Reza Ghadiri. *ACS Med.Chem.Lett.* **2012,** *3*.

177. He, B.; Velaparthi, S.; Pieffet, G.; Pennington, C.; Mahesh, A.; Holzle, D. L.; Brunsteiner, M.; van Breemen, R.; Blond, S. Y.; Petukhov, P. A. *J. Med. Chem.* **2009,** *52*, 7003.

178. Condorelli, F.; Gnemmi, I.; Vallario, A.; Genazzani, A. A.; Canonico, P. L. *Br. J. Pharmacol.* **2008,** *153*, 657.

179. Muhlethaler-Mottet, A.; Meier, R.; Flahaut, M.; Bourloud, K. B.; Nardou, K.; Joseph, J. M.; Gross, N. *Mol. Cancer.* **2008,** *7*, 55.

180. Witt, O.; Deubzer, H. E.; Lodrini, M.; Milde, T.; Oehme, I. *Curr. Pharm. Des.* **2009,** *15*, 436.

181. Oehme, I.; Deubzer, H. E.; Lodrini, M.; Milde, T.; Witt, O. *Expert. Opin. Investig. Drugs.* **2009,** *18*, 1605.

182. Oehme, I.; Deubzer, H. E.; Wegener, D.; Pickert, D.; Linke, J. P.; Hero, B.; Kopp-Schneider, A.; Westermann, F.; Ulrich, S. M.; von Deimling, A.; Fischer, M.; Witt, O. *Clin. Cancer. Res.* **2009,** *15*, 91.

183. Fass, D. M.; Reis, S. A.; Ghosh, B.; Hennig, K. M.; Joseph, N. F.; Zhao, W. N.; Nieland, T. J.; Guan, J. S.; Groves Kuhnle, C. E.; Tang, W.; Barker, D. D.; Mazitschek, R.; Schreiber, S. L.; Tsai, L. H.; Haggarty, S. J. *Neuropharmacology* **2012**.

184. Verdonk, M. L.; Cole, J. C.; Hartshorn, M. J.; Murray, C. W.; Taylor, R. D. *Proteins* **2003,** *52*, 609.

185. Zhang, C. J.; Li, L.; Chen, G. Y.; Xu, Q. H.; Yao, S. Q. *Org. Lett.* **2011,** *13*, 4160.

186. Zhao, Y. L.; Dichtel, W. R.; Trabolsi, A.; Saha, S.; Aprahamian, I.; Stoddart, J. F. *J. Am. Chem. Soc.* **2008,** *130*, 11294.

187. Neelarapu, R.; Holzle, D. L.; Velaparthi, S.; Bai, H.; Brunsteiner, M.; Blond, S. Y.; Petukhov, P. A. *J. Med. Chem.* **2011,** *54*, 4350.

188. Dowling, D. P.; Gattis, S. G.; Fierke, C. A.; Christianson, D. W. *Biochemistry* **2010,** *49*, 5048.

189. Butler, K. V.; Kalin, J.; Brochier, C.; Vistoli, G.; Langley, B.; Kozikowski, A. P. *J. Am. Chem. Soc.* **2010,** *132*, 10842.

190. Paquin, I.; Raeppel, S.; Leit, S.; Gaudette, F.; Zhou, N.; Moradei, O.; Saavedra, O.; Bernstein, N.; Raeppel, F.; Bouchain, G.; Frechette, S.; Woo, S. H.; Vaisburg, A.; Fournel, M.; Kalita, A.; Robert, M. F.; Lu, A.; Trachy-Bourget, M. C.; Yan, P. T.; Liu, J.; Rahil, J.; MacLeod, A. R.; Besterman, J. M.; Li, Z.; Delorme, D. *Bioorg Med Chem Lett* **2008,** *18*, 1067.

191. Bressi, J. C.; Jennings, A. J.; Skene, R.; Wu, Y.; Melkus, R.; De Jong, R.; O'Connell, S.; Grimshaw, C. E.; Navre, M.; Gangloff, A. R. *Bioorg. Med. Chem. Lett.* **2010,** *20*, 3142.

192. Watson, P. J.; Fairall, L.; Santos, G. M.; Schwabe, J. W. *Nature* **2012,** *481*, 335.

193. Jones, G.; Willett, P.; Glen, R. C.; Leach, A. R.; Taylor, R. *J. Mol. Biol.* **1997,** *267*, 727.

194. Inc., M. USA Patent PCT/US2007/060045; **2007**.

195. D. Gowda, B. M., & G. Shankare. *Ind. J. Chem. Sect. B* **2001,** *40*, 75.

196. Suzuki, T.; Ando, T.; Tsuchiya, K.; Fukazawa, N.; Saito, A.; Mariko, Y.; Yamashita, T.; Nakanishi, O. *J Med Chem* **1999,** *42*, 3001.

197. Umezawa, N.; Matsumoto, N.; Iwama, S.; Kato, N.; Higuchi, T. *Bioorg Med Chem* **2010,** *18*, 6340.

198. Chou, C. J.; Herman, D.; Gottesfeld, J. M. *J Biol Chem* **2008,** *283*, 35402.

199. Salisbury, C. M.; Cravatt, B. F. *J. Am. Chem. Soc.* **2008,** *130*, 2184.

200. Methot, J. L.; Chakravarty, P. K.; Chenard, M.; Close, J.; Cruz, J. C.; Dahlberg, W. K.; Fleming, J.; Hamblett, C. L.; Hamill, J. E.; Harrington, P.; Harsch, A.; Heidebrecht, R.; Hughes, B.; Jung, J.; Kenific, C. M.; Kral, A. M.; Meinke, P. T.; Middleton, R. E.; Ozerova, N.; Sloman, D. L.; Stanton, M. G.; Szewczak, A. A.; Tyagarajan, S.; Witter, D. J.; Secrist, J. P.; Miller, T. A. *Bioorg. Med. Chem. Lett.* **2008,** *18*, 973.

201. Suzuki, J.; Chen, Y. Y.; Scott, G. K.; Devries, S.; Chin, K.; Benz, C. C.; Waldman, F. M.; Hwang, E. S. *Clin Cancer Res* **2009,** *15*, 3163.

VITA

ADITYA S. VAIDYA

246 W Big Springs Rd, Apt F
Riverside, CA-92507
312-208-7590

aditya_dv@yahoo.com
addyvaidya@gmail.com

EDUCATION

Ph.D., Medicinal Chemistry, University of Illinois at Chicago, 2008-present
Advisor: Dr. Pavel A. Petukhov

B.Tech. Pharmaceutical Sciences and Technology, Institute of Chemical Technology, Mumbai, 2008.
Thesis title: "Aprotic diazotization-iodination of aromatic amines"
Advisor: Dr. K.G. Akamanchi.

RESEARCH EXPERIENCE

2013-Present Junior Specialist, University of California at Riverside
Mentor: Dr. Sean Cutler

- Involved in the design and synthesis of Abscisic acid receptor agonists.

2009-2013 Graduate Assistant, University of Illinois at Chicago
Advisor: Dr. Pavel A. Petukhov

- Developed potent and selective photoreactive benzamide probes for mapping the binding site of histone deacetylase 2.
- Designed a set of photoaffinity probes to validate the binding modes of novel series of ligands targeting a secondary binding site in histone deactylase 8.
- Established a fluorogenic assay for screening of multitude of inhibitors/probes against histone deacetylase 2.
- Experienced in research techniques such as immunoblotting, fluorescence spectrophotometry, cell culture, protein purification and LCMS.
- Gained experience in molecular modeling studies, using Molecular operating environment (MOE).

2008 Undergraduate research assistant, Institute of Chemical Technology, Mumbai

Advisor: Dr. K.G.Akamanchi

- Studied aprotic diazotization iodination reaction for the synthesis of o-iodobenzoic acid, a major precursor in the synthesis of hypervalent organoiodine reagents.

2007 Internship at Nicholas Piramal India Ltd.
Studied synthesis of Vitamin A.

2006 Research Trainee, Sangene Biotech Ltd.
Studied molecular biology techniques such as gel electrophoresis and immunoblotting.

SCHOLARSHIPS AND AWARDS

- Chancellor's Fellowship, University of Illinois at Chicago (2013)
- ADDF, Young Investigator Scholarship (2012)
- W.E. van Doren Scholar Award (2012)
- Graduate College Presenters Award, University of Illinois at Chicago (2011)
- Graduate Student Council Travel Award, University of Illinois at Chicago (2011)
- ADDF, Young Investigator Scholarship (2011)
- Oscar Robert Oldberg Prize, University of Illinois at Chicago (2010)
- IDMA (Indian Drug Manufacturer's Association) G.P.Nair Award (2009)
- Indian Pharmaceutical Association Award (2009)
- K.C. Mahindra Scholarship for Post Graduate Studies abroad (2008)
- Mrs. Soonabhai Dadabhoy Master Scholarship(2008)
- Mrs. R.B. Foster Book Prize(2008)
- Mrs. Usha /S.M.Joshi Award, Institute of Chemical Technology(2008)
- Dr. M.K Rangnekar Memorial Medal, University of Mumbai (2008)
- Prof. M.L.Khorana Memorial Prize for being the topper in B.Tech Pharma(2008)
- Prof. J.G.Kane Memorial Award for being the topper in all branches of ICT(2008)
- Prof. G.M.Nabar Prize for 2008 for being topper in B.Tech/B.Chem/B.Pharm branches of ICT(2008)
- ICT Department & Golden Jubilee Scholarship(2008)
- Sir Ratan Tata Scholarship(2007)
- John Kapoor Charitable Endowment Scholarship(2007)

PRESENTATIONS

- Aditya S. Vaidya, Emma Mendonca, Bhargava Karumudi, Antonett Madriaga, Pavel A. Petukhov, Novel photoreactive diazide based benzamide probes for mapping the binding site of HDAC2, College of Pharmacy Research Day,UIC, March 9th, 2012, Chicago, IL.

- Aditya S. Vaidya, Emma Mendonca, Bhargava Karumudi, Antonett Madriaga, Pavel A. Petukhov, Novel photoreactive diazide based benzamide probes for mapping the binding site of HDAC2, 6th DRUG DISCOVERY FOR NEURODEGENERATION: An Intensive Course on Translating Research into Drugs, February 12th-14th, 2012, New York, NY.
- Aditya S. Vaidya, Emma Mendonca, Bai He, Raghupathi Neelarapu, Pavel A. Petukhov, Exploring a secondary binding site in histone deacetylases for design of inhibitors lacking zinc binding group. 49th Annual MIKI Meeting, 2011, University of Kansas, Lawrence, KS.
- Aditya S. Vaidya, Emma Mendonca, Bai He, Raghupathi Neelarapu, Pavel A. Petukhov, Exploring a secondary binding site in histone deacetylases for design of inhibitors lacking zinc binding group. 5th DRUG DISCOVERY FOR NEURODEGENERATION: An Intensive Course on Translating Research into Drugs, February 6th-8th, 2012, San Diego, CA.

PUBLICATIONS

- **Vaidya, A.S**.; Neelarapu, R; Madriaga, A; Bai, H; Mendonca, E; Abdelkarim, H; van Breemen, R.B; Blond, S. Y.; Petukhov, P.A. *Bioorg. Med. Chem. Lett*, **2012,** 22, 6621.
- **Vaidya, A.S**.; Karumudi, B; Mendonca, E; Madriaga, A; Abdelkarim, H; van Breemen, R. B.; Petukhov, P. A. *Bioorg. Med. Chem. Lett*. **2012,** 22, 5025.
- Patel HK, Siklos MI, Abdelkarim H, Mendonca EL, **Vaidya A**, Petukhov P. A, Thatcher GR. ChemMedChem. **2013**, PMID 23956109
- Probing the protonation state of Asp^{101} "hot spot" in class I histone deacetylases using novel amine based ligands, Neelarapu, R; Mendonca, E; Abdelkarim, A; **Vaidya A.S**; Bai, H; Madriaga, A; Brunsteiner, M; Petukhov, P.A. (Manuscript in progress)
- Synthesis and biological evaluation of phenothiazine-based HDAC inhibitors.. Madriaga A.P, **Vaidya. A.S** and Petukhov P.A(Manuscript in progress).

AFFILIATIONS

American Association of Pharmaceutical Scientists
American Chemical Society